

9-19-2013

Development and Characterization of Microfabricated Device for Real-Time Measurement of the Size and Number of Airborne Ultrafine Particles

Terence Barrett
University of Vermont

Follow this and additional works at: <http://scholarworks.uvm.edu/graddis>

Recommended Citation

Barrett, Terence, "Development and Characterization of Microfabricated Device for Real-Time Measurement of the Size and Number of Airborne Ultrafine Particles" (2013). *Graduate College Dissertations and Theses*. Paper 17.

This Thesis is brought to you for free and open access by the Dissertations and Theses at ScholarWorks @ UVM. It has been accepted for inclusion in Graduate College Dissertations and Theses by an authorized administrator of ScholarWorks @ UVM. For more information, please contact donna.omalley@uvm.edu.

DEVELOPMENT AND CHARACTERIZATION OF A MICROFABRICATED
DEVICE FOR REAL-TIME MEASUREMENT OF THE SIZE AND NUMBER OF
AIRBORNE ULTRAFINE PARTICLES

A Thesis Presented

by

Terence Barrett

to

The Faculty of the Graduate College

of

The University of Vermont

In Partial Fulfillment of the Requirements
for the Degree of Master of Science
Specializing in Civil & Environmental Engineering

October 2011

Accepted by the Faculty of the Graduate College, The University of Vermont, in partial fulfillment of the requirements for the degree of Master of Science, specializing in Civil & Environmental Engineering.

Thesis Examination Committee:

Britt A. Holmén, Ph.D. **Advisor**

George Pinder, Ph.D.

Jeffrey Marshall, Ph.D.

Jeffrey Frolik, Ph.D. **Chairperson**

Domenico Grasso, Ph.D. **Dean, Graduate College**

Date: June 23rd, 2011

ABSTRACT

Ultrafine particle emissions in motor-vehicle exhaust are associated with cardiopulmonary health impacts and increased mortality. The emission, evolution, and exposure-uptake of these particles, one hundred nanometers and smaller in diameter, are fundamentally quantified by the number concentration as a function of particle size. Ultrafine particle number distributions are widely varying and fast changing as they are strongly influenced by local environmental conditions and variation in vehicle operation and maintenance. Research and regulation to quantify and control such emissions rely on measurement of the number distribution of ultrafine particles in vehicle exhaust and by the roadside. Instruments to make such measurements are commercially available, but they are expensive, non-portable, and have slow response times.

A new instrument, the NanoAPA, is being developed for these in-situ applications as an inexpensive, portable, and real-time instrument. The instrument is designed to perform ultrafine particle sizing and counting through electronic control of a microfabricated device that charges sampled airborne particles with a corona ionizer and then incrementally size-separates, collects, and counts the number of particles in the aerosol.

The focus of this thesis was the development and characterization of the smallest device known that can perform these sizing and counting functions. The device miniaturizes a classical instrument from the aerosol field, the double-condenser of Whipple (1960) used for the sizing and counting of atmospheric ions, into a microfabricated device designed to utilize voltage-and-flowrate-variable electrophoresis to measure ultrafine particle aerosols.

Performance characterization of the microfabricated device required development of an apparatus for the generation and conditioning of aerosols appropriate to this application. This Standard Aerosol apparatus was demonstrated to produce repeatable, temperature and humidity stable, charge-neutral, monodisperse exhaust-analog aerosols of particles 10 to 100 nanometer in diameter.

The microfabricated device was characterized with the Standard Aerosol apparatus for the operating conditions of 0.1 to 1.5 liter per minute flow rate and 0 to 3000 volt separator voltage. Results of the characterization demonstrated effective selection and collection of solvent droplets in the diameter range 10-100nm. The selection and collection results for engine-exhaust analog particles were inconclusive, likely due to particle re-entrainment. Repeatable measurements of particle number proved elusive, likely due to electrical field interference, the limited particle concentration obtainable from the Standard Aerosol apparatus, and signal-to-noise and temporal stability issues with the electrometer electronics. Recommendations are made for approaches likely to overcome these issues.

TABLE OF CONTENTS

	Page
LIST OF TABLES.....	vi
LIST OF FIGURES	viii
1.0 INTRODUCTION	1
1.1 Motivation.....	1
1.2 Research applications	5
1.2.1 On-board measurements	5
1.2.2 Road-proximate evolution and dispersion	6
1.2.3 Lab dynamometer	7
1.3 Regulation applications	7
1.3.1 Vehicle inspection and air quality monitoring.....	7
1.3.2 On-board diagnostics and control.....	8
1.4 Literature review.....	8
1.4.1 Instruments that count and size airborne ultrafine particles	8
1.4.1.1 Current instruments	8
1.4.1.2 Historical instruments	11
1.4.1.3 Portable instruments	13
1.5 New instrument needs.....	15
2.0 RESEARCH OBJECTIVES	16
2.1 Research Objective 1: Design and develop a micro-fabricated ultrafine particle sorting and counting device capable of forming the core of a new instrument for	

quantifying vehicle exhaust number distributions of particles in the diameter range 10-100nm.....	16
2.2 Research Objective 2: Characterize the particle sizing and counting capabilities of the device in Objective 1 using laboratory-generated particles with properties similar to vehicle exhaust particulate.	16
3.0 PRELIMINARY WORK.....	18
3.1 Acquisition and evaluation of the instrument prototype – the MicroAPA.....	18
3.2 NanoAPAv.1.....	20
3.3 Options for instrument re-design.....	24
3.3.1 Charger + single condenser (Israel 1970).....	25
3.3.2 Charger + two condensers in series (Whipple 1960).....	26
3.3.3 Charger + two condensers in series; sweep V and/or Q(Ungethüm 1974; Dhanorkar and Kamra 1991; Dhanorkar and Kamra 1993)	29
3.3.4 Charger + series/parallel condensers (Israel 1970).....	29
4.0 EXPERIMENTAL METHODS.....	31
4.1 Generation of a standard aerosol	32
4.2 Development of the electrostatic precipitator and neutralizer.....	38
4.2.1 Development of the ²¹⁰ Po neutralizer	38
4.2.2 Development of the electrostatic precipitator.....	40
4.3 Spec/design/build NanoAPAv2.....	51
4.4 Proof-of-concept of serial condenser.....	55
4.5 Characterization of the proof-of-concept double condenser	59

4.5.1 Particle collection	59
4.5.2 Particle concentration measurement	60
4.5.3 Electrometer circuit robustness.....	60
4.5.4 Whipple calculation with the best database subset.....	61
5.0 RESULTS & DISCUSSION.....	62
5.1 Standard aerosol capability.....	62
5.1.1 Dilution linearity and control range.....	62
5.1.2 Temperature settings.....	63
5.1.3 Standard aerosols	65
5.1.4 ESP and ²¹⁰ Po neutralizer leak check and high-voltage characterization.....	68
5.1.4 Charged particle removal with ²¹⁰ Po neutralizer and ESP.....	71
5.2 Design and build the NanoAPAv2/POC instrument	74
5.2.1 Leak checking of the microfabricated devices	74
5.2.2 High-voltage characterization of the microfabricated devices	75
5.2.3 Calculation of Reynolds number	76
5.2.4 Channel flow simulation.....	79
5.2.5 Electrometer selection and evaluation	80
5.3 Characterize the micro-fabricated double condenser	86
5.3.1 Particle collection efficiency	88
5.3.2 Correlate current signal to aerosol concentration	92
5.3.3 Characterize performance of the electrical circuitry.....	94
5.3.3.1 Capacitive coupling	94
5.3.3.2 Temporal instability of electrometer.....	96
5.3.4 Whipple calculation with the best database subset.....	101
5.3.5 Whipple calculation with the TI electrometer	108
5.3.6 Leakage current	114
5.3.7 Uncertainty analysis.....	118

6.0 SUMMARY & CONCLUSIONS.....	126
6.1 Summary.....	126
6.2 Conclusions and future work.....	130
6.3 Patent process	134
6.4 Post-thesis extensions for a fully functional portable instrument.....	134
REFERENCES	136
Appendix A. Standard Operating Procedure for Standard Aerosol Generation	141
Appendix B. Standard Operating Procedure for NanoAPAv.2 Instrument	149
Appendix C. Datasets for Double Condenser Proof-of-Concept.....	153
Appendix D. Matlab Programs	163
Appendix E. Reynolds number calculations.....	215
Appendix F. Electrical Schematics.....	216
Appendix G. Labview virtual instrument programs	218
Appendix H. TI DDC-EVM hardware and software operation.....	220

LIST OF TABLES

Table	Page
Table 1. Chemical information.	34
Table 2. Properties of radionuclides for use in ion generation. (Flagan 2001).	39
Table 3. ²¹⁰ Po Neutralizer parts list.	40
Table 4. ESP sizing calculations.	46
Table 5. ESP mechanical parts list.	50
Table 6. Particle concentration vs. diameter for IPA background.	67
Table 7. High voltage performance of the ESPs.	70
Table 8. Boltzmann Distribution (Hinds 1999).	71
Table 9. Calculation of concentration-drift-corrected Neutralizer/ESP performance.	73
Table 10. Uncertainty calculations for electrometer output voltage data.	121
Table 11. Number of samples used in electrometer uncertainty calculations.	122
Table 12. Uncertainty calculations for CPC particle concentration data.	124
Table 13. Number of samples used in CPC uncertainty calculations.	125

Table 14. Database of experimental data. 154

Table 15. Range selection of the DDC112 electrometer. 222

LIST OF FIGURES

Figure	Page
Figure 1. Increased mortality over time due to increase of $10\mu\text{g}/\text{m}^3$ in $\text{PM}_{2.5}$	2
Figure 2. EPA data on the spatial distribution of $\text{PM}_{2.5}$ concentration in the United States.	2
Figure 3. Human lung deposition of airborne particles.	4
Figure 4. Typical diesel engine exhaust size distributions.	4
Figure 5. Operating principles of the SMPS instrument.	11
Figure 6. Operating principles of the EAA instrument.	12
Figure 7. The MicroAPA instrument prototype.	18
Figure 8. The microfabricated ultrafine particle charging and separating device.	20
Figure 9. NanoAPAv.1 instrument, the 2008 upgrade of the original MicroAPA.	21
Figure 10. Operational flow of the NanoAPAv.1 instrument.	21
Figure 11. Comparison of separator effectiveness before and after the electronic redesign.	22
Figure 12. Separator performance characterization of the microfabricated device. ...	23

Figure 13. Method of determining size distribution with a single condenser.	25
Figure 14. The double condenser design of (Whipple 1960).	27
Figure 15. Trajectories through the double condenser of particles with different values of electrical mobility.	28
Figure 16. Series/parallel condenser design for direct measurement of the particle size distribution.	30
Figure 17. Diagram of the Standard Aerosol apparatus.	33
Figure 18. ^{210}Po Neutralizer mechanical schematic.	39
Figure 19. Cross section of the annular ESP design.	42
Figure 20. Electric field strength in the annular space between a wire and a tube.	48
Figure 21. Mechanical schematic of ESP.	50
Figure 22. Utilizing two of the microfabricated devices to implement the double condenser design.	52
Figure 23. Operational flow for the NanoAPAv.2, adapted from the segmented condenser design of Whipple 1960.	52
Figure 24. Three dimensional model of the microfabricated device.	53

Figure 25. Calculation verifying scalability of (Whipple 1960) design to NanoAPA dimensions and operating parameter ranges.	54
Figure 26. Electrical mobility versus particle diameter.	55
Figure 27. Operational flow of NanoAPAv.2 proof-of-concept instrument.	57
Figure 28. Photo of the NanoAPAv.2 proof-of-concept instrument.	57
Figure 29. Schematic of the proof-of-concept instrument.	58
Figure 30. The Standard Aerosol apparatus modified to characterize the proof-of-concept instrument.	58
Figure 31. Standard Aerosol apparatus as built.	62
Figure 32. Evaluation of linearity and control range of MD19 dilution.	63
Figure 33. Effect of ASET temperature on mean aerosol diameter of IPA droplets.	64
Figure 34. Effect of ASET temperature on downstream concentration of 10 nm particles.	65
Figure 35. Particle concentration vs. diameter for IPA background, Emery/IPA, and Oleic/IPA.	66
Figure 36. ²¹⁰ Po Neutralizer.	68
Figure 37. Electrostatic precipitator, high-voltage power supplies, and DC source.	68

Figure 38. Leak checking the neutralizer and ESP#2.	69
Figure 39. Leak checking ESP#2.	70
Figure 40. Fractional removal of Neutralizer/ESP combination vs. that predicted by theory.	72
Figure 41. Leak checking of microfabricated devices.	75
Figure 42. High-voltage characteristic curves for the microfabricated devices.	76
Figure 43. Re number analysis for the macro model.	77
Figure 44. Re number analysis for the pillar model, as-designed channel.	78
Figure 45. Re number analysis for the pillar model, as-built channel.	78
Figure 46. U2Rans-simulated flow through the one-condenser macro model.	80
Figure 47. Response of MicroAPA and Keithley electrometers to the 0-6 pA reference signal from the Parametric Analyzer.	81
Figure 48. Diagnosing lack of MicroAPA electrometer response.	82
Figure 49. Stability of the Keithley 616 electrometer.	83
Figure 50. Evaluation of the response of the TI DDC112 EVM electrometer to reference signals generated by the Parametric Analyzer.	84
Figure 51. Example data collection for the proof-of-concept experiments.	88

Figure 52. Particle pass-through ratio for datasets of IPA aerosol.	90
Figure 53. Particle pass-through ratio for datasets of Oleic Acid aerosol.	91
Figure 54. Keithley electrometer response plotted against the aerosol concentration at the microfabricated device.	92
Figure 55. Linear regressions of subsets of the data.	93
Figure 56. Electrometer current induced by condenser voltage.	95
Figure 57. Long-term temporal stability of the Keithley electrometer.	96
Figure 58. Short-term instability of the Keithley electrometer.	97
Figure 59. Long-term temporal stability of the TI electrometer.	99
Figure 60. Short-term temporal stability of the TI electrometer.	100
Figure 61. Current-to-concentration linear regression of the database subset.	101
Figure 62. The I_{signal} and I_{diff} data in the database for the selected subset of experiments.	102
Figure 63. The concentration drift factor and particle pass-through ratio data in the database for the selected subset of experiments.	103
Figure 64. An enlarged view of the I_{diff} data for the experiment subset.	106

Figure 65. The Whipple characteristic curves calculated for each dataset in the subset.	107
Figure 66. The Whipple size-distributions for the datasets in the subset.	108
Figure 67. Current-to-concentration correlation for experiments employing the TI electrometer.	109
Figure 68. The I_{signal} and I_{diff} data in the database for the TI electrometer experiments.	110
Figure 69. The concentration drift factor and particle pass-through ratio data in the database for the TI electrometer experiments.	111
Figure 70. An enlarged view of the I_{diff} data for the TI experiments.	112
Figure 71. The Whipple characteristic curves calculated for the TI experiments.	113
Figure 72. The Whipple size-distributions for the TI experiments.	114
Figure 73. I_{signal} and I_{diff} data for the TI electrometer experiments with the minimum and maximum estimated values of leakage current.	116
Figure 74. Long-term temporal stability of the Keithley and TI electrometers.	117
Figure 75. NanoAPAv.2 block diagram.	149
Figure 76. I_{signal} and I_{diff} for experiment sets 1 through 3.	155

Figure 77. Concentration drift factor and particle pass-through ratio for experiment sets 1 through 3.	156
Figure 78. I_{signal} and I_{diff} for experiment sets 4 through 8.	157
Figure 79. Concentration drift factor and particle pass-through ratio for experiment sets 4 through 8.	158
Figure 80. I_{signal} and I_{diff} for experiment sets 9 through 13.	159
Figure 81. Concentration drift factor and particle pass-through ratio for experiment sets 9 through 13.	160
Figure 82. I_{signal} and I_{diff} for experiment set 14.	161
Figure 83. Concentration drift factor and particle pass-through ratio for experiment set 14.	162
Figure 84. Spreadsheet for the calculation of Reynolds number.	215
Figure 85. Electrical schematic of MicroAPA prototype.	216
Figure 86. Electrical schematic of NanoAPA v1 instrument.	217
Figure 87. NanoAPA_2.vi Front Panel.	218
Figure 88. NanoAPA_2.vi Block Diagram.	218
Figure 89. NanoAPA_3.vi Front Panel.	219

Figure 90. NanoAPA_3.vi Block Diagram.	219
Figure 91. TI EVM Front Panel.	220
Figure 92. Integration/conversion timing of a dual DDC112 A/D converter.	221

1.0 INTRODUCTION

1.1 Motivation

Small diameter particulate matter ($<1 \mu\text{m}$) suspended in the air has serious deleterious effect on human health. (HEI 2007; Grahame and Schlesinger 2009; Pope, Majid et al. 2009) In May 2010 a panel of the American Heart Association, after reviewing recent epidemiological, molecular, and toxicological studies, issued a statement declaring that “Particulate matter appears to directly increase risk by triggering events in susceptible individuals within hours to days of an increased level of exposure, even among those who otherwise may have been healthy for years.”; “Growing evidence also shows that longer-term $\text{PM}_{2.5}$ [<2.5 micrometer-diameter particle] exposures ... contributes to cardiovascular morbidity and mortality.”; and “[There is] no ‘safe’ level of $\text{PM}_{2.5}$ exposure.”; the results of numerous studies showing an increase of mortality over time for low levels of particle exposure are shown in Figure 1. (AHA 2010) Steady increases of increased mortality are apparent, with the largest magnitude being about 16% increased mortality after 10 years of $10 \text{ ug}/\text{m}^3$ increase in exposure to $\text{PM}_{2.5}$.

The EPA’s latest Integrated Science Assessment for Particulate Matter chronicles numerous studies demonstrating adverse health effects of fine particles, and provides data showing that roughly one hundred million people in the US live in counties with $\text{PM}_{2.5}$ concentrations $12 \text{ ug}/\text{m}^3$ and above; see Figure 2. (EPA 2009)

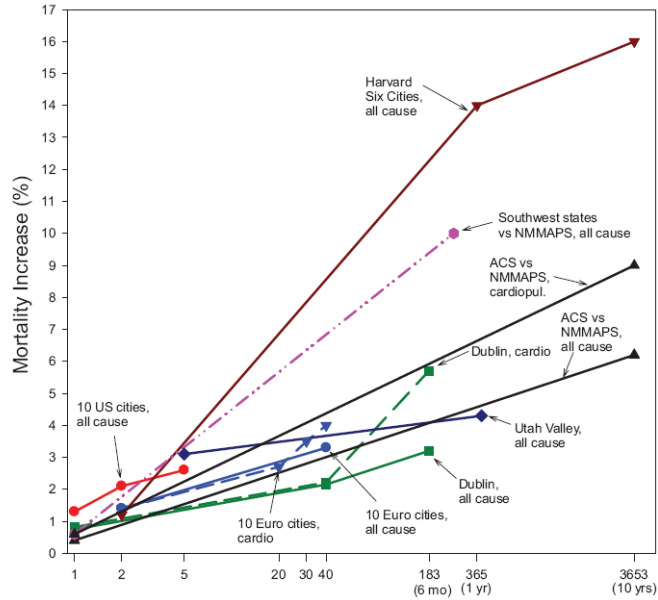


Figure 1. Compilation of cohort-based studies that show increased mortality over time due to increase of $10\mu\text{g}/\text{m}^3$ in $\text{PM}_{2.5}$ (Harvard six-cities: 8000 people, 1974-1991; and others) or $20\mu\text{g}/\text{m}^3$ of PM_{10} . (Brook, Rajagopalan et al. 2010)

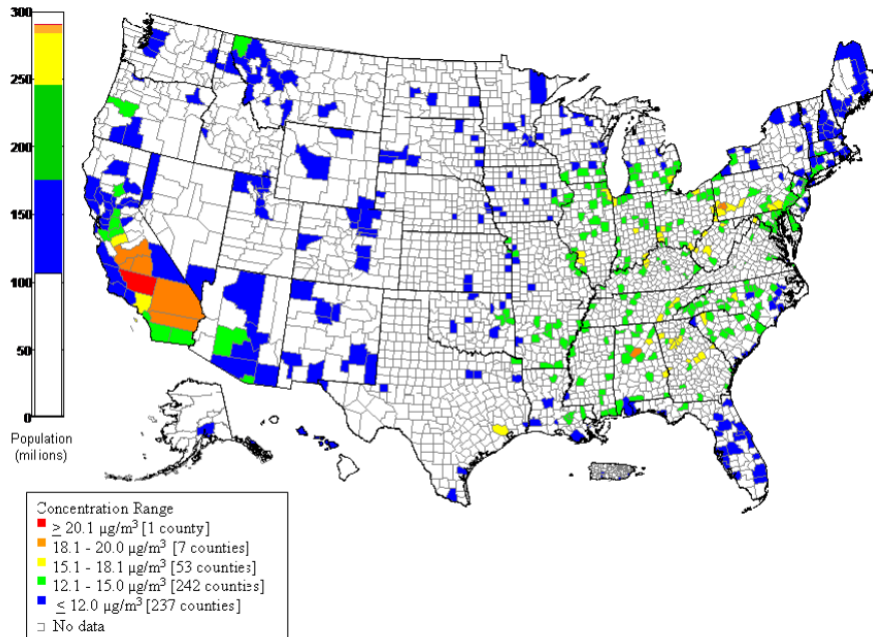


Figure 2. EPA data on the spatial distribution of $\text{PM}_{2.5}$ concentration in the United States. “Three-yr average 24-hour $\text{PM}_{2.5}$ concentration by county 2005-2007. The population bar shows the number of people residing within counties that reported county-wide average concentrations within the specified ranges.” (EPA 2009)

Such particles are produced in significant numbers by mobile sources, primarily on-road vehicles. (Sawyer, Harley et al. 2000; Colvile, Hutchinson et al. 2001; Niemeier 2005) For society to be able to fully quantify the health effects of the transportation sector, measurements of sub-micrometer particle-size concentrations will be needed for many diverse transportation-related situations, in fine spatial and temporal resolution. (McCarthy, Eisinger et al. 2006) Current instruments that can size and count these ultrafine particles at sufficient resolution are expensive, bulky, and non-portable, and so only a smattering of the necessary data has been collected to date.

Particles in ambient air are currently regulated in the United States by measuring the mass of particles below a certain aerodynamic size collected on a filter, at the levels of PM_{2.5} (particles 2.5 micrometer and smaller in aerodynamic diameter) and PM₁₀ (10 micrometer or smaller). (EPA 2009) However, it is the number of particles in the classification of ultrafine particles (diameter less than 100nm) that is most correlated with health effects because these numerous tiny particles travel deeper into the lungs than the larger particles; the smallest may even pass directly into the blood stream; see Figure 3. (Kittelson 2002) The exact mechanisms are not yet fully understood, but various cardiovascular problems have been linked to exposure to the ultrafine particles of vehicle exhaust. The total mass of these small particles in vehicle exhaust is often miniscule when compared to that of the larger particles, and so hardly register on the mass tests; Figure 4 shows the difference in the size distribution of diesel exhaust when weighted by mass and number. As shown and stated in the figure,

90% of the particles are in the nuclei mode (the left most peak) but they account for only 2.8% of the volume (and so mass) of the total. (Kittelson 1998)

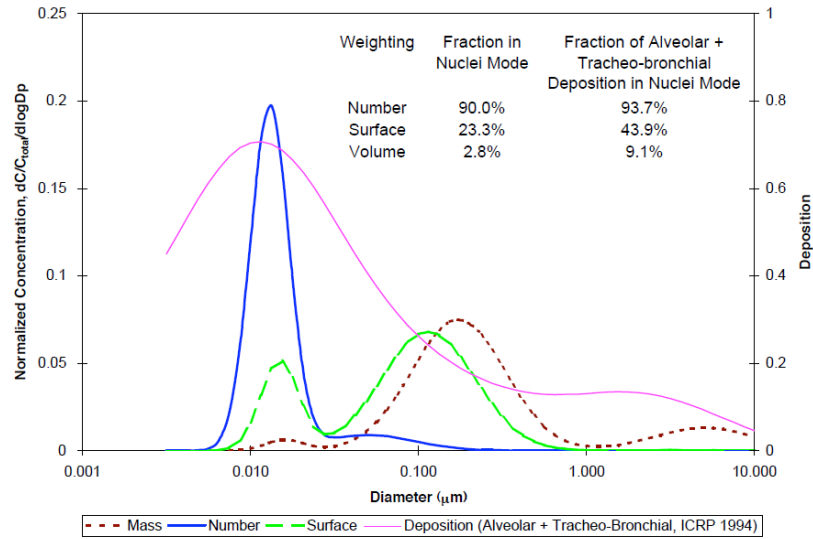


Figure 3. Human lung deposition of airborne particles as a function of particle diameter superimposed over a typical distribution of particles from engine exhaust weighted by mass, surface area, and number. (Kittleson 2002)

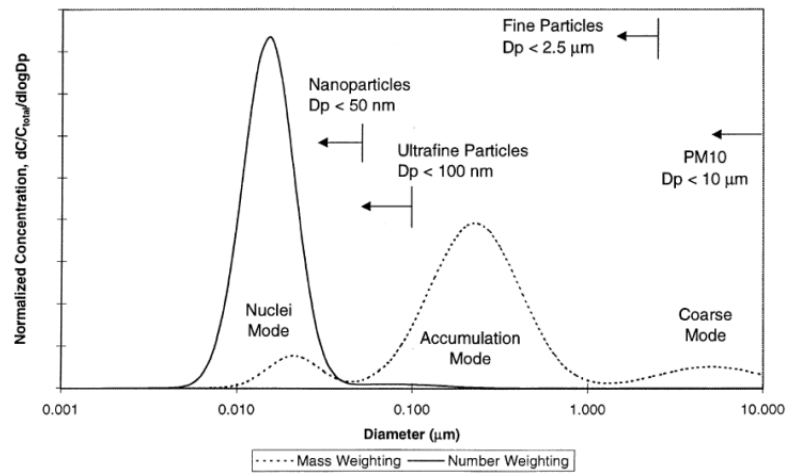


Figure 4. Typical diesel engine exhaust size distribution, weighted by mass and number. (Kittelson 1998).

1.2 Research applications

Research on particulate matter (PM) emission from vehicles is a growing area of research, both driven by and driving regulation that aims to limit its negative effects on human health. The U.S. Federal Highway Administration spearheaded a recent effort to bring together a cross-section of transportation-sector and university partners to determine research priorities; the highest-rated research priorities for PM research that were agreed upon: “monitoring near roadways, evaluating hot-spot models, developing and evaluating PM emissions models, and evaluating control-strategy programs”; all of these priorities would be benefited by development of low-cost, portable PM measuring instruments. In addition, many of the medium priority areas consisted directly of instrument development issues: “improving PM measurements, increasing the spatial extent and temporal resolution of PM measurements, and collecting exhaust emissions from gross emitters”, among others. (McCarthy, Eisinger et al. 2006)

1.2.1 On-board measurements

Mobile emission inventories have traditionally been based on average emission performance of small data sets of new car, small-scale used car, or road side measurements. All of these are only approximations to the continuously varying emissions of real-world vehicles. To accurately predict the inventory of local-specific vehicle fleets, driving behavior, car maintenance, and fuel blends, there has been increasing research interest in quantifying emissions directly on-board vehicles on a

second-by-second basis. (Jackson, Qu et al. 2006) This work has been slowed by the lack of truly portable instruments that can both size and count particles.

1.2.2 Road-proximate evolution and dispersion

The distribution of particle size emitted in vehicle exhaust and its evolution through condensation and coagulation as it disperses from the roadway is an active area of research that is also limited by the availability of portable instruments with adequate size and temporal resolution that are inexpensive enough for wide spread deployment. Many studies wind up relying on modeling for extrapolation from a few measurement points taken with a single, expensive instrument; for an example, see (Zhang, Wexler et al. 2004).

Particle formation through complex chemical reactions of precursor gases from mobile sources, fixed sources, and natural sources is a newly emerging branch of inquiry, described well in (Dusek 2000). The complex and time-dependent aspects of these processes call for much more measurement in the world outside the laboratory, and on fast time scales.

Other common methods of road-proximate particle matter analysis are tunnel measurements and street canyon studies, both of which are limited in their predictive scope due to either aggregated measurements or reliance on a single, expensive, non-portable instrument. (Kirchstetter, Harley et al. 1999; Kumar, Fennell et al. 2008; Kumar, Fennell et al. 2008)

1.2.3 Lab dynamometer

Even the research done in laboratories with vehicles on dynamometers would benefit from the development of fast and inexpensive portable particle instruments, as then the same instruments deployed widely in the field for collecting large data sets could be coupled with identical measurements in the lab to produce solid correlations. A recent study used various commercial instruments for simultaneous measurements of diesel PM on a laboratory-dynamometer setup, and pointed out the challenges of cross-correlating dissimilar instruments. (Kinsey, Mitchell et al. 2006) Another issue driving the need for increased temporal resolution measurements is to support the capability of on-road emissions models such as EPA's MOVES model that can now handle data sampled at one measurement per second. (EPA 2011)

1.3 Regulation applications

The US tradition of regulating particles continues to be based on mass measurements, missing most of the ultrafine particles most dangerous to health. (EPA 2000) The European Union has been more responsive to health studies implicating ultrafine particles, and thus is shifting their regulatory focus to particle number. (Andersson and Clarke 2004; Andersson, Clarke et al. 2004; Andersson 2005)

1.3.1 Vehicle inspection and air quality monitoring

The case for finer spatial and temporal measurements of particle number concentration to enable more beneficial regulation continues to grow: "Direct monitoring ... demonstrates that the levels a person is exposed to vary drastically during the day, and that the ambient, outdoor air quality, regulated by various limit

values do not describe the overall load, even in industrialised [sic] countries.” (Fenger 1999) A 2003 EPA study inspecting gasoline vehicles in Kansas City for particulate emissions clearly spelled out a need for inexpensive instrument development: “[There is] no technique available to quickly and inexpensively screen PM emissions.” (EPA and Baldauf 2003)

1.3.2 On-board diagnostics and control

Heavy-duty diesel vehicle PM on-board diagnostics will be required in the US starting in 2012. (EPA 2008) Industry is responding with systems designed to support this regulation. The RAVEM system, a commercial partial-flow constant volume sampling system weighing 120kg is available to measure emissions, including PM, in heavy duty diesel vehicles, but is limited to bag collection, with PM size/count assessed in an off-line laboratory, which provides information on total particle emissions over the collection time, and no information about the second-by-second size distribution. (Weaver and Petty 2004) There is also a newly published method proposing a corona leakage current monitoring design that may result in an instrument design that would non-invasively size and count on-board diesel particle number (PN). (Rostedt, Marjamäki et al. 2009)

1.4 Literature review

1.4.1 Instruments that count and size airborne ultrafine particles

1.4.1.1 Current instruments

The current standard instrument for measuring the size/number distribution of particles is the TSI, Inc. (Shoreview, MN) Scanning Mobility Particle Sizer (SMPS).

The latest models of this instrument can measure mobility diameters from 0.0025 μm to 1 μm and produce a particle diameter vs. count distribution in approximately two minutes. Alternatively, the instrument can be run in a mode by which a single monodisperse band of particles is selected from an inlet polydisperse stream, and this selected monodisperse flow can be used for any number of uses, including characterizing other particle measuring instruments. The SMPS has been used to characterize the performance of most, if not all, modern portable and semi-portable instruments. The instrument is not ideal for non-laboratory use however, because it is expensive, heavy (approx. 80lb.), consumes a lot of power (approx. 400W at 120VAC), and is slow, taking two minutes to make a single size distribution measurement. There is another commercial instrument with similar capabilities, the MSP Scanning Mobility Particle Spectrometer, but it is not nearly as ubiquitous as TSI's instrument.

It is useful to separate the functions of particle charging, sizing, and counting. In the SMPS the charging is done by passing the aerosol through a ^{85}Kr radioactive chamber to engender a Boltzmann distribution of charges to the particles. Sizing is done by a differential mobility analyzer (DMA), and the counting by a condensation particle counter (CPC); Figure 5 presents a schematic diagram of the SMPS instrument. (Hinds 1999) The DMA was first described in (Knutson and Whitby 1975). The current standard instrument tailored for use with nano-sized particles is the TSI, Inc. NanoDMA. (Chen, Pui et al. 1998) In the DMA design, charged particles pass through an annular space between a high-voltage (HV) rod and a grounded cylinder; only

particles with a certain electrical mobility can exit through a mono-disperse exit at the end of the HV rod.

The CPC-type counting method goes back to beginning of the field – it was first described in 1888 (Walton and Vincent 1998) – but the modern development as a commercial instrument as described in (Agarwal and Sem 1980) has continued its relevance through today with advances in optics and lasers, allowing smaller particles to be measured, down to $0.0025\mu\text{m}$ in the latest instrument from TSI. A CPC works by first passing the particles through the area above a volatile liquid, then the particles in the vapor pass into a cooled condenser in which the liquid condenses on the particles, which then pass by a collimated laser beam whose light is scattered by the enlarged particles, thus counting them one by one. (Sem 2002)

Other lab instrument designs include multi-DMA coupled with multi-electrometers such as the GRIMM Fast Aerosol Particle Emission Spectrometer (FAPES) (GRIMM 2011); DMA/multi-electrometer combos such as the TSI Engine Exhaust Particle Sizer (EEPS) (TSI 2011) and Cambustion's line of Fast Response Differential Mobility Spectrometers (FR-DMS) (Cambustion 2011); and cascade impactors coupled with multi-electrometers such as the Dekati Electrical Low Pressure Impactor (ELPI, ELPI+) (Dekati 2011) . These electrical instruments make very fast measurements of the particle number-size distribution (up to ten measurements per second), but their electronics are very sensitive to vibration, which limits their resolution in the ultrafine particle diameters when used in applications on board vehicles.

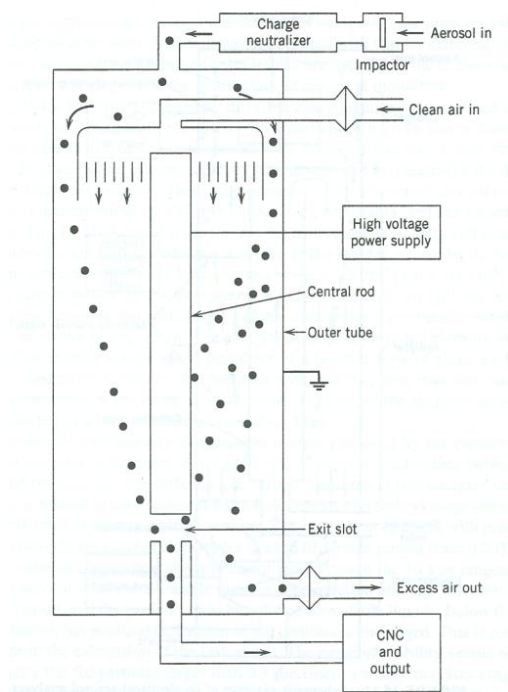


Figure 5. Simplified diagram depicting the operating principles of the SMPS instrument (^{85}Kr charger + DMA + CPC) (Hinds 1999).

1.4.1.2 Historical instruments

The instrument that the SMPS replaced was first described in 1966 as the Whitby Aerosol Analyzer (WAA) (Whitby and Clark 1966), commercialized by TSI as the Electrical Aerosol Analyzer (EAA), and later improved upon in 1975 (Liu and Pui 1975), when the DMA became available to characterize its performance with more monodisperse aerosols. In the EAA, the particles were charged by a corona ionizer, sized by an arrangement similar to the DMA except that it worked like a low-pass filter of electrical mobility, and counting was done by a Faraday cup coupled with an electrometer; a schematic representation of the operation of the EAA is shown in Figure 6. (Hinds 1999) The EAA was capable of measuring particles 10nm to 1 μm in

diameter at a flowrate of 4 liters per minute (Liu and Pui 1975), completing a ten-bin size distribution measurement in approximately two minutes. (Whitby 1976)

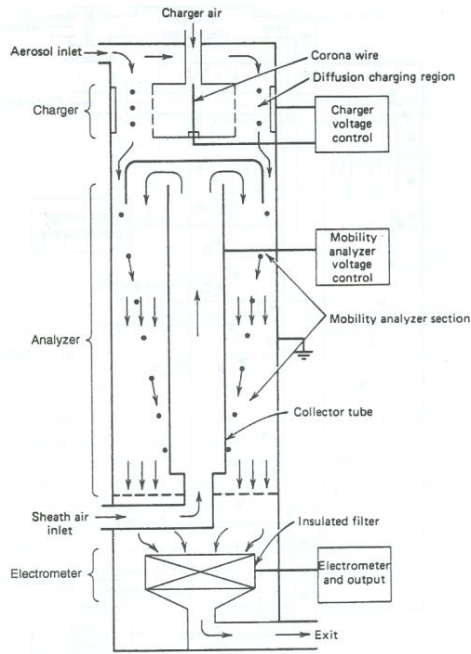


Figure 6. Simplified diagram depicting the operating principles of the EAA instrument (corona charger + low-pass electrical mobility filter + Faraday cup & electrometer circuit) (Hinds 1999).

The ion condenser, also known as the aspirated capacitor, was the first instrument in the field of electrical mobility measurement, developed in the latter part of the 19th century, and was used to measure the ambient ionization of the atmosphere – conductivity and discrete electrical mobilities – and before they were known to be there, particles as well. The historical development of this instrument is well described in the literature. (Israel 1970; Flagan 1998) The important aspect of this instrument was its simplicity: two parallel plates were held at a voltage potential difference, and the current flowing through the circuit, formed by charged particles landing on the plates and passing their carried electrons into the circuit, was counted by amplifying the signal

with an electrometer circuit. Because of its simplicity, development and refinement of this instrument type has continued through the present with modifications of: sheath air (Yeh, Raabe et al. 1973), parallel condensers (Dhanorkar and Kamra 1993), sweeping the condenser voltage (Ungethüm 1974), arranging multiple condensers as series-parallel (Israel 1970), sweeping both the aerosol flowrate as well as the condenser voltage (Whipple 1960), and integration with modern computer control and design for portability (Aplin and Harrison 2000; Aplin and Harrison 2001). This historical instrument served as inspiration for the work of this project, and as such is described in detail in Section 3.3.

1.4.1.3 Portable instruments

All of this background leads up to the question: What portable particle sizing instruments are available or still need to be developed, and how are they designed?

Portable instruments for sizing/counting of particles have mostly been achieved by using small versions of the above designs, taking advantage of the on-going miniaturization of the necessary electronics. The GRIMM Nanocheck is a commercial instrument that uses corona charging, an electrical conductivity measurement, and a Faraday cup electrometer. (Pesch, Grimm et al. 2009) The conductivity measurement is closely related to the traditional condenser design. The Portable Aerosol Spectrometer for Nanoparticles (PAMS) instrument, in development, consists of a unipole charger, a mini-disk DMA, and a portable TSI water-based CPC. (Qi, Chen et al. 2008; Qi, Chen et al. 2008; Li, Chen et al. 2009) Particle Measuring Systems has recently begun offering a commercial instrument of similar design, the Nano-ID, in a portable package

weighing 7 kg; the performance of the instrument is waiting evaluation by researchers in the field. The National Institute for Occupational Safety and Health (NIOSH) is nearing the end of a four-year project to develop a portable instrument for nanoparticle exposure measurement, the Personal Nanoaerosol Sizer (NIOSH 2010). These instruments are approaching portability by way of further miniaturization of the SMPS-type lab equipment. Another portable instrument in development is the Mini Electrical Diffusion Battery (Mini-EDB) consisting of a diffusion battery coupled with multi-electrometers. (Fierz, Weimer et al. 2009) This instrument also harkens back to traditional design, with its simply-baffled diffusion battery, repeating the theme of bringing back early simple designs to achieve portability. Researchers at Clarkson have had some initial success with two portable instruments, the Miniature Electrical-mobility Aerosol Spectrometer (MEAS) for size distributions, and the Tailored Electrode Concentration Sensor (TECS) for linear concentration measurements at a single, hardware-customizable window of particle diameter. (Ranjan and Dhaniyala 2008; Ranjan and Dhaniyala 2009)

More recently, progress has been made in making core devices for potentially very small instruments. These devices are based around microfabricated components for charging/sizing/counting. Some examples from the literature are: MicroAPA-Ionizer and DMA (Chua, Wexler et al. 2008), SMAC Surface Discharge Microplasma Aerosol Charger (AAAR 2009: Fujimora, Kanazawa U., Japan), the Nano-Particle Cross-Flow DMA (NCDMA) (Song and Dhaniyala 2007), an electrically tunable airborne particle classifier using a virtual impactor (Kim, Park et al. 2008), and the

Nano Electrical Mobility Analyzer (nEMA) (Il-Hyun, Yong-Ho et al. 2008). These instruments are taking the paradigm of simple design to its logical extreme, fabricating the simplest of instrument designs with microchip fabrication equipment. The miniaturization of such micro-instruments will be limited only by the micro-fluidic aerosol effects in their tiny flow channels and particle adherence, clogging, and cleaning. (Marshall 2007)

1.5 New instrument needs

Research studies are demonstrating that ultrafine particles produced by mobile sources such as highway vehicles are deleterious to health. There are instruments available to measure the size and count of such particles, but they are mostly expensive and non-portable. A few portable instruments are available, or may soon be, but they are not yet small or cheap enough to make all the measurements that are needed to support the research and regulation needed to secure the public's health. Instruments based around microfabricated devices that are themselves based on simple historical designs are the likely solution to this problem, and research efforts, coupled with government support, are working together toward inexpensive, portable instruments for use in laboratories, by the road-side, and in vehicles themselves.

To summarize the two-fold need for a new instrument: An inexpensive, portable instrument would be used in greater numbers, increasing the spatial extent and depth of relevant emission data, and a fast, real-time instrument would increase the temporal resolution of emission data leading to more accurate modeling and correlation with other parameters. This thesis project is an attempt to fill this two-fold need.

2.0 RESEARCH OBJECTIVES

Research was performed that addressed the following objectives:

2.1 Research Objective 1: Design and develop a micro-fabricated ultrafine particle sorting and counting device capable of forming the core of a new instrument for quantifying vehicle exhaust number distributions of particles in the diameter range 10-100nm.

Completion of this objective would make possible further development of a new portable instrument for use in on-board and road-side sampling. This would likely be the smallest, simplest, and least expensive instrument with these measurement capabilities in the field, allowing for far more measurements to be taken in more applications, and moving closer toward integration in every vehicle with an internal combustion engine.

2.2 Research Objective 2: Characterize the particle sizing and counting capabilities of the device in Objective 1 using laboratory-generated particles with properties similar to vehicle exhaust particulate.

To characterize this new aerosol measurement device, repeatable aerosol with particular specifications would be required, and so as a part of this research, a new apparatus would need to be custom-designed and built. After qualifying this new apparatus as providing useful experimental aerosols, the apparatus would be employed

to characterize the sizing and counting performance of the device developed and built in Research Objective 1. Completion of Objective 2, with proper attention to both the generation of standard aerosols that emulate the particles in engine exhaust and to the systematic characterization of the performance of the new device, would provide valuable input to the eventual development of an efficacious new ultrafine particle sizing and counting instrument.

The Ph.D. research of Dr. Beelee Chua, et al. at UC Davis (Chua, Niemeier et al. 2006) was used as a jumping off point for this research. The next section explains the preliminary work of my thesis project conducted to acquire and evaluate the UC Davis research group's instrument prototype, to identify required areas of further development, and to redesign that instrument in support of the above research objectives.

3.0 PRELIMINARY WORK

3.1 Acquisition and evaluation of the instrument prototype – the MicroAPA

The UC Davis MicroAPA instrument prototype as acquired is described in (Chua, Wexler et al. 2005; Chua, Niemeier et al. 2006; Chua, Wexler et al. 2009), and is shown in Figure 7. The prototype operated by pulling an aerosol sample into the instrument with a 1.5 LPM air pump, charging and separating the aerosol in a microfabricated device, collecting the separated charged particles in a Faraday cup, and amplifying the collected-charge signal with an electrometer circuit. A small flow meter monitored the flowrate of the remaining aerosol before its exit back to the ambient air; and a programmable logic board set the voltage supplied by high-voltage power supplies and returned the electrometer counts to an attached laptop.

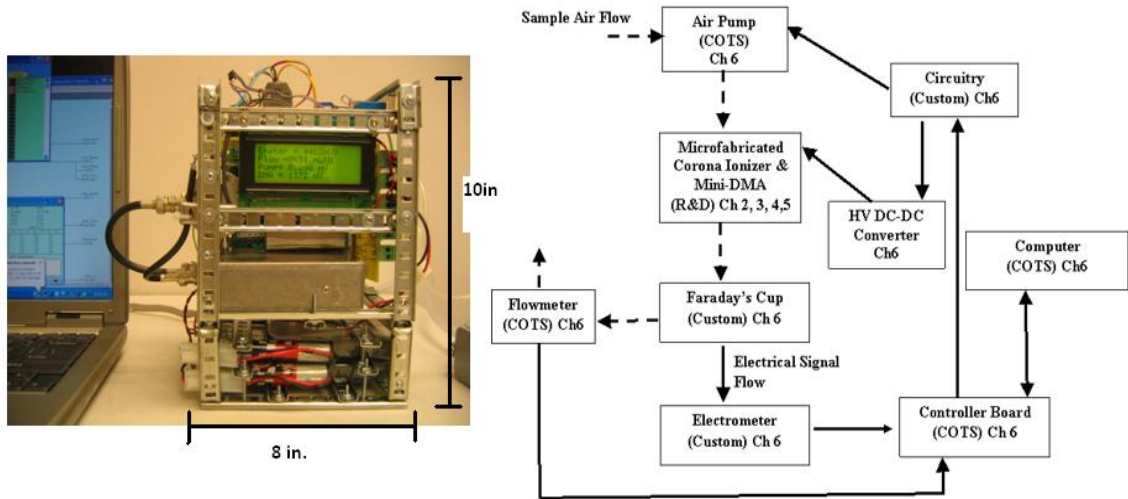


Figure 7. The MicroAPA instrument prototype (Chua et al. 2006).

A preliminary evaluation of the MicroAPA instrument prototype revealed that its components were functional and ultrafine particle signals were detectable, but also that its electrical circuitry was undocumented, some components weren't intended for use past the proof-of-concept phase, the high-voltage power supplies were not stable enough for reliable measurements, and the Faraday cup collection efficiency and operational stability were unknown. In order to fully evaluate the design, the electronic package of the prototype needed to be redesigned and rebuilt.

The prototype's core device, a microfabricated ultrafine particle charging and sorting device is shown in Figure 8. It consists of two parts: a micro-corona ionizer and a separator section, both on a glass substrate. In the charging/sorting device, aerosol first passes through two parallel plates with a pin between them; an electric field between the pin and plates causes a corona to form on the tip of the pin, and electrons from the corona drift to the plates. Particles passing through this charging section pick up electrons, increasing their negative ionization charge. The particles next flow through a section of two long parallel plates where a second electric field generated between the plates captures the charged particles on the plates. As described in the next section, this device was retained in the re-designed instrument, and new electronics were built around it.

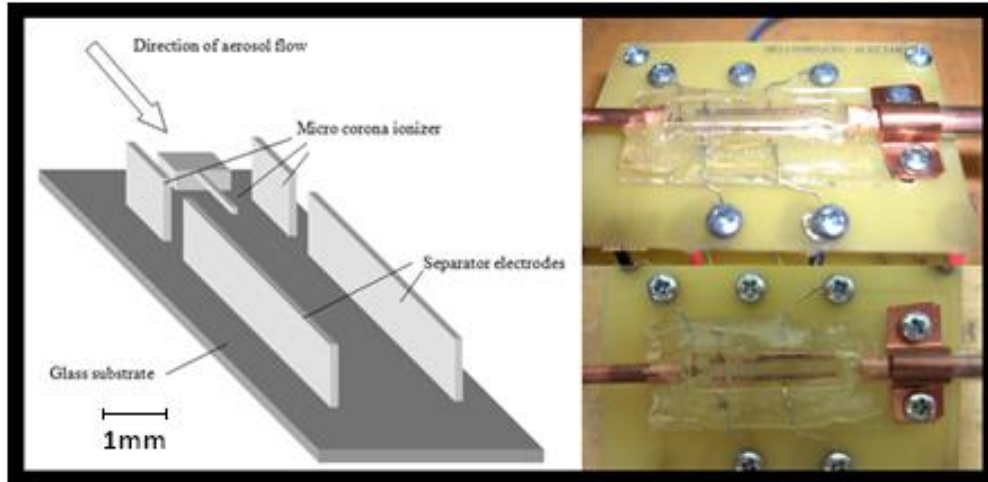


Figure 8. The microfabricated ultrafine particle charging and separating device, as a diagram (left) and in photos of two views of the actual device (right). (Diagram: Chua et al. 2008)

3.2 NanoAPAv.1

The electronic package of the MicroAPA prototype instrument was completely redesigned and rebuilt with the assistance of Kurt Anthony, an electrical technician in the UVM School of Engineering. See Appendix F for the electrical schematics before and after the re-design. The new instrument, named the NanoAPAv.1, featured stable power supplies for both the charging and separating stages; user-selectable voltages for the charger as well as the separator; a high-voltage control circuit stream-lined by use of transistor-based devices; feedback control of pump, charger, and separator; a simplified power system (from three sets of batteries of various voltages to one 12 VDC supply); and the use of circuit boards securely attached to a steel plate for improved robustness of the instrument package. A diagram and photo of the NanoAPAv1 instrument as built is shown in Figure 9, and an operational flowchart of its operation is shown in Figure 10.

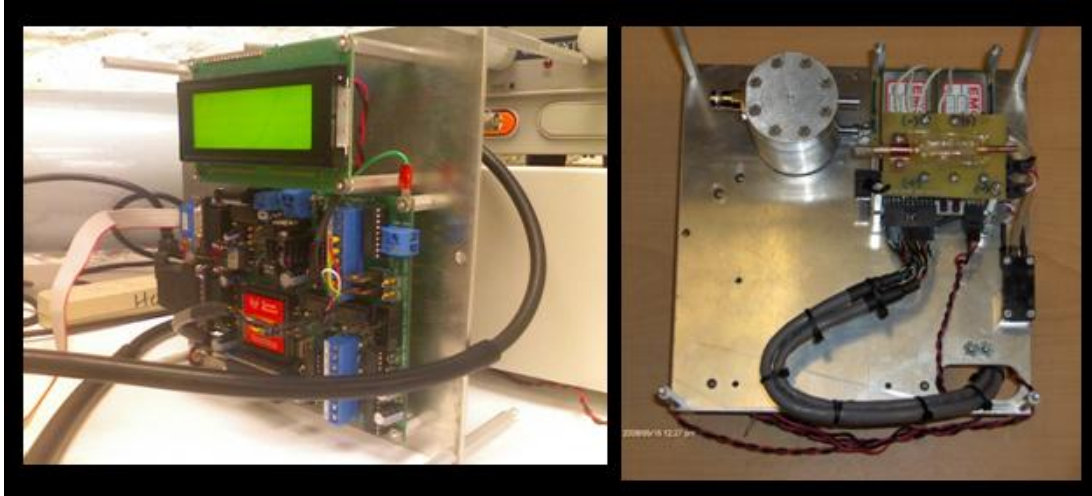


Figure 9. NanoAPAv.1 instrument, the 2008 upgrade of the original MicroAPA.

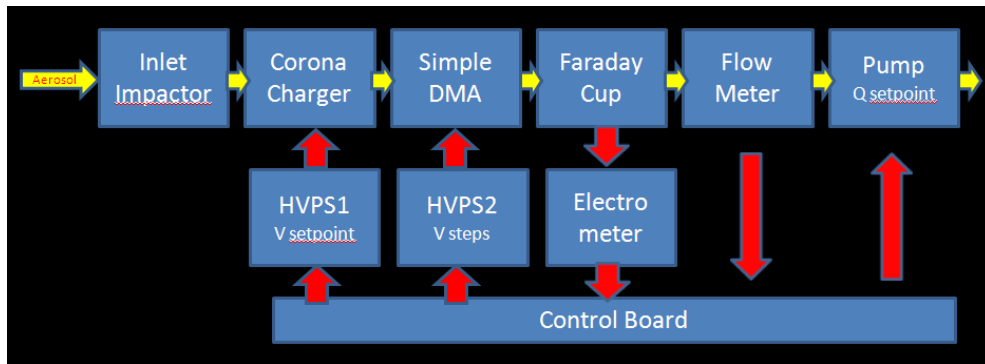


Figure 10. Operational flow of the NanoAPAv.1 instrument.

The upgraded electronics improved the electrical stability, reduced the signal noise, and increased the particle selection of the microfabricated device; see Figure 11. In these tests, a monodisperse aerosol flow of charged 10 nm particles was delivered by the TSI Electrostatic Classifier to the device, and the maximum tolerable voltage to the device was turned on for a set period of time, and then turned off. The output of the device was connected to the TSI CPC, which counted all the particles that were not

collected by the separator. As can be seen in Figure 11, the post-upgrade electronics provided increased particle collection, with less noise.

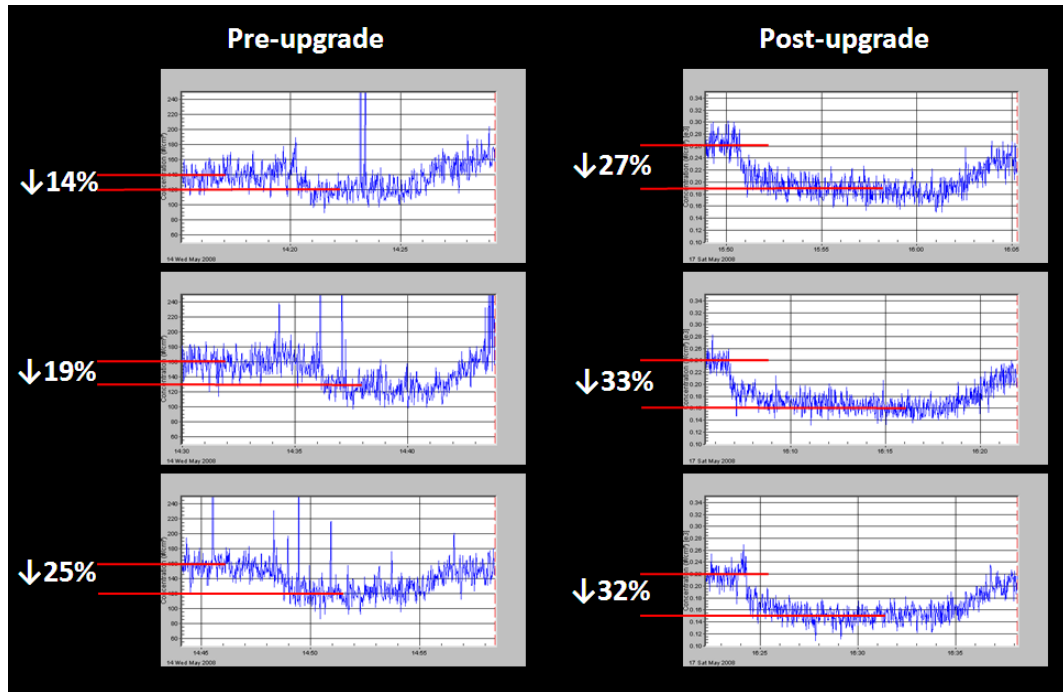


Figure 11. Comparison of separator effectiveness before and after the electronic redesign; 10nm ambient aerosol, charger off; three experiment replications each Note decreases in noise and increase in deflection with the upgraded electronic package. Microfabricated device in-line within SMPS.

Characterization results measuring the particle pass-through ratio of the separator are shown in Figure 12. Particle pass-through ratio (PPR) is the ratio of the particle concentration exiting the separator at a particular voltage setting to the concentration with the separator voltage off, and is an indicator of particle collection performance. This test showed that the device could deflect particles effectively in the desired range, but also that all particles started being collected as soon as voltage was applied. Because of this overlap of the signals for all particle sizes, the design was inadequate to measure size distributions of polydisperse aerosols.

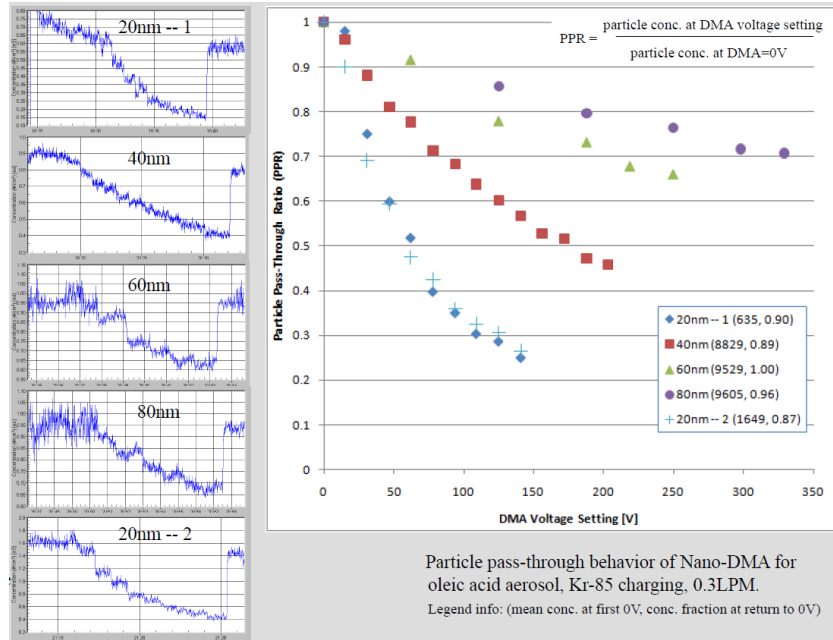


Figure 12. Separator performance characterization of the microfabricated device in-line within SMPS, charging accomplished with ^{85}Kr charger.

The extreme miniaturization of the core functions of the instrument resulted in an overly-simplified design that prevented the MicroAPA from functioning as a DMA-type instrument as originally intended. Existing DMA instruments all incorporate sheath air in the design, which separates the signals of different particle sizes. (Knutson and Whitby 1975) Without the sheath air to separate the response of the different particle diameters in the mobility spectrum, individual particle diameter concentration can only be deduced in a polydisperse measurement by two mathematical differentiations of the PPR data, and so any calculated size distribution would likely be overwhelmed by the systematic errors in the measurement data. (Israel 1970) In addition to this, a review of the methods by which the EAA and DMA instruments were characterized made it clear that another design simplification of the MicroAPA

microfabricated device made in order to miniaturize it would prevent this device from operating as intended. This was the fact that the separator immediately follows the charger without an intervening ion trap. (Knutson and Whitby 1975; Liu and Pui 1975; Whitby 1976) Without an ion trap, the air molecules ionized in the charger continue charging the aerosol through its traversal of the separator, leading to combined field and diffusion charging, which has two effects: it narrows the particle size range that the device can detect, and it reduces the dynamic response of the measurement over the range it could measure. (Hinds 1999) Therefore, it was apparent that the NanoAPAv.1 instrument needed to be modified for it to be able to provide a reliable size distribution of a sampled polydisperse aerosol.

3.3 Options for instrument re-design

A review of the literature for simple instrument designs brought out that the earliest instrument used to measure particle size distributions through electrical means - the ion condenser – behaved like the NanoAPA’s PPR vs. voltage response, with the same limitations noted as were discovered for the NanoAPA design. (Israel 1970; Flagan 1998) However, this condenser design was extended over the hundred years or so since its first use with multiple design modifications that purported to overcome both the sheath air and combined charging issues, some of which also appeared extendable to the NanoAPA’s dimensions and operating conditions. The basic element of the condenser design is that parallel plates are held at a potential difference and the current through that circuit is monitored as the charged particles of the sample aerosol are collected on one of the plates and release their electrons. Reconfiguring the NanoAPA

device for this design (in particular, repurposing the separator portion of the microfabricated device as a condenser) would have the added benefit of removing the need for a separate particle collection step using a Faraday cup; this would further reduce the size and weight of the instrument.

Four options for redesigning the NanoAPA as a condenser-type instrument were examined:

3.3.1 Charger + single condenser (Israel 1970)

This design would use the single, existing microfabricated device plus an electrometer circuit to measure the current induced by the charges collected to the separator plates. This design would still require a mathematical double differentiation of the data – but of the current/voltage (I/V) curve. Operationally, this would be accomplished as two single differentiations for the tangent intercepts to determine the number of particles in a single size bin, see Figure 13.

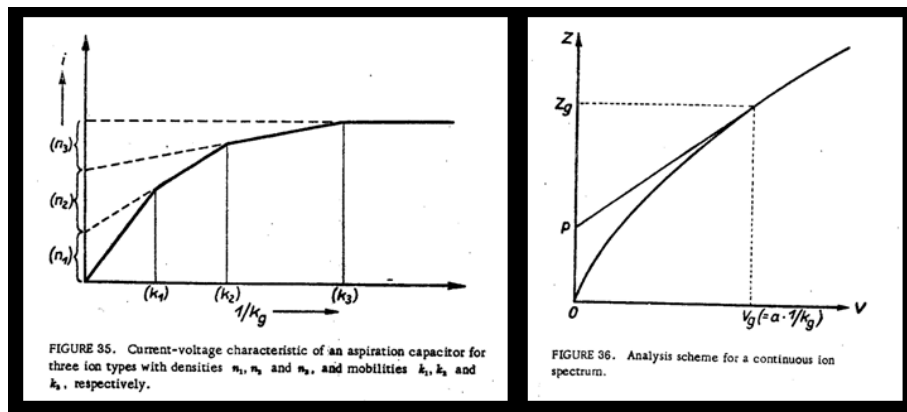


Figure 13. Method of determining size distribution with a single condenser. (Israel 1970)

The issue of combined charging would remain for this simple design that contains no ion trap; in fact this would likely be an even more difficult issue here, as the charged air ions entering the condenser could confound the I/V curve.

3.3.2 Charger + two condensers in series (Whipple 1960)

This design would use the two existing microfabricated devices in series (the one currently in the NanoAPA plus the one spare) plus three electrometer circuits. Both condensers would nominally be held at the same voltage, but they would require separate high voltage power supplies so that the current signals to the respective electrometers would not be confounded; therefore an additional high voltage power supply would be needed. In this arrangement, a single differentiation of the I/V curve of the second condenser would give the number of particles in a given size bin. The first condenser serves two critical functions: it acts like the sheath air in the DMA design, separating the response of the different particle sizes so they are not confounded, and it also serves as an ion trap, reducing the prevalence of combined charging in the second condenser. With this design, the I/V vs. particle electrical mobility (k) characteristic equation is the same for a given set of design parameters, and so various settings of potential (V) and flowrate (Q) can be selected that will maximize the possible range of sampled critical mobilities. See Figure 14.

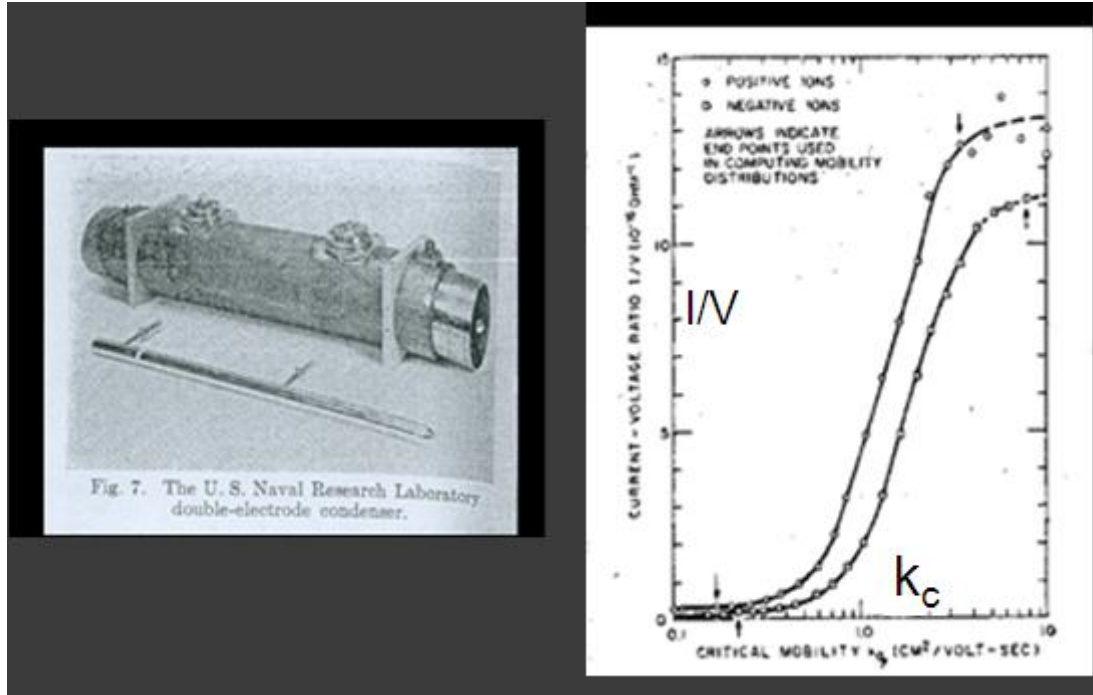


Figure 14. The double condenser design of (Whipple 1960).

The size distribution is determined from the I/V vs. k characteristic as follows (adapted from (Whipple 1960)):

$$\frac{I_3}{V_3} = 4\pi e \left[C_1 k_c \int_{k_d}^{k_c} f(k) dk + (C_1 + C_2) \int_0^{k_d} k f(k) dk - C_1 \int_0^{k_c} k f(k) dk \right] \quad (3-1)$$

Where I_3 and V_3 are the current and voltage for the second condenser; C_1 and C_2 are the capacitances of the two condensers; e is the charge of an electron; k_c and k_d are the critical mobilities of the first condenser and of the first and second condensers combined, respectively; and $f(k)$ is the mobility spectrum (number-size distribution) of the polydisperse sample aerosol.

Electrical mobility, Z , (units: $\text{length}^2 / \text{V s}$) relates the terminal velocity of a charged particle to the strength of the electrical field propelling it: $U_{\text{term,field}} = Z E$.

Critical mobility, k , indicates the smallest electrical mobility (and so largest particle) that will be completely captured by a device at a particular operating condition: $k = Q / 4\pi CV$. In the Whipple design, k_c is the critical mobility of the first condenser, and k_d the critical mobility of both condensers together; see Figure 15.

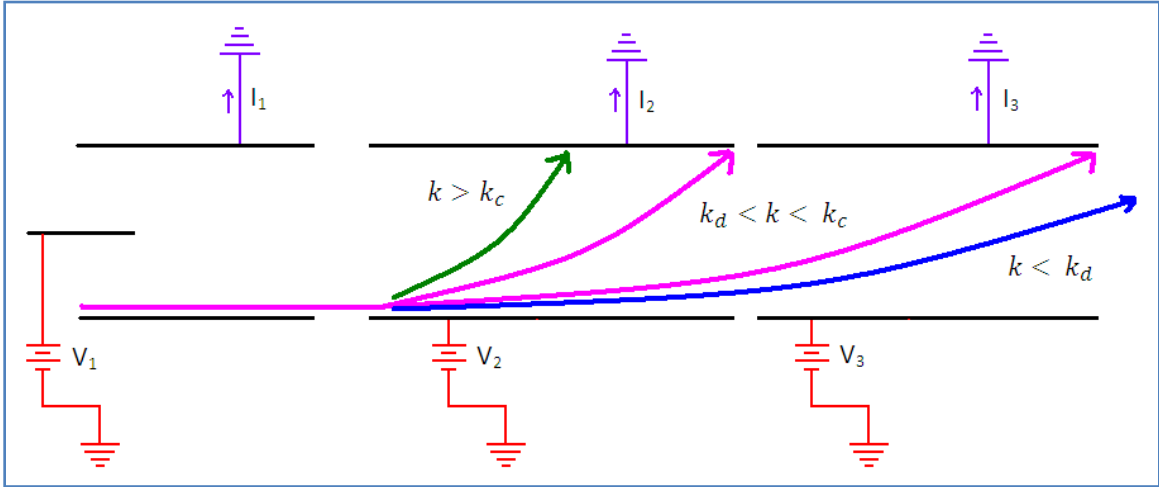


Figure 15. Trajectories through the double condenser of particles with different values of electrical mobility.

Differentiating Equation 3-1 with respect to k_c :

$$\frac{d(\frac{I_3}{V_3})}{d k_c} = \frac{\partial(\frac{I_3}{V_3})}{\partial k_c} + \frac{\partial(\frac{I_3}{V_3})}{\partial k_d} \frac{d k_d}{d k_c} = 4\pi e C_1 \int_{k_d}^{k_c} f(k) dk \quad (3-2)$$

Rearranging Equation 3-2 to get the particle size distribution:

$$Particle\ Conc. (k_d \rightarrow k_c) = \int_{k_d}^{k_c} f(k) dk = \frac{1}{4\pi e C_1} \frac{d(\frac{I_3}{V_3})}{d k_c} \quad (3-3)$$

And so if all measured values of I_3 , for all settings of V_3 and Q , are plotted as I_3/V_3 vs. k_c (see plot, Figure 14), the slope of this curve at each selected value of k_c provides the number of particles in the mobility range k_d to k_c .

3.3.3 Charger + two condensers in series; sweep V and/or Q(Ungethüm 1974; Dhanorkar and Kamra 1991; Dhanorkar and Kamra 1993)

This design would require a more extensive electronic redesign and new components in order to support the linear sweep of voltage and/or flowrate, and to be able to measure a continuously varying I/V response. However, (Flagan 1998) predicts that the condenser design could be extended in this way to give a direct (non-differentiated) measurement of the particle size distribution. The linear sweeping of V and Q is predicted to obviate the need to differentiate the resulting I/V curve.

3.3.4 Charger + series/parallel condensers (Israel 1970)

This design (see Figure 16) would require the fabrication of an additional microfabricated device for an additional separator stage, or the fabrication of a new microfabricated device integrating the function of three of the current devices, as well as additional electronic components and control design. However, the theory behind this design from Benndorf (as translated and related by Israel 1970) attests to a direct (non-differentiated) measurement of the particle size distribution. In essence, the parallel condensers (held at slightly different voltages) do the work of the double differentiation described above.

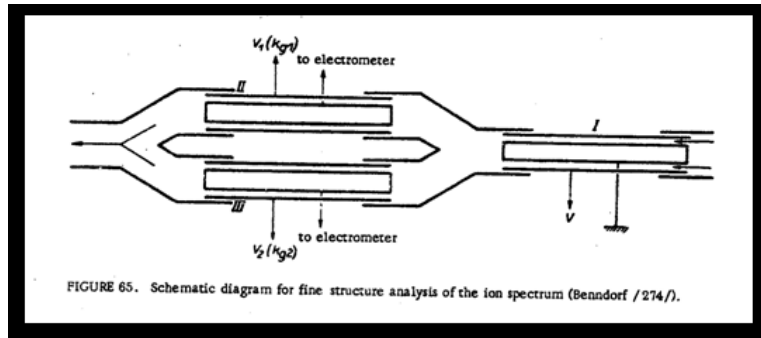


Figure 16. Series/parallel condenser design for direct measurement of the particle size distribution. (Israel 1970)

4.0 EXPERIMENTAL METHODS

The NanoAPAv.2 instrument, based on re-design option #2 described in Section 3.3.2, above, is intended for two applications, the road side and on-board monitoring of vehicle exhaust. As such, it will need to handle a temperature range of approx. -20 to 300C (from the ambient temperatures in the winter of northern climates to tailpipe exhaust temperatures); relative humidity from zero to fully saturated (encountered in both the ambient air and in direct vehicle exhaust); particle compositions both hydrophobic and hydrophilic; particle morphologies both simple and agglomerated (to cover both the nucleation and the accumulation modes of the particle spectrum, the latter especially an issue with diesel exhaust, which forms long-chain agglomerates); a particle diameter range of 10-300nm to cover the high end of the nucleation mode and the low end of the accumulation mode; and a size-bin resolution sufficient to clearly differentiate the two modes.

For this phase of the project, the core measuring device of NanoAPA instrument was characterized over a more restricted range of operating parameters. For particle composition two organic compounds were aerosolized, partially-hydrophobic oleic acid (molecular formula: $\text{CH}_3(\text{CH}_2)_7\text{CH}=\text{CH}(\text{CH}_2)_7\text{COOH}$; IUPAC name: (9Z)-Octadec-9-enoic acid; manufacturer: Sigma-Aldrich, St. Louis, MO; purity: >99% chromatography grade) and hydrophobic emery oil (molecular formula: 75% $[\text{CH}_2-\text{CH}_2-(\text{CH}_2)_7-\text{CH}_3]_3$ 25% $[\text{CH}_2-\text{CH}_2-(\text{CH}_2)_7-\text{CH}_3]_4$; IUPAC name: unknown, trade name: Synfluid® PAO 4 cSt; manufacturer: Chevron Phillips, The Woodlands, TX; purity:

unknown), both from isopropyl alcohol (IPA) (molecular formula: $\text{CH}_3\text{-CHOH-CH}_3$; IUPAC name: isopropyl alcohol; manufacturer: Fisher Chemical, Fairlawn, NJ; purity: >99.9% HPLC grade)) suspensions. The characterized measurement range for this condenser design, mindful of the limiting factors of diffusion and edge-effects, was 10-100 nm. The temperature was maintained at 80°C (in order to ensure evaporation of the aerosolized solution's carrier solvent, IPA); relative humidity was maintained at near zero (through the use of a diffusion dryer); and simple spherical, non-agglomerated morphology was maintained (by keeping aerosol lines short and by not using a mixing chamber). Two NanaoAPA operating parameters were varied across the full permitted range in order to achieve the range of critical mobility to cover the size measurement range: the aerosol flowrate was varied from 0.1 to 1.5 LPM, and the voltage on the condensers was varied from 0 to 3000 Volts. Particle charging was handled externally, by the EC instrument in the standard aerosol apparatus.

4.1 Generation of a standard aerosol

The objective of developing a “standard aerosol” apparatus was the generation and conditioning of a repeatable, temperature and humidity stable, charge-free, monodisperse, 10-100 nm selectable diameter, 0.1-1.5 LPM selectable flowrate, exhaust-analog aerosol with less than ten percent by number of carrier-solvent particles, for use in characterizing new particle analyzing instruments.

A diagram showing the apparatus developed to meet this need is shown in Figure 17. The process flow started with clean, dry, particle-free air from a pressurized cylinder (AirGas UltraZero Air) routed to a Collison-type atomizer, either the small and

simple TSI, Inc. Model 9302 Single Jet Atomizer (SJA, used for earlier experiments) or the more robust, longer-running, and more stable TSI, Inc. Model 3076 Constant Output Atomizer (COA, used in later experiments). Both atomizers work by impinging a jet of air into a solution made up of two parts: a solute that is the desired particle composition and a carrier solvent that dissolves the solute and can be effectively removed by evaporation further in the apparatus. The SJA atomizer was placed in a circulating, constant-temperature bath (B.Braun 350-208 Temperature Bath with Thermomix 1441 Heater/Circulator) to improve the stability of the aerosol it produced; the COA atomizer did not require the bath.

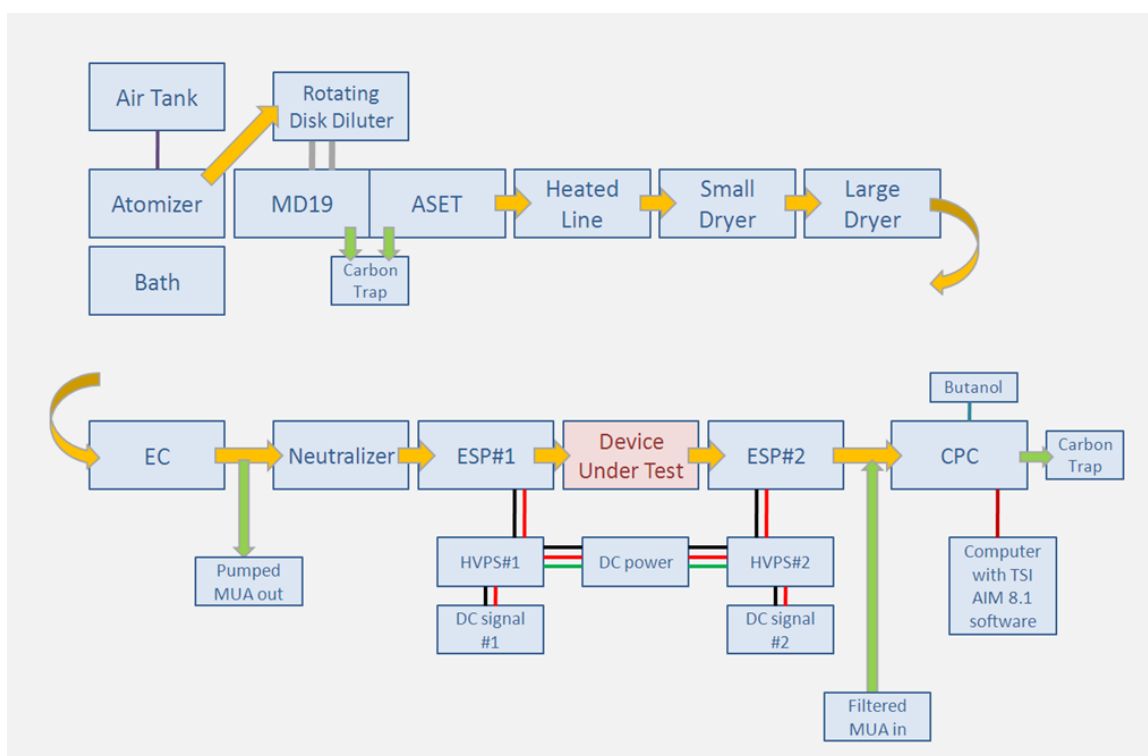
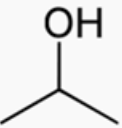

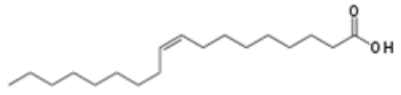
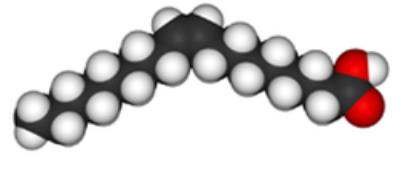


Figure 17. Diagram of the Standard Aerosol apparatus.

The chemicals used for the atomizer solutions are listed in Table 1. Two target-particle solutes were tested: oleic acid and emery oil. Oleic acid is semi-hydrophobic, and emery oil fully hydrophobic, and so when they are atomized and purified of their carrier solvent, both produce engine-exhaust analogue aerosols. Isopropanol was used as the carrier solvent because it fully dissolves both solutes of interest, and can be removed by straight-forward evaporation means later in the apparatus.

Table 1. Chemical information.

isopropyl alcohol	C_3H_8O	$CH_3-CHOH-CH_3$
oleic acid	$C_{18}H_{34}O_2$	$CH_3(CH_2)_7CH=CH(CH_2)_7COOH$
monounsaturated omega-9 fatty acid		
emery oil	$(C_{10}H_{21}) \times 3,4$	75% $[•CH_2-CH_2-(CH_2)_7-CH_3]_3$ 25% $[•CH_2-CH_2-(CH_2)_7-CH_3]_4$
highly branched isoparaffinic polyalphaolefin		

isopropyl alcohol		Oleic acid	
			

Both atomizers produced aerosol at a high concentration ($\sim 10^7$ particles/cm³) with only limited ability for adjustment, and at a higher flowrate than desired (~ 6 LPM for the SJA and ~ 3 LPM for the COA), and so to dilute the aerosol produced by the atomizers and to balance the flowrate with the downstream section of the apparatus, the Matter Engineering MD-19 2E rotating disk diluter (aka MD19) was employed. This

diluter grabs packets of input aerosol in hemispherical divots of a rotating disk (heated to prevent condensation) with selectable rotation speed and so provides adjustment over an order of magnitude in particle concentration.

To enable removal of enough of the carrier solvent in the apparatus, the particle concentration needed to be decreased further, and heated to a temperature sufficient to evaporate the solvent but not evaporate the solute. This was accomplished by a TSI, Inc. Model 379030 Thermal Conditioner Air Supply ASET-15. The additional stage of dilution resulted in concentrations 0.05-0.5% of the input concentration, with the 1.5 LPM flowrate pulled by the CPC at the end of the apparatus. The ASET-15 dilution air temperature setting used to evaporate the solvent but not the solute was set at 400°C (maximum setting). Melting and boiling points for IPA, oleic acid, and emery oil conform to the plan to vaporize all components of the aerosol but capture only the evaporated IPA with 0.2 s residence time in the 400°C ASET evaporation tube and 100°C heated line. (Giechaskiel and Drossinos 2010) The flow balancing resulted in the aerosol being pushed into and pulled from the MD19/ASET instrument. The MD19 and ASET each produce an excess exhaust flow containing aerosol, which was trapped by a carbon trap or vented through a fume hood.

The aerosol exiting the dilution instruments was of much lower concentration of solute particles, but still in a mixture of air and evaporated solvent. To remove the carrier solvent from the aerosol, it was carried by a heated line (AtmoSeal IGH-120-CS-6/X-D48 Heated Line, held at 100°C) to two stages of vapor-phase activated carbon (Chemical Connection Large Air Phase Pellets, 1L-EYMO-5VI7), first a five-channel

small dryer (five 2 cm diameter screen flow paths through a 8cm diameter channel of 15cm length) and then the first half of a single-channel large dryer (4cm diameter screen flow path through 17cm diameter channel of 81cm length). To remove any water that may have been included in the bulk solvent, the second half of the large dryer was filled with silica desiccant beads (Fisher Scientific, grade 48, 4-10 mesh).

The dry, diluted aerosol of solute particles was still polydisperse at the exit of the large dryer (see Figure 17, above), with a log-normal distribution covering a range of particle diameters of approximately 5-200nm. For effective use in characterization, a monodisperse aerosol of selectable diameter was needed, and the TSI, Inc. Model 3080 Electrostatic Classifier (EC) was employed for this purpose. As described above, this instrument engenders a Boltzmann distribution of charges onto the aerosol and then selects particles of a certain small window of electrical mobility from the aerosol and provides the now mono-disperse aerosol at the exit port.

The aerosol exiting the EC is charged (as this is how it is selected) and a repeatable standard aerosol needs to be neutrally charged, so another neutralization stage was required. This neutralization apparatus was designed and built in-house, and was comprised of two components: a Neutralizer and an Electrostatic Precipitator (ESP). These are described in detail in the next section.

The aerosol at exiting the ESP (see ESP#1 in Figure 17, above) was now mono-disperse, dry, of a selected particle diameter and concentration, and ready for use as a standard aerosol for use in characterizing the particle measuring equipment.

The last element of the standard aerosol apparatus was the TSI, Inc. Model 3025A Ultrafine Condensation Particle Counter (CPC), which has a pump that pulled the aerosol through the apparatus from the diluter onwards, at flowrates of 0.3 or 1.5LPM. The device measures the concentration of aerosol using butanol-based condensation growth and optical scattering counting, as described above. The butanol bottle attaches to the unit and is placed on top of it to ensure butanol is available when the instrument calls for replenishment of its reservoir. The exhaust of the unit contains toxic butanol vapor, and so was routed through a carbon trap or to a fume hood.

To select continuous values of flowrate in the range of 0.1-1.5 LPM, two make-up air units (MUA) were included in the apparatus. The EC and CPC operate most efficiently at a flowrate of 1.5 LPM, and so the MUAs were located after the EC and before the CPC, so these instruments could run at optimum flow while the device under test (DUT) could be challenged with lower flowrates. The first MUA consisted of a digital flow meter (TSI Inc. Model 4100) and pump (Gilian Model 5000) to pull air out of the aerosol flow, and the second consisted of a critical orifice and HEPA filter to bring in particle-free make-up air at a known dilution ratio.

All tubing in the apparatus that carried the standard aerosol consisted of either stainless steel or conductive silicon tubing (0.19"ID and 0.31"ID, TSI Inc. 3001788 and 3001789 respectively), grounded through the instruments they connected. Grounded conductive tubing was necessary to minimize the collection of charged particles to tubing walls. (Hinds 1999)

The Standard Operating Procedure (SOP) for the Standard Aerosol Apparatus is included as Appendix A.

4.2 Development of the electrostatic precipitator and neutralizer

Two of the instruments required to complete the Standard Aerosol apparatus were designed and built as part of the project: a neutralizing chamber and an electrostatic precipitator. The development process for each is described below.

4.2.1 Development of the ^{210}Po neutralizer

To add capability for neutralizing the aerosol flow at locations other than in the EC, an additional radioactive neutralizer was needed. As the commercially available options were expensive, and the design straightforward, a commercial design was replicated in stainless steel vacuum parts, with the radioactivity supplied by sealed strips of ^{210}Po , readily available for anti-static applications. The new neutralizer was designed by replicating the design of a commercially available device using A&N ISO Quick-Flange stainless steel vacuum fittings, utilizing the α -radiation from the ^{210}Po in two Static Master Anti-Stat 2U500 strips fixed inside the tube with UniStrut springs. The radiation imparted a Boltzmann charge distribution to the aerosol. Design of the neutralizer was similar to that described in (Tsai, Lin et al. 2005).

How does aerosol charging/ neutralizing with ^{210}Po compare to that using ^{85}Kr (the isotope used in the TSI EC)? Both isotopes generate ion pairs, and so both will impart a Boltzmann charge distribution to the aerosol. The generation rate is similar for both at about 1 ion pair per 35 eV, but the charging mechanisms are different: ^{210}Po generates α radiation (He nuclei) that travel in straight lines, reaching about 4cm away,

and ^{85}Kr generates β radiation (electrons) that travel much further along a wandering path. As can be seen in Table 2, ^{210}Po has about 10x the energy density of ^{85}Kr , but decays much faster (138 days vs. 10.76 years).

Table 2. Properties of radionuclides for use in ion generation. (Flagan 2001)

Source	$\tau_{\frac{1}{2}}$	Radiation Type	Energy (MeV)	R_{air} (cm)	μ (cm^{-1})	k (ion pairs/cm)
^{63}Ni	100 yr	β	0.065		0.449	
^{90}Sr	27.7 yr	β	0.546 (max)		0.044	230
^{90}Y	2.7 d	β	2.18 (max)		0.0089	196
^{85}Kr	10.76 yr	β	0.67 (max)		0.035	220
		γ	0.514 (0.41%)			
^{241}Am	458.6 yr	α	5.49 (85%)	4.0		
			5.44 (13%)	4.0		
^{210}Po	138.4 d	α	5.30 (100%)	3.8		

Therefore the newly designed neutralizer should work like the TSI neutralizer in the EC, but the ^{210}Po strips in the new neutralizer will need to be replaced on a more regular basis, every six months to one year. The mechanical design of the ^{210}Po Neutralizer is shown in Figure 18, and the list of parts is in Table 3.

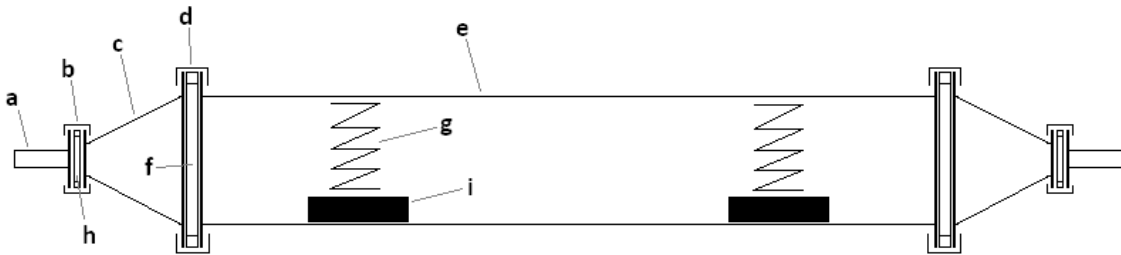


Figure 18. ^{210}Po Neutralizer mechanical schematic (not to scale).

Table 3. ²¹⁰Po Neutralizer parts list.

Callout	Description	Vendor	Part Number
a	adapter to 1/4" Swagelok, stainless steel	IES / A&S	QF16X25-SWG
b	small clamp	IES / A&S	QF16-CT
c	conical reducer, stainless steel	IES / A&S	QF40X16-CR
d	large clamp	IES / A&S	QF40-CT
e	12" flanged tube, 1.5" diameter, stainless steel	IES / A&S	QF40-150-NL
f	large O-ring	IES / A&S	QF40-150-SR-S
g	unistrut spring	shop supplies	
h	small O-ring	IES / A&S	QF16-075-SR-S
i	Static Master Anti-Stat 2U500	VWR	11298-062

4.2.2 Development of the electrostatic precipitator

To fulfill one of the performance objectives of the Standard Aerosol apparatus, all charged particles need to be removed from the aerosol stream before they are introduced to the device under test. Devices to perform this function are called electrostatic precipitators (ESP) and are commercially available for many applications from air purifiers to fly ash collection in coal fired electrical plants. However, even the small devices are quite expensive, and the design is relatively straightforward, and so a device was designed and built with the assistance of the mechanical and electrical technicians of the UVM School of Engineering, Floyd Vilmont and Kurt Anthony, respectively. The ESP was designed and built based on the one used in (Alonso, Martin et al. 2006), in which the aerosol is passed through a grounded cylindrical tube with a rod at its center held at a sufficiently high voltage (produced by an EMCO C50 High Voltage Power Supply, itself powered and controlled by a Mastech HY3010 DC power supply) to collect all charged particles up to a certain flowrate. If the device under test charges the particles as part of its operation, a second ESP/HVPS is needed

to characterize the charging efficiency (Alonso, Martin et al. 2006) and so two ESPs (see ESP#1 and #2 in Figure 17, above) were built to the same specifications.

After the aerosol particles have been re-neutralized, the particles in the aerosol again have a Boltzmann distribution of charges – some particles will be uncharged, and approximately equal fractions will have positive and negative charges. A properly designed ESP in-line after re-neutralization will remove all charged particles.

As a starting point for the design, the device used in (Alonso, Martin et al. 2006) was specified for a similar application to ours, and so the researcher was contacted to ask for advice. Alonso sent a sketch of a cylindrical device that he had built with a diameter of 100 mm, internal diameter of 10 mm, and a wire centered in the cylinder to carry the high-voltage to establish the electrical field. The aerosol inlets and outlets were perpendicular near the ends of the cylinder.

To determine if this design and dimensions were suitable for our application, the characteristic equations governing ESP operation were derived and applied to this configuration.

The electric field in the annular space between concentric cylinders is (Hinds 1999):

$$E = \frac{V_{diff}}{R \ln(d_t/d_w)} \quad (4-1)$$

Where V_{diff} is the electrical potential difference between the tube and wire, R is the radial distance from the concentric axis, d_t is the inner diameter of the tube, and d_w is the outer diameter of the wire; see Figure 19.

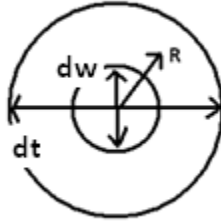


Figure 19. Cross section of the annular ESP design.

According to Eq. 4-1, the electric field varies continuously from wire to cylinder, but if we assume that the field is constant (an assumption that will be verified later) at the value it has at average R distance:

$$R_{ave} = \frac{d_t + d_w}{2} \quad (4-2)$$

Substituting Eq. 4-2 into Eq. 4-1 gives an expression for value of the average electrical field strength:

$$E_{ave} = \frac{4 V_{diff}}{(d_t + d_w) \ln (d_t / d_w)} \quad (4-3)$$

The terminal velocity of a charged particle in an electric field in air is given by (Hinds 1999):

$$U_{term,field} = Z E_{ave} \quad (4-4)$$

where Z is the electrical mobility of the particle.

Substituting Eq. 4-3 into Eq. 4-4:

$$U_{term,field} = \frac{4 Z V_{diff}}{(d_t + d_w) \ln (d_t / d_w)} \quad (4-5)$$

Assuming a fully developed laminar flow regime (which will also be verified later) the maximum velocity of the air passing through the annulus will be twice the average velocity:

$$U_{flow,max} = \frac{2Q}{A} \quad (4-6)$$

Where Q is the volumetric flow rate through the annulus and A is the cross sectional area of the annulus:

$$A = \frac{\pi}{4} (d_t^2 - d_w^2) \quad (4-7)$$

Substituting Eq. 4-7 into Eq. 4-6:

$$U_{flow,max} = \frac{8Q}{\pi (d_t^2 - d_w^2)} \quad (4-8)$$

The minimum residence time for a particle to pass through the length of the tube, l , is:

$$t_{res} = \frac{l}{U_{flow,max}} \quad (4-9)$$

Substituting Eq. 4-8 into Eq. 4-9:

$$t_{res} = \frac{\pi l (d_t^2 - d_w^2)}{8Q} \quad (4-10)$$

The minimum velocity that a particle must have in order to traverse across the full annular distance, required for all charged particles to be collected by the device, with those right at the inside of the tube or at the wire being the worst case (requiring the longest residence time for capture), is given by:

$$U_{term,res} = \frac{d_t - d_w}{2 t_{res}} \quad (4-11)$$

Substituting Eq. 4-10 into Eq. 4-11:

$$U_{term,res} = \frac{4Q}{\pi l (d_t + d_w)} \quad (4-12)$$

The ESP will collect all charged particles if the slowest particles travel at $U_{term,field}$ or faster across the annular dimension and at $U_{term,res}$ or slower along the long dimension of the device, and so the performance equation of the device is found by setting these two velocities equal to each other.

Setting $U_{term,field} = U_{term,res}$ and solving for the tube length, l , required to collect all charged particles in the aerosol gives:

$$l = \frac{Q}{\pi Z V_{diff}} \ln \frac{d_t}{d_w} \quad (4-13)$$

The smallest device possible is desired, and as V_{diff} is in the denominator of Eq. 4-13, the larger the value of V_{diff} , the shorter the device will need to be. However, there is an additional constraint to the design: The electric field strength that V_{diff} engenders must remain less than that which would cause dielectric breakdown of the air in the tube. In dielectric breakdown, air becomes conductive, and so there would be electrical discharge from the wire to the tube, which would cause the re-entrainment of particles formerly held to the tube and wire, as well as damage to the high-voltage power supply connected to the wire. Dielectric breakdown of air occurs at an electrical field strength of approximately 3×10^6 V/m. (Cheng 1992) To provide a margin of safety, the ESP device was designed to operate at a maximum electric field strength of 80% that which would cause breakdown: $E_{max} = 0.8 \times 3 \times 10^6$ V/m = 2.4×10^6 V/m.

Returning to Eq. 4-1, and recognizing that the maximum electric field strength in the annular space will occur at the wire, $R = d_w/2$:

$$E_{max} = \frac{2 V_{diff,max}}{d_w \ln (d_t/d_w)} \quad (4-14)$$

Rearranging Eq. 4-14 for the maximum electrical potential that can applied between the tube and wire:

$$V_{diff,max} = \frac{E_{max} d_w \ln (d_t/d_w)}{2} \quad (4-15)$$

For an ESP device operating at the maximum value of electrical potential, the minimum length would be (substituting Eq. 4-15 into Eq. 4-13):

$$l_{maxE} = \frac{2 Q_{max}}{\pi E_{max} Z_{min} d_w} \quad (4-16)$$

The lowest electrical mobility will be the value of Z for the largest particle needing to be captured, carrying a single charge. For this application, the largest particle used was 100 nm in diameter, and for a singly charged 100 nm diameter particle, Hinds (1999) gives a mobility value of $2.7 \times 10^{-8} \text{ m}^2/\text{Vs}$. The maximum volumetric flowrate, Q, in this application was 1.5 LPM. As a starting point for fixing the design, the inner diameter of the tube, d_t , was held at 10mm, the dimension recommended by Alonso.

Alonso did not give a recommendation for the wire diameter, and so a range of wire diameters from 0.5 to 9mm were considered. Table 4 shows the calculation of minimum tube length for these wire diameters, along with the maximum electrical potential that would be required to generate the requisite electrical field for that wire diameter.

Table 4. ESP sizing calculations.

		L_{maxE} [cm]	Vdiff.max [volt]	A [cm ²]	U_{mean} [cm/s]	D_H [cm]	Re
d_w [mm]	d_w [cm]	Eq. 4-16	Eq. 4-15	Eq. 4-7	Q_{max}/A	d_t-d_w	Eq. 4-17
0.5	0.05	49.1	1797	0.78	32	0.95	201
1	0.1	24.6	2763	0.78	32	0.90	192
2	0.2	12.3	3863	0.75	33	0.80	176
3	0.3	8.2	4334	0.71	35	0.70	162
4	0.4	6.1	4398	0.66	38	0.60	150
5	0.5	4.9	4159	0.59	42	0.50	140
6	0.6	4.1	3678	0.50	50	0.40	132
7	0.7	3.5	2996	0.40	62	0.30	124
8	0.8	3.1	2142	0.28	88	0.20	117
9	0.9	2.7	1138	0.15	168	0.10	111

d_t	10 mm	1 cm
E_{max}	2.40E+06 V/m	2.40E+04 V/cm
Q_{max}	1.5 liter/min	25 cm ³ /s
Z_{min}	2.70E-08 m ² /Vs	2.70E-04 cm ² /Vs
v	1.51E-05 m ² /s	1.51E-01 cm ² /s

The minimum lengths range from 2.7 cm to 49.1 cm; the largest length that seemed reasonable for the instrument was about 25 cm, which limited the acceptable wire diameters to 1 mm and above. Deflection of the 1 and 2 mm wires over their required lengths of 25 and 12 cm would likely be more than advisable to keep the electric field uniform along the tube length, and so this limited the wire diameter to 3 mm and above. The maximum potential required ranged from about 1.1 to 4.4 kV, all of which were easily achievable in a controlled manner with the same type of high-voltage power supplies used in the NanoAPA instrument, and so voltage was not a limiting factor in selection of wire diameter.

One of the assumptions underlying this analysis was that the flow was in the laminar regime. For flow through an annular tube, the flow is considered laminar if the

Reynolds number is below approximately 2300 (Finnemore and Franzini 2002), when the Reynolds number is calculated as:

$$Re = \frac{U_{mean} D_H}{\nu} \quad (4-17)$$

Where U_{mean} is the mean air velocity through the annular space, Q / A ; D_H is the hydraulic diameter, $d_t - d_w$; and ν is the dynamic viscosity of air at 20°C, 15.11×10^{-6} m²/s. (Finnemore and Franzini 2002)

The values of Reynolds number for the wire diameters under consideration were also calculated and are shown in the last column of Table 4, above. All of the values of Reynolds number were under about 200, all comfortably in the laminar regime, and so Reynolds number was also not a limiting factor in selection of wire diameter.

The other assumption underlying this analysis was that the electric field was uniform enough across the annular space to assume it constant. To investigate if this is achievable with this geometry, and if so, to see how the field uniformity could inform selection of wire diameter, the electric field strength (Eq. 4-1) was plotted as a function of radial distance through the annular space, for each of the wire diameters under consideration; see Figure 20.

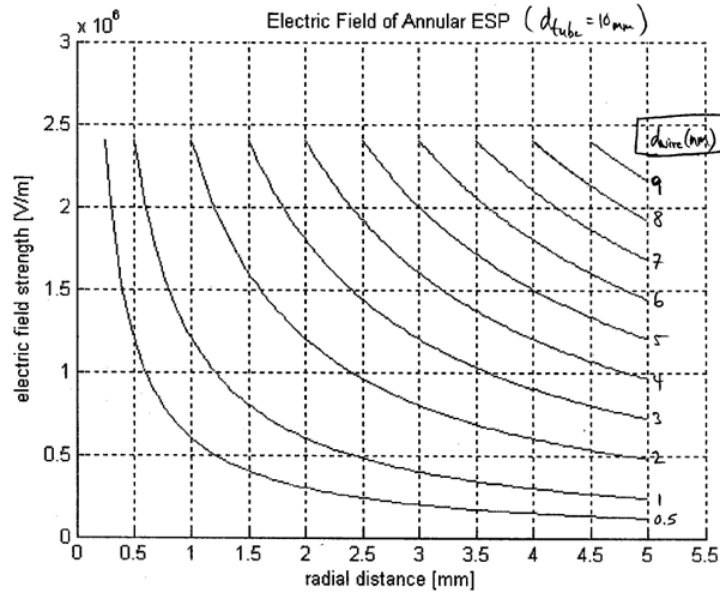


Figure 20. Electric field strength (Eq. 4-1) in the annular space between a wire and a tube; tube inner diameter of 10mm, various wire diameters comprise the family of curves. .

The electric field is very non-uniform with the smallest wire sizes, and becomes more uniform at the largest wire sizes. This result implies that for field uniformity, the largest wire size possible is desired.

Another consideration is that the airflow through the device should have the least disruption, both in terms of acceleration and direction changes. The inlet and outlet connections of the device were planned to be ¼ inch tubing, to match the size of the tubing used to carry the aerosol through most of the standard aerosol apparatus. This tubing has an inner diameter of approximately 6 mm, and so at the maximum flowrate of 1.5 liter/min, the average velocity of the aerosol in the tubing is the volumetric flowrate divided by the cross-section of the inner diameter of the tubing:

$$25[\text{cm}^3/\text{s}] / (\pi (0.6/2)[\text{cm}])^2 \text{ or } 88.4 \text{ cm/s}$$

which is closest to the average flowrate for an annular device with an 8mm “wire”. In terms of direction changes, since the inlet and outlet are perpendicular to the tubing, they point directly toward the inner wire, and so the smaller the wire is, the least direction disruption to the flow will occur, and the more uniformly the flow will spread around the annular space.

Taking all of these factors into account, as well as the readily available tubing sizes and fittings, a wire diameter of 3mm was chosen, with a tube length of 10 cm, about 25% longer than the minimum required of 8.2 cm, to ensure that the moderate amount of electric field non-uniformity in this configuration would not allow any charged particles of interest to pass through.

The mechanical aspect of the ESP design was realized according to the schematic in Figure 21 and parts list in Table 5.

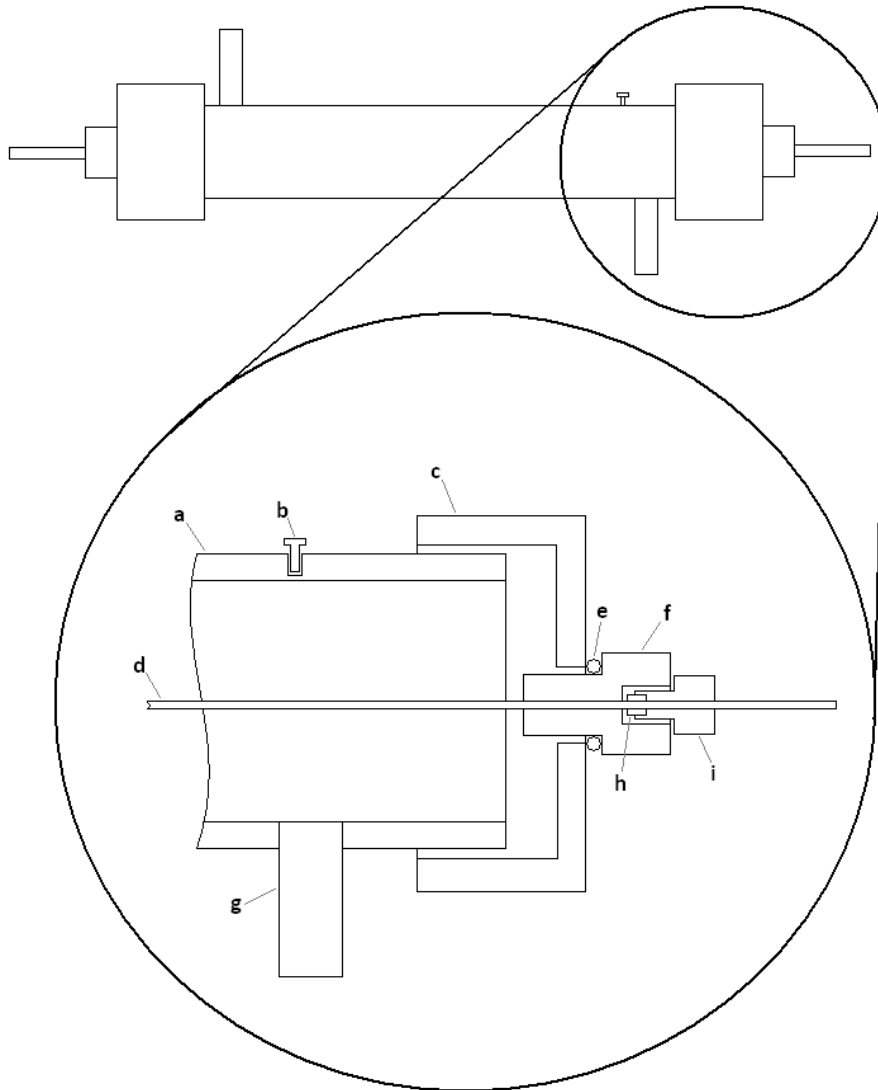


Figure 21. Mechanical schematic of ESP (not to scale).

Table 5. ESP mechanical parts list.

Callout	Description	Vendor	Part Number
a	4" long stainless steel flat-sided tube w/ male NPT ends	Swagelok	SS-6-HLN-4.00
b	grounding screw	shop supplies	
c	stainless steel endcaps, NPT; hole for (f) drilled and threaded	Swagelok	SS-6-CP
d	stainless steel shaft, 3mm diameter	McMaster-Carr	1174K35
e	silicone O-ring	shop supplies	
f	threaded port adapter, 5/16-24 male to 1/4-28 female, KEL-F(PCTFE)	IDEX	P-718
g	barbed nipple for 1/4" tubing; press-fit through hole drilled in (a)	shop supplies	
h	ferrule, flangeless, for 3mm tubing	IDEX	P-343x
i	nut, flangeless, 1/4-28, Delrin (ACETAL)	IDEX	P-301x

Electrically, the design was implemented in a straight-forward manner. An EMCO C50 High Voltage Power Supply, powered (14 V) and controlled (0-5 V) by two Mastech 3010X DC Power Supplies was connected to the ESP; the high voltage lead was connected by an alligator clip to one end of the rod protruding from the device and covered with a plastic shield, and the high-voltage return lead was connected by a terminal lug to the grounding screw attached to the tube. In normal operation the EMCO was set to an input of 5 V, which provided a 5 kV potential to the ESP.

4.3 Spec/design/build NanoAPA v2

For the NanoAPA instrument re-design, the four re-design options described in Section 3.3 were considered. Design option 1 had similar limitations to the MicroAPA design, and so was not a viable alternative. Design options 3 and 4 seemed optimum choices, but they would have required more time and resource for redesign and fabrication of new hardware than was available in the project. Design option 2, featuring two condensers in series (see Figure 22), based on the design of (Whipple 1960), would result in a single-differentiation measurement and would require only minimal changes to the current hardware and control design, and so this design was selected. The operational flow of Version 2 of the NanoAPA is shown in Figure 23. A three dimensional model of the device is shown in Figure 24.

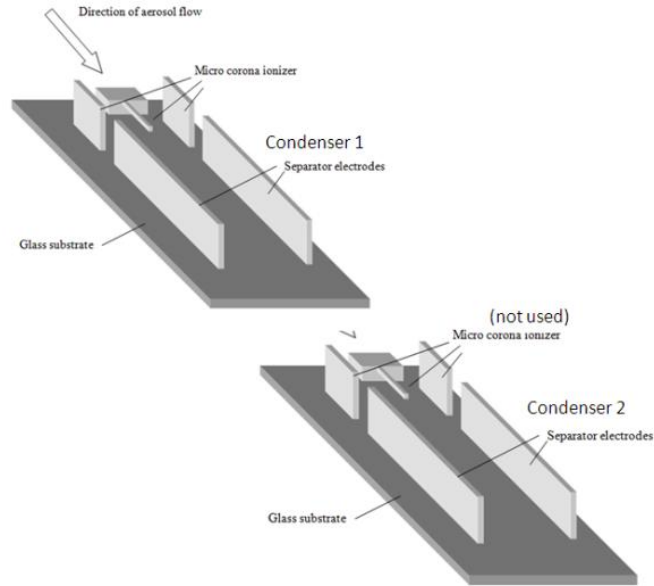


Figure 22. Utilizing two of the microfabricated devices to implement the double condenser design (source: Chua, B., A. S. Wexler, et al. (2009))

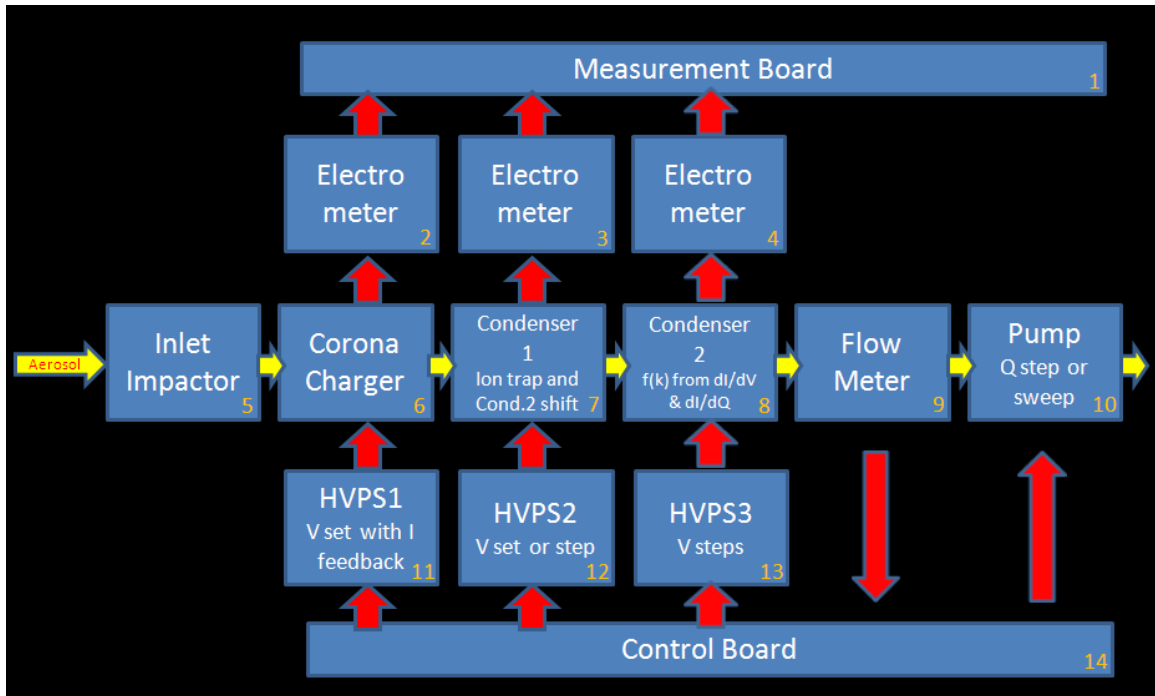


Figure 23. Operational flow for the NanoAPAv2, adapted from the segmented condenser design of Whipple 1960.

A calculation was made using the performance equations given by Whipple using the dimensions and parameter ranges (Q_a , flowrate and V , condenser voltage) of the NanoAPA design to determine if the design was scalable to the NanoAPA's much reduced critical dimensions: $k_c = Q_a / (4\pi CAP_1 V)$, the critical mobility of the first condenser, $k_d = Q_a / (4\pi (CAP_1 + CAP_2) V)$, the critical mobility of the two condensers taken together; the capacitances of the condensers (CAP_1 , CAP_2) were estimated by $A/(4\pi d)$, (A = plate area, d = plate separation). For this design, a size bin is determined by a mobility range k_d to k_c ; the aerosol flowrate and condenser potentials would be varied to achieve the range of necessary critical mobilities.

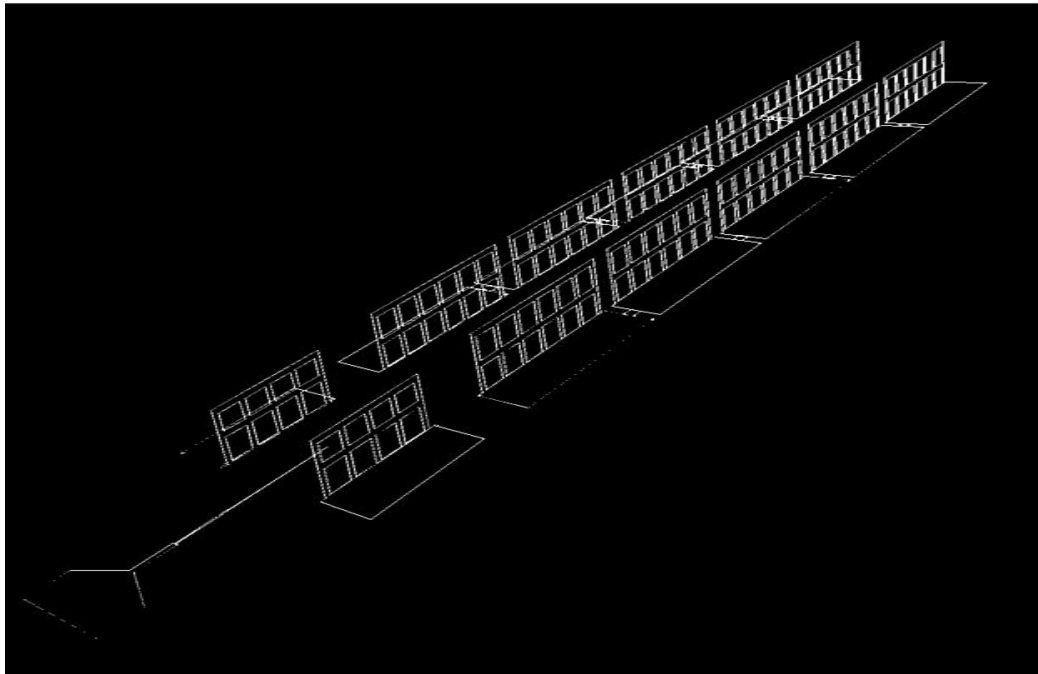


Figure 24. Three dimensional model of the microfabricated device created using Pointwise.

The results of these calculations for four size bins that make use of the full range of voltage and flowrate capability of the NanoAPA instrument package (shown in Figure 25, as compared to Figure 26) predict that the hardware used in the NanoAPAv1 could be converted into a double-condenser design following (Whipple 1960) that would (ideally, before diffusion and edge effects are considered) measure the size distribution of particles from single nanometers in the lowest bin up to about 100nm in the highest bin, a range suitable to this project's applications.

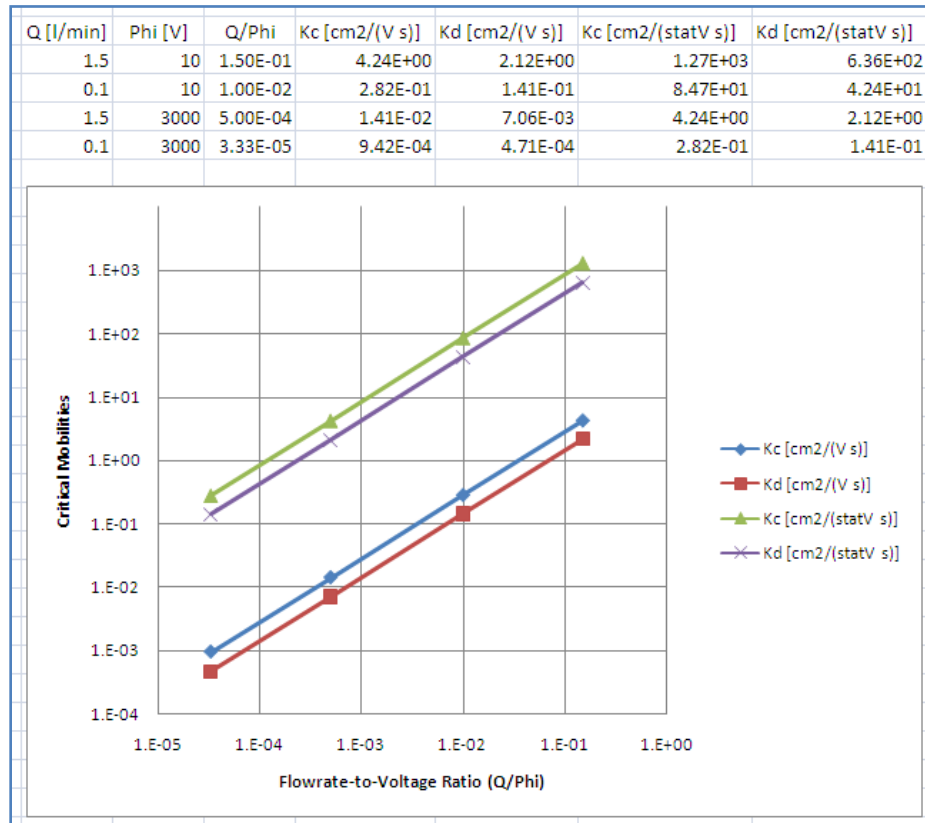


Figure 25. Calculation verifying scalability of (Whipple 1960) design to NanoAPA dimensions and operating parameter ranges. These critical mobility ranges are referenced to the mobility vs. particle size charts in Figure 26 to find the predicted size range that would be measured by the NanoAPA instrument re-purposed to the (Whipple 1960) design.

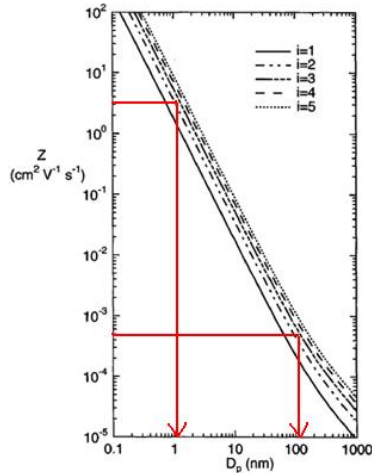


Fig. 18-1. Variation of particle mobility with size.

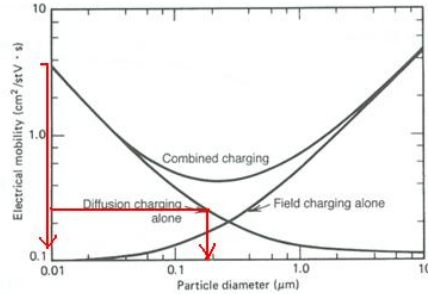


FIGURE 15.4 Electrical mobility versus particle size for diffusion, field, and combined charging at $E = 500 \text{ kV/m}$ [5 kV/cm] and $N_t t = 10^{13} \text{ s/m}^3$ [10^7 s/cm^3].

Figure 26. Electrical mobility versus particle diameter from Flagan 1998 (on left, in volts) and Hinds 1999 (on right, in stat-volts). Red arrows follow the estimated electrical mobility extremes for the microfabricated device (shown in Figure 25) to the particle diameters predicted by these charging models; the Flagan model is in SI units (volts), and the Hinds 1999 model is in a cgs unit system (stat-volts).

Based on the literature that describes these designs, there are a few other issues that may limit the effectiveness of the proposed design: oxidation and particle build-up on the condenser plates causing electrometer drift; edge effects introduced by using parallel plates instead of coaxial cylinders; and the resolution trade-offs necessary to limit the errors generated by mathematical differentiation of data collected at different voltage and flow settings.

4.4 Proof-of-concept of serial condenser

To build the NanoAPAv.2 as designed, another micro-fabricated device identical to the one available from the MicroAPA prototype (DEV#1) was required. An attempt was made to modify the one available spare (DEV#2) to allow its integration, but epoxy infiltrated the device, rendering it unusable. Dr. Chua agreed to

fabricate two new devices, but also experienced issues with epoxy infiltration, and so only one device was immediately forthcoming. This device (DEV#3) had uneven and too-close electrode spacing, and so was not capable of handling the specified range of voltages with simultaneous operation of charger and condenser, and even the condenser operated on its own was able to achieve only 2500 V without experiencing arcing. In addition, the MicroAPA electrometer was found to be non-operational, and there was a wait for the specified replacement electrometer (TI DDC112) to arrive.

To enable the project to go forward, a modified instrument was developed to demonstrate a proof-of-concept of the serial condenser design, the section of the instrument that was the key new idea to be tested. This instrument was comprised of DEV#3 as the first condenser stage and DEV#1 as the second condenser stage; a Keithley616 analog electrometer was used to measure the current collected from particles captured by the second condenser; a single EMCO C50 high-voltage power supply provided the potential to both condensers and was manually controlled by a Mastech HY-3010 power supply; charging was accomplished by the TSI EC (the Standard Aerosol neutralizer and ESP were removed to allow the charged mono-disperse aerosol exiting the DMA to flow directly into the double condenser; the National Instruments Data Acquisition Card (NI DAQ 6009) along with a custom Labview v.7 virtual instrument (VI) program (shown in Appendix G) collected and logged the electrometer output for analysis by the Whipple method. The proof-of-concept instrument is shown in Figures 27 through 30.

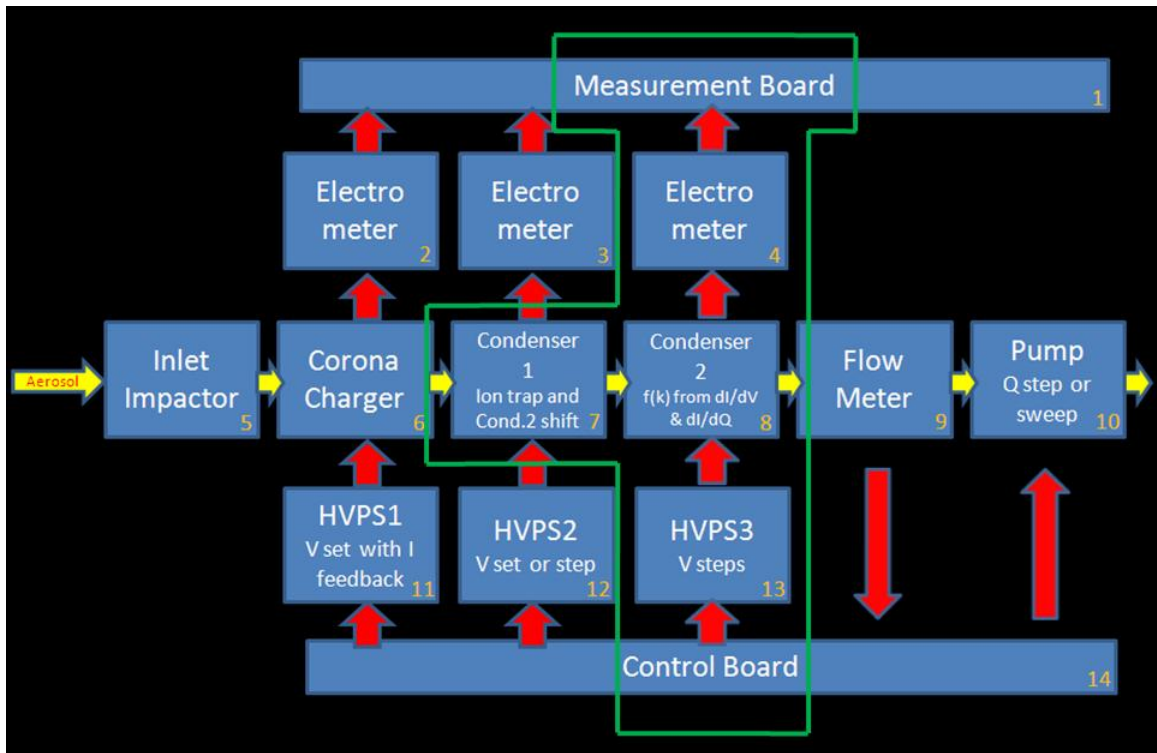


Figure 27. Operational flow of NanoAPAv.2 proof-of-concept instrument (subset in green box).

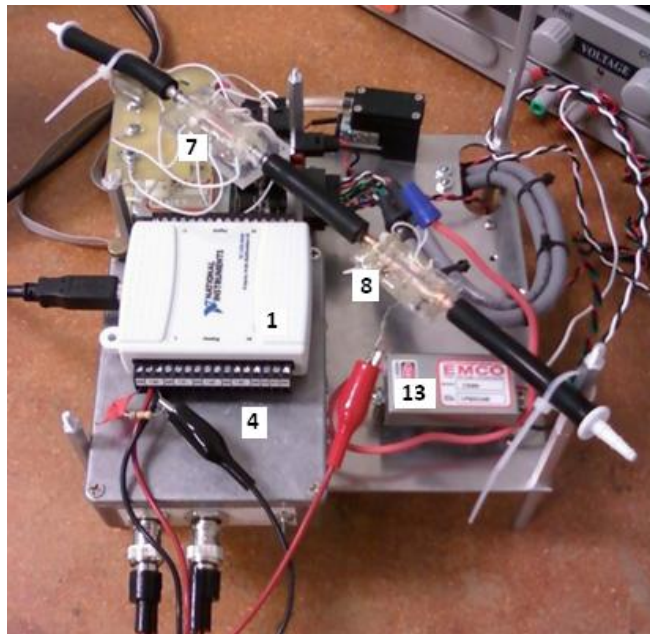


Figure 28. Photo of the NanoAPAv2 proof-of-concept instrument with labels for components matching the numbers of Figure 27, above.

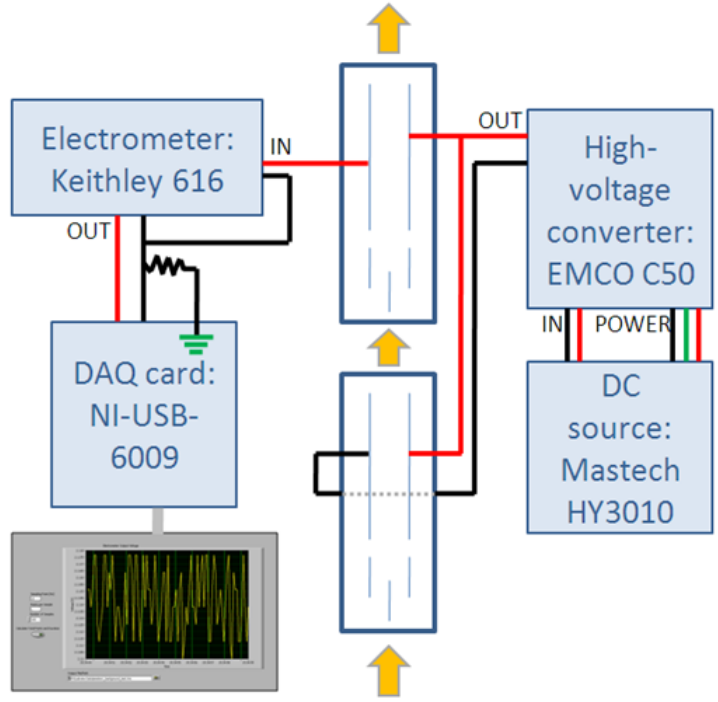


Figure 29. Schematic of the proof-of-concept instrument developed to test re-design option 2 (Whipple 1960) using two microfabricated condensers in series. The microfabricated devices changed between experiments; see Appendix C.

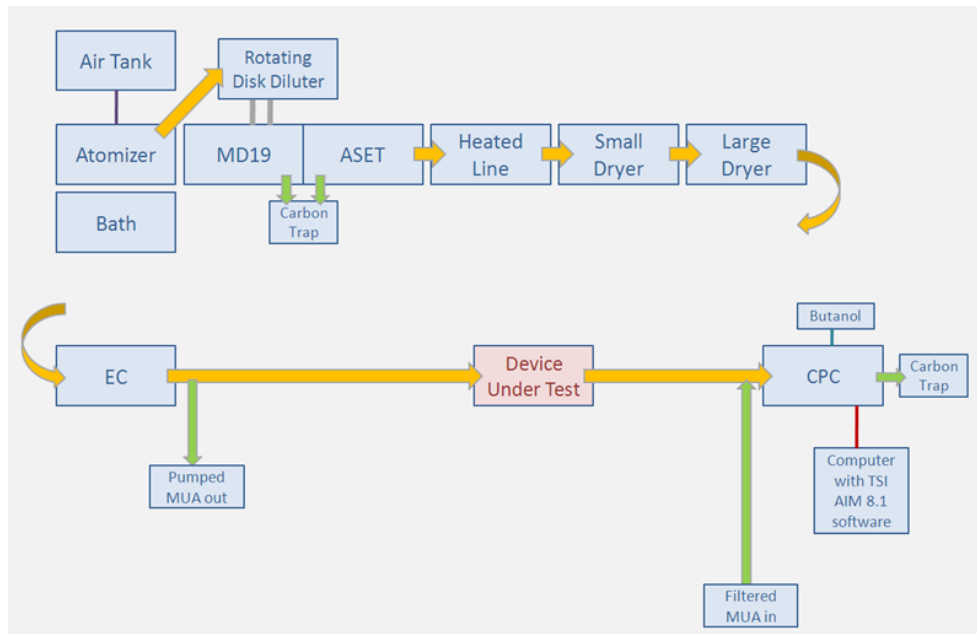


Figure 30. The Standard Aerosol apparatus modified to characterize the proof-of-concept instrument.

4.5 Characterization of the proof-of-concept double condenser

The general method of running the experiments on the proof-of-concept double condenser as the device under test (DUT, see Figure 30, above), was comprised of four steps: 1) Establish a sufficient concentration of a standard aerosol (SA) of a certain composition flowing through the DUT when electrically cold, based on CPC measurement downstream of the DUT; 2) Disconnect the DUT from the SA and determine the background electrometer signals from the DUT for the voltage settings of interest; 3) Reconnect the DUT to the SA, step the DUT through the voltage steps of interest, recording the electrometer signals and CPC concentration signals for each; and 4) repeat step 2, so that the background electrometer signals were recorded both before and after the DUT was challenged with an aerosol.

4.5.1 Particle collection

The first area to be investigated was the particle collection efficiency of the device through the NanoAPA operational ranges of voltage and flowrate. The most basic issue to start with was to check if the single condenser could generate an electrical field, use that field to deflect particles to the electrodes, hold the deflected particles on the electrodes, and then release them when the electric field was removed. Further, there should be more particle collection with increasing electrical field strength, and less with increasing flowrate. Once the operation of the single condenser was verified in this way, the same tests were repeated on the two condensers in series.

These tests were carried out with the standard aerosol apparatus as described above, by establishing the flow of aerosol at a certain flowrate (from 0.1 to 1.5LPM)

and concentration (from about 100 to 10, 000 p/cm³) with the voltage to the electrodes set to zero. The CPC-measured concentration at the initial (voltage zero) settings provided the background concentration information. The voltage to the electrodes was then increased in five to ten steps from the minimum settable value of 200V to just below the voltage that would cause arcing, which varied from 2000-3000V depending on the exact device and wiring configuration. At each voltage step, the difference of the CPC-measured concentration divided by the zero-voltage background concentration provided the particle pass-through ratio (PPR) at those settings. If the devices operated as expected, for each composition type and flowrate setting, the PPR would decrease with increasing voltage until reaching zero, and would return to a value of one, or the same as the background concentration, when the voltage was again turned off.

4.5.2 Particle concentration measurement

The next step was to evaluate the electrometer output response to challenge aerosols over a range of particle concentrations. Correlation of the aerosol concentration that passed through the device with trends in corrected current (electrometer current with aerosol minus the current without aerosol) was evaluated for all datasets collected. At a minimum, the instrument should show an increasing electrometer signal response to increasing particle number concentration.

4.5.3 Electrometer circuit robustness

To characterize the performance of the three electrometers available in the project: the original electrometer that came with the MicroAPA prototype, the Keithley 616 analog electrometer, and the TI DDC-112EVM digital electrometer evaluation

module, two areas were investigated: The relative importance of the electrometer zero-flow background signal on the measurement of particle collection and the relative impact of the electrometer's temporal stability on the ability to make a size-distribution measurement.

4.5.4 Whipple calculation with the best database subset

A subset of the database comprised of datasets with correlated electrometer measurement to concentration signal was indentified, and these datasets were put through the complete Whipple calculation as described in section 3.3.2. The end results of this calculation were number-size particle distributions.

5.0 RESULTS & DISCUSSION

5.1 Standard aerosol capability

5.1.1 Dilution linearity and control range

To characterize the ability of the Standard Aerosol apparatus (see Figure 31) to provide selectable concentrations of aerosol concentration, the MD19 dilution setting was adjusted and the resulting dilution was calculated by the ratio of output concentration at that diluter setting to the concentration without the diluter; see Figure 32. As can be seen in Figure 32, the standard aerosol apparatus was able to provide linear selection of particle concentration dilution over a range from 0.05% to 0.5% of input (atomizer) concentration.

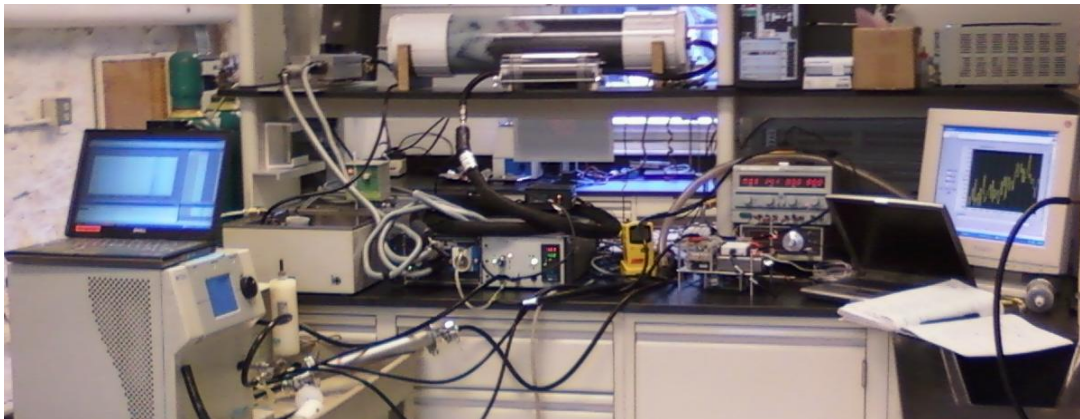


Figure 31. Standard Aerosol apparatus as built.

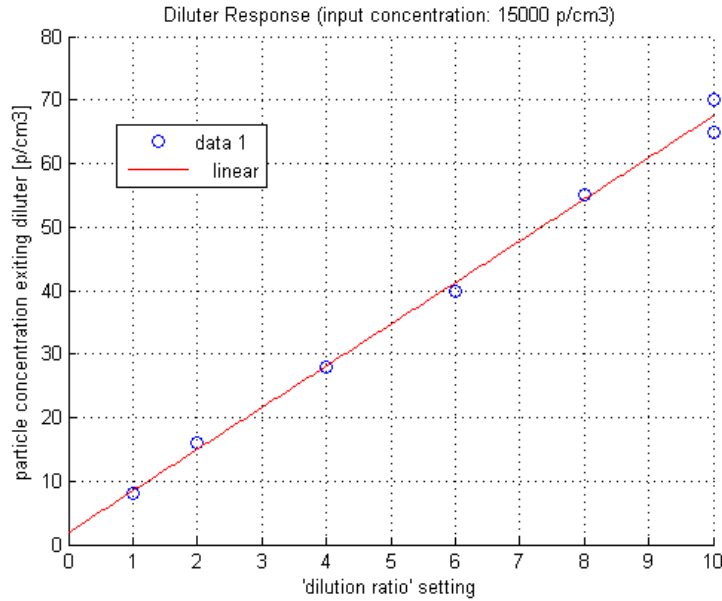


Figure 32. Evaluation of linearity and control range of MD19 dilution.

5.1.2 Temperature settings

A key objective in developing the Standard Aerosol apparatus was a pure aerosol of target particles. The apparatus began with a pressurized jet to aerosolize a solution of the target particle material in a carrier solvent, isopropyl alcohol (IPA). The IPA needed to be evaporated for the output aerosol to resemble engine exhaust, as intended. The first goal was to aerosolize IPA only, and to find the apparatus settings that would completely evaporate this aerosol; these settings would then be used with the target particle solution. Temperatures in the heated line and ASET instrument above the boiling point of IPA successfully evaporated the solvent; see Figure 33.

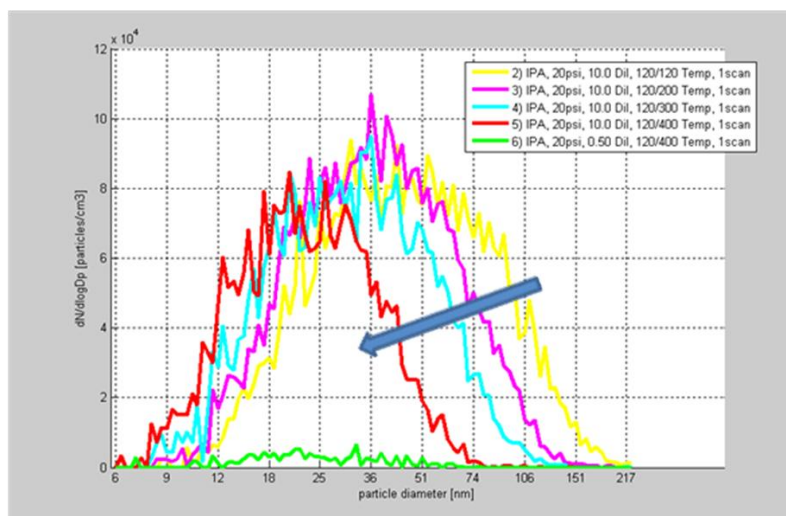


Figure 33. Effect of ASET temperature on mean aerosol diameter of IPA droplets. Temperature set points of the heated line and ASET, respectively, are listed in the legend. The blue arrow shows that for increasing set points of ASET temperature, the mean diameter of IPA aerosol was reduced.

As can be seen in Figure 33, increasing the ASET temperature (follow the arrow from the yellow line (120°C) to the red line (400°C)) decreased the mean diameter of the IPA aerosol, and so it was inferred that the particles were evaporating. However, at the maximum diluted concentration (10.0 Dil) there was still a significant concentration of IPA detected by the CPC. Decreasing the dilution setting to its minimum setting (0.5 Dil) resulted in much more evaporation of the IPA aerosol, but not complete removal of the IPA particles.

Next the target-particle solutions were aerosolized at the best-case settings for IPA. The effect of ASET temperature on target particle concentration was examined for 1% Emery oil in IPA. As shown in Figure 34, 10 nm particle counts decreased as the ASET temperature was lowered, from a maximum of 90p/cm³ at 400°C to a minimum of 0 at 156°C, and back up to about 15p/cm³ at lower temperatures; see

Figure 34. It appeared that at high temperatures the ASET was vaporizing the emery oil particles, which then re-nucleated downstream. This result was advantageous to the generation of the smallest particles desired for this study, and so these temperature settings were confirmed.

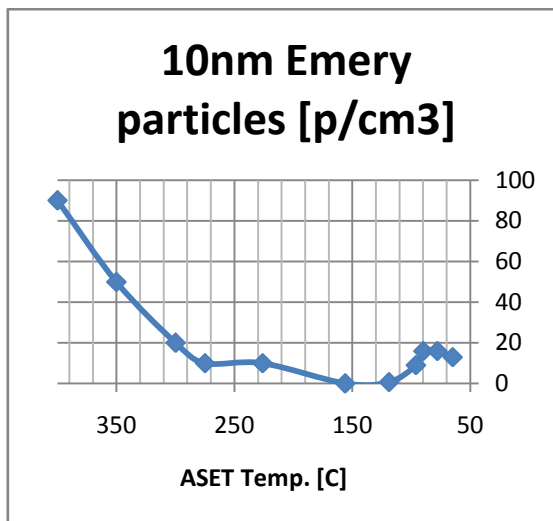


Figure 34. Effect of ASET temperature on downstream concentration of 10nm particles.

5.1.3 Standard aerosols

Examining different settings of operational parameters for the Standard Aerosol apparatus resulted in the apparatus configuration and default operating parameters as detailed in Appendix A. It was determined that no combination of settings and configurations would provide complete evaporation of the carrier solvent without also completely evaporating the target particles as well, but settings and configuration were able to be determined that would provide 10-100 nm target particles with a maximum of 10% carrier solvent remaining; see Figure 35 and Table 6. These settings were used for all subsequent tests with the NanoAPAv.2.

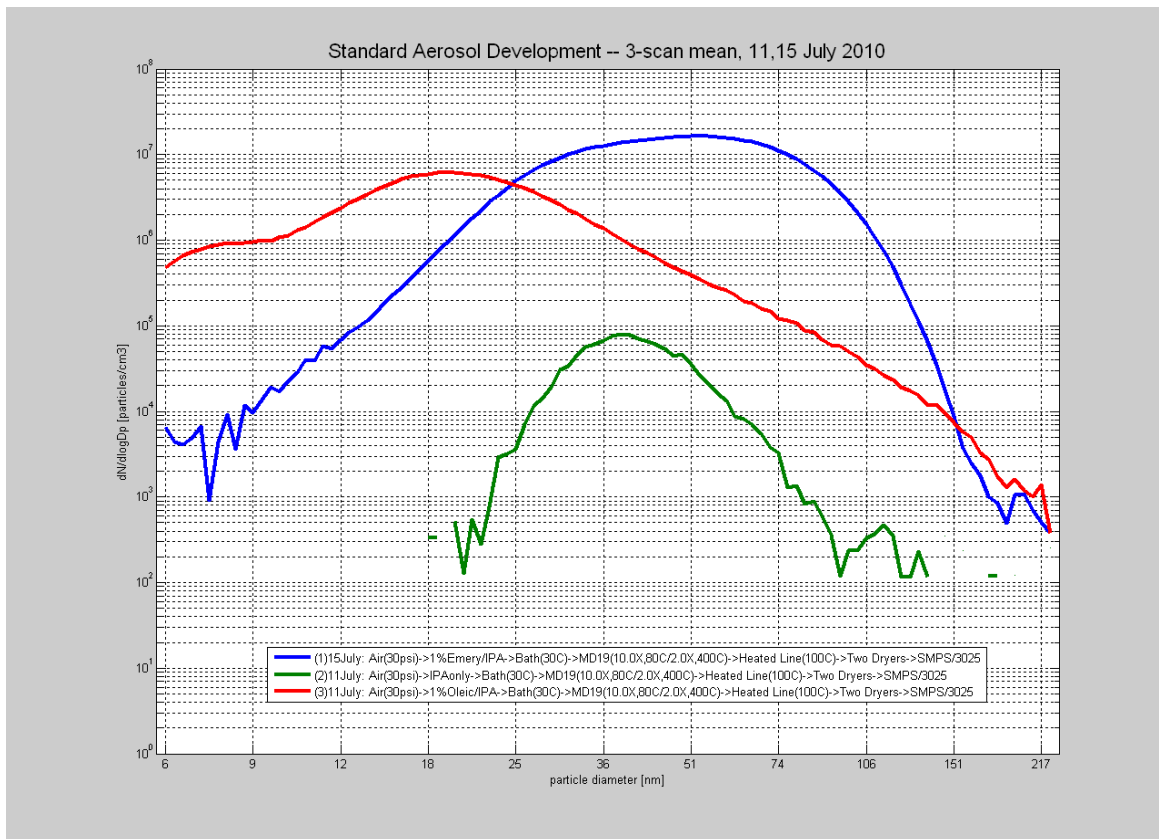


Figure 35. Particle concentration vs. diameter for IPA background, Emery/IPA, Oleic/IPA with EC → CPC, as SMPS (in analog-control scan mode). Standard aerosol generation for Oleic Acid/IPA (red), Emery Oil/IPA (blue), and IPA background (green).

Table 6. Particle concentration vs. diameter for IPA background, Emery/IPA, Oleic/IPA with EC (panel control) to CPC (recording counts at single diameter set by the EC).

Date	Aerosol Conditions					CPC Concentration Data			
	Atomizer Solution	Atomizer Pressure [psi]	EC Dia. [nm]	MD19 Dilution Factor	DMA Sheath Flowrate [LPM]	Mean concentration [p/cm ³]	Std. dev. of conc. [p/cm ³]	Duration of 1/sec data [minutes]	Solvent Background [% of Target Particles]
15-Jul	1%Emery/IPA	30	10	10	15	2	0	1.2	0.6
15-Jul	1%Emery/IPA	30	20	10	15	232	18	1.7	5.4
15-Jul	1%Emery/IPA	30	50	10	15	71482	1580	1.7	0.2
15-Jul	1%Emery/IPA	30	100	10	15	82828	3635	1.7	0.0
15-Jul	1%Emery/IPA	30	10	10	5	1	0	1.3	85.9
15-Jul	1%Emery/IPA	30	20	10	5	537	30	1.7	27.7
11-Jul	1%Oleic/IPA	30	10	10	15	2786	74	4.2	0.0
11-Jul	1%Oleic/IPA	30	20	10	15	9657	478	2.5	0.1
11-Jul	1%Oleic/IPA	30	50	10	15	1302	54	2.0	9.6
11-Jul	1%Oleic/IPA	30	100	10	15	252	15	2.5	1.1
11-Jul	1%Oleic/IPA	30	10	10	5	8944	134	2.7	0.0
11-Jul	1%Oleic/IPA	30	20	10	5	34770	894	1.7	0.4
11-Jul	1%Oleic/IPA	30	50	10	5	4096	130	1.8	9.5
11-Jul	1%Oleic/IPA	30	100	10	5	780	26	2.3	1.2
11-Jul	IPA	30	10	10	15	0	0	1.2	
11-Jul	IPA	30	20	10	15	13	1	1.1	
11-Jul	IPA	30	50	10	15	126	12	2.2	
11-Jul	IPA	30	100	10	15	3	0	1.2	
11-Jul	IPA	30	10	10	5	1	0	0.8	
11-Jul	IPA	30	20	10	5	149	14	1.5	
11-Jul	IPA	30	50	10	5	389	15	0.8	
11-Jul	IPA	30	100	10	5	10	0	0.7	

The oleic acid rows of Table 6 show that oleic acid particles were generated for diameters of 10 to 100 nm with IPA background fractions of less than 0.1, or 10%. The apparatus could provide the smallest particles 10-20 nm in maximum concentrations of only a few thousand particles per cubic centimeters; this was likely due to diffusion loss in the long apparatus, and the low Boltzmann charge distribution fractions at small diameters. (Hinds 1999) It was recognized that operating the EC sheath flow at the standard setting of 15 LPM provided the tightest monodisperse window of about 1 nm at the smallest diameter set points, but distributions of a few nanometer were allowable for the instrument characterization in the project. By lowering the sheath flow rate to 5 LPM, this widening of the particle diameter window was achieved, resulting in the

expected increase in the particle concentration, and as shown in Table 6 in the rows with DMA Sheath Flowrate of 5 LPM.

5.1.4 ESP and ^{210}Po neutralizer leak check and high-voltage characterization

Photos of the ^{210}Po Neutralizer and ESP, as built, are shown in Figures 36 and 37.

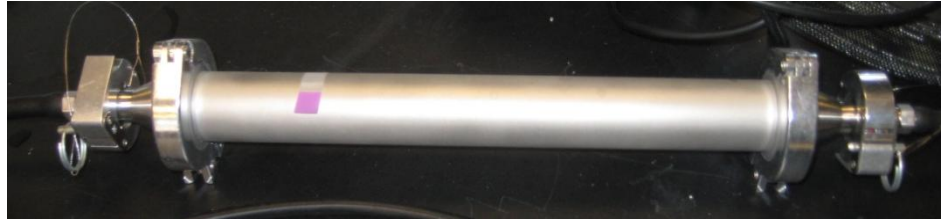


Figure 36. ^{210}Po Neutralizer

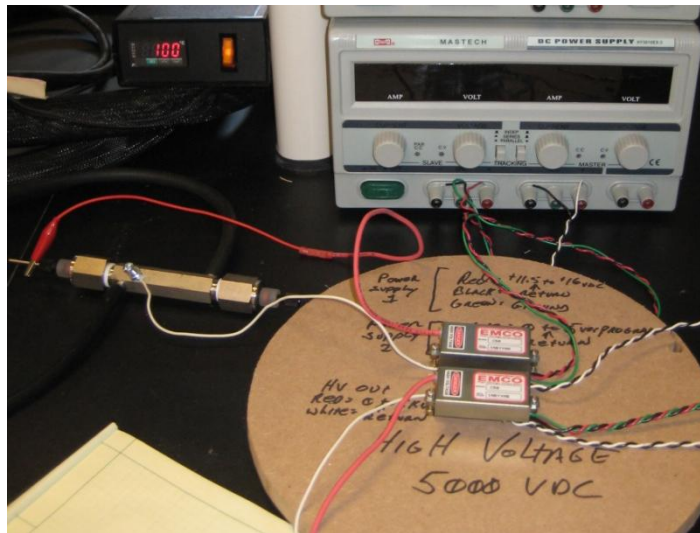


Figure 37. Electrostatic precipitator (left), high-voltage power supplies (right front), and DC source (right rear).

In order for the ESPs and neutralizer to function properly, they needed to be leak-free; in addition, the ESPs would need to maintain the high-voltage required for operation. The first requirement was considered to be met if the two new instruments

could pass the leak-check specification of the CPC instrument, which states that a vacuum of at least 30 cm of Hg needed to be maintained for ten minutes. The neutralizer passed on the first attempt; see Figure 38. ESP#2 required a few rounds of leak identification and then fitting tightening and sealing before passing the leak check; see Figures 38 and 39. Only one ESP, ESP#2, was needed in the apparatus for the testing to follow.

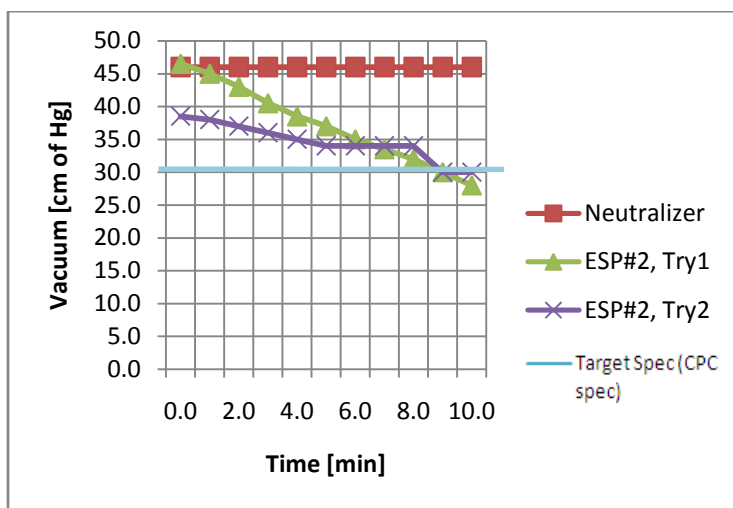


Figure 38. Leak checking the neutralizer (successful) and ESP#2 (unsuccessful).

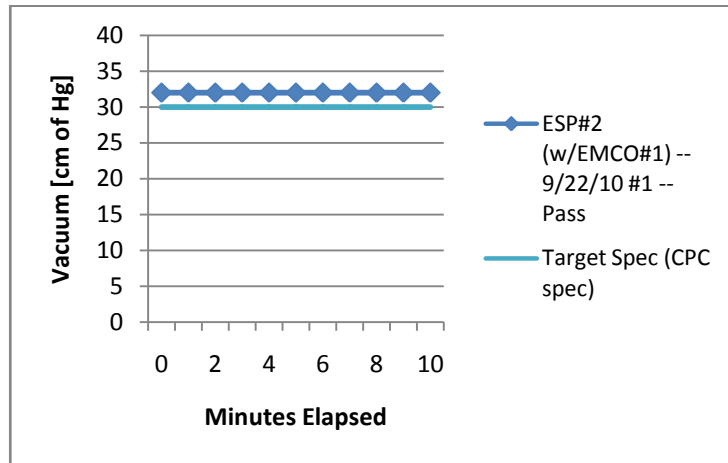


Figure 39. Leak checking ESP#2 (successful).

Concerning high-voltage operation, both ESPs were able to handle the full range of EMCO voltage without shorting or arcing, meaning they could be operated up to at least 4840 Volts; see Table 7. The ESP design predicts that 4330 Volts will capture all charged particles less than 100 nm in diameter for an ESP of these dimensions, and so this test was passed.

Table 7. High voltage performance of the ESPs.

	Program voltage [V]	High-Voltage probe voltage [V]	Actual voltage on ESP [V]
ESP#1/EMCO#1	0.0	0.05	50
	1.0	1.01	1010
	2.0	1.99	1990
	3.0	2.96	2960
	4.0	3.89	3890
	5.0	4.85	4850
ESP#2/EMCO#1	0.0	0.05	50
	1.0	1.03	1030
	2.0	2.00	2000
	3.0	2.96	2960
	4.0	3.86	3860
	5.0	4.83	4830

5.1.4 Charged particle removal with ²¹⁰Po neutralizer and ESP

The new neutralizer and ESP#2 were evaluated in tandem to determine if they were operating correctly to re-neutralize the aerosol and then remove all of the charged particles from the aerosol, thereby providing a completely neutral aerosol at the exit of the neutralizer-ESP combination, as desired. As described above, if the neutralizer was operating as designed, any aerosol entering the unit should exit the unit with a Boltzmann distribution of charges; see Table 8.

Table 8. Boltzmann Distribution (Hinds 1999); particle diameters of interest marked in green.

TABLE 15.4 Distribution of Charge on Aerosol Particles at Boltzmann Equilibrium

Particle Diameter (µm)	Average Number of Charges	Percentage of Particles Carrying the Indicated Number of Charges								
		< -3	-3	-2	-1	0	+1	+2	+3	>+3
0.01	0.007				0.3	99.3	0.3			
0.02	0.104				5.2	89.6	5.2			
0.05	0.411			0.6	19.3	60.2	19.3	0.6		
0.1	0.672		0.3	4.4	24.1	42.6	24.1	4.4	0.3	
0.2	1.00	0.3	2.3	9.6	22.6	30.1	22.6	9.6	2.3	0.3
0.5	1.64	4.6	6.8	12.1	17.0	19.0	17.0	12.1	6.8	4.6
1.0	2.34	11.8	8.1	10.7	12.7	13.5	12.7	10.7	8.1	11.8
2.0	3.33	20.1	7.4	8.5	9.3	9.5	9.3	8.5	7.4	20.1
5.0	5.28	29.8	5.4	5.8	6.0	6.0	6.0	5.8	5.4	29.8
10.0	7.47	35.4	4.0	4.2	4.2	4.3	4.2	4.2	4.0	35.4

10-100nm range of NanoAPA

And then if the ESP was operating correctly, all particles entering the unit with a charge would be trapped and prevented from exiting the unit. Therefore, the fraction of particle concentration removed by the paired neutralizer-ESP instruments could be predicted to be the total of the charged particles in the Table 8: ~1% of 10 nm particles and ~57% of 100 nm particles. The paired instruments were tested with 10, 20, 50, and 100 nm aerosol of IPA and oleic acid, and the results were as shown in Figure 40 and Table 9.

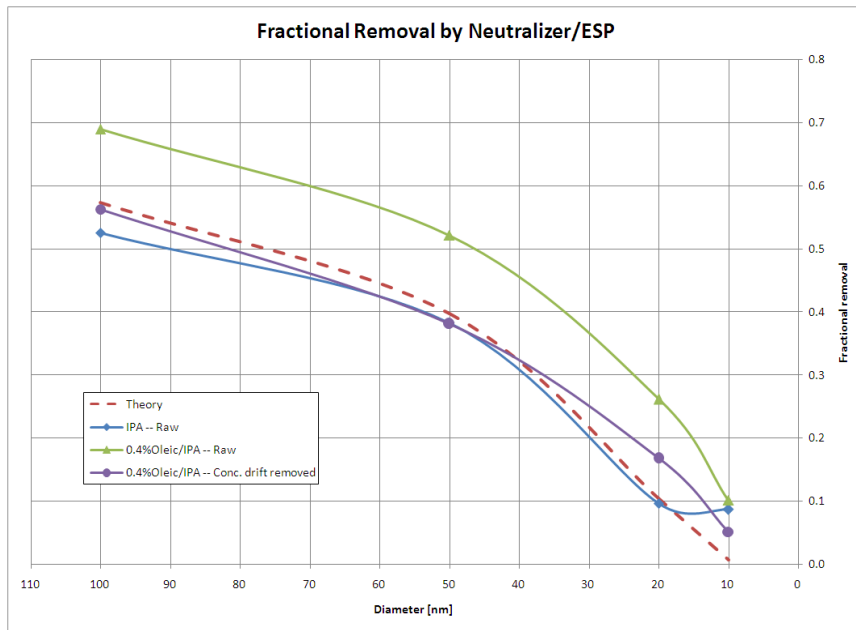


Figure 40. Fractional removal of Neutralizer/ESP combination vs. that predicted by theory.

A direct comparison of aerosol concentration with and without the Neutralizer/ESP units in line in the Standard Aerosol apparatus resulted in the IPA aerosols (Figure 40, “IPA- raw”) following the predicted removal line well (Table 9, sub-table e), but that the aerosol of Oleic acid (Figure 40, “Oleic – raw”) did not (Table 9, sub-table a).

Table 9. Calculation of concentration-drift-corrected Neutralizer/ESP performance.

a	Particle Type	Date	Dia. [nm]	ESP state	Mean conc [p/cm ³]	Std. Dev. conc [p/cm ³]	Sample time [min]	Electrostatic Fraction Removed (exp)	Electrostatic Fraction Removed (theory)			
	See Hinds p.337											
Without Consideration of Concentration Drift	0.4%Oleic/IPA	29-Jul	100	on	139	12	1.67	0.690	0.574			
	0.4%Oleic/IPA	29-Jul	50	on	692	26	1.67	0.522	0.398			
	0.4%Oleic/IPA	29-Jul	20	on	960	46	1.67	0.262	0.104			
	0.4%Oleic/IPA	29-Jul	10	on	132	10	1.67	0.101	0.007			
	0.4%Oleic/IPA	29-Jul	100	off	449	23	1.67					
	0.4%Oleic/IPA	29-Jul	50	off	1447	57	1.67					
	0.4%Oleic/IPA	29-Jul	20	off	1300	49	1.67					
	0.4%Oleic/IPA	29-Jul	10	off	147	13	1.67					
b	Particle Type	Date	Dia. [nm]	ESP state	Mean conc [p/cm ³]	Std. Dev. conc [p/cm ³]	Sample time [min]	Midpoint elapsed time [s]	Time diff. [s]	Conc change	Conc. change per second	Avg (mean conc)
	Analysis of Concentration Drift											
Analysis of Concentration Drift	0.4%Oleic/IPA	29-Jul	100	no, before	329	19	1.67	550				
	0.4%Oleic/IPA	29-Jul	100	no, after	509	26	1.67	2260	1710	180	0.11	419
	0.4%Oleic/IPA	29-Jul	50	no, before	1248	50	1.67	370				
	0.4%Oleic/IPA	29-Jul	50	no, after	2007	178	1.67	2400	2030	760	0.37	1627
	0.4%Oleic/IPA	29-Jul	20	no, before	1647	59	1.67	230				
	0.4%Oleic/IPA	29-Jul	20	no, after	2227	61	1.67	2510	2280	580	0.25	1937
	0.4%Oleic/IPA	29-Jul	10	no, before	352	19	1.67	100				
	0.4%Oleic/IPA	29-Jul	10	no, after	442	29	1.67	2670	2570	90	0.04	397
c	Particle Type	Date	Dia. [nm]	ESP state	Mean conc [p/cm ³]	Std. Dev. conc [p/cm ³]	Sample time [min]	Midpoint elapsed time [s]	Time diff. [s]	Conc offset	Corrected Conc.	
	Correction of "ESP off" counts											
Correction of "ESP off" counts	0.4%Oleic/IPA	29-Jul	100	on	139	12	1.67	870				
	0.4%Oleic/IPA	29-Jul	100	off	449	23	1.67	2110	1240	-130	318	
	0.4%Oleic/IPA	29-Jul	50	on	692	26	1.67	1050				
	0.4%Oleic/IPA	29-Jul	50	off	1447	57	1.67	1930	880	-329	1118	
	0.4%Oleic/IPA	29-Jul	20	on	960	46	1.67	1210				
	0.4%Oleic/IPA	29-Jul	20	off	1300	49	1.67	1790	580	-148	1153	
	0.4%Oleic/IPA	29-Jul	10	on	132	10	1.67	1370				
	0.4%Oleic/IPA	29-Jul	10	off	147	13	1.67	1590	220	-8	139	
d	Particle Type	Date	Dia. [nm]	ESP state	Mean conc [p/cm ³]	Std. Dev. conc [p/cm ³]	Sample time [min]	Electrostatic Fraction Removed (exp)	Electrostatic Fraction Removed (theory)			
	See Hinds p.337											
With Consideration of Concentration Drift	0.4%Oleic/IPA	29-Jul	100	on	139	12	1.67	0.563	0.574			
	0.4%Oleic/IPA	29-Jul	50	on	692	26	1.67	0.381	0.398			
	0.4%Oleic/IPA	29-Jul	20	on	960	46	1.67	0.168	0.104			
	0.4%Oleic/IPA	29-Jul	10	on	132	10	1.67	0.052	0.007			
	0.4%Oleic/IPA	29-Jul	100	off	318		1.67					
	0.4%Oleic/IPA	29-Jul	50	off	1118		1.67					
	0.4%Oleic/IPA	29-Jul	20	off	1153		1.67					
	0.4%Oleic/IPA	29-Jul	10	off	139		1.67					
e	Particle Type	Date	Dia. [nm]	ESP state	Mean conc [p/cm ³]	Std. Dev. conc [p/cm ³]	Sample time [min]	Electrostatic Fraction Removed (exp)	Electrostatic Fraction Removed (theory)			
	IPA data											
IPA data	IPA	24-Jul	100	off	1481	47	1.67					
	IPA	24-Jul	50	off	2392	73	1.67					
	IPA	24-Jul	20	off	293	17	1.67					
	IPA	24-Jul	10	off	31	1	1.67					
	IPA	24-Jul	100	on	703	22	1.67	0.525	0.574			
	IPA	24-Jul	50	on	1476	56	1.67	0.383	0.398			
	IPA	24-Jul	20	on	265	17	1.67	0.096	0.104			
	IPA	24-Jul	10	on	29	1	1.67	0.087	0.007			

Notes on sub-tables: (a) Oleic acid data without considering concentration drift; (b) Analysis of concentration drift of Oleic acid particles (ESP “no” means the ESP was removed for these measurements); (c) Correcting the “ESP off” Oleic data; (d) Oleic acid data with consideration of concentration drift; (e) IPA data, did not need correction, because didn’t drift.

Investigation revealed that the concentration of Oleic acid particles flowing through the apparatus changed rapidly, increasing with time. This effect was known to be a result of the concentration of the target particle in the SJA atomizer solution increasing with time, as the solvent evaporated and left with the vapor phase of the exit aerosol at a much faster rate than that of the target particle solution. To correct the data for this evaporation effect, a linear increase of particle concentration with time was assumed, calculated for the Oleic acid solution (Table 9, sub-table b), removed from the “ESP-off” concentration values (Table 9, sub-table c), and then these values were used to recalculate the fraction removed by the ESP (Table 9, sub-table d). After correcting the oleic aerosol data for atomizer concentration-drift, the concentration-drift-corrected calculations of fractional removal showed very good match to that predicted by theory (Figure 40, “Oleic – Conc. drift removed”).

Thus the ^{210}Po Neutralizer and ESP instrument pair were qualified and integrated into the Standard Aerosol apparatus.

5.2 Design and build the NanoAPAv2/POC instrument

5.2.1 Leak checking of the microfabricated devices

As built, the microfabricated devices were initially unable to maintain the vacuum specification to match the CPC performance; see Figure 41. The devices were leaked checked by plugging the outlet and attaching a vacuum gauge, shutoff valve, and vacuum pump to the inlet. The pump was used to draw the device down to 30 or more [cm of Hg], and then the shutoff valve was closed. The value of vacuum was read from the gauge every minute for ten minutes. If a vacuum equal to or greater than

30 cm of Hg could be maintained for the full ten minutes, the device was considered to be at least as resistant to leaks as the CPC instrument. To enable the devices to hold the required vacuum, a number of layers of additional sealant (cyanoacrylate, Krazy Glue) were applied to the devices until they could pass the spec, as shown in the final runs of Figure 41.

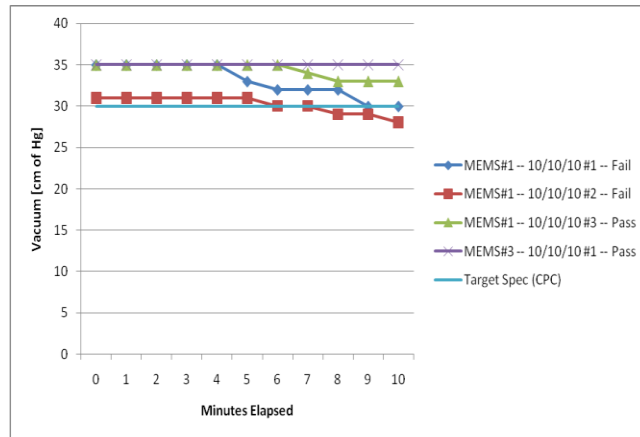


Figure 41. Leak checking of microfabricated devices.

5.2.2 High-voltage characterization of the microfabricated devices

To determine the actual voltage value applied by the high-voltage power supply to the condensers in the microfabricated devices and to determine the repeatability of that voltage setting, a Fluke 80K high-voltage probe was used to measure voltage on the condenser leads through sweeps of the programmed voltage steps; see Figure 42. The actual voltages were stable and linear, with a small offset of the linear trend at 0 V.

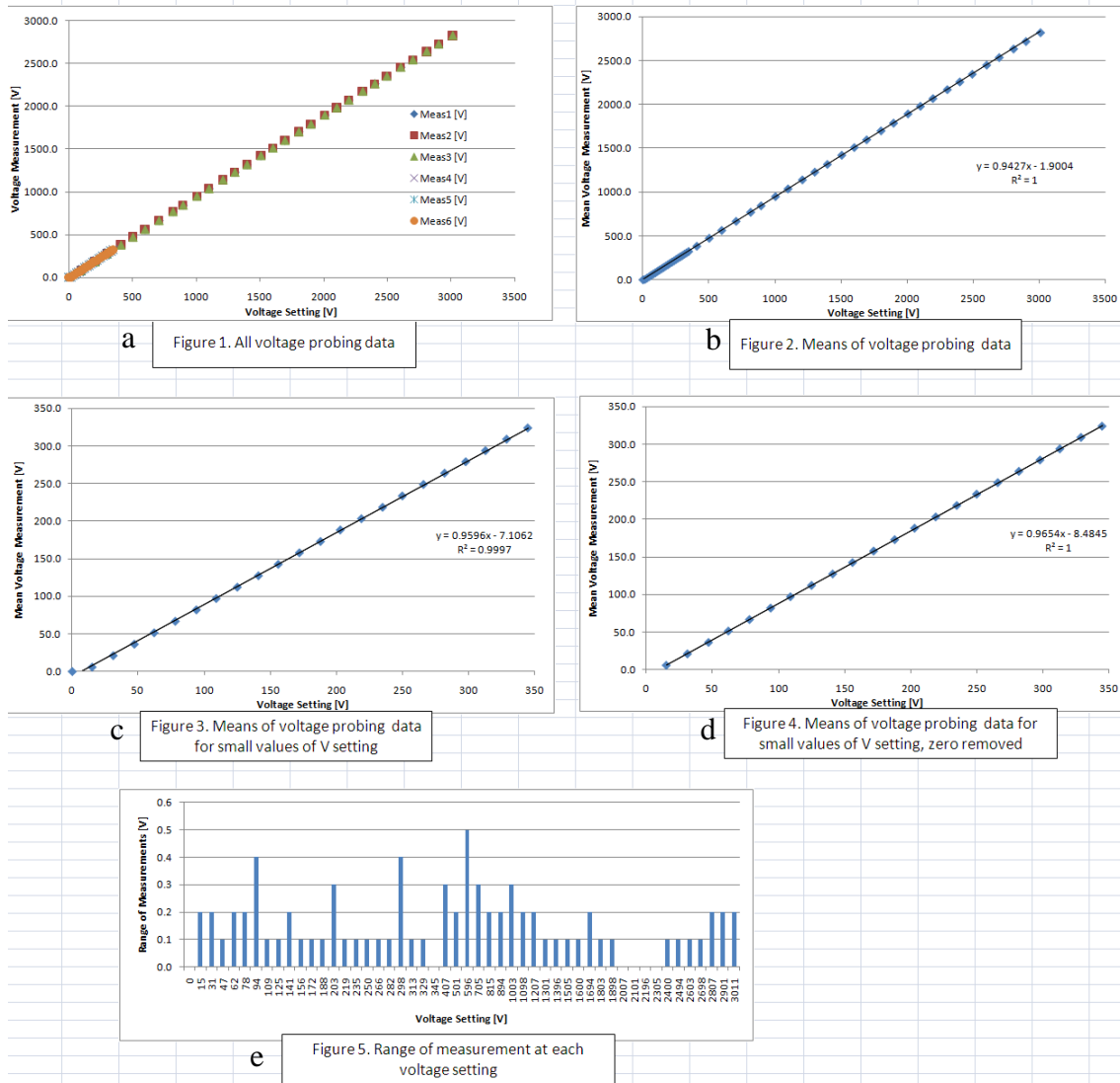


Figure 42. High-voltage characteristic curves for the microfabricated devices.

5.2.3 Calculation of Reynolds number

To determine the flow condition (laminar/transition/turbulent) of the aerosol through the microfabricated devices, the Reynolds number was calculated as a function of temperature to cover possible applications of the NanoAPA instrument (ambient in cold weather up through tailpipe exhaust temps); through channel size to cover

designed vs. as-built channel cross-section dimensions (2.2x1.0mm vs. 3.2x2.0mm(est.)); through a range of sample flowrates to cover the possible operating range of instrument; and for both the a macro model, a smooth walled channel, and one pillar of a micro model – a segment of the microfabricated screen transverse to the flow. See Figures 43 through 45.

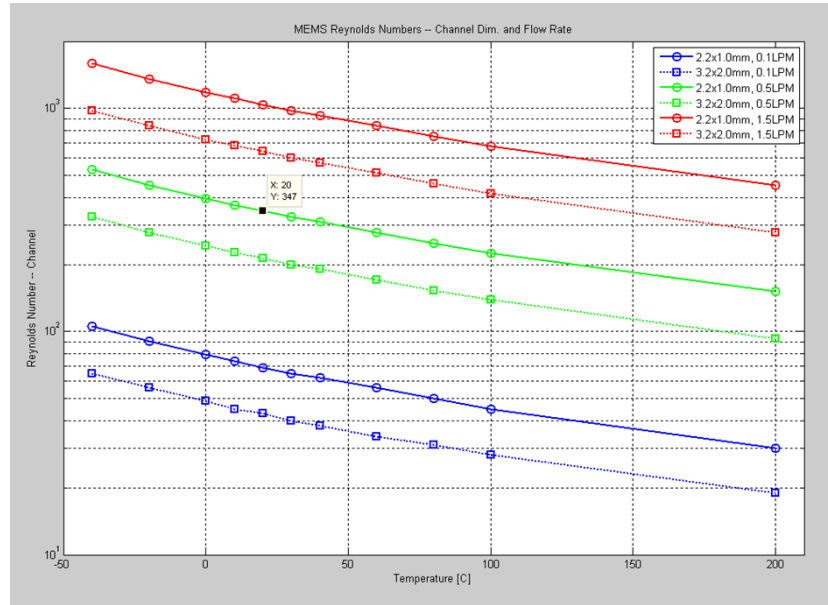


Figure 43. Re number analysis for the macro model.

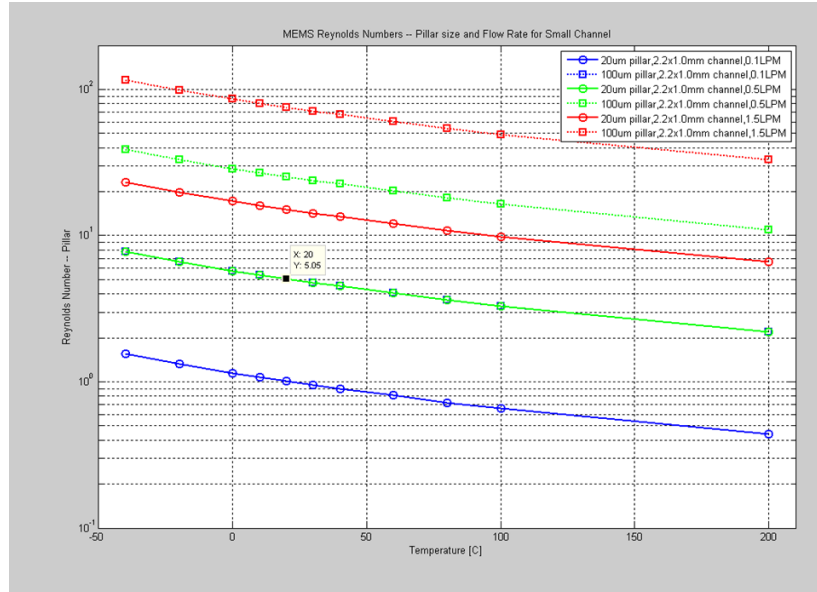


Figure 44. Re number analysis for the pillar model, as-designed channel.

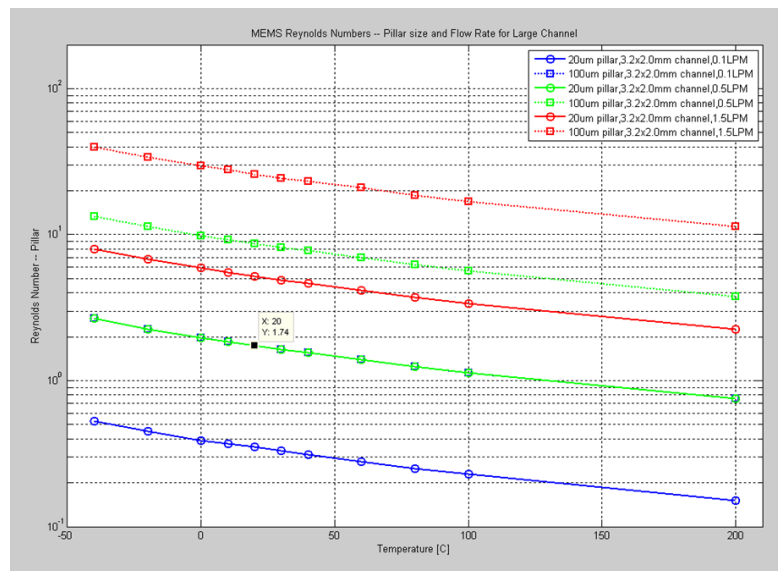


Figure 45. Re number analysis for the pillar model, as-built channel.

The Reynolds numbers for microfabricated device at maximum flowrate (1.5LPM), as-designed channel cross section (2.2mmx1.0mm), ambient air at 20°C as taken from Figures 43-45, based on the equation $Re = \frac{DH U}{\nu}$ (DH hydraulic

diameter; U mean velocity; ν kinematic viscosity): Re for channel bulk flow ($DH = 4$ (cross-section area) / (cross-section perimeter)): 1000; Re for pillar face normal parallel to bulk flow ($DH = \text{pillar face} = 20\text{nm}$): 15; and Re for pillar face normal perpendicular to bulk flow ($DH = \text{pillar face} = 100\text{nm}$): 75.

Details for the Re number calculation are shown in Appendix E. All Reynolds numbers were comfortably in the laminar regime.

5.2.4 Channel flow simulation

Concerned that the screen design of the microfabricated devices may introduce challenges to understanding the operating performance of the future instrument, collaboration was initiated with Prof. Marshall and his research group in order to complement the laboratory characterization of the microfabricated devices with simulation of their function. The Marshall codes comprise fluid flow, electrostatic fields, and particle adherence and are described in (Marshall 2007; Liu, Marshall et al. 2009). Preliminary modeling plan was for a “macro” model of a smooth channel, and a “micro” model of one pillar of the condenser screens. These two solid models of the microfabricated devices were created and set up to be run through the Marshall codes. The "macro" model was successfully run through the fluid-flow portion of the code at the nominal model conditions: as-designed channel dimensions (1.0x2.2x30mm), 0.5LPM, std. temp and pressure. See Figure 46 for a plot with three contour-plot slices of velocity in +Z direction and a rake of streamlines starting at equal intervals along the inlet diagonal. Flow through the channel develops as expected for this laminar-flow, smooth-walled simulation: the air near the walls slows into a boundary layer, and the

air in the center of the channel speeds up to nearly twice the average velocity (as determined from the 0.5LPM flowrate) of 3.8m/s.

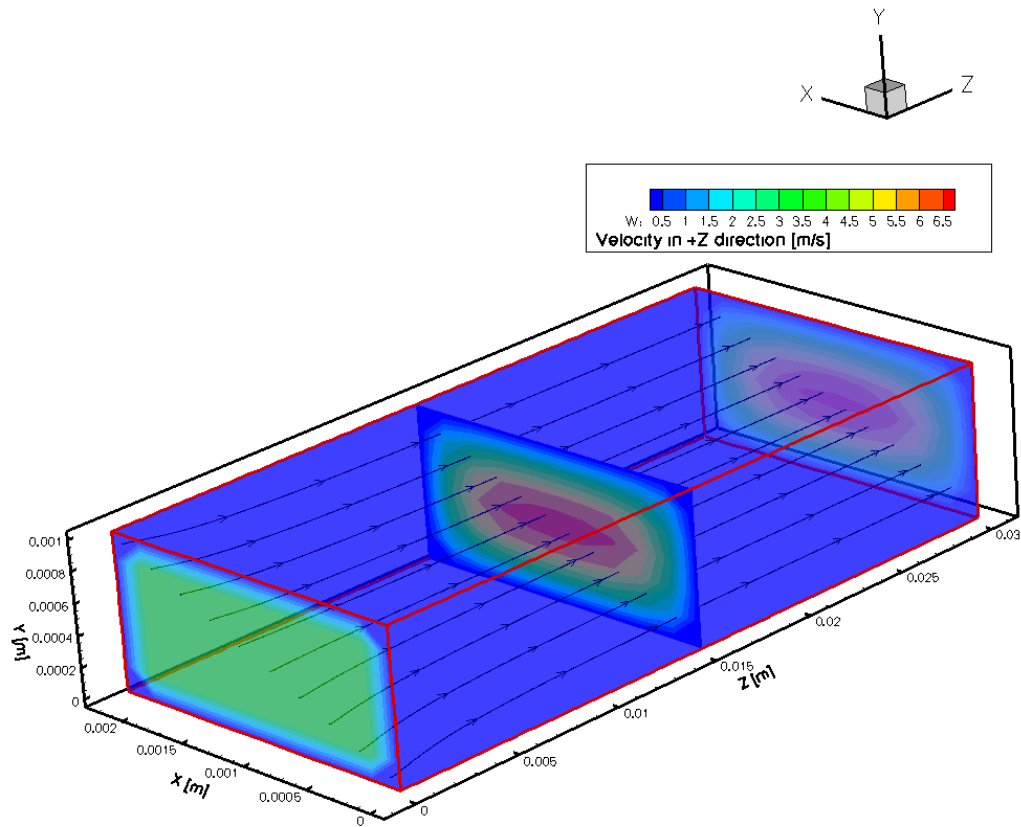


Figure 46. U2Rans -Simulated Flow through the one-condenser macro model.

The determination that an additional instrument re-design and build was required in the project necessitated that this simulation aspect of the project be shelved due to time constraints.

5.2.5 Electrometer selection and evaluation

The first electrometer investigated for its applicability to the new instrument design was the electrometer provided with the MicroAPA prototype. A reference signal of 0-6pA (the specified operating range of the MicroAPA electrometer) was

sourced from an HP 4156c Semiconductor Parameter Analyzer in steps of 100fA. As can be seen in Figure 47, the output voltage signal of the MicroAPA electrometer did not show a detectable correlation to the input current signal as it was designed to.

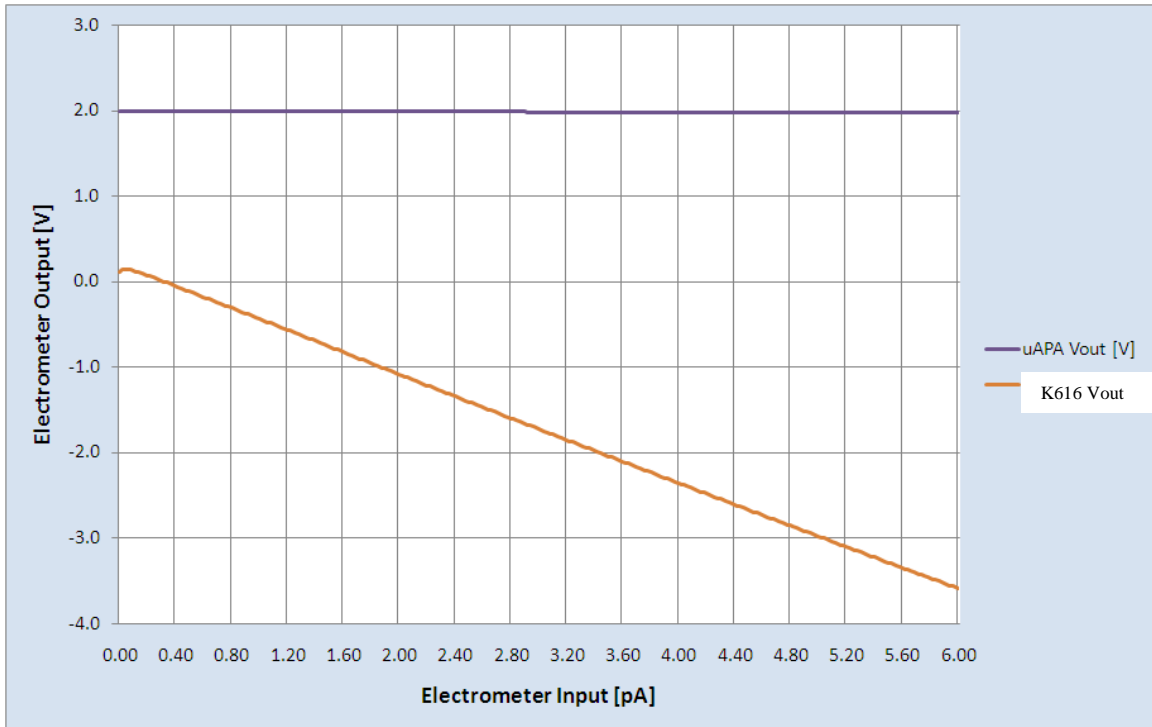


Figure 47. Response of MicroAPA and Keithley electrometers to the 0-6pA reference signal from the Parametric Analyzer. The MicroAPA response is shown in blue and labeled "uAPA" and the response of the Keithley electrometer is shown in orange and labeled "K616".

A comparison of the MicroAPA electrometer's output voltage signal to the voltage at the input (measured by the Parametric Analyzer) is shown in the top graph of Figure 48. It can be seen that electrometer's output voltage is following the voltage of the input signal 1:1, and thus is only passing the signal through instead of providing a measurement of it. This implies that the MicroAPA electrometer circuit was damaged/short-circuited: unfortunately, because the circuit board was covered in opaque epoxy to keep its design a secret, further diagnosis and repair were impossible.

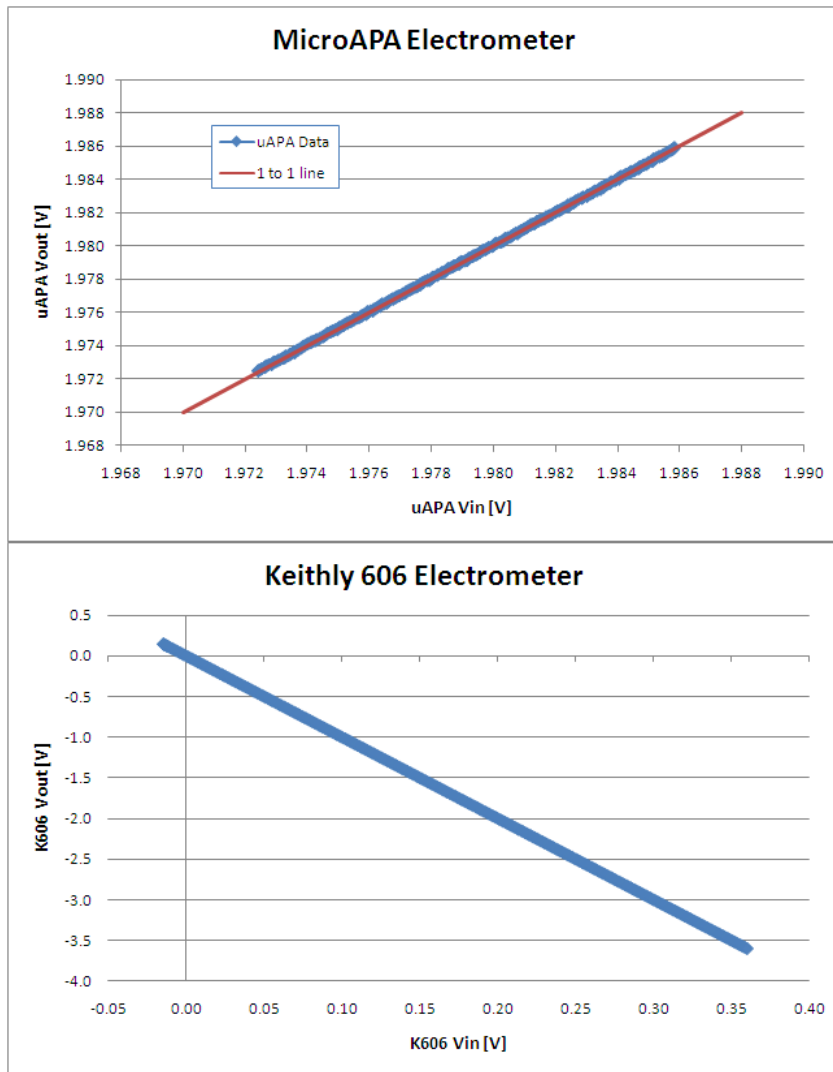


Figure 48. Diagnosing the lack of MicroAPA electrometer response to the current of the input (top graph) and employing a similar analysis to the Keithly electrometer to confirm it is operating correctly. The voltage of the signal input to the respective electrometer is compared to the voltage of the electrometer’s output signal. The MicroAPA electrometer’s output voltage follows the input voltage exactly; the Keithly electrometer’s does not.

After demonstrating that the MicroAPA electrometer was non-functioning, a Keithly 616 analog electrometer was borrowed and evaluated in the same way; see Figures 47 and 48. This electrometer’s voltage output was correlated with the current input, and was linear over the range from 0.1 pA to at least 6 pA, a range adequate to

characterize the performance of the NanoAPAv.2 instrument. Next, the warm-up period was checked for the Keithley electrometer; see Figure 49. Significant drift in the Keithley electrometer's measurement of a constant input was observed; the electrometer achieved stability in about 45 minutes.

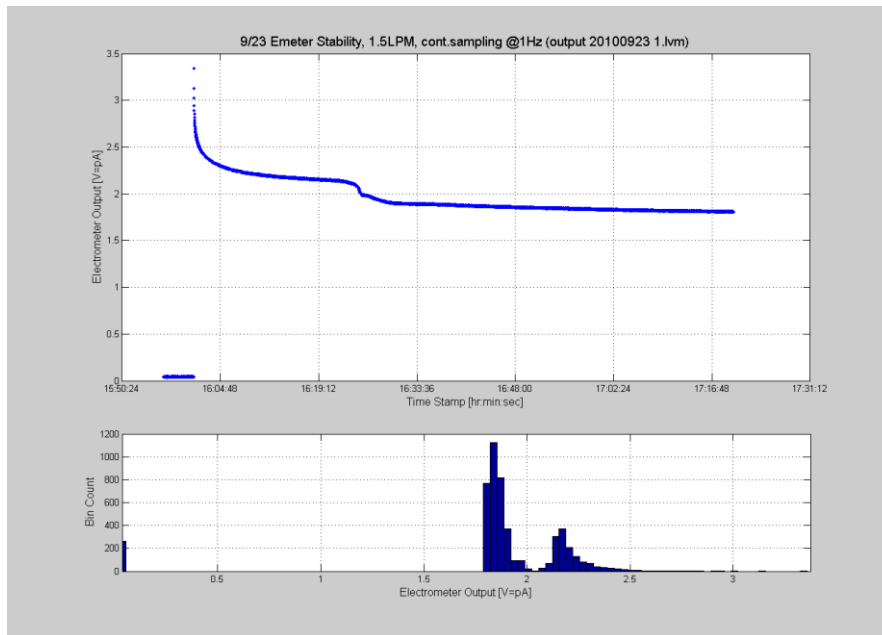


Figure 49. Stability of the Keithley 616 electrometer.

The lab-bench application Keithley electrometer would not be suitable for integration into a field-deployed NanoAPAv.2 instrument, and so a long-term solution was pursued; the Keithley electrometer was employed to characterize the instrument performance until the final electrometer could be acquired and integrated. Most of the data collected in this project employed this electrometer.

A digital electrometer evaluation kit (TI DDC112EVM) was acquired and qualified near the end of the project. The evaluation of the TI electrometer to the reference signals from the Parametric Analyzer is shown in Figure 50.

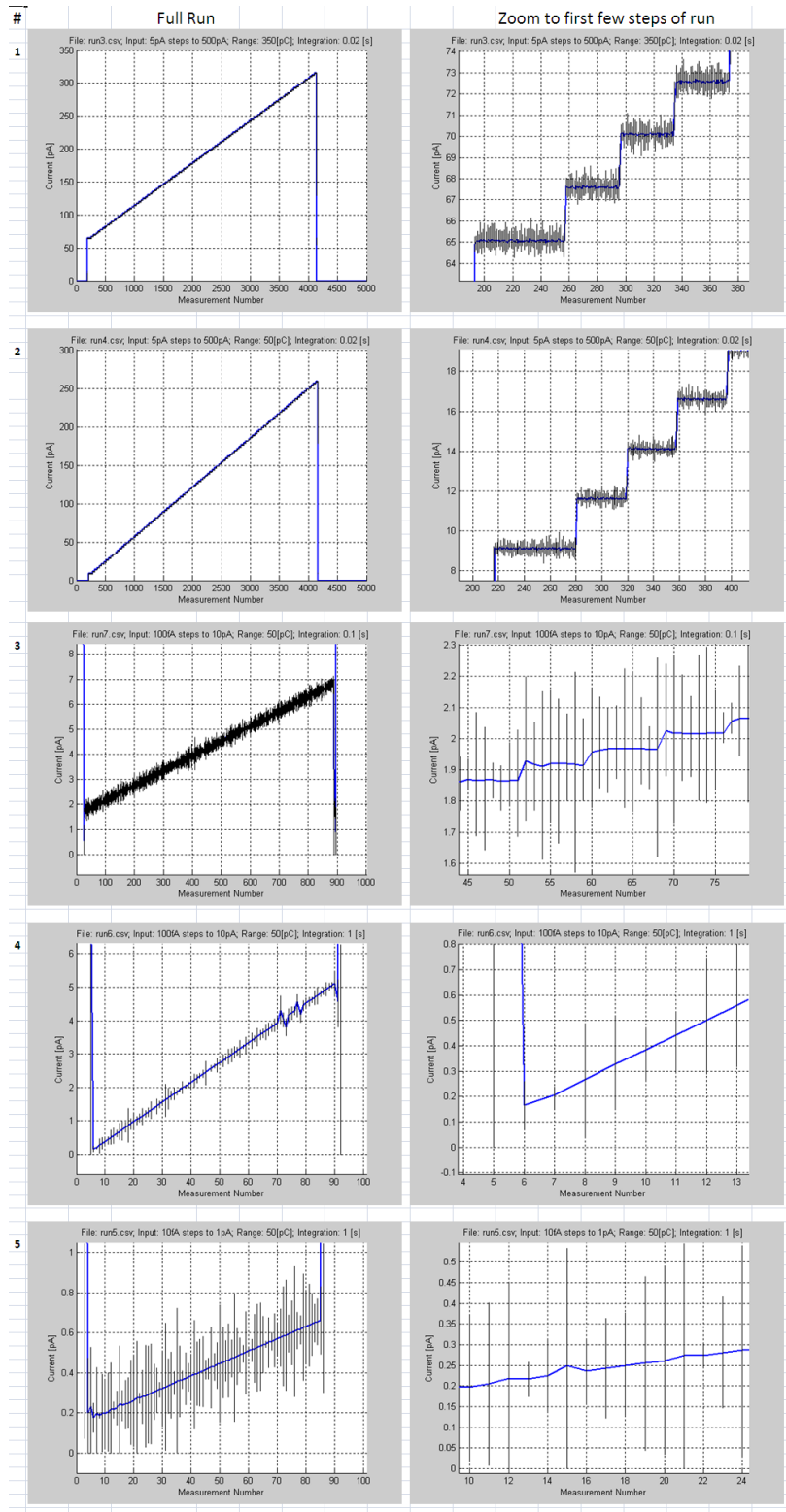


Figure 50. Evaluation of the response of the TI DDC112 EVM electrometer to reference signals generated by the Parametric Analyzer.

Various step sizes and maximum currents were sent to the TI electrometer, which was configured with various sensitivity settings; see Appendix H for a description of the operation of this electrometer. The five runs with the most useful data are shown in Figure 50 ordered from least sensitive, largest range to most sensitive, smallest range. In the tested configuration there were four "channels" of data recorded from one combined input -- each of the two physical channels has two "half-cycle" measurements, denoted "A" and "B"; the mean of the four is shown as the blue line, and the range of the four is shown by the vertical black line for each measurement; see Figure 50

Plots #1 and #2 of Figure 50 show that 5pA steps were clearly detectable and linear over a 0-500 pA input range, and that the measurement noise was reduced by switching to the smaller-range setting. Plots #3 and #4 show that 100 fA steps were detectable and linear over a 0-10 pA input range. (Note: The input steps were programmed to be about a second in duration each, hence the lack of obvious steps in plot#4 which was for an integration time of 1 second.) Plot 5 shows that 10 fA steps were detectable and linear from about 50 fA and up; an impressive capability. There was a large variation apparent between the four "channels" that oscillates though the measurements -- this was likely caused by the Parametric Analyzer struggling to maintain a steady signal at these very low currents, and so this should not be a factor for non-sourced measurements. Ignoring offset in the measured zero-current level run-to-run, it appears that the DDC112 measured a current half as large as the Parametric Analyzer was programmed to source.

These results showed that the TI DDC112 would make an excellent electrometer for the NanoAPA, provide a usable measurement range of 50fA to 50pA, covering the full range of likely NanoAPA measurement capability.

5.3 Characterize the micro-fabricated double condenser

To characterize the performance of the proof-of-concept double condenser, experiments with various SA parameters, DUT configurations, and operating parameters were performed. The full list of experiments with relevant DUT and SA parameters is shown in a table in Appendix C. The database includes 77 experiments run over the course of about two months time; with challenge aerosols of diameters from 8 to 100 nm; with flowrates ranging from 0.1 to 1.5 LPM; with aerosol compositions of IPA-only, oleic acid in IPA, and a few with engine residual trapped in the ASET after the instrument was used for on-board data collection; with aerosol concentration (at the DUT) of near zero to nearly 90,000 p/cm³; with one or two devices as condenser stage #1; with positive and negative condenser polarities; with positive and negative charging polarity; with Keithley and TI electrometers; and with various serial-numbered condensers used as condenser stage #1. All experiments in the database were performed with DEV#1 as condenser stage #2 (the one critical for measurement).

The control of the electrical potential to the DUT was performed by the Labview VI NanoAPA_3.vi, shown in Appendix G. Each of the database items with no aerosol flow (Composition = N) were comprised of 1 Hz electrometer output voltage recorded by the Labview VI NanoAPA_2.vi, shown in Appendix G. For each voltage

setting listed in the database, the electrometer output was monitored until it stabilized, and this value was used in the analysis as the background electrometer current for that voltage setting at that time. For database items with aerosol flow (Composition \neq N) a minute of stabilized 1 Hz electrometer measurements were recorded and the mean of these values are shown for each experiment as I_{signal} in Appendix C plots. I_{signal} minus the background voltage is shown as I_{diff} in the Appendix. To account for the drift in aerosol concentration the DUT saw during the experiment (an issue primarily in experiments using the SJA atomizer) the concentrations recorded by the CPC both before and after the experiment were used to establish a linear drift in concentration; see Figure 51 (dashed blue line). This linear concentration, normalized to the concentration at the 500V setting, provided the values of ConcDrift in Appendix C. The Matlab programs used to generate the database of experimental data, and for the analysis below, are shown in Appendix D.

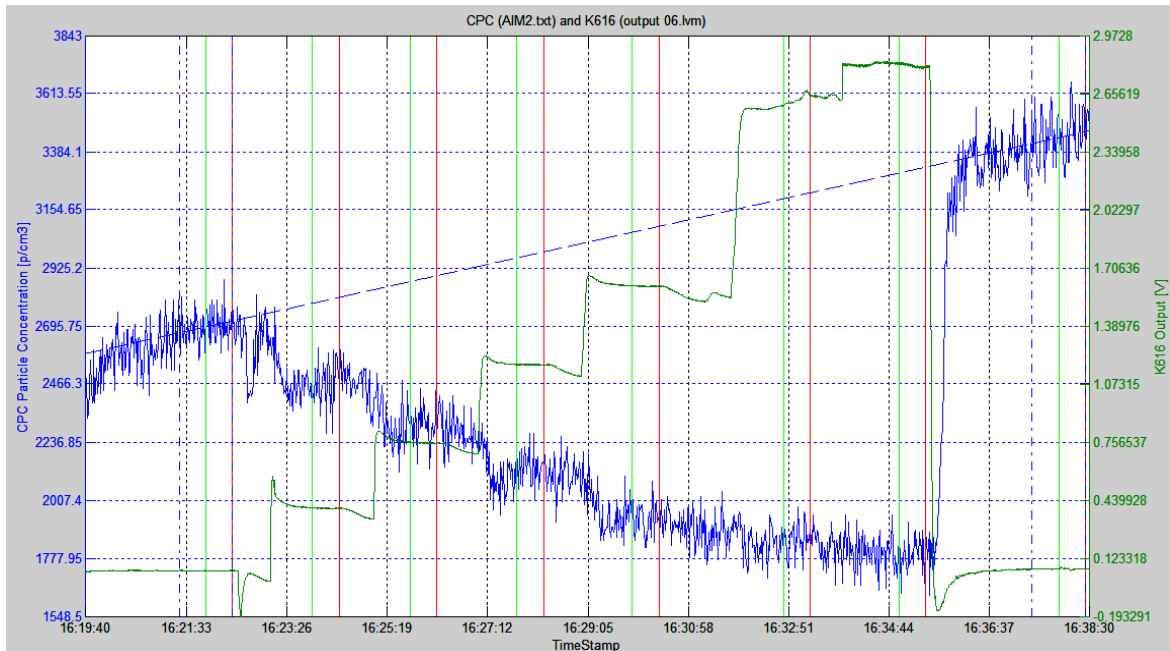


Figure 51. Example data collection for the proof-of-concept (POC) experiments. Particle concentration as recorded by the CPC are in blue, Electrometer output as recorded by the DAQ+VI are in green.

5.3.1 Particle collection efficiency

The characterization results of particle collection efficiency for the double condenser design device for two compositions, IPA and oleic acid, are shown in Figures 52 and 53 where PPR is plotted as a function of applied high voltage. The plots in Figure 52 show that for IPA, all diameter particles were collected through voltage, with the smaller particles completely collected at all flowrates, and the larger particles experienced collection efficiencies (efficiency = 1-PPR) corresponding to their size. Furthermore, all the particle diameters of IPA composition returned to a PPR of very near one when the voltage was returned to zero, as expected. The oleic particles (Figure 53) behaved quite differently, however; only a few of the early experiments exhibited smooth collection like the IPA aerosol. The remainder showed a PPR that

fluctuated both above and below zero, with large spikes above zero at the higher voltages. This behavior is likely due to the oleic (or other) particles attached to the condenser plates during previous experiments being re-entrained into the aerosol flow by the new particles colliding into them during collection, and particles may also have been sputtered off the condenser plates by local electric field anomalies at the screen edges. The IPA particles would not have been prone to these issues, because when they were collected to the condenser plates, they likely burst and evaporated.

The IPA results (Figure 52) demonstrate the effectiveness of the microfabricated device at collecting particles of the specified diameters; the oleic acid results possibly demonstrate the need for the instrument that this device will eventually be used in to have a cleaning protocol to remove particle build-up on the condenser plates.

It is important to note that re-entrainment of particles should not have affected the number-size measurement by the microfabricated device, because as long as the new particles being collected give up their charges when they hit the condenser plates, the electrometer will measure the resulting current. Once the charge is measured, the measurement is not affected by whether particles stay on the plates or re-entrain into the aerosol flow. However, particle adhesion to the plates will have a long-term effect on instrument measurement capability and stability, due to the changing conditions near the plate surfaces, and so an appropriate cleaning and calibration procedures will be required for the final instrument to be field-deployable.

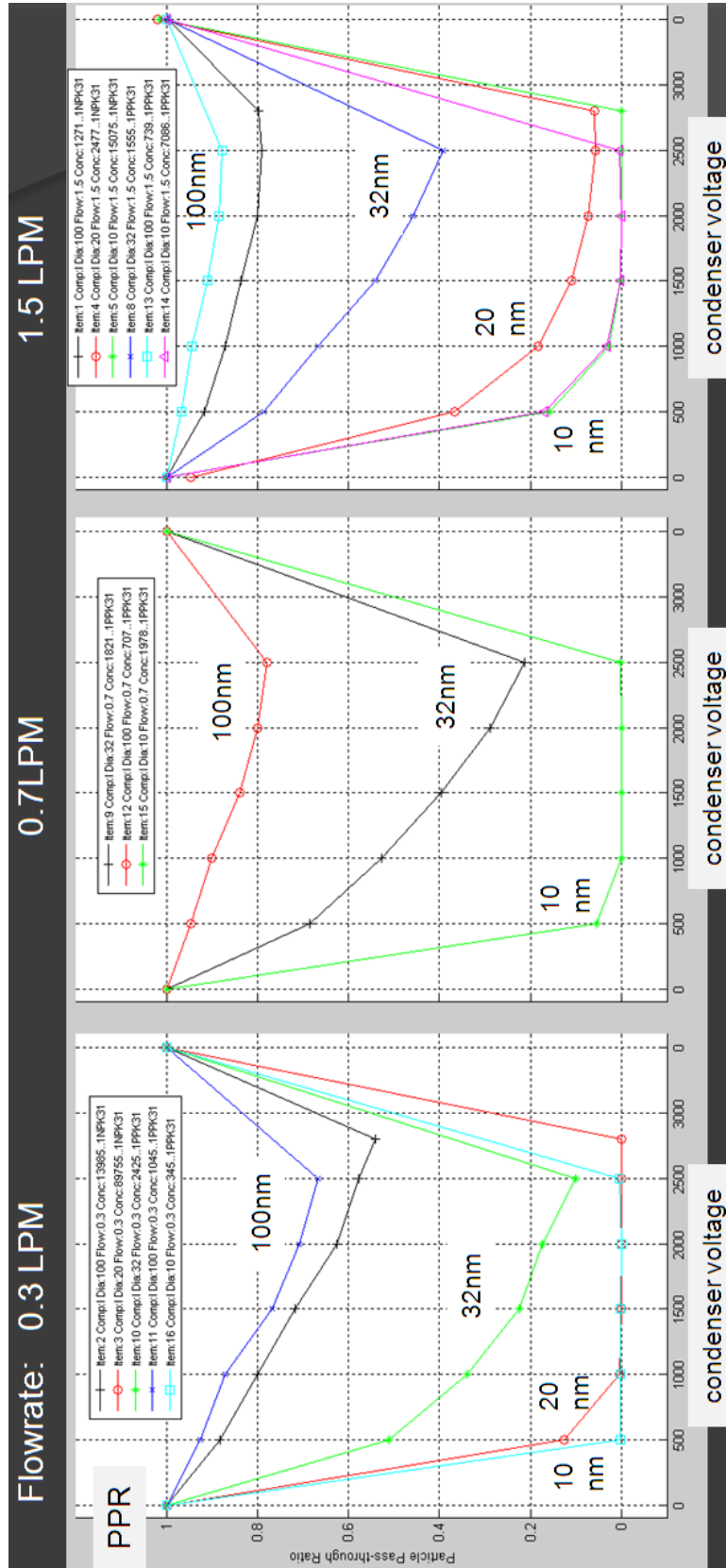


Figure 52. Particle pass-through ratio for datasets of IPA aerosol. (Left plot: 0.3 LPM flowrate; middle plot: 0.7LPM; right plot: 1.5 LPM)

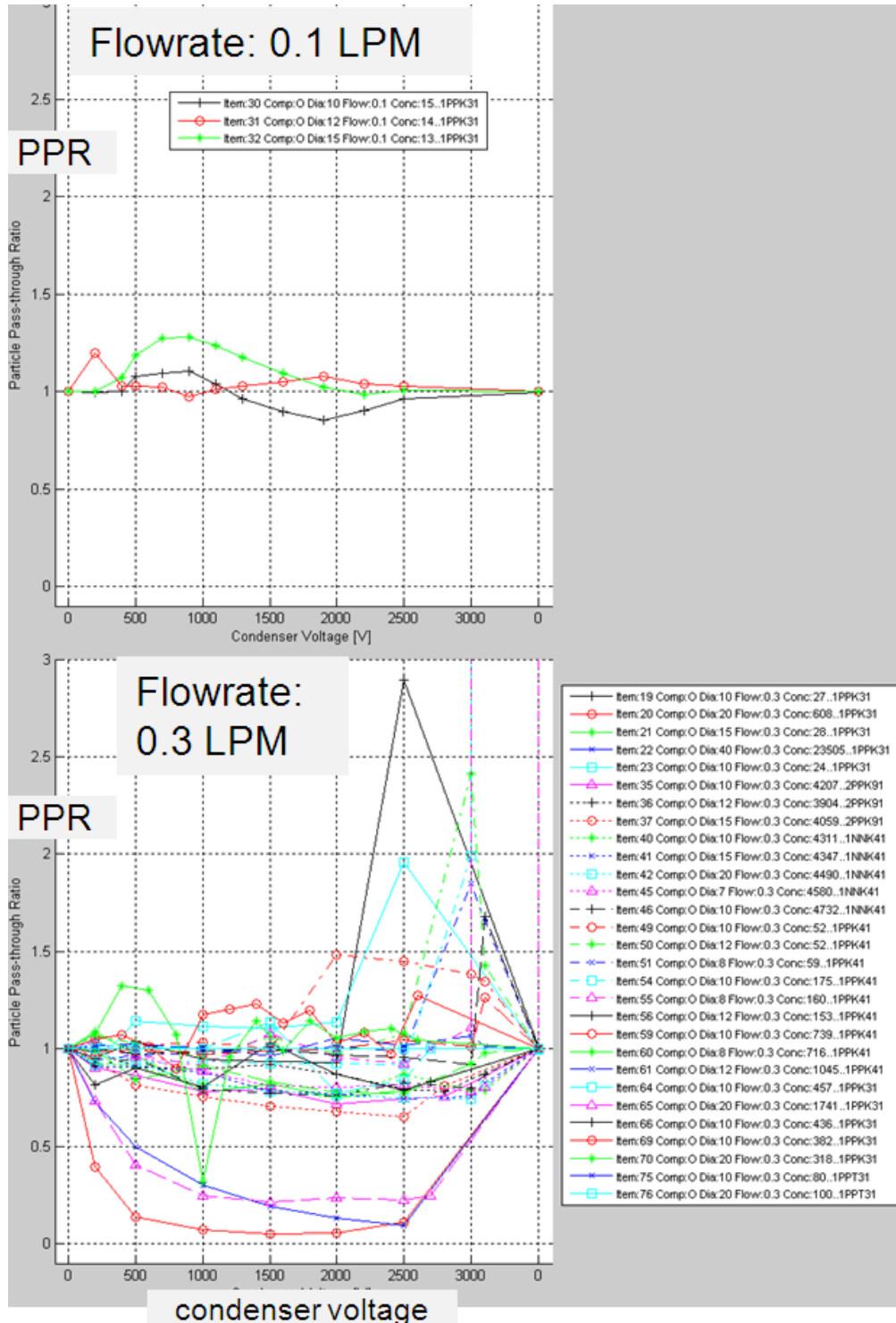


Figure 53. Particle pass-through ratio for datasets of Oleic Acid aerosol. (Top plot: 0.1 LPM flowrate; bottom plot: 0.3LPM)

5.3.2 Correlate current signal to aerosol concentration

To verify that aerosols over a range of particle concentrations result in linear signals from the electrometer output, a metric derived from the measurement of electrometer current, maximum absolute value of I_{diff} , was compared to the aerosol concentration at the double condenser, for all non-background datasets in the database measured by the Keithley electrometer; see Figure 54.

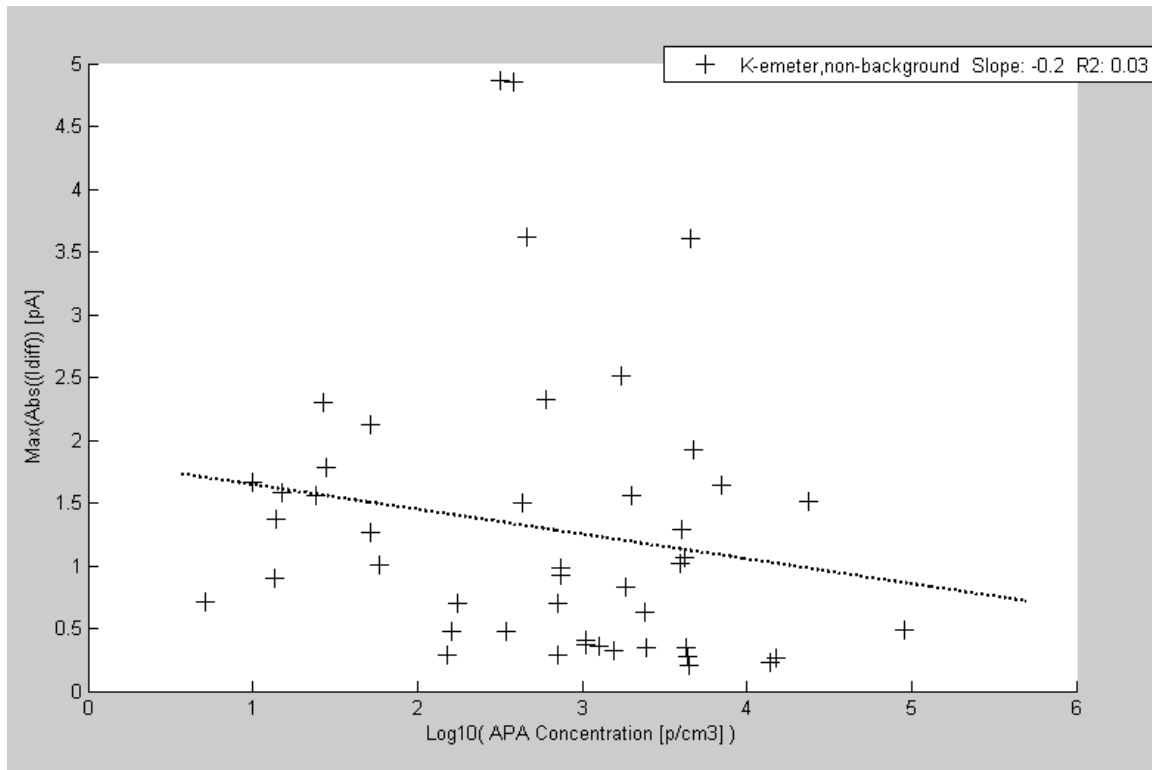


Figure 54. Keithley electrometer response (as the maximum absolute value of the I_{diff} signal) plotted against the aerosol concentration at the microfabricated device, for all non-background datasets (all aerosol compositions) in the database. No correlation is apparent.

No correlation is apparent in Figure 54; a linear fit of the current signal to the aerosol concentration has a slope near zero, with an R^2 value of only 0.03.

Some correlation of all datasets would have been encouraging, but a lack of such a correlation was not necessarily expected; the datasets included experiments at varying particle diameters, flowrates, and so on. Sub-setting the experiments into groups with small ranges of operating parameters, however, allowed interesting patterns to emerge; see Figure 55.

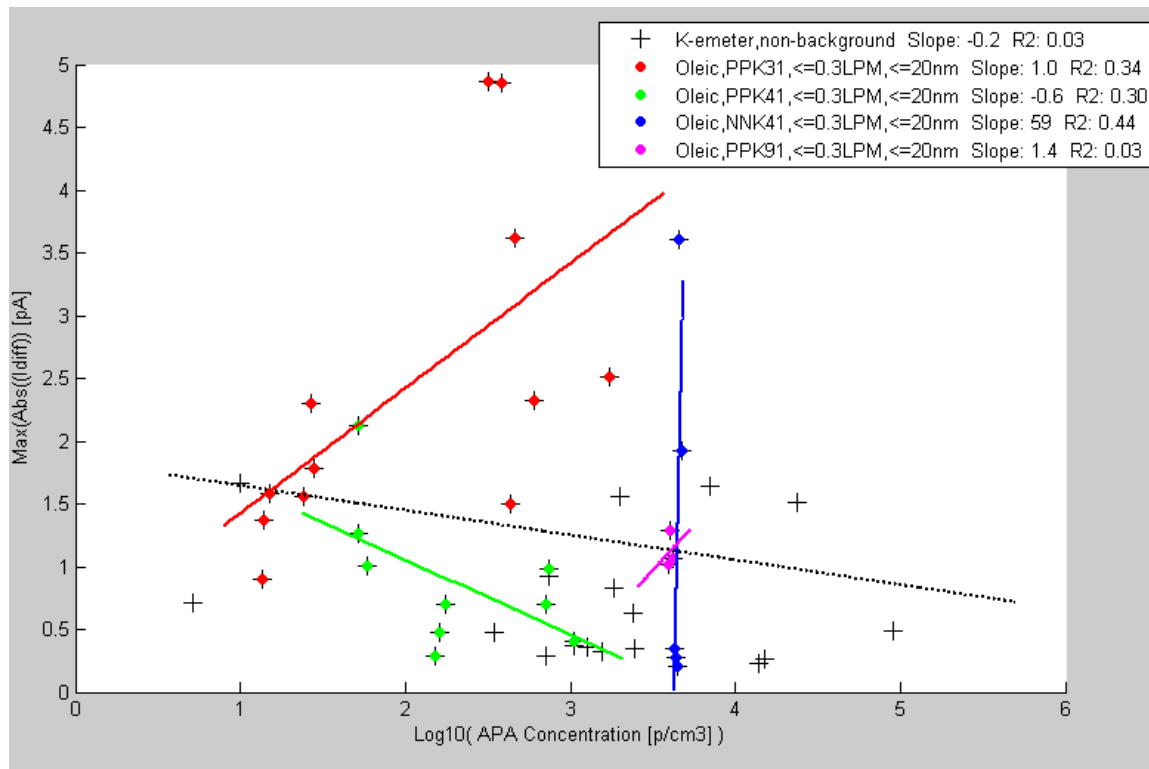


Figure 55. Linear regressions of subsets of the data from Figure 54, selected for similarity in operating parameters. The subset marked in red is the only subset with a positively correlated signal and sufficient data to examine further.

As can be seen in Figure 55, one sub-set of experiments (marked in red), comprised of experiments with oleic acid particles of 20nm or smaller diameters, for flowrates of 0.3 LPM or less, and with hardware configuration PPK31 (positive condenser polarity, positive charging polarity, Keithley electrometer, DEV#3 as

condenser#1, and DEV#1 as condenser#2), resulted in a positive correlation of electrometer current to particle concentration of 1.0 pA per $\log_{10}(\text{concentration [p/cm}^3\text{)})$. The other subsets did not provide the relationship expected from the design, likely because of electrometer circuit stability and design issues that will be examined below.

5.3.3 Characterize performance of the electrical circuitry

Two issues with the electrical circuitry of the proof-of-concept instrument became apparent during the characterization work: capacitive coupling between the high-voltage circuit and the electrometer circuit, and temporal stability of the Keithley electrometer, both short and long-term.

5.3.3.1 Capacitive coupling

The system as tested exhibited a significant magnitude of capacitive coupling, here defined as a non-aerosol-induced current measurement in the electrometer circuit caused by the applied high-voltage circuit. The two circuits are not physically “connected” but “coupled”, when aerosol is not flowing, by the electric field (and dry air) in the second condenser (which functions electrically as a capacitor). Figure 56 shows the effect for an example run.

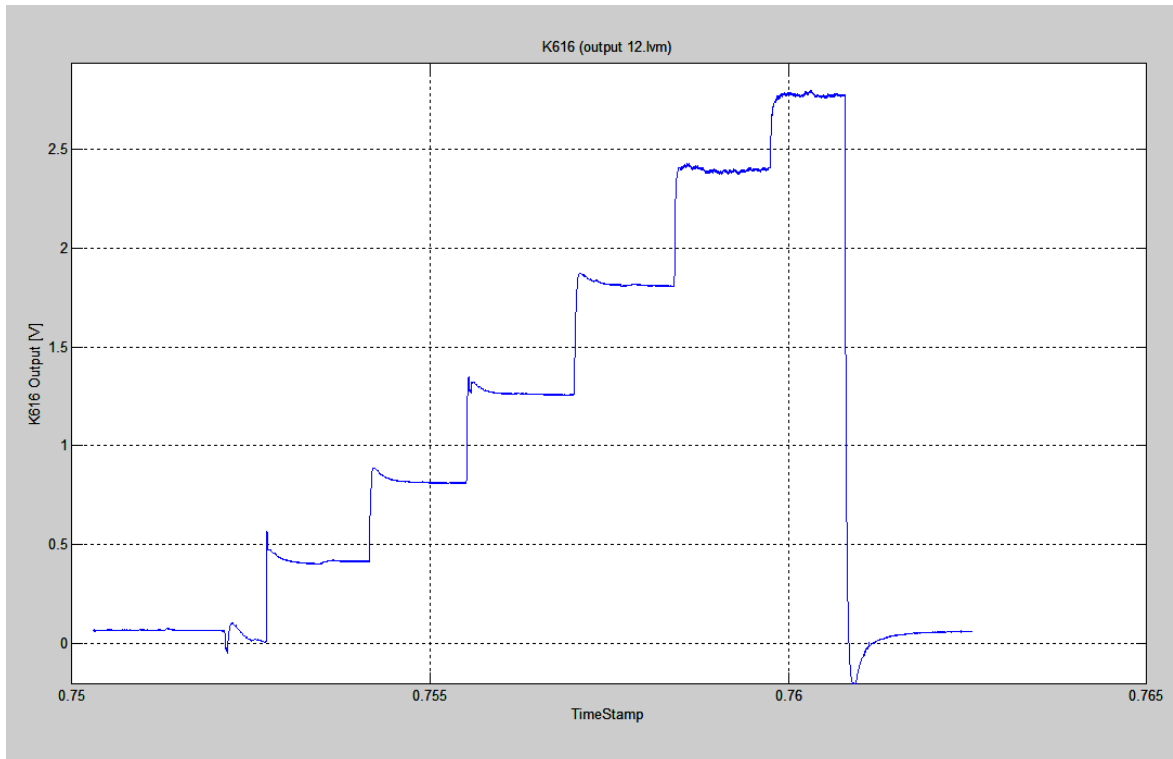


Figure 56. Electrometer current induced by condenser voltage. At increasing voltage settings (from 0 to 2500 Volts) with zero aerosol flow, background measurement of current by the Keithley electrometer (as reported in voltage on the y-axis) are in the same range as readings due to actual particle collection.

Capacitive coupling between condenser and electrometer was not reported by Whipple or for any other of the surveyed macro-scale devices, except for the continuous voltage-sweep design of Ungethüm et al., which described the development of a circuit expressly designed to compensate for the effect. Since the NanoAPAv.2 design called for a stepped, not swept, voltage, capacitive coupling was not expected to have a significant impact on the instrument's operation. However, it appears that with the extreme minaturiation of the condenser design in the NanoAPAv.2 instrument, the capacitive coupling effect is now a major impact on the operation of the design.

This issue will be returned to in Section 5.3.5, after a context has been established with Whipple-method analysis of experimental data.

5.3.3.2 Temporal instability of electrometer

Temporal instability was significant for both electrometers tested, both analog (Keithley 616) and digital (TI DDC112 EVM). Long term stability for the Keithley electrometer was examined by plotting the average value of I_{signal} at the 2500 V condenser setting for all the background datasets employing that electrometer; see Figure 57. The data shows that the electrometer had a drift of about 8 pA through the period of testing reported in the database, with short-term jumps at the earliest and latest tests, and a long decrease in the background value through the bulk of the testing.

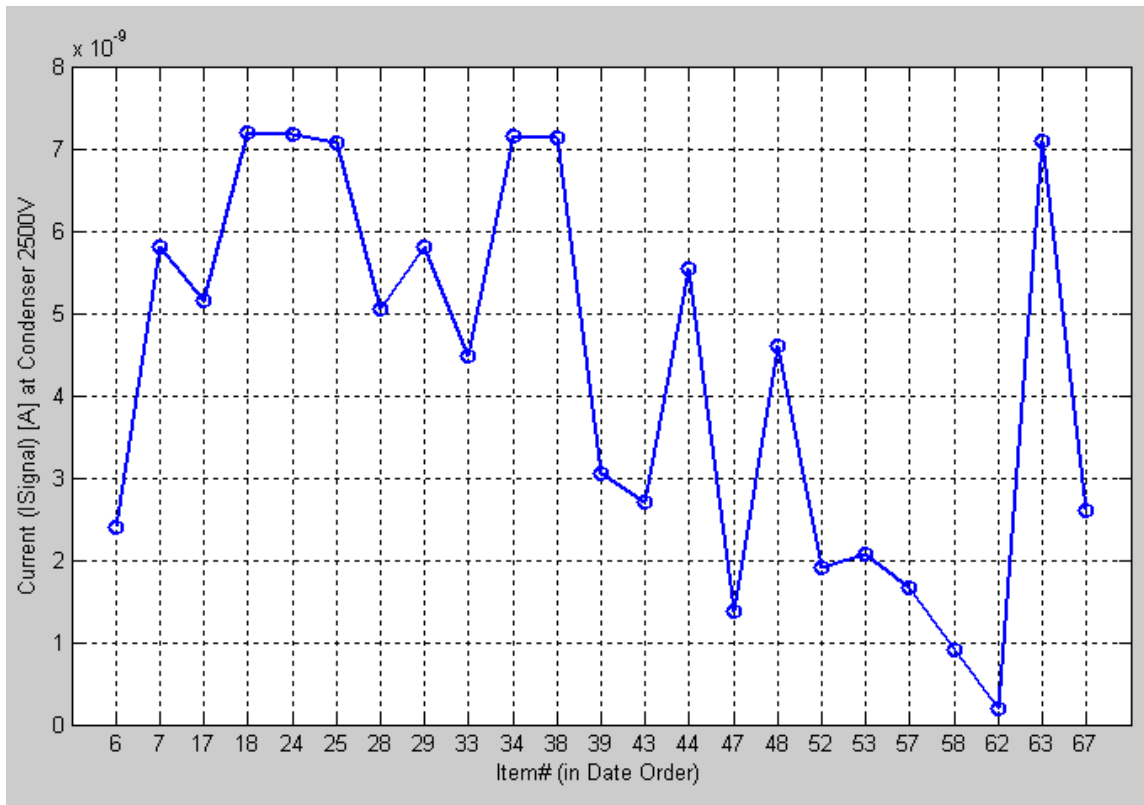


Figure 57. Long-term temporal stability of the Keithley electrometer with condensers set at 2500V and no aerosol flow.

The Keithley electrometer also experienced significant short-term drift, evidenced in the drift of the background measurements of electrometer current taken before and after sets of experiments. For an example of such measurements near the beginning and end of testing, see Figure 58.

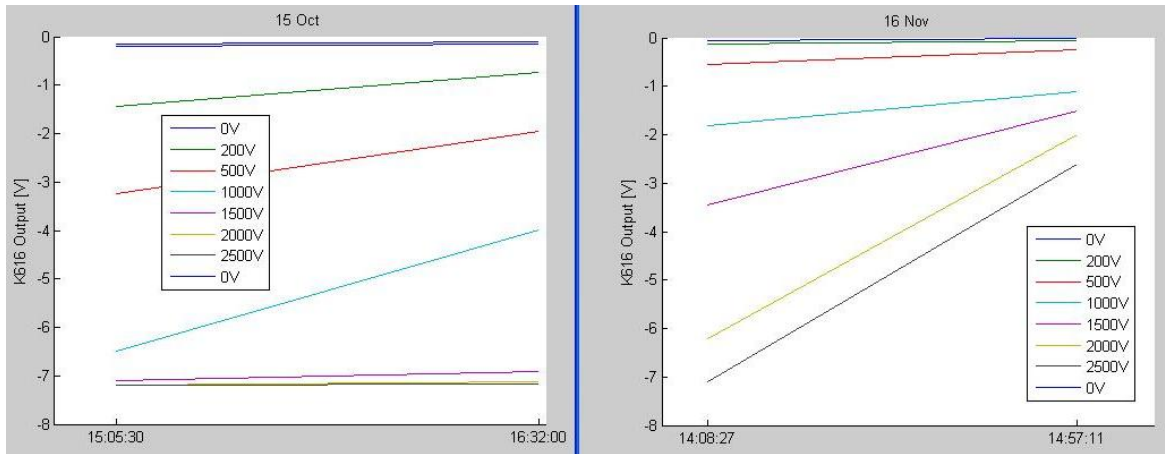


Figure 58. Short-term instability of the Keithley electrometer as evidenced by electrometer readings for each condenser voltage setting, taken before and after a set of experiments. The data on the left graph was taken on 15 October, and that on the right, 16 November. Over the course of that month, the short-term electrometer drift as a function of condenser voltage changed dramatically.

By deriving the values of I_{diff} from I_{signal} for each experiment, as described above, long-term electrometer drift and the linear portion of short-term drift should have been adequately compensated for.

The long-term drift in the analog, twenty-year old Keithley electrometer was likely due to temperature fluctuation of the device and the lab, and deterioration of the components in the electrometer. The latter may explain the increase in the non-homogeneity of the short-term drift as seen above. Other influences may have been oscillations in voltage at the condenser induced by the design of the EMCO high-

voltage converters, settling of displacement currents (currents induced by the change in voltage of a capacitor) incurred at the steps though voltage, and interference from other electric fields.

Clarkson University's MEAS device is similar in dimension to the NanoAPA microfabricated device and was found to experience similar problems: Capacitive coupling was identified as the reason the first generation MEAS had to be run at constant voltage (no voltage steps) and at flowrates less than 5 LPM, significantly reduced from their original design, and the reason that aerosol concentrations of 10^6 p/cm³ were needed to get 30-400fA signals from the instrument's electrometer and so provide an adequate signal-to-noise ratio. (Ranjan and Dhaniyala 2008)

To get electrometer noise down to levels that enabled the second generation MEAS device to make measurements over 10-100nm down to concentrations of 10^4 p/cm³, the device needed to be put into a shielded housing and its signal lines were converted from co-axial to tri-axial cables. (Ranjan and Dhaniyala 2008) Similar design changes would likely improve the performance of the NanoAPA instrument as well.

The TI DDC-112 EVM electrometer, used in the final few experiments in this project, had markedly better long-term stability; see Figure 59.

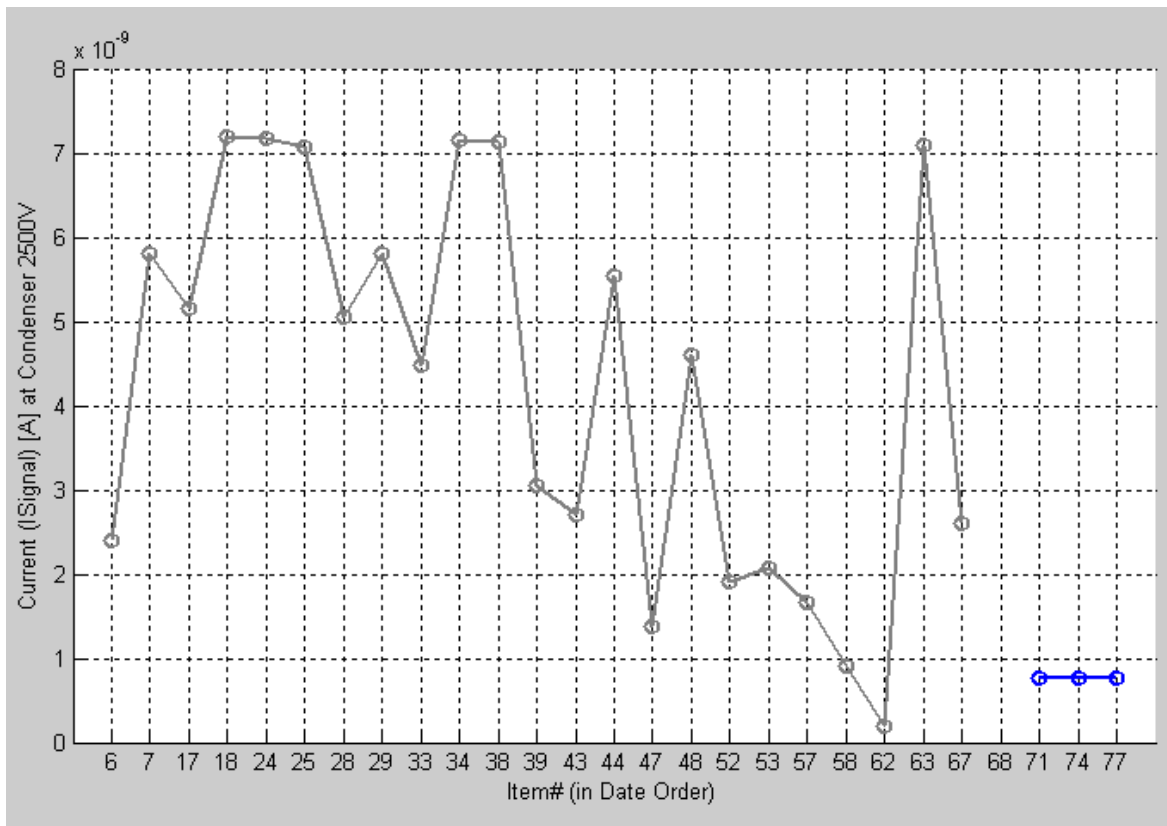


Figure 59. Long-term temporal stability of the TI electrometer (in blue) with condensers set at 2500V and no aerosol flow, compared to that of the Keithley electrometer (grey).

However, the TI electrometer’s short-term stability was as problematic as that of the Keithley electrometer; see Figure 60.

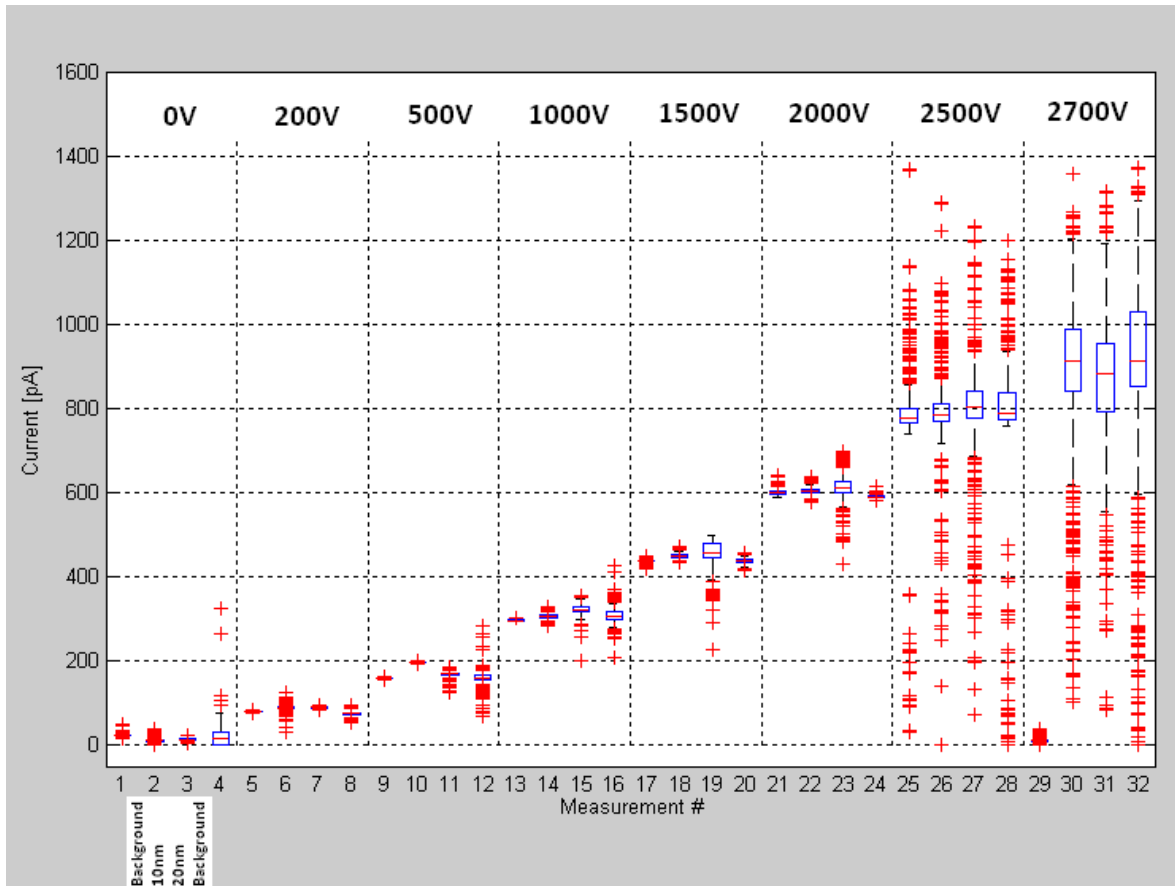


Figure 60. Short-term temporal stability of the TI electrometer, shown with box plots of the data in database items 71-74. N=600 for each measurement. The four database items correspond to measurement number as follows: 71) background, 72) 10nm, 73) 20nm, 74) background for the first voltage step, 0 Volts (see top of plot), are measurement # 1 through #4. This pattern repeats for every voltage step.

Figure 60 shows that the TI electrometers measurement of both the background and aerosol flow experiments had a large increased spread of the data as the condenser voltage increased. The issues identified above of power supply oscillations and electrical field interference were likely also responsible here as well.

5.3.4 Whipple calculation with the best database subset

To see if the datasets collected could provide size distributions following the equations and data-reduction methods described by Whipple (1960), the best-performing subset of the data as identified above was used. The current-concentration linear regression for this subset, Oleic acid, PPK31, ≤ 0.3 LPM, ≤ 20 nm, is shown again in Figure 61.

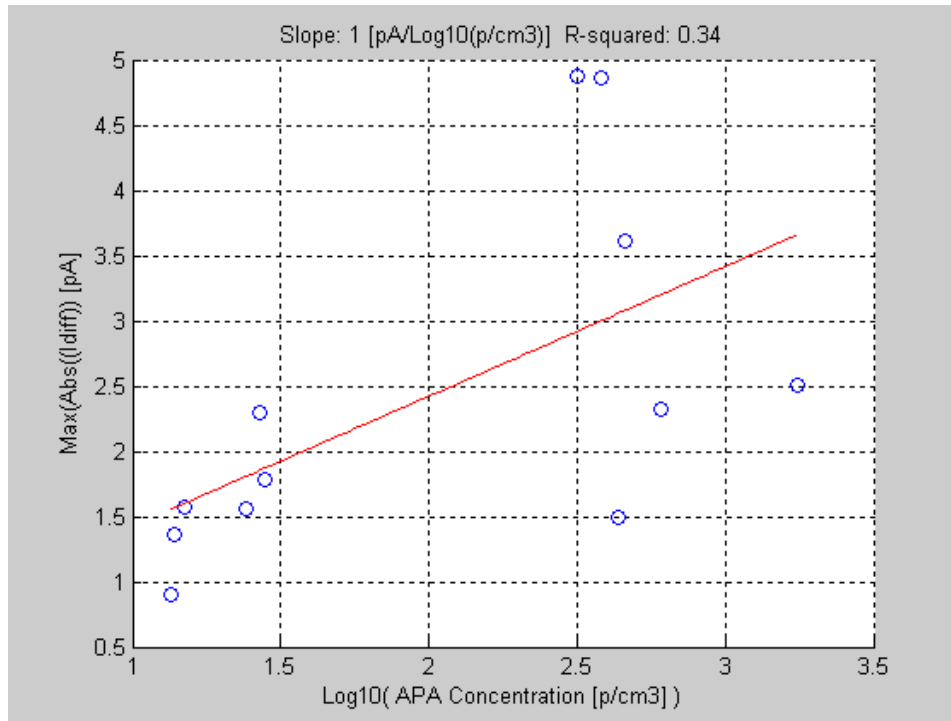


Figure 61. Current-to-concentration linear regression of the database subset.

The database entries of data for these experiments are shown in Figures 62 and 63. The datasets contained in the database: I_{source} , I_{diff} , Concentration Drift Factor, and Particle Pass-through Ratio were described in the introduction to Section 5.3. The concentration drift factors for this subset of experiments (Figure 63, left plot) have both positive and negative slopes because the particle concentration produced by the

Standard Aerosol apparatus increased over time during some experiments (positive slope), and decreased over time for other experiments (negative slope). The only known cause for concentration drift was increase in atomizer solute concentration during an experiment, as described in the introduction to Section 5.3 and explained in more detail in the standard operating procedure of the Standard Aerosol apparatus in Appendix A; the cause for decrease in particle concentration during some of the experiments is unknown.

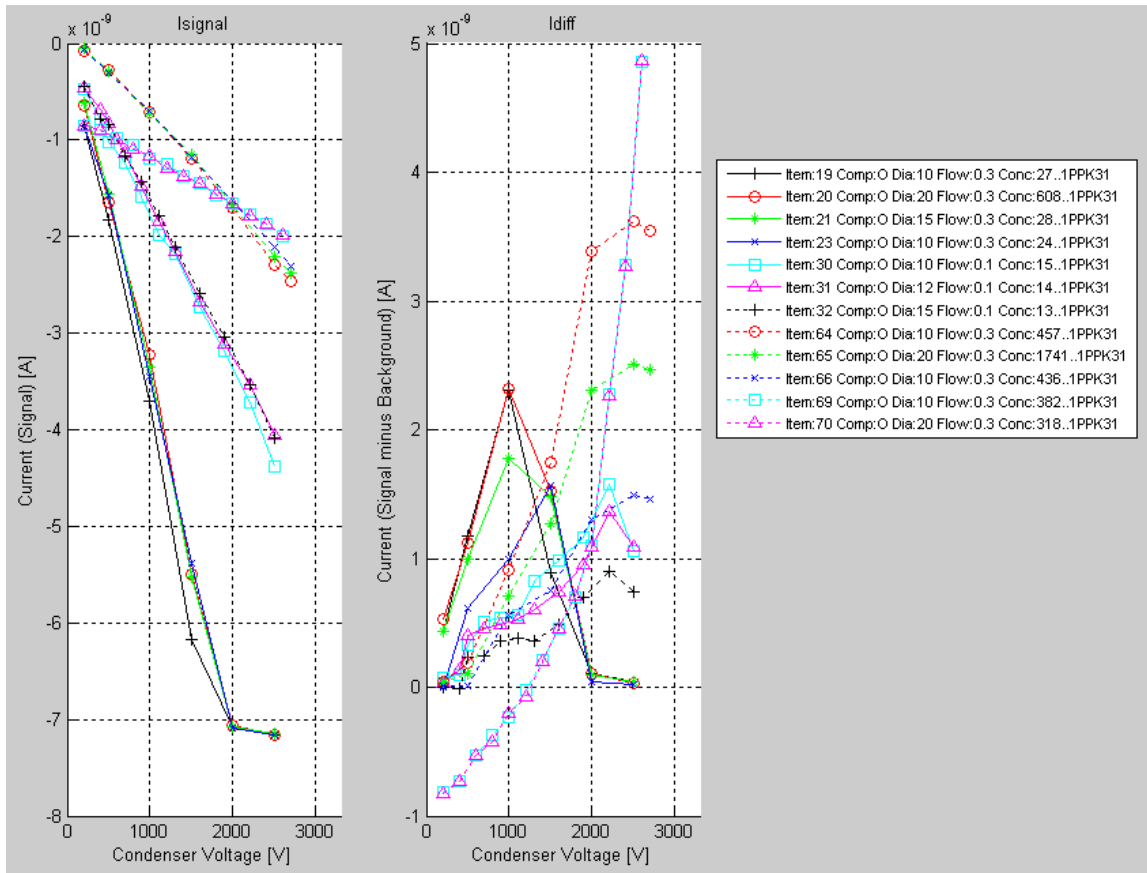


Figure 62. The I_{signal} and I_{diff} data in the database for the selected subset of experiments.

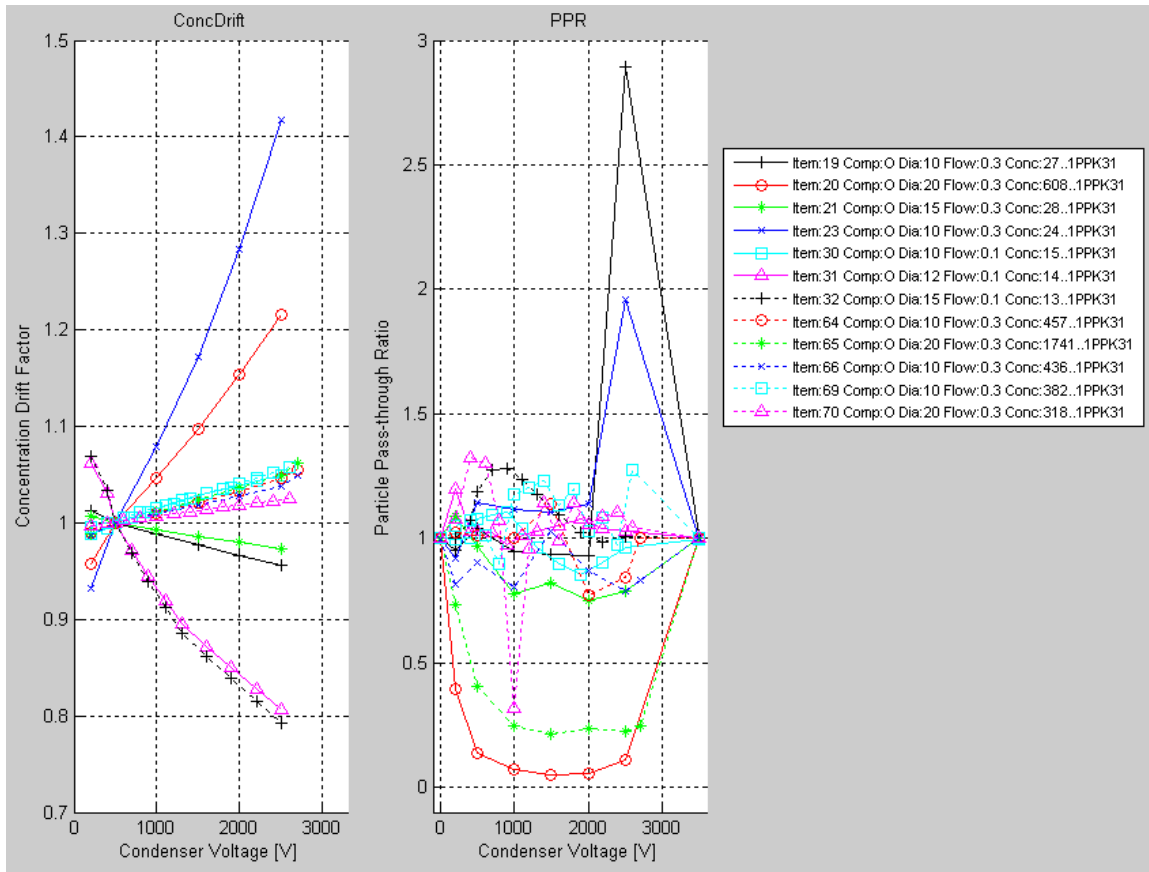


Figure 63. The Concentration drift factor and particle pass-through ratio data in the database for the selected subset of experiments.

Figures 64, 65, and 66 show the calculation of the number-size distributions according to the Whipple method. The theoretical particle diameter used for the x-axis of Figure 66 was determined from the critical mobility (x-axis of Figure 64 and 65) using the relationship of particle diameter to critical mobility of Flagan (1998) as shown in Figure 26.

The first few experiments (items #19 to 23) in the subset had characteristic I/V curves (Figure 65) as expected from the Whipple method (refer to Figure 14) and single peaks in the size distribution (Figure 66) as expected from the monodisperse input

aerosol, but these results were not replicated in the further experiments. Furthermore, the input particle diameters for these four experiments varied, and the peaks for each did not follow the input particle diameter. The input particle diameters for these experiments were #19: 10nm (black line), #20: 20nm (red line), #21: 15nm (green line), and #23: 10nm (blue line); see Figure 66. The first 10nm experiment (#19, black line) produced a peak at 6.3 nm theoretical diameter, but the repeat 10nm experiment (#23, blue line) did not find a peak; at 6.3 nm theoretical diameter its size distribution was still increasing. The 20nm experiment (#20, red line) had a peak at 6.3nm, like the first 10nm experiment; the 20nm peak was expected to be at correspondingly larger theoretical diameter. The 15nm experiment (#15, green line) appeared to be heading for a peak larger than 6.3 nm, which makes sense in relation to only the first 10nm experiment.

The early experiments show distributions with similar maximum particle distributions on the order of 10^{10} p/cm³ (Figure 66), much higher than the actual concentrations (see “Conc” in the figure legends), and they are very similar to each other, even though each experiment had quite different concentration. In the Whipple method, the particle concentration is indirectly proportional to the capacitance of the condenser (refer to Equation 3-3 in Section 3.3.2) and so the inflated values of particle concentration found in this analysis could have come from an under-estimated value of condenser capacitance. As described in Section 4.3, the capacitance of the condenser was estimated directly from its designed dimensions; for future work on the NanoAPA instrument, the actual capacitance of the condenser, as built, should be measured.

After the first set of experiments, run at 0.3 LPM (items 19 to 23, Figures 64 to 66), in this subset had inconclusive results, the apparatus was set to a flowrate of 0.1 LPM for the next set of experiments (items 30 to 32, Figures 64 to 66) to enable measurements into larger particle diameters, but these results showed no peaks. If a single peak was not found by the analysis, then the size distribution of the input monodisperse aerosol was not measured; a size distribution of a monodisperse aerosol is comprised of a single peak. (Hinds 1999)

Finally, a set of experiments (items 64 to 70, Figures 64 to 66) were performed that attempted to identically replicate the first set of experiments, but these also showed inconclusive data. The reason the instrument was unable to measure even a part of a size distribution for any experiment after #23 was likely due to the long term and short-term temporal instability of the Keithley electrometer described in Section 5.3.3.2. The instability of the electrometer caused the measurements of background (zero-flow) electrometer output to differ within run and run-to-run by a magnitude larger than the I_{diff} signal derived using those background measurements and used to calculate the size distribution.

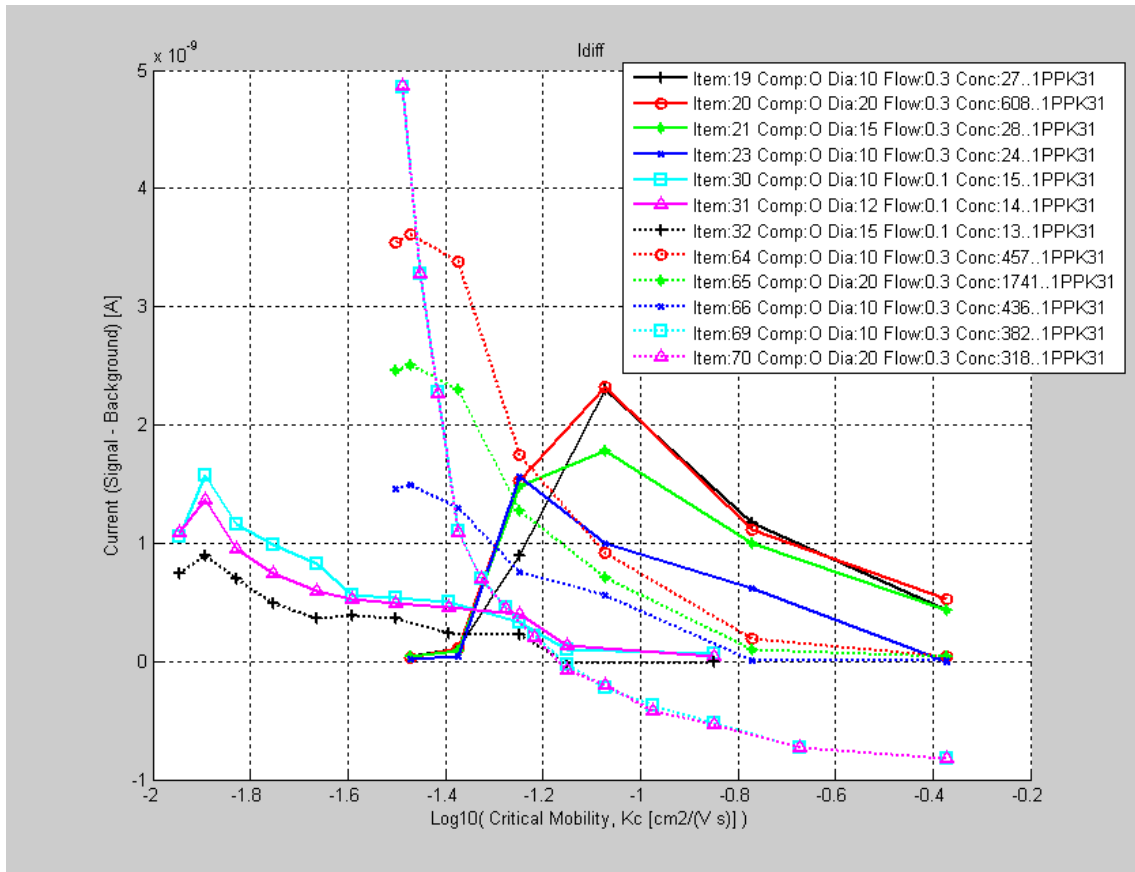


Figure 64. An enlarged view of the I_{diff} data for the experiment subset.

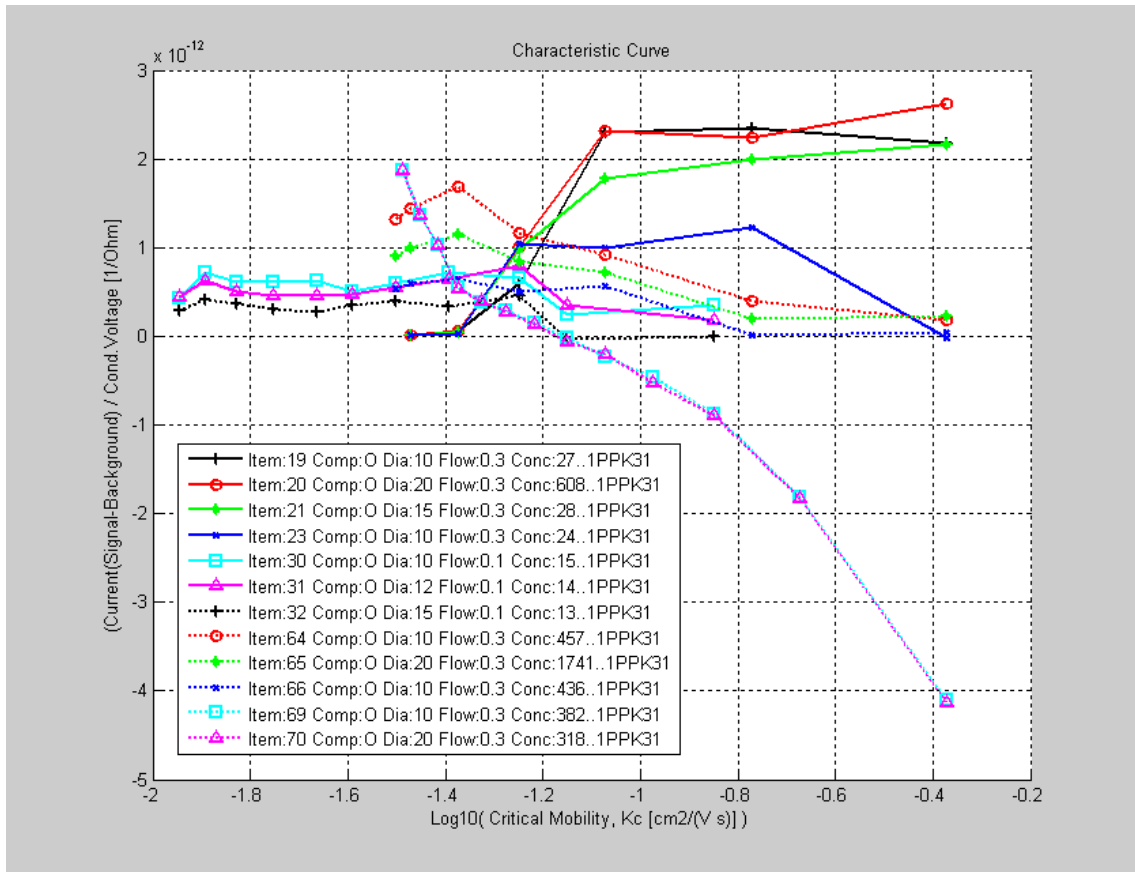


Figure 65. The Whipple characteristic curves calculated for each dataset in the subset.

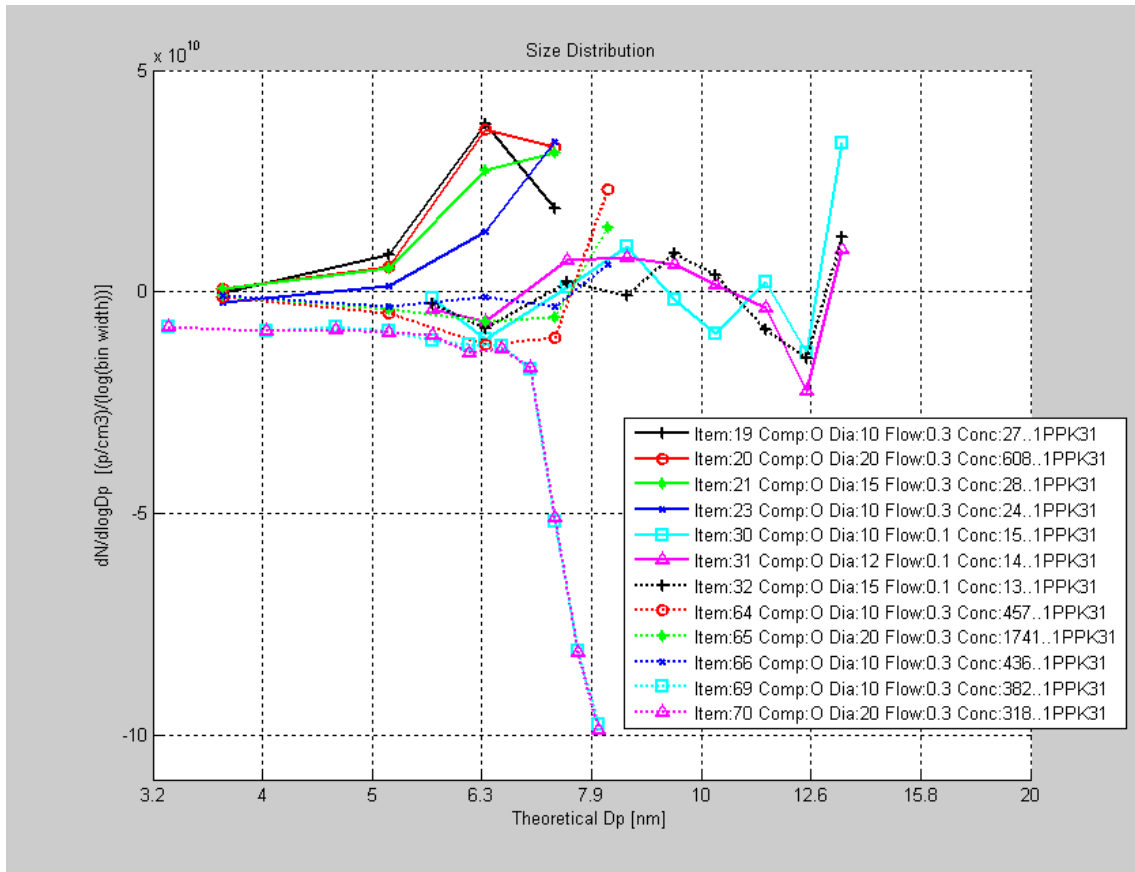


Figure 66. The Whipple size-distributions for the datasets in the subset.

5.3.5 Whipple calculation with the TI electrometer

When the TI electrometer had been acquired and qualified for operation, a few experiments were run at settings similar to those for the database subset above, to see if this new, digital, electrometer could produce usable size distributions.

The current-to-concentration data for these experiments are shown in Figure 67. They showed a negative correlation, not what was expected according to the design.

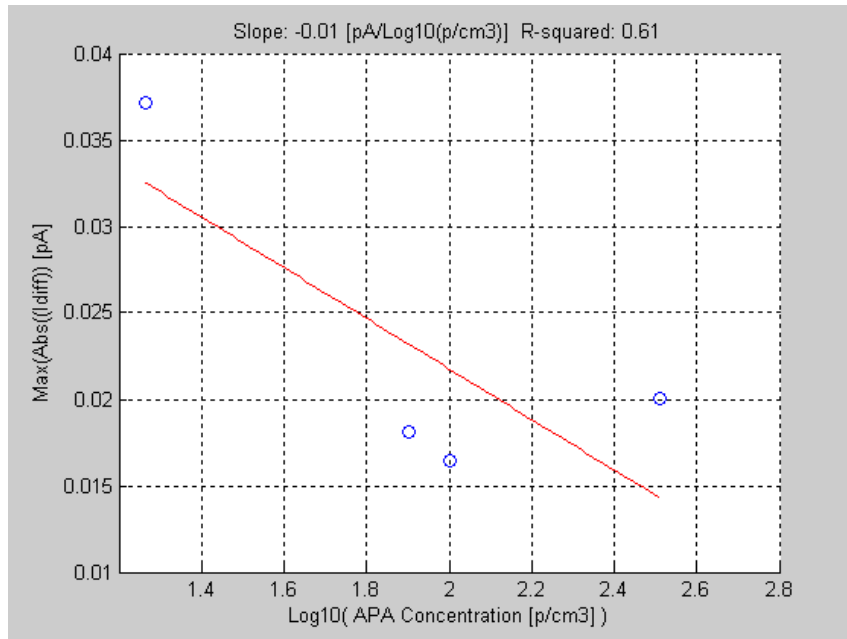


Figure 67. Current-to-concentration correlation for experiments employing the TI electrometer.

Figures 68 through 72 show the rest of the Whipple analysis for the TI experiments, using the same analysis steps as described in Section 5.3.4. No usable size distributions were obtained; the short-term electrometer drift issue described in Section 5.3.3.2 likely prevented successful measurement, and so the digital TI electrometer, as implemented, did not provide the expected improvement over that of the analog Keithley electrometer. These issues will be discussed further in the following two sections, 5.3.6 and 5.3.7, and in the conclusion section, Section 6.2.

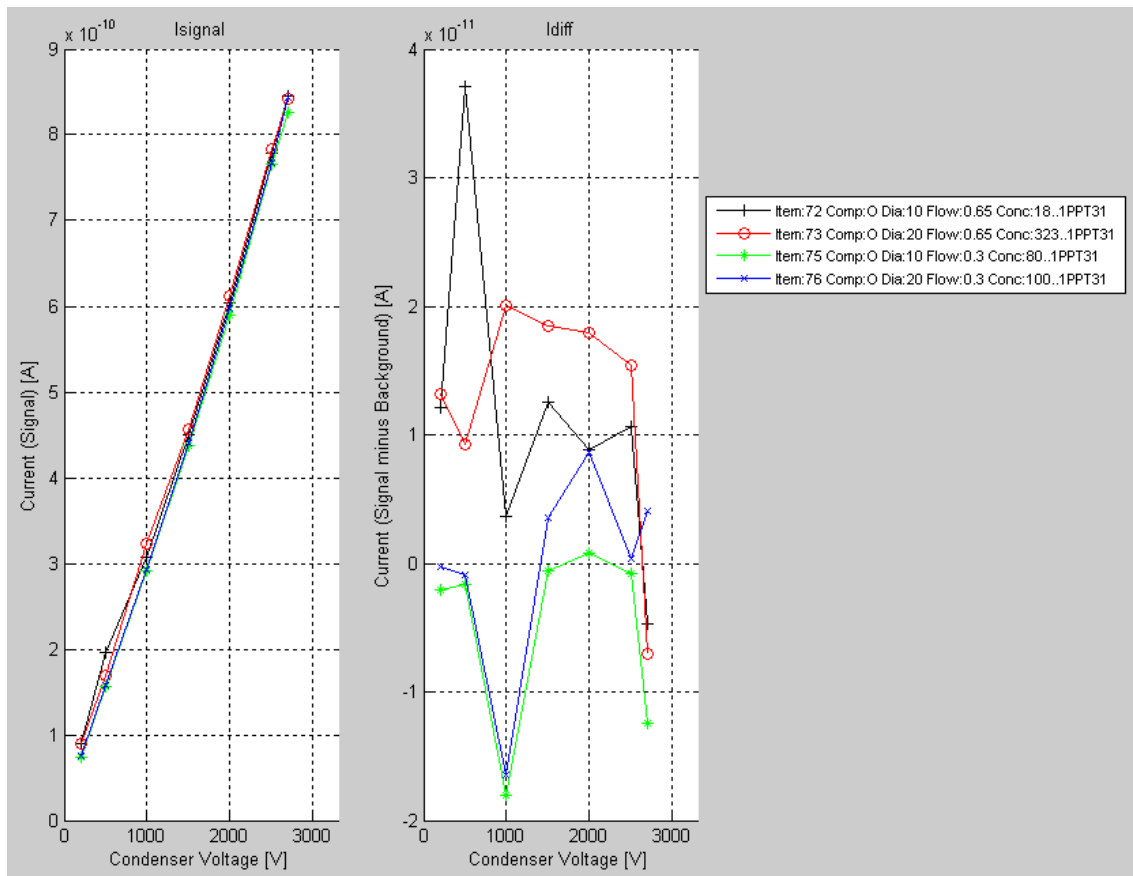


Figure 68. The I_{signal} and I_{diff} data in the database for the TI electrometer experiments.

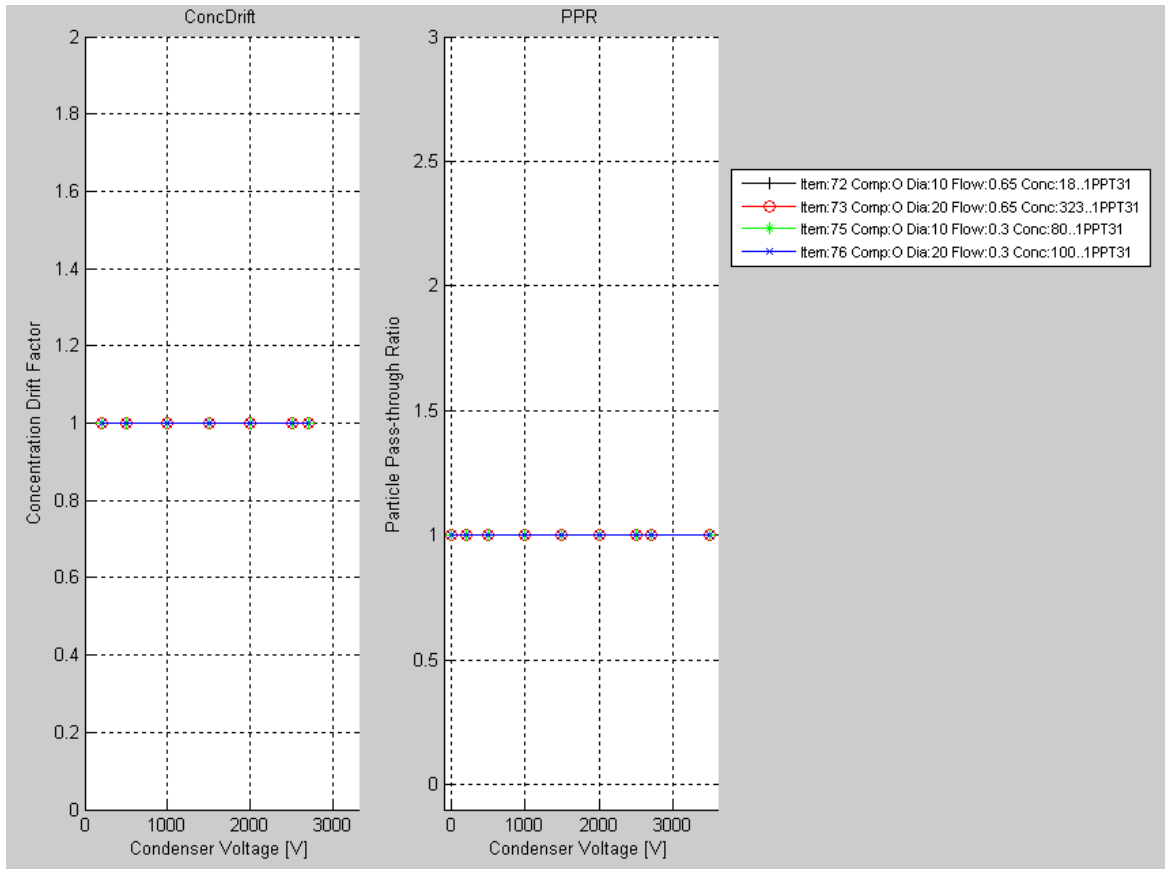


Figure 69. The Concentration drift factor and particle pass-through ratio data in the database for the TI electrometer experiments. (The CPC for these experiments was not set up to record concentration measurements, and so the database has no data for these parameters; however, the COA atomizer was being used in the Standard Aerosol apparatus for these experiments, and the concentration drift was therefore negligible.)

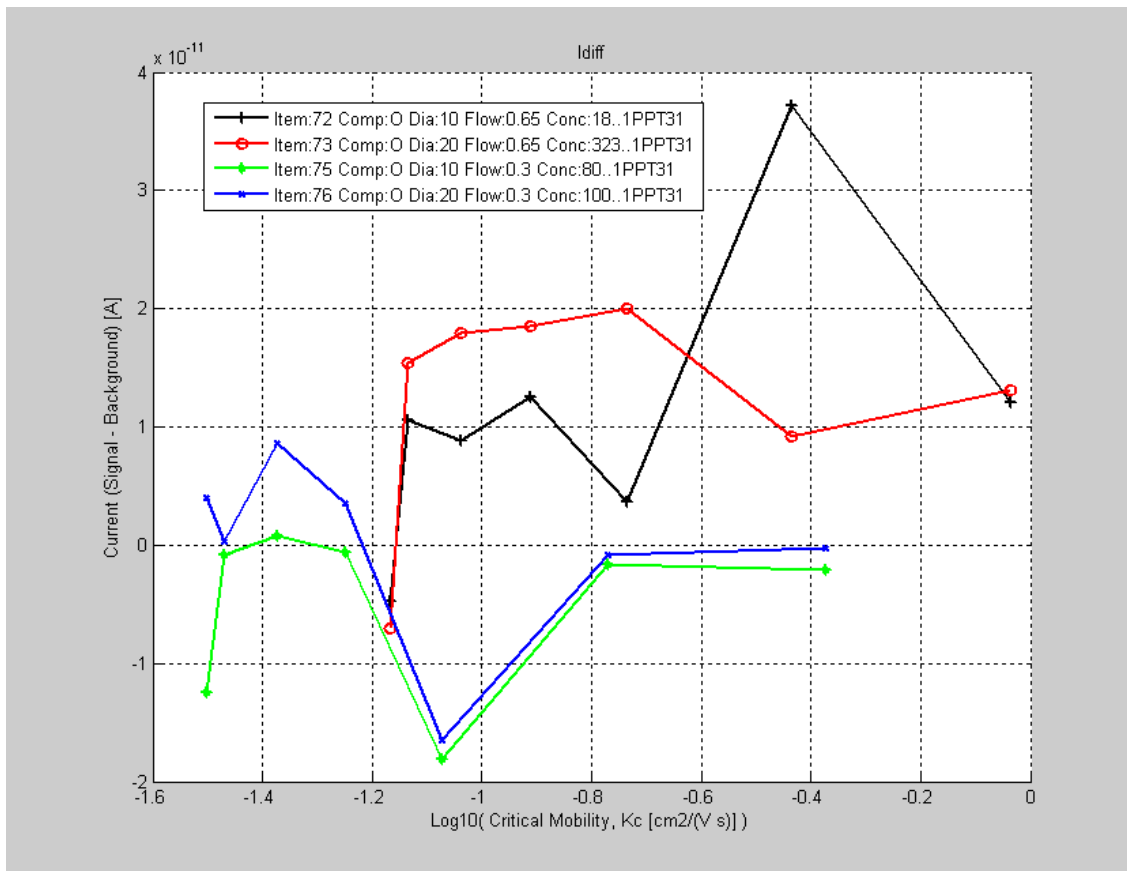


Figure 70. An enlarged view of the I_{diff} data for the TI experiments.

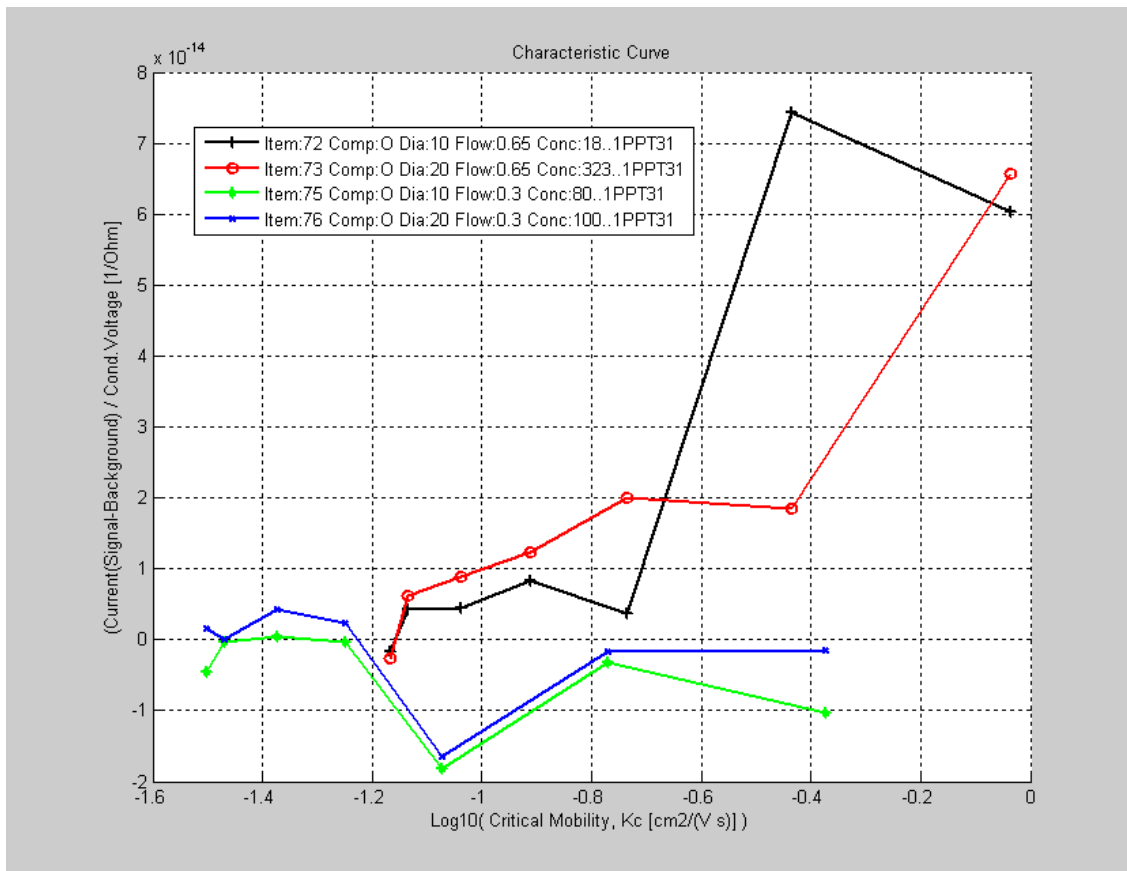


Figure 71. The Whipple characteristic curves calculated for the TI experiments.

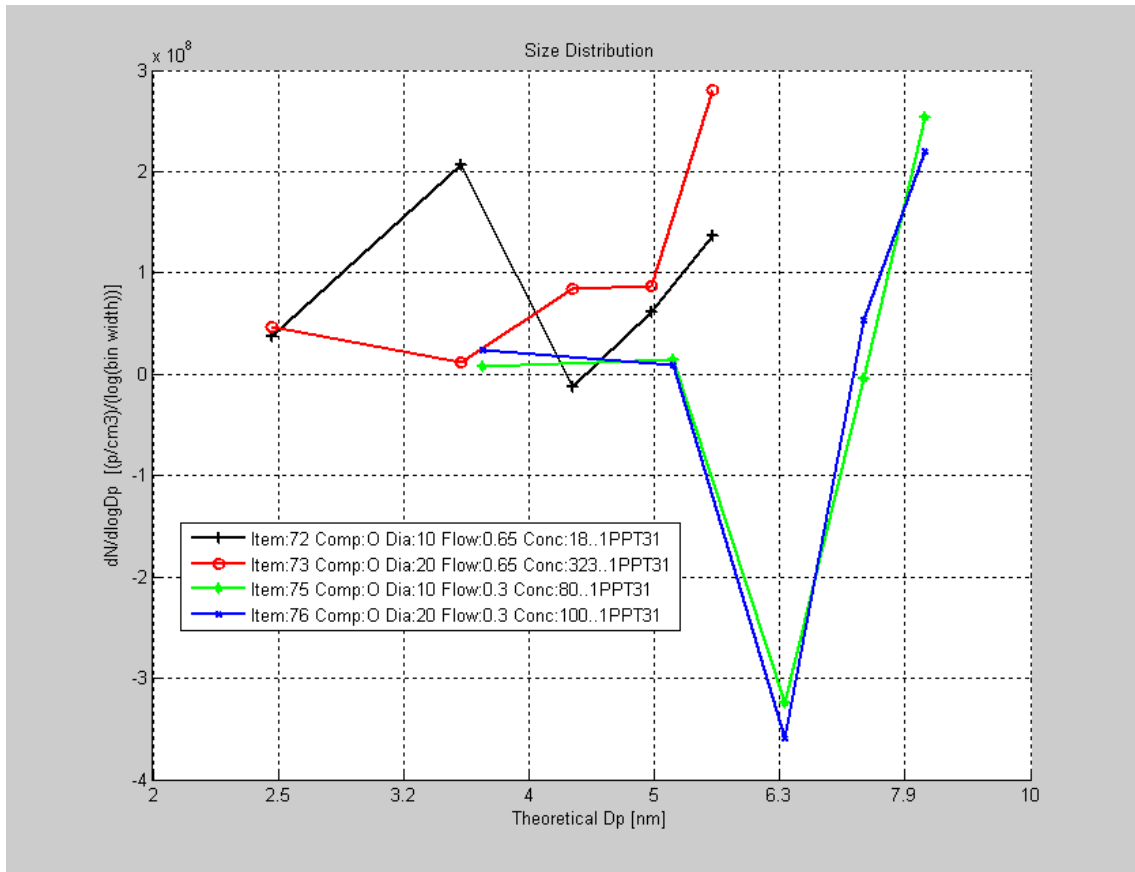


Figure 72. The Whipple size-distributions for the TI experiments.

5.3.6 Leakage current

Although air is a dielectric and so is normally considered to be non-conductive below the threshold for dielectric breakdown, all physical dielectrics in a capacitor will experience some, very small, current known as “leakage current”. (Bobrow 1985) A calculation of the leakage current for the microfabricated device was performed as follows.

The resistance, R [Ω (ohms)], of a homogenous material of uniform cross section in a capacitor for steady current is $R = d / (\sigma A)$, where d is the separation

distance between the capacitor plates (2mm, see above), σ is the electrical conductivity of the dielectric, and A is the effective area of the capacitor. (Cheng 1992) The electrical conductivity of dry air at sea level is 2.5×10^{-14} [$1/(\Omega \text{ m})$]. (Weast 1983) Only one condenser was evaluated for leakage current, the second (Condenser 2, Figure 27), because the first condenser (Condenser 1, Figure 27) was connected to the high-voltage return of the power supply, and so did not have a path to leak current to the electrometer. The actual effective area of the capacitor was unknown, but a likely minimum and maximum value was estimated: The minimum likely effective area was the area of the facing screen plates as designed, 1.18 mm^2 . The maximum likely effective area was the full facing area covered by the screen plates (i.e., without the holes in the screen subtracted out), 3.1 mm^2 . The actual effective area was somewhere between these two values. Therefore, the likely range of the value of the electrical resistance of the air in the condenser was calculated to be $2.58\text{--}6.78 \times 10^{12} \Omega$. Using the relation $I = V / R$, minimum and maximum estimates of leakage current in the second condenser were calculated at each of the condenser voltage set points, and plotted with the I_{signal} and I_{diff} data from the TI electrometer experiments; see Figure 73.

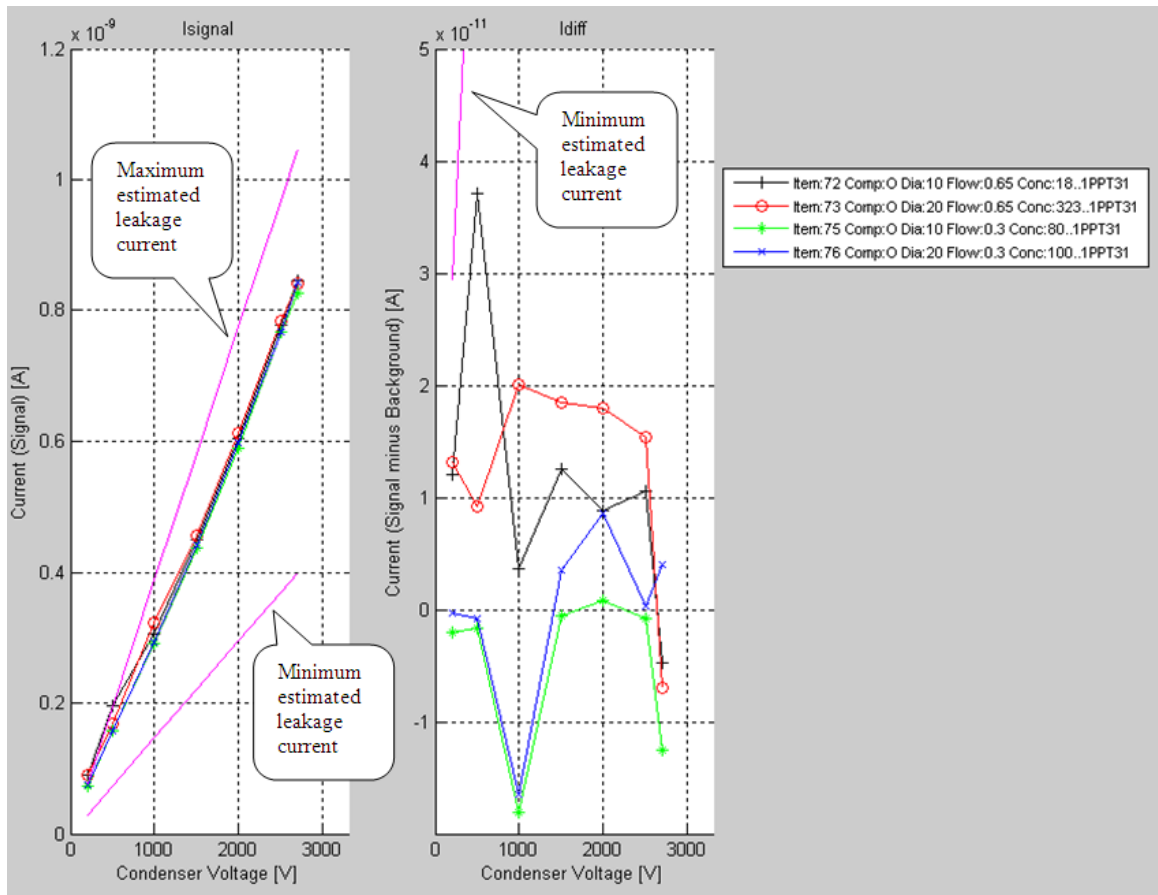


Figure 73. I_{signal} and I_{diff} data for the TI electrometer experiments with the minimum and maximum estimated values of leakage current shown as solid lines.

It can be seen in the left chart of the Figure 73 that all the I_{signal} values in the TI electrometer experiments fall inside the range of estimated leakage current, and in the right chart that all the I_{diff} values are below the minimum estimated leakage current. Therefore, it is likely that the leakage current from the second condenser was much larger in magnitude than any particle-count signal. This, coupled with low concentrations of generated aerosols in these experiments, may explain why the much more stable and calibrated TI electrometer also failed to produce repeatable size distribution measurements.

With this new insight, the Keithley experiments were revisited by adding the estimated leakage current to the long-term stability chart in Figure 74.

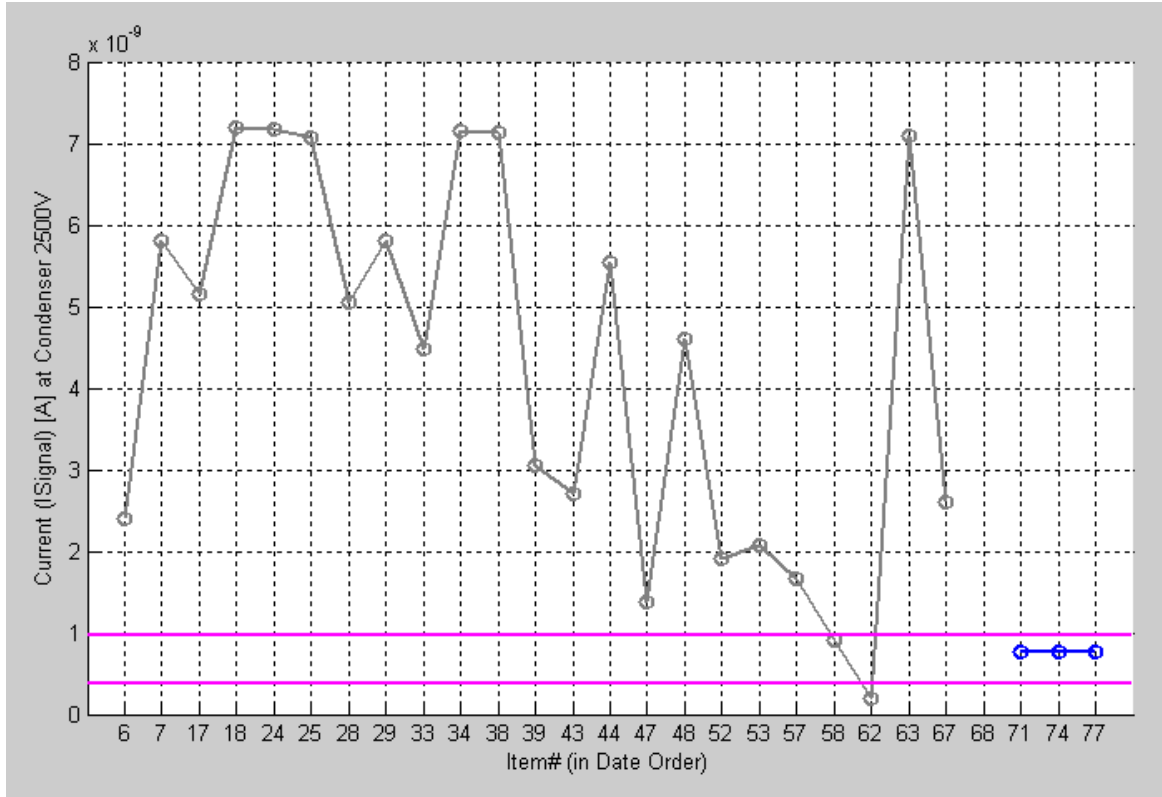


Figure 74. Long-term temporal stability of the Keithley electrometer (grey) and TI electrometer (blue) with condensers set at 2500V and no aerosol flow, with the range of estimated leakage current at 2500V shown as horizontal lines.

There are a number of Keithley experiments in the database above the maximum estimated leakage current, but the temporal drifts, long and short term, of that electrometer prevented any calibrated examination of the actual signal-to-leakage ratio in those experiments.

5.3.7 Uncertainty analysis

The NanoAPAv.2 proof-of-concept instrument's inability to produce repeatable size distribution measurements could also have been caused by inadequate ability of the electrometers and CPC instrument to record repeatable measurements (of electrometer output voltage and particle concentration, respectively) free of systematic errors. To evaluate the uncertainty in the measurements involved in the proof-of-concept testing, the 1Hz data of CPC particle concentration and Labview electrometer output voltages were examined. For each condenser voltage setting in all the non-background experiments, each set of raw data was submitted to a statistical analysis which resulted in values of mean, standard deviation, coefficient of variance (COV), and number of samples. The COV was calculated as the standard deviation divided by the mean.

The result of the uncertainty analysis for a subset of condenser voltage settings shared by most of the experiments, the set [0 500 1000 1500 2000 2500 0] Volts, is shown in Tables 10 through 13. Tables 10 and 11 list the uncertainty calculations for the electrometer data, and Tables 12 and 13 for the CPC data.

Considering the electrometer uncertainty first, the data for the first zero voltage settings in Table 10 demonstrates that the Keithley electrometer (experiments 1-70) showed a general trend of increasing electrical circuit noise over the course of all experiments, as measured by COV, with the early experiments (experiment #32 and lower) having COV less than about 5%, but then by the later experiments (experiment #35 and higher) had much higher COV values, as high as 25 and 50%. This is another perspective on the temporal stability of the Keithley electrometer described above in

section 5.3.3.2. Comparing the calculations for the first zero settings with the final zero setting at the other side of the table, it can be seen that the noise (COV) was much higher throughout the Keithley electrometer experiments, with the COV values at the return-to-zero in the hundreds of %. This was likely due to residual effects on the electrometer circuit from previous settings of high voltage; there were transient oscillations in the circuit that had not settled out by the time the final zero volt measurements were taken. A longer delay time than the one minute used in these characterization tests may be required for future measurements in order to limit the impact of this effect. The four entries in Table 10 for the TI electrometer (experiments 72-76) all exhibit high COV at zero voltage; this is a reflection of the large spread in the measurements with this electrometer shown above in Figure 60. As for the uncertainty in the electrometer data at the non-zero values of condenser voltage (Table 10), both electrometers exhibited good performance with low COV throughout the voltage settings 500 to 2000 Volts, most at 2% or lower, and the highest value, 7%. The Keithley electrometer performed well at 2500V, but the TI electrometer exhibited COV of about 20 to 40% at that voltage; the reason proposed earlier for this behavior was the increased sensitivity of the TI electrometer responding to the oscillations produced by the voltage regulation of the EMCO high voltage power supply. Table 11 lists the number of samples in each calculation of electrometer uncertainty; most of the calculations used 30 or more data points which provided stable statistics. A few isolated calculations (and all of experiments 69 and 70) were performed on ten data

points or less, providing less reliable measurements of uncertainty. As these were only a few calculations, they do not cast doubt on the conclusions made above.

Table 11. Number of samples used in electrometer uncertainty calculations.

Exp#	Condenser Setting [V]						
	0	500	1000	1500	2000	2500	0
1	300	300	300	300	300	300	300
2	300	300	300	300	300	300	300
3	300	300	300	300	300	300	299
4	300	300	300	300	300	300	300
5	300	300	300	300	300	300	300
8	30	25	30	30	30	25	30
9	30	30	30	30	30	30	30
10	30	30	30	30	30	30	30
11	30	30	30	30	30	30	30
12	30	30	30	30	30	20	30
13	30	30	30	30	30	20	30
14	30	30	30	30	30	25	30
15	31	30	31	30	20	30	31
16	30	25	30	30	30	30	20
19	30	30	30	30	30	20	30
20	30	30	30	30	30	30	30
21	30	30	30	30	30	30	30
22	30	30	30	30	30	30	30
23	30	30	30	30	30	30	30
26	30	30				30	30
27	30	30				30	30
30	30	30				30	30
31	30	30				10	30
32	30	30				10	30
35	10	30	30	30	30	30	30
36	30	30	30	30	30	30	30
37	10	30	30	30	30	30	30
40	30	30	30	30	20	25	30
41	30	30	30	30	30	20	30
42	25	30	30	30	30	30	30
45	30	30	30	30	30	30	30
46	30	30	30	30	30	25	30
49	30	30	30	30	30	30	30
50	31	30	30	30	29	15	30
51	30	30	30	30	30	8	30
54	30	30	30	30	30	30	30
55	30	30	30	30	25	10	30
56	30	30	30	30	30	15	30
59	30	30	30	30	30	30	30
60	30	30	30	30	30	30	30
61	30	24	30	30	30	30	30
64	30	31	30	30	31	10	30
65	30	30	30	30	30	30	30
66	30	30	19	15	30	30	30
69	10		10		10		5
70	10		10		10		5
72	600	600	600	600	600	600	
73	600	600	600	600	600	600	
75	600	600	600	600	600	600	
76	600	600	600	600	600	600	

The uncertainty metrics for the CPC particle concentration data for the non-background experiments are shown in Tables 12 and 13. The COV values for both zero voltage settings (Table 12) are nearly all below 10%, and are similar for both zero voltage measurements, demonstrating that the experimental methods worked fine for the particle concentration measurements; there was no increasing trend through time or carryover effect of high voltages as seen in the electrometer uncertainty calculations. However, the COV values for the non-zero condenser value settings are highly variable, and without much of a trend other than degrading from the sub-5% values of the very early experiments to values above 10% and some over 100% on later experiments. This result confirms the observations made above in Section 5.3.1: it appears that oleic acid particles accumulated on the condenser plates experiment after experiment, resulting in particles captured in previous experiments being released and counted by the CPC during subsequent experiments. Concerning the number of samples for the uncertainty calculations, Table 13 shows a similar situation for the CPC calculations as that for the electrometer calculations – a few scattered calculations were performed with less than ten data points, but most were performed with 30 or more data points.

The uncertainty calculations support the observations of electrometer instability, electrometer drift, and particle re-entrainment noted during the testing of the proof-of-concept instrument.

Table 12. Uncertainty calculations for CPC particle concentration data: mean, standard deviation, and coefficient of variance for data at different voltage settings with proof-of-concept instrument.

Exp#	Condenser Setting [V]														
	0	500	500	1000	1000	1500	1500	2000	2000	2500	2500	2500	0	0	0
	Mean	St.D.	COV	Mean	St.D.	COV	Mean	St.D.	COV	Mean	St.D.	COV	Mean	St.D.	COV
	[p/cm ³]	[p/cm ³]	[%]	[p/cm ³]	[p/cm ³]	[%]	[p/cm ³]	[p/cm ³]	[%]	[p/cm ³]	[p/cm ³]	[%]	[p/cm ³]	[p/cm ³]	[%]
1	1.18E+03	3.63E+01	3	1.16E+03	5.30E+01	5	1.18E+03	4.92E+01	4	1.21E+03	5.18E+01	4	1.22E+03	5.40E+01	4
2	2.70E+03	6.92E+01	3	2.47E+03	9.42E+01	4	2.30E+03	7.24E+01	3	2.14E+03	6.86E+01	3	1.96E+03	6.18E+01	3
3	1.60E+04	6.50E+02	4	2.27E+03	8.01E+01	4	9.29E+01	2.84E+01	3	6.18E+00	1.88E+00	44	4.27E+00	6.43E-01	15
4	1.43E+03	4.88E+01	3	9.10E+02	3.24E+01	4	4.06E+02	1.51E+01	4	4.47E+02	3.59E+01	8	7.05E+02	6.37E+02	9
5	1.56E+04	8.95E+02	6	2.36E+03	7.01E+01	3	3.88E+02	2.42E+01	6	3.12E+01	1.12E+00	7	2.56E+00	1.59E-01	6
8	4.86E+02	2.01E+01	2	5.82E+02	1.88E+01	3	4.49E+02	2.15E+01	5	3.39E+02	2.24E+01	7	6.51E+02	4.90E+01	8
9	1.52E+03	7.39E+01	5	1.22E+03	4.75E+01	4	1.06E+03	5.06E+01	5	8.70E+02	3.86E+01	6	7.50E+02	3.96E+01	5
10	4.83E+02	2.09E+01	4	2.48E+02	1.28E+01	5	1.65E+02	9.30E+00	6	1.09E+02	9.71E+00	9	8.58E-01	2.25E+00	3
11	2.07E+02	1.76E+01	9	1.93E+02	1.27E+01	7	1.83E+02	1.43E+01	8	1.63E+02	1.40E+01	9	1.52E+02	1.41E+01	9
12	3.29E+02	1.46E+01	4	3.12E+02	1.79E+01	6	2.98E+02	1.58E+01	5	2.78E+02	1.53E+01	6	2.66E+02	1.91E+01	7
13	7.23E+02	2.29E+01	3	7.15E+02	3.75E+01	5	7.13E+02	1.99E+01	3	7.01E+02	2.30E+01	3	6.95E+02	3.28E+01	5
14	7.08E+03	1.57E+02	2	1.20E+03	6.62E+01	6	2.29E+02	1.46E+01	6	1.95E+01	7.05E-01	4	1.74E+00	2.75E-01	16
15	9.30E+02	4.05E+01	4	5.07E+01	1.25E+00	2	1.59E-01	9.83E-02	62	1.00E-01	4.24E-17	0	4.89E-01	1.52E-01	31
16	7.12E+01	1.09E+00	2	1.00E-01	2.84E-17	0	1.00E-01	4.24E-17	0	1.00E-01	4.24E-17	0	2.59E-02	2.64E-02	102
19	2.68E+01	1.04E+00	4	2.85E+01	1.07E+00	4	2.63E+01	7.00E-01	3	2.62E+01	2.54E+00	10	2.64E+01	1.35E+00	5
20	6.62E+02	3.95E+01	6	8.23E+01	4.33E+00	5	4.13E+01	7.19E+00	17	2.72E+01	1.07E+00	4	2.85E+01	1.57E+00	6
21	2.81E+01	1.12E+00	4	2.75E+01	9.81E-01	4	2.23E+01	2.64E+00	12	2.37E+01	2.07E+00	9	2.19E+01	7.14E-01	3
22	2.41E+04	7.75E+02	3	1.17E+04	5.87E+02	5	7.06E+03	2.22E+02	3	4.45E+03	1.69E+02	4	2.95E+03	1.53E+02	5
23	2.73E+01	1.19E+00	4	2.71E+01	9.08E-01	3	2.47E+01	2.30E+00	9	2.23E+01	4.72E-01	2	2.10E+01	3.95E-01	2
26	4.71E-01	2.07E-02	4	4.46E-01	1.24E-02	3									
27	4.80E-01	1.77E-02	4	4.71E-01	1.19E-02	3									
30	5.09E+00	5.64E-01	11	5.38E+00	5.10E-02	1									
31	4.20E+00	5.35E-01	13	4.74E+00	1.04E-01	2									
32	4.10E+00	3.27E-02	1	5.39E+00	1.10E-01	2									
35	4.40E+03	1.53E+02	3	3.64E+03	1.18E+02	3	3.20E+03	9.14E+01	3	3.18E+03	3.01E+02	9	2.80E+03	8.01E+01	3
36	3.93E+03	1.34E+02	3	3.56E+03	1.59E+02	4	3.49E+03	1.23E+02	4	3.58E+03	1.57E+02	4	3.37E+03	9.99E+01	3
37	4.21E+03	1.45E+02	3	3.31E+03	8.72E+01	3	3.01E+03	9.62E+01	3	2.75E+03	9.21E+01	3	2.59E+03	1.02E+02	4
40	4.31E+03	1.34E+02	3	3.91E+03	2.23E+03	57	3.53E+03	1.18E+02	3	3.44E+03	9.10E+01	3	3.24E+03	7.87E+01	2
41	4.26E+03	1.51E+02	4	3.96E+03	1.21E+02	3	3.87E+03	1.30E+02	3	3.47E+03	8.56E+01	2	3.45E+03	9.34E+01	3
42	4.48E+03	8.60E+01	2	4.19E+03	2.52E+02	6	3.70E+03	8.83E+01	2	3.52E+03	1.11E+02	3	3.42E+03	1.07E+02	3
45	4.60E+03	1.29E+02	3	4.39E+03	1.06E+02	2	4.05E+03	1.35E+02	3	3.68E+03	1.14E+02	3	3.65E+03	9.52E+01	3
46	4.83E+03	2.09E+02	4	4.51E+03	2.79E+02	6	3.72E+03	1.18E+02	3	3.58E+03	1.03E+02	3	3.48E+03	8.82E+01	3
49	5.17E+01	1.26E+00	2	5.28E+01	1.43E+00	3	5.37E+01	2.59E+00	5	5.23E+01	9.28E-01	2	7.74E+01	1.15E+01	15
50	5.04E+01	1.39E+00	3	5.36E+01	1.08E+00	2	5.05E+01	2.70E+00	5	5.68E+01	9.81E-01	2	5.28E+01	1.65E+00	3
51	6.02E+01	3.37E+00	6	5.73E+01	1.79E+00	3	5.77E+01	1.92E+00	3	5.77E+01	8.25E-01	1	5.83E+01	2.67E+00	5
54	1.77E+02	1.61E+01	9	1.63E+02	1.43E+01	9	1.63E+02	1.02E+01	6	1.61E+02	1.66E+01	10	1.58E+02	1.12E+01	7
55	1.58E+02	1.17E+01	7	1.55E+02	1.74E+01	11	1.46E+02	1.29E+02	74	1.55E+02	1.43E+01	10	1.55E+02	1.43E+01	9
56	1.53E+02	1.23E+01	8	1.49E+02	1.34E+01	9	1.51E+02	1.27E+01	8	1.52E+02	1.42E+01	9	1.46E+02	1.64E+01	11
59	7.56E+02	5.39E+01	7	7.37E+02	7.59E+01	10	7.10E+02	5.46E+01	8	7.13E+02	6.43E+01	9	7.37E+02	7.73E+01	11
60	6.64E+02	4.07E+01	6	6.02E+02	3.20E+01	5	6.78E+02	5.83E+01	9	6.37E+02	5.29E+01	8	6.15E+02	5.03E+01	8
61	1.08E+03	6.15E+01	6	1.07E+03	8.88E+01	8	1.04E+03	7.06E+01	7	9.81E+02	5.31E+01	5	1.06E+03	8.31E+01	8
64	4.67E+02	2.62E+01	6	4.63E+02	4.22E+01	9	4.52E+02	6.62E+01	15	5.09E+02	6.01E+01	12	3.44E+02	3.99E+02	116
65	1.78E+03	7.55E+01	4	7.04E+02	4.85E+01	7	4.29E+02	3.33E+01	8	3.66E+02	3.52E+01	10	3.95E+02	2.93E+01	7
66	4.46E+02	3.82E+01	9	3.94E+02	3.43E+01	9	3.49E+02	4.01E+01	11	4.41E+02	2.94E+01	7	3.70E+02	5.67E+01	15
69	3.88E+02	2.67E+01	7				4.44E+02	3.57E+01	8				3.79E+02	1.53E+01	4
70	3.21E+02	2.08E+01	6				1.01E+02	9.59E+00	10				3.30E+02	2.46E+01	7

Table 13. Number of samples used in CPC uncertainty calculations.

Exp#	Condenser Setting [V]						
	0	500	1000	1500	2000	2500	0
1	29	29	29	29	29	29	29
2	29	29	29	29	29	29	29
3	29	29	29	29	29	29	29
4	29	29	29	29	29	29	29
5	29	29	29	29	29	29	29
8	29	24	29	29	29	24	29
9	29	29	29	29	29	29	29
10	29	29	29	29	29	29	29
11	29	29	29	29	29	29	29
12	29	29	29	29	29	19	29
13	29	29	29	29	29	19	29
14	29	29	29	29	29	24	29
15	29	29	29	29	19	29	29
16	29	24	29	29	29	29	19
19	29	29	29	30	29	19	30
20	29	30	29	29	30	29	30
21	29	30	29	29	30	29	29
22	30	29	30	29	29	30	29
23	30	29	30	29	29	30	29
26	29	29				29	29
27	29	29				29	29
30	29	29				29	29
31	29	29				9	29
32	29	29				9	29
35	9	29	29	29	29	29	29
36	29	29	29	29	29	29	29
37	9	29	29	29	29	29	29
40	29	29	29	29	19	24	29
41	29	29	29	29	29	19	29
42	24	29	29	29	29	29	29
45	29	29	29	29	29	29	29
46	29	29	29	29	29	24	29
49	29	29	29	29	29	29	29
50	29	29	29	29	29	13	29
51	29	29	29	29	29	7	29
54	29	29	29	29	29	29	29
55	29	29	29	29	24	9	29
56	29	29	29	29	29	14	29
59	29	29	29	29	29	29	29
60	29	29	29	29	29	29	29
61	29	23	29	29	29	29	29
64	29	29	29	29	29	9	29
65	29	29	29	29	29	29	29
66	29	29	18	14	29	29	29
69	9		9		9		4
70	9		9		9		4

6.0 SUMMARY & CONCLUSIONS

6.1 Summary

In this project, two research objectives were successfully completed: 1) An apparatus (the Standard Aerosol apparatus) was developed that provides engine-exhaust-analog standard aerosols, and 2) A novel, microfabricated design (the smallest distribution measurement device attempted to date) for the core of a portable particle number-size measurement instrument, the NanoAPAv.2, was developed, built, and characterized with the Standard Aerosol apparatus.

This Summary section briefly summarizes the contents of Chapters 1 to 5 of this thesis document and the Conclusions section highlights the major findings and recommendations for future work.

The motivation for this research, detailed in Section 1, can be summarized in five statements: Particulate matter suspended in the air is detrimental to human health; dangerous concentrations of airborne particulate matter are widespread and a major contributor to them is engine exhaust; it is the number, not the mass, of particles that is important for both engine emissions and lung deposition; current instruments that measure number-size distributions are large, expensive, and/or slow; and greater measurement density (both spatial and temporal) of vehicle exhaust is needed in support of regulation, research, and modeling.

Section 1 continues with a description of the research and regulation needs for a new, portable particle size-distribution measurement instrument relevant for on-board

and road-side measurement of vehicle exhaust. A literature review was conducted that surveyed the field of aerosol electrical mobility measurement instruments, back to the earliest instruments in the field developed at the end of the 19th century.

The preliminary work of this research project, described in Section 3, included a description of the MicroAPA instrument prototype, an evaluation of that prototype that found a need to redesign the electronic package of the instrument to enable a full characterization, the successful electronic redesign into an instrument named the NanoAPAv.1, and evaluation of that redesigned instrument that found the intended function of the core microfabricated devices as a differential mobility analyzer to be inadequate for the project's research objectives. Four re-design options were described, including the double-condenser design of Whipple (1960) that was used in the remainder of the project.

The experimental methods to complete the two research objectives were described in Section 4. The design and evaluation plan for the Standard Aerosol apparatus described a design for a complex apparatus consisting of multiple commercial and custom-built instruments that would produce a repeatable, temperature and humidity stable, charge-free, mono-disperse, 10-100 nm selectable diameter, 0.1-1.5 LPM selectable flowrate, exhaust-analog aerosol. Two of the components of the Standard Aerosol apparatus required a complete design, build, and test program that was fully described: a ²¹⁰Po aerosol charge neutralizer, and an electrostatic precipitator (ESP) to remove charged particles from the aerosol.

Next, the experimental methods to design, build, and test the NanoAPAv.2 instrument, a redesign of the NanoAPAv.1 instrument using a reconfiguration of the microfabricated devices into a configuration emulating that of Whipple (1960), were described in the second part of Section 4. The tests designed to evaluate the new instrument included particle pass-through ratio, correlation of electrometer output voltage to particle concentration, electrometer circuit temporal stability, and implementation of the Whipple (1960) size-distribution calculation.

The results of the characterization tests described in Section 4 were communicated in Section 5. The Standard Aerosol apparatus was successfully evaluated in terms of dilution linearity, predicted temperature effects, production of standard aerosols of oleic acid with ten percent or less by number of carrier solvent, and paired ^{210}Po neutralizer and ESP instrument performance matching that predicted by the Boltzmann particle charging distribution.

The evaluation of the NanoAPAv.2 proof-of-concept instrument demonstrated that the microfabricated devices were leak-proof with linear voltage response through 3000 Volts; a Reynolds number analysis and flow simulation ensured that all instrument flowrates up to 1.5 LPM would exhibit laminar flow regimes; and evaluation of the three electrometers used in the project (the MicroAPA prototype electrometer, the Keithley 616 analog electrometer, and the TI DDC-112 digital electrometer) demonstrated capability of the Keithley and TI electrometers, but also short-and long term temporal stability issues that would limit the usefulness of size measurements of the proof-of-concept instrument.

The final section of Section 5 described the characterization of the NanoAPAv.2 proof-of-concept instrument with the Standard Aerosol apparatus. The particle pass-through ratio (PPR) test demonstrated collection of IPA particles as expected in the design, but the other, engine-analog, particle compositions exhibited adhesion and re-entrainment behavior that obscured the expected collection behavior. The relationship of electrometer output voltage to inlet particle concentration produced the expected linear response for only a subset of the oleic acid particle data at small diameter (less than 20nm) and low flowrates (less than 0.3 LPM). The number-size distributions from the early experiments of this sub-set produced the expected single-peak size distributions with the Whipple calculation, but the remainder of the experiments did not produce repeatable results. A key issue for the miniaturization of particle sizing instruments was identified, namely, that for microfabricated capacitor-based devices, capacitive coupling leakage current between the high voltage supply and the electrometer circuit can overwhelm the measurement signals if the core device is not shielded from the interference of other electric fields. In the final section of Section 5, an uncertainty analysis of the electrometer output voltage and CPC concentration datasets demonstrated that there were no systematic interactions of the characterization instruments with the NanoAPAv.2 proof-of-concept instrument, but confirmed the electrometer temporal stability/drift and particle re-entrainment issues observed earlier in the project.

6.2 Conclusions and future work

In this project, a novel, microfabricated design – the smallest and simplest distribution measurement device attempted to date – for the core of a portable particle number-size measurement instrument was developed, built, and characterized over a range of voltages, flowrates, and aerosol compositions and concentrations. This design of an unshielded microfabricated double-condenser tied directly to an uncompensated electrometer circuit was unable to produce a usable size-distribution measurement, due to electrical field interference and electrometer instability. However, evidence was found for possible areas of improvement in microfabricated number-size measurement devices, useful for future iterations of microfabricated aerosol instrument design.

There are some electrical issues that arise with miniaturization of measurement devices to microfabricated dimensions that were not examined in this research project, and that will need to be examined for future work on this project: particle Brownian motion, electrical dielectrophoretic force, and the need to electrically shield the microfabricated device from external electrical fields.

Brownian motion is the random, diffusion-like, motion of particles that are small enough to approach the size of the vibrating air molecules, and is more dominant the smaller the size of the particles in the aerosol. For particles of diameters of 100nm and less, this is an important effect that needs to be considered in measurement of particle concentration, since a sizable fraction of the particles of these dimensions will diffuse to surfaces within the instrument, be captured by van der Waals forces on the surfaces, and not be measured, (Hinds 1999) In this research project, relative particle

concentration through particle diameter was the goal – in other words, measuring the shape of the number-size distribution, in order to demonstrate the capability of a miniaturized Whipple double condenser with microfabricated components. Ultimately, the absolute particle concentration at each particle diameter will be required for a complete measurement, and so further research on this instrument design needs to include an evaluation of the fraction of particles that are captured by the device independent of condenser voltage. This can be accomplished by applying the diffusion-loss testing methods of (Alonso, Martin et al. 2006) to both the charging and condenser stages.

In this research project, the sole electrical effect on the particles considered was that of the Coulomb force, the simple attraction of bodies with opposite charge. (Cheng 1992) But there is another electrical effect that becomes important for nano-sized particles, the dielectrophoretic force: “The dielectrophoretic force on a particle with induced electric dipole causes the particle to be attracted to regions of high electric field magnitude. For particles very close to the surface panels on the macroscopic body, the variation in electric field strength over the panel surface can lead near-surface particles to be attracted preferentially to the panel edges.” (Liu, Marshall et al. 2009) Since the electrodes of the condensers in the microfabricated device used in the NanoAPAv.2 are fabricated as screens, they have many edges, and so the dielectrophoretic effect may be important for the characterization and operation of the instrument, and so needs to be examined in future work on the instrument.

The temporal instability of the output voltage of both the Keithley and TI electrometers was partially attributed to the effect of external electric fields in this research project, and so it was recommended that electrically shielding the microfabricated device and the cables that connect to it directly would be necessary for future development of the instrument. This effect has been reported by others in the field, notably by (Ranjan and Dhaniyala 2008) in which a particle measuring device (known as MEAS) of dimensions approaching that of the NanoAPA's microfabricated device was initially able to measure concentrations only down to 10^6 p/cm³ at a sufficient signal-to-noise ratio, a result they attributed to the interference of external electrical fields. These researchers then electrically shielded their measurement device and changed all the cables that connected to it to tri-axial cables (which provide more electrical shielding than co-axial cables) which resulted in measurements down to the 10^4 p/cm³ range. Thus, the fact that the NanoAPA v.2 proof-of-concept device, unshielded and interconnected with unshielded wires, was unable to produce a repeatable size-distribution measurement at particle concentrations often below 10^3 p/cm³ matches other results from the field, and emphasizes the need for careful attention to these issues for any future development of the instrument.

There is an also an issue with the standard aerosol apparatus that was not studied in this research project, but is known to be important for testing of portable particle measuring instruments: The relative humidity (RH) of the aerosol has a strong effect on the charging and adhesion of particles. (Hinds 1999) Engine exhaust has a high relative humidity, but the Standard Aerosol apparatus developed and used in this

project to characterize the NanoAPA instrument provided aerosols of near-zero RH. For future work on NanoAPA instrument development, the instrument will need to be characterized with aerosols of various relative humidity. Fortunately, another student researcher, Tamara Stone, has developed a temperature and humidity add-on to the Standard Aerosol apparatus that may be used for this future work.

Lastly, there are unanswered questions about non-IPA-particle adhesion and re-entrainment that arose from the analysis in this project, as described in Section 5.3.1. In this project IPA particles were tested first, followed by the engine-analog particles, mainly oleic acid. The particle pass-through ratio (PPR) results for the IPA test (Figure 52) demonstrate the expected behavior: an increasing fraction of particles were collected with increasing voltage, and a larger fraction of smaller particles were collected than larger particles at the same voltage setting. However, the oleic acid PPR results (Figure 53) did not follow these expected patterns. The first few experiments showed the same behavior as the IPA results, but subsequent tests did not; in many of the later experiments particles appeared to be produced by the device ($PPR > 1$), which was attributed to particle adhesion in previous experiments being re-entrained during subsequent tests, likely due to oleic acid's viscous nature. However, to confirm that this explanation is correct, another set of IPA experiments would need to be conducted after a series of Oleic acid experiments, which should repeat the results of the earlier IPA experiments. This change in the experimental method should be implemented for any future work.

6.3 Patent process

A patent application for the microfabricated double-condenser design was filed 31 March 2011 by a patent attorney contracted by the UVM Office of Technology Commercialization, application number 13/077768.

6.4 Post-thesis extensions for a fully functional portable instrument

To produce a complete instrument, the remaining OEM components of pump, flow meter, inlet impactor, and battery pack must be specified, acquired, and characterized individually.

Next, all the individual components will need to be integrated and calibrated as a field-deployable instrument. This will include: the design and fabrication of an expanded power/control/measurement board; instrument case design and build; arrangement for the fabrication of microfabricated device spares; and the development of a cleaning protocol for the microfabricated devices and aerosol lines.

Three demonstrations of the capability of the integrated instrument should be conducted: lab (vs. SMPS); on-board (integrated into the TOTEMS systems currently in use by the Holmén research group); and by the roadside.

The work on this project may be further extended by designing and acquiring a single new microfabricated device that implements the Benndorf series/parallel design for direct measurement of the size distribution or a microfabricated device and electronic circuit suitable to implement the V and/or Q sweep method of Ungethüm or Dhanorkar and Kamra; and by electrically shielding the microfabricated devices and all

cables that connect to them; increasing the standard aerosol output at small particle diameters; and designing an application-specific electrometer circuit.

REFERENCES

- Agarwal, J. K. and G. J. Sem (1980). "Continuous flow, single-particle-counting condensation nucleus counter." Journal of Aerosol Science 11(4): 343-357.
- AHA (2010) "Evidence growing of air pollution's link to heart disease, death."
- Alonso, M., M. I. Martin, et al. (2006). "The measurement of charging efficiencies and losses of aerosol nanoparticles in a corona charger." Journal of Electrostatics 64(3-4): 203-214.
- Andersson, J. and D. Clarke (2004). UN-GRPE PMP Phase 3 Inter-laboratory Correlation Exercise: Framework and Laboratory Guide, A Document For The UK Department for Transport. RD 04/80801.5
- Andersson, J. C., D. (2005). UN-GRPE PMP Phase 3: Inter-laboratory correlation exercise: Framework and laboratory guide.
<<http://www.unece.org/trans/doc/2005/wp29grpe/>> PMP-2005-14-01e.pdf.
- Andersson, J. D., D. P. Clarke, et al. (2004). UK Particulate Measurement Programme (PMP): A Near US 2007 Approach To Heavy Duty Diesel Particulate Measurements - Comparison With The Standard European Method. SAE 2004-01-1990.
- Aplin, K. L. and R. G. Harrison (2000). "A computer-controlled Gerdien atmospheric ion counter." Review of Scientific Instruments 71(8): 3037-3041.
- Aplin, K. L. and R. G. Harrison (2001). "A self-calibrating programmable mobility spectrometer for atmospheric ion measurements." Review of Scientific Instruments 72(8): 3467-3469.
- Bobrow, L. S. (1985). Fundamentals of Electrical Engineering. Fort Worth, Holt, Rinehart and Winston, Inc.
- Brook, R. D., S. Rajagopalan, et al. (2010). "Particulate Matter Air Pollution and Cardiovascular Disease: An Update to the Scientific Statement From the American Heart Association." Circulation 121(21): 2331-2378.
- Cambustion. (2011). "Particulate & Aerosol Measurement Products." from <http://www.cambustion.com/products>.
- Chen, D. R., D. Y. H. Pui, et al. (1998). "Design and evaluation of a nanometer aerosol differential mobility analyzer (Nano-DMA)." Journal of Aerosol Science 29(5-6): 497-509.
- Cheng, D. K. (1992). Field and Wave Electromagnetics. Reading, Massachusetts, Addison-Wesley Publishing Company.
- Chua, B., D. A. Niemeier, et al. (2006). Micro Air Borne Particulate Analyzer (MicroAPA) Final Report, The California Air Resources Board.
- Chua, B., A. S. Wexler, et al. (2008). "Design, fabrication, and testing of a microfabricated corona ionizer." Journal of Microelectromechanical Systems 17(No. 1): 115-123.

- Chua, B., A. S. Wexler, et al. (2009). "Electrical Mobility Separation of Airborne Particles Using Integrated Microfabricated Corona Ionizer and Separator Electrodes." Microelectromechanical Systems, Journal of 18(1): 4-13.
- Chua, B. L., A. S. Wexler, et al. (2005). Microfabricated device for selectively removing and analyzing airborne particulates from an airstream. USPO.
- Colville, R. N., E. J. Hutchinson, et al. (2001). "The transport sector as a source of air pollution." Atmospheric Environment 35: 1537-1565.
- Dekati. (2011). "ELPI+." from <http://www.dekati.com/cms/elpiplus>.
- Dhanorkar, S. and A. K. Kamra (1991). "Measurement of mobility spectrum and concentration of all atmospheric ions with a single apparatus." Journal of Geophysical Research 96(D10): 18671-18678.
- Dhanorkar, S. and A. K. Kamra (1993). "Diurnal Variations Of The Mobility Spectrum Of Ions And Size Distribution Of Fine Aerosols In The Atmosphere." J. Geophys. Res. 98.
- Dusek, U. (2000). Secondary Organic Aerosol – Formation Mechanisms and Source Contributions in Europe, International Institute for Applied Systems Analysis.
- EPA (2000). Emissions Standards <http://www.epa.gov/OMS/stds-ld.htm>.
- EPA (2008). Regulations Requiring Onboard Diagnostic Systems on 2010 and Later Heavy-Duty Engines Used in Highway Vehicles Over 14,000 Pounds; Revisions to Onboard Diagnostic Requirements for Diesel Highway Vehicles Under 14,000 Pounds
- EPA (2009). Integrated Science Assessment for Particulate Matter (Final Report). Washington, DC, U.S. Environmental Protection Agency.
- EPA. (2011). "MOVES (Motor Vehicle Emission Simulator)", from <http://www.epa.gov/otaq/models/moves/index.htm>.
- EPA, U. S. and Baldauf (2003). The Kansas City Light-Duty Vehicle Emissions Study: Assessing PM Emissions From Gasoline Powered Motor Vehicles. International Emissions Inventory Conference, Mobile Source Session. Clearwater, Florida.
- Fenger, J. (1999). "Urban air quality." Atmospheric Environment 33: 4877-4900.
- Fierz, M., S. Weimer, et al. (2009). "Design and performance of an optimized electrical diffusion battery." Journal of Aerosol Science 40(2): 152-163.
- Finnemore, E. J. and J. B. Franzini (2002). Fluid Mechanics with Engineering Applications. Boston, McGraw Hill.
- Flagan, R. C. (1998). "History of electrical aerosol measurements." Aerosol science and technology 28(4): 301-380.
- Giechaskiel, B. and Y. Drossinos (2010). "Theoretical Investigation of Volatile Removal Efficiency of Particle Number Measurement Systems." SAE International Journal of Engines 3(1): 1140-1151.
- Grahame, T. and R. Schlesinger (2009). Cardiovascular health and particulate vehicular emissions: a critical evaluation of the evidence. Air Quality, Atmosphere & Health.
- GRIMM. (2011). "Fast Aerosol Particle Emission Spectrometer (FAPES)." from http://www.grimm-aerosol.com/downloads/datasheets/en/GrimmAerosolTechnik_Nano_FAPES.pdf.

- HEI (2007). *Mobile-Source Air Toxics: A Critical Review of the Literature on Exposure and Health Effects. Special Report 16.* H. A. T. R. Panel. Boston, Massachusetts, Health Effects Institute.
- Hinds, W. C. (1999). Aerosol Technology: Properties, Behavior, and Measurement of Airborne Particles. New York, John Wiley & Sons.
- Il-Hyun, J., K. Yong-Ho, et al. (2008). Micromachined electrical mobility analyzer for wide range airborne particle classification. Micro Electro Mechanical Systems, 2008. MEMS 2008. IEEE 21st International Conference.
- Israel, H. (1970). Atmospheric Electricity Vol1. Jerusalem, Israel Program for Scientific Translations.
- Jackson, E., Y. Qu, et al. (2006). Driver and Road Type Effects on Light-duty Gas and Particulate Emissions. Transportation Research Board 85th Annual Meeting.
- Kim, Y. H., D. Park, et al. (2008). Electrically tunable airborne particle classifier using a virtual impactor. Micro Electro Mechanical Systems, 2008. MEMS 2008. IEEE 21st International Conference.
- Kinsey, J. S., W. A. Mitchell, et al. (2006). "Evaluation of methods for the determination of diesel-generated fine particulate matter: Physical characterization results." Journal of Aerosol Science 37(1): 63-87.
- Kirchstetter, T. W., R. A. Harley, et al. (1999). "On-road measurement of fine particle and nitrogen oxide emissions from light- and heavy-duty motor vehicles." Atmospheric Environment 33: 2955-2968.
- Kittelson, D. B. (1998). "Engines and nanoparticles: a review." Journal of Aerosol Science 29(5-6): 575-588.
- Kittelson, D. B. (2002). Characteristics and Measurement of Nanoparticles. Engines, Chairman's Air Pollution Seminar, Sacramento, CA.
- Knutson, E. O. and K. T. Whitby (1975). "Accurate measurement of aerosol electric mobility moments." Journal of Aerosol Science 6(6): 453-460.
- Knutson, E. O. and K. T. Whitby (1975). "Aerosol classification by electric mobility: apparatus, theory, and applications." Journal of Aerosol Science 6(6): 443-451.
- Kumar, P., P. Fennell, et al. (2008). "Measurements of particles in the 5-1000 nm range close to road level in an urban street canyon." Science of The Total Environment 390(2-3): 437-447.
- Kumar, P., P. Fennell, et al. (2008). "Pseudo-simultaneous measurements for the vertical variation of coarse, fine and ultrafine particles in an urban street canyon." Atmospheric Environment 42(18): 4304-4319.
- Li, L., D.-R. Chen, et al. (2009). "A miniature disk electrostatic aerosol classifier (mini-disk EAC) for personal nanoparticle sizers." Journal of Aerosol Science 40(11): 982-992.
- Liu, B. Y. H. and D. Y. H. Pui (1975). "On the performance of the electrical aerosol analyzer." Journal of Aerosol Science 6(3-4): 249-264.
- Liu, G. Q., J. S. Marshall, et al. (2009). Discrete-element method for particle capture by a body in an electrostatic field.
- Marshall, J. S. (2007). "Particle aggregation and capture by walls in a particulate aerosol channel flow." Aerosol Science 38: 333-351.

- McCarthy, M. C., D. S. Eisinger, et al. (2006). "Particulate Matter: A Strategic Vision for Transportation-Related Research." Environmental Science & Technology (SEPTEMBER 15, 2006): 5593- 5599.
- Niemeier, D. (2005). Mobile Source Emissions: An Overview of the Regulatory and Modeling Frameworks. Transportation Engineering Handbook: Planning Methods and Applications. K. Goulias, CRC Press.
- NIOSH. (2010). "927ZBCQ - Real-time Instrument for Nanoaerosol Exposure Measurement
<http://www.cdc.gov/niosh/programs/manuf/noragoals/projects/927ZBCQ.html>."
- Pesch, M., H. Grimm, et al. (2009). NanoCheck, a Valuable Tool for Size Range Expansions of Optical Particle Counters for Environmental Applications. European Aerosol Conference 2009. Karlsruhe.
- Pope, C. A., E. Majid, et al. (2009). "Fine-particulate air pollution and life expectancy in the United States." New England Journal of Medicine 360(4): 376-386.
- Qi, C., D.-R. Chen, et al. (2008). "Fundamental Study of a Miniaturized Disk-Type Electrostatic Aerosol Precipitator for a Personal Nanoparticle Sizer." Aerosol Science & Technology 42(7): 505-512.
- Qi, C., D.-R. Chen, et al. (2008). "Performance study of a unipolar aerosol mini-charger for a personal nanoparticle sizer." Journal of Aerosol Science 39(5): 450-459.
- Ranjan, M. and S. Dhaniyala (2008). "A new miniature electrical aerosol spectrometer (MEAS): Experimental characterization." Journal of Aerosol Science 39(8): 710-722.
- Ranjan, M. and S. Dhaniyala (2009). "A novel electrical-mobility-based instrument for total number concentration measurements of ultrafine particles." Journal of Aerosol Science 40(5): 439-450.
- Rostedt, A., M. Marjamäki, et al. (2009). "Non-Collecting Electrical Sensor for Particle Concentration Measurement." Aerosol and Air Quality Research 9: 470-477.
- Sawyer, R. F., R. A. Harley, et al. (2000). "Mobile sources critical review: 1998 NARSTO assessment." Atmospheric Environment 34: 2161-2181.
- Sem, G. J. (2002). "Design and performance characteristics of three continuous-flow condensation particle counters: a summary." Atmospheric Research 62(3-4): 267-294.
- Song, D. K. and S. Dhaniyala (2007). "Nanoparticle cross-flow differential mobility analyzer (NCDMA): Theory and design." Journal of Aerosol Science 38(9): 964-979.
- Tsai, C. J., J. S. Lin, et al. (2005). "Electrostatic Charge Measurement and Charge Neutralization of Fine Aerosol Particles during the Generation Process." Particle & Particle Systems Characterization 22(5): 293-298.
- TSI. (2011). "Engine Exhaust Particle Sizer Spectrometer." from http://www.tsi.com/en-1033/segments/particle_instruments/2208/engine_exhaust_particle_sizer%E2%84%A2_spectrometer.aspx.
- Ungethüm, E. (1974). "The mobilities of small ions in the atmosphere and their relationship." Journal of Aerosol Science 5(1): 25-37.

- Walton, W. H. and J. H. Vincent (1998). "Aerosol Instrumentation in Occupational Hygiene: An Historical Perspective." Aerosol Science and Technology 28(5): 417 - 438.
- Weast, R. C., Ed. (1983). CRC Handbook of Chemistry and Physics. Boca Raton, Florida, CRC Press Inc.
- Weaver, C. S. and L. E. Petty (2004). Reproducibility and Accuracy of On-Board Emission Measurements Using the RAVEM™ System, Engine, Fuel, and Emissions Engineering, Inc.
- Whipple, E. C. (1960). "An Improved Technique for Obtaining Atmospheric Ion Mobility Distributions." J. Geophys. Res. 65(11): 3679-3684.
- Whitby, K. T. (1976). Electrical Measurement of Aerosols. Fine particles : aerosol generation, measurement, sampling, and analysis : [papers] / edited by Benjamin Y. H. Liu, B. Y. H. Liu. New York, Academic Press: 581-623.
- Whitby, K. T. and W. E. Clark (1966). "Electrical aerosol particle counting and size distribution measuring system for the 0.015 to 1 um size range." Tellus 18: 573-586.
- Yeh, H. C., O. G. Raabe, et al. (1973). Development of a miniature aerosol charge spectrometer. Annual report of the Inhalation Toxicology Research Institute, October 1, 1972--September 30, 1973: 16-20.
- Zhang, K. M., A. S. Wexler, et al. (2004). "Evolution of particle number distribution near roadways, Part II: the 'Road-to-Ambient' process." Atmospheric Environment 38(38): 6655-6665.

Appendix A. Standard Operating Procedure for Standard Aerosol Generation

Objective:

The generation and conditioning of a repeatable, neutral charge, mono-disperse, 10-100nm selectable-diameter exhaust-analog aerosol (with less than 10% by number of carrier-solvent particles) for use in characterizing new particle charging, counting, and sizing instruments.

I. Equipment required

1. UltraZero Air cylinder with regulator and shutoff valve
2. TSI Model 9302 Single Jet Atomizer (SJA) or Model 3076 Constant Output Atomizer (COA)
3. B.Braun 350-208 Temperature Bath with Thermomix 1441 Heater/Circulator (Needed for SJA, not for COA)
4. TSI Model 379020A Rotating Disk Thermodiluter + Model 379030 Thermal Conditioner Air Supply (MD19+ASET)
5. AtmoSeal IGH-120-CS-6/X-D48 Heated Line
6. Large, single channel dryer, half silica dessicator beads and half vapor-phase activated carbon
7. Small, five-channel dryer, filled with vapor-phase activated carbon
8. Neutralizer, containing two 2U500 strips of ^{210}Po
9. (2x) Electrostatic precipitator (ESP)

10. (2x) HY3010 DC Power Supply;
11. (2x) EMCO C50 High Voltage Power Supply (HVPS)
12. TSI Model 3080 Electrostatic Classifier (EC)
13. TSI Model 3025a Condensation Particle Counter (CPC)
14. HEPA filter (for dry blank runs)
15. Carbon Traps (for MD19/ASET and CPC exhaust; or exhaust through tubing out a window or into a hood)
16. Conductive tubing (for equipment interconnect)

II. Chemicals required

1. Isopropyl alcohol: 99.9% HPLC Grade
2. Emery oil: SynFluid PAO4cSt
3. Oleic acid: >99% GC grade; bulk quantity is stored in the Votey 122 freezer.
4. Butanol (for CPC operation)

Note: Working quantities of solutions should be stored in a flammables cabinet when not testing.

III. Apparatus default operating conditions

1. Air Tank: 30psi
2. Atomizer: 30psi
3. Bath: 30°C

4. MD19: Dilution Factor 10.0; Temp 80°C (ready lights all green)
5. ASET: Dilution Factor 2.0; Temp 400°C (ready lights all green)
6. Heated Line: 100°C
7. Large Dryer: Carbon on inlet side
8. EC: Panel Control; Sheath Flowrate 15lpm (as in normal SMPS operation)
9. DC Power Supply for ESP HVPSs: 14V (for both)
10. ESP#1: Set DC signal #1 to 5V so that HVPS#1 provides 5kV to the ESP.
Be careful not to exceed 5V as this may damage the HVPS. Control wires:
black → black supply; white → red supply. CAUTION: HIGH VOLTAGE
11. ESP#2: Set DC signal #2 to 0V; ESP#2 is used only for device under test (DUT) charger characterization.
12. CPC: High Flow mode (1.5lpm, as in normal SMPS operation); valve on HEPA inlet closed; butanol bottle placed atop CPC (can be run without bottle attached, but if instrument call for Butanol and can't get it, the run will need to re-run.) Disregard flowrate reading on SMPS panel unless recently calibrated; CPC is calibrated and this is what should be monitored by TSI flow meter occasionally.
13. Computer: AIM software version 8.1 opened with a .C25 file for recording particle concentration every second.

IV. Notes on setup

1. So that there are no low spots in the line from the atomizer to the rotating disk part of the MD19, position the rotating disk above the atomizer and use a piece of tubing just long enough to make the connection without extra. This ensures that any liquid formed in this line from the condensation of atomizer liquid particles does not block the line, but runs back into the atomizer. Optionally, a condenser bottle could be added to the line.

3. The CPC pump pulls 1.5 lpm (high-flow mode) or 0.3 lpm (low-flow mode) through the apparatus; open the CPC inlet bypass valve to achieve lower flowrates.

4. Minimize the length of tubing connecting the pieces of the apparatus; this minimizes diffusion loss and unwanted temperature changes.

5. The ^{210}Po strips in the neutralizer have an operational life of approximately six months; the currently installed strips have a manufacture date of May 2010.

V. Apparatus zeroing, calibration, and cleaning

1. Dry Blank (perform at the start of every testing session): With apparatus assembled, run with air flowing and atomizer empty until particle concentration is consistently zero. This ensures that there are no leaks or contamination in the apparatus.

2. Wet Blank (perform after Dry Blank and after every change of solution type): Rinse atomizer with IPA three times and fill with fresh IPA. (Dispose waste solvent in appropriately marked waste solvent container, stored in a flammables

cabinet.) Run system with air flowing until particle concentration is stable. Record this information for use in calculating the fraction of the IPA carrier solvent remaining in target aerosol flow. Track this information over time to monitor absorbance of activated carbon – when this concentration jumps up to a higher level, the activated carbon may need to be replaced.

3. Compensating for concentration drift (performed during every test with Emery Oil or Oleic Acid solutions): When a solution of Emery Oil or Oleic Acid in IPA is used to generate particles, the particle concentration of the standard aerosol increases steadily over time. This occurs because evaporation of the solvent leads to higher concentration of solute, and so the fraction of the Emery or Oleic in the solution increases over time; higher fractions cause higher particle concentrations. This is compensated for by taking baseline measurements of concentration before and after testing of the DUT,. The concentration found in these baseline measurements can be fit with a linear fit (for the SJA atomizer, the effect is linear until the atomizer has about 0.5cm of solution remaining) and the slope of this line is then removed from the time-series measurements made during the DUT testing.

4. Cleaning: Rinse atomizer with IPA three times when switching between solution types, and then run SMPS scans until back to wet blank levels; this ensures that the next user gets a clean instrument. Empty atomizer and fill with IPA at the end of every session; when starting a new session, empty the atomizer and rinse with IPA before starting again. Waste solution is disposed in the appropriate waste accumulation container.

5. Stabilization: After any change in the apparatus settings or reconfiguration, monitor concentration on the AIM software until it stabilizes before continuing with testing.

6. Monitor pressure to atomizer to maintain set point (the air pressure drops as cylinder empties).

7. Monitor lights on MD19/ASET to ensure no flow imbalance or backpressure situation develops (red lights). If lights go red, shut down and investigate.

8. Monitor CPC sample flowrate; adjust valve inside if necessary to return to spec range.

VI. Adjustable parameters

1. Air pressure: (5-40psi) Higher pressure produces higher particle concentrations, but results in shorter duration before refill. (Note: the SJA atomizer leaks aerosol at higher pressures.)

2. Solute/solvent fraction: Emery oil remains in solution to 1%v/v; Oleic acid to at least 2%v/v; lower fractions produce lower particle concentrations.

3. Temperatures

Bath: (For SJA atomizer only) Temps higher than the 30°C default (50°C was tested) lead to higher concentration of background solvent in the particle signal, likely because more solvent vapor accompanies the atomized droplets.

MD19: Limited data on temperatures other than the 80°C default have been collected, but the MD19 heater can be set at 80°/120°/150°C or off – but note: setting at 150°C never gives a green ready light.

ASET: Default temp of 400°C is highest setting, causes evaporation and later nucleation of particles resulting in more particles 20nm and less in diameter, but ASET heater can be set at any temperature 400°C or lower to a precision of 1 degree, or be turned off.

Heated Line: Off to 250°C is possible; 250°C was investigated, but this resulted in very few target particles likely because the Emery/Oleic target particles were vaporized and trapped along with the carrier solvent.

4. Dilution Factors:

MD19: Lower dilution factors (1.0 is lowest recommended setting) result in lower particle concentrations.

ASET: Higher dilution factors (7.0 is highest recommended setting – limited by maximum with yellow ready light lit; if light turns red -- too high) may result in higher or lower particle concentrations – both have been observed.

5. Sheath-air flowrate – EC: Lowering the EC Sheath flowrate from the standard setting of 15 lpm (minimum recommended is 5 lpm) increases the width of the particle band, and so increases the particle concentration.

6. Bypass of one or both dryers: This results in more particles at smaller diameters, likely because there is less diffusion loss and time to agglomerate.

7. ESP#2 Voltage: 0-5V on DC Source#2 results in HVPS#2 providing 0-5kV to ESP#2, which is needed for characterization of the DUT's charging capabilities. Be careful not to exceed 5V as this may damage the HVPS. CAUTION: HIGH VOLTAGE

VII. Health & Safety

1. Use a ventilation hood for solvent mixing and instrument exhaust. Note: lab windows and doors must be shut for this ventilation to work properly.
2. Personal Protective Gear: nitrile gloves; respirator if solvent fumes are detectable in the lab.
3. Note location of the Lab Safety Folder; consult for MSDSs and other reference information.
4. Waste solvent needs to be stored in a properly marked bottle kept in a flammables cabinet; contact for removal when full.
5. For unattended operation, ensure that there is no exposed high voltage and post the approved sign on all doors to the lab.
6. In case of emergency, call 911 on the UVM phone to reach UVM response team.

Appendix B. Standard Operating Procedure for NanoAPAv.2 Instrument

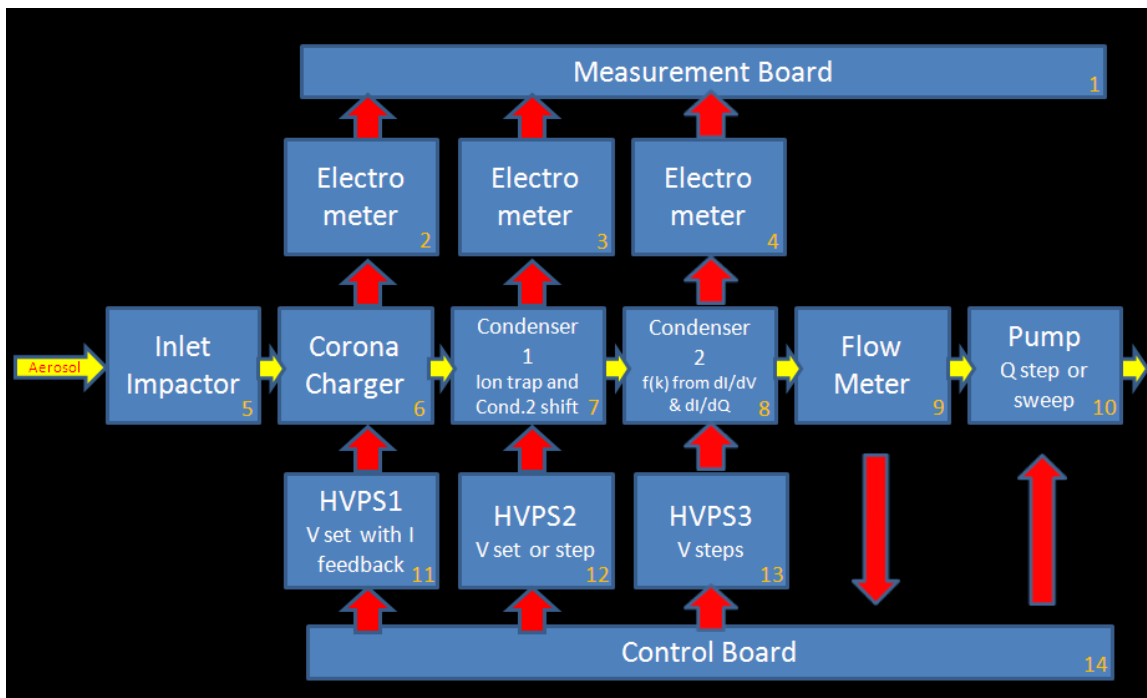


Figure 75. NanoAPAv.2 Block Diagram (Red arrows indicate flow of information; yellow arrows indicate the flow of the aerosol sample under test.)

Refer to Figure 75 for the operational flow of the NanoAPAv.2 instrument.

1. The control board (14) applies a control voltage to the high voltage power supply (HVPS, 11) which converts this to a high voltage output (V_1) and passes this to the microfabricated corona charger (6). A corona develops on the end of the pin, and electrons from the corona drift to the plates, propelled by the electrical field. This establishes a leakage current between pin and plates which is amplified by an electrometer (2) and recorded by a measurement board (1). The charging model having

been earlier established, the average number of charges acquired by each particle is known as a function of charger voltage, aerosol flowrate, and particle diameter.

2. From here on, all control is understood to be performed by the control board (14) and all measurement by the measurement board (1).

3. The pump (10) is set to pull a certain flowrate (Q_a) through the instrument; this is monitored by the flow meter (9); and so an aerosol sample is drawn into the instrument.

4. Two HVPSs (12, 13) provide high voltage outputs (V_2 , V_3) that establish electric fields in the two condensers (7, 8).

5. The aerosol sample first passes through an inertial impactor (5), designed to allow only particles of 300nm or smaller diameter to pass; the larger particles are collected on a plate that is periodically cleaned.

6. The aerosol then passes through the corona charger (6) and its particles pick up electrons.

7. The charged particles of the aerosol then flow into the first condenser (7) and begin to flow toward the plate with the opposite charge. The charged particles with an electrical mobility greater than the critical mobility of the condenser for this flowrate and voltage are completely collected on the condenser plate. (This includes the air molecules ionized by the corona.) The critical mobility of the first condenser is $k_c = Q_a / (4\pi C_1 V_2)$ where C_1 is the capacitance of the condenser, estimated by: $C_1 = A / 4\pi d$ (A is the plate area and d the plate separation).

8. When the particles stick to the condenser plate, they give up their charges, which become a current that is amplified by the electrometer (3) and recorded for diagnostic information.

9. The charged particles not collected by the first condenser flow into the second condenser (8), where they are driven to the opposite charged plate of this condenser as in the earlier one. Particles with a critical mobility greater than the critical mobility of both condensers combined, $k_d = Q_a / (4\pi(C_1 + C_2)V_3)$ but less than k_c (since they made it through the first condenser) are collected in the second condenser. There is also a fraction of the charged particles with electrical mobility less than k_d that get collected; this is predictable and is taken into account in the data analysis below. Prior characterization work has established a relationship between a particle's mobility and its diameter.

10. The current from these collected charges is amplified by electrometer (4) and recorded as the raw data for the measurement.

11. The aerosol with whatever particles still remain in it passes through the flow meter and pump and exits the instrument.

12. This process is repeated over a range of airflow (Q_a) and voltage (V_2, V_3) values, with the current from the second condenser (I_3) recorded at each setting. The airflow and voltage values are selected to provide values of critical mobility that define particle diameter ranges of interest.

13. The data is arranged as I_3/V_3 vs. k_c and differentiated once. This information, along with the equation below, and the corrections calculated from the

instrument characterization (and described above) results in the number vs. diameter distribution, $f(k)$, of the aerosol sample, the desired measurement.

$$\frac{I_3}{V_3} = 4\pi e \left[C_1 k_c \int_{k_d}^{k_c} f(k) dk + (C_1 + C_2) \int_0^{k_d} k f(k) dk - C_1 \int_0^{k_c} k f(k) dk \right]$$

$$\frac{d\left(\frac{I_3}{V_3}\right)}{d k_c} = \frac{\partial\left(\frac{I_3}{V_3}\right)}{\partial k_c} + \frac{\partial\left(\frac{I_3}{V_3}\right)}{\partial k_d} \frac{d k_d}{d k_c} = 4\pi e C_1 \int_{k_d}^{k_c} f(k) dk$$

Appendix C. Datasets for Double Condenser Proof-of-Concept

The database shown below contains seventy-seven datasets of electrometer current, background-corrected current, concentration drift, and particle pass-through ratio, all recorded at a series of condenser voltage steps. Table 10 shows the entries indexed by particle diameter, aerosol flowrate, particle composition, and hardware configuration. The datasets are shown in Figures 76 through 83; for the values of each plotted point, refer to the Matlab program `Full_dataset_2.m` in Appendix D.

Table 14. Database of experimental data.

Datasets for Double Condenser Proof-of-Concept															Composition: O=oleic acid; I= IPA; E=engine residual; N=no aerosol		
T. Barrett 1/18/2011															MEMS#9 = MEMS#3+MEMS#4		
Item#	Set#	Date	Run#	Dia. (nm)	Flow (lpm)	Composition	Starting conc. @CPC	Bypass factor	Conc. @APA [p/cm3]	#Cond1	Condenser Polarity	Charging Polarity	Emeter Type	Cond1 MEMS#	Cond2 MEMS#		
1	1	10/9/2010	4	100.0	1.50	I	1271	1.0	1271	1	N	P	K	3	1		
2	1	10/9/2010	6	100.0	0.30	I	2797	5.0	13985	1	N	P	K	3	1		
3	1	10/9/2010	8	20.0	0.30	I	17951	5.0	89755	1	N	P	K	3	1		
4	1	10/9/2010	9	20.0	1.50	I	2477	1.0	2477	1	N	P	K	3	1		
5	1	10/9/2010	10	10.0	1.50	I	15075	1.0	15075	1	N	P	K	3	1		
6	1	10/9/2010	12	0.0	0.00	N	0	1.0	0	1	N	P	K	3	1		
7	2	10/13/2010	3	0.0	0.00	N	0	1.0	0	1	P	P	K	3	1		
8	2	10/13/2010	4	31.6	1.50	I	1555	1.0	1555	1	P	P	K	3	1		
9	2	10/13/2010	5	31.6	0.70	I	850	2.1	1821	1	P	P	K	3	1		
10	2	10/13/2010	6	31.6	0.30	I	485	5.0	2425	1	P	P	K	3	1		
11	2	10/13/2010	7	100.0	0.30	I	209	5.0	1045	1	P	P	K	3	1		
12	2	10/13/2010	8	100.0	0.70	I	330	2.1	707	1	P	P	K	3	1		
13	2	10/13/2010	9	100.0	1.50	I	739	1.0	739	1	P	P	K	3	1		
14	2	10/13/2010	10	10.0	1.50	I	7086	1.0	7086	1	P	P	K	3	1		
15	2	10/13/2010	11	10.0	0.70	I	923	2.1	1978	1	P	P	K	3	1		
16	2	10/13/2010	12	10.0	0.30	I	69	5.0	345	1	P	P	K	3	1		
17	2	10/13/2010	13	0.0	0.00	N	0	1.0	0	1	P	P	K	3	1		
18	3	10/15/2010	1	0.0	0.00	N	0	1.0	0	1	P	P	K	3	1		
19	3	10/15/2010	5	10.0	0.30	O	27	1.0	27	1	P	P	K	3	1		
20	3	10/15/2010	6	20.0	0.30	O	608	1.0	608	1	P	P	K	3	1		
21	3	10/15/2010	7	15.0	0.30	O	28	1.0	28	1	P	P	K	3	1		
22	3	10/15/2010	8a	40.0	0.30	O	23505	1.0	23505	1	P	P	K	3	1		
23	3	10/15/2010	8b	10.0	0.30	O	24	1.0	24	1	P	P	K	3	1		
24	3	10/15/2010	9	0.0	0.00	N	0	1.0	0	1	P	P	K	3	1		
25	4	10/20/2010	1	0.0	0.00	N	0	1.0	0	1	P	P	K	3	1		
26	4	10/20/2010	2	10.0	0.10	E	3	3.0	10	1	P	P	K	3	1		
27	4	10/20/2010	3	15.0	0.10	E	2	3.0	5	1	P	P	K	3	1		
28	4	10/20/2010	4	0.0	0.00	N	0	1.0	0	1	P	P	K	3	1		
29	5	10/20/2010	6	0.0	0.00	N	0	1.0	0	1	P	P	K	3	1		
30	5	10/20/2010	7	10.0	0.10	O	5	3.0	15	1	P	P	K	3	1		
31	5	10/20/2010	9	12.0	0.10	O	5	3.0	14	1	P	P	K	3	1		
32	5	10/20/2010	10	15.0	0.10	O	5	3.0	14	1	P	P	K	3	1		
33	5	10/20/2010	11	0.0	0.00	N	0	1.0	0	1	P	P	K	3	1		
34	6	11/5/2010	3	0.0	0.00	N	0	1.0	0	2	P	P	K	9	1		
35	6	11/5/2010	5	10.0	0.30	O	4207	1.0	4207	2	P	P	K	9	1		
36	6	11/5/2010	6	12.0	0.30	O	3904	1.0	3904	2	P	P	K	9	1		
37	6	11/5/2010	7	15.0	0.30	O	4059	1.0	4059	2	P	P	K	9	1		
38	6	11/5/2010	8	0.0	0.00	N	0	1.0	0	2	P	P	K	9	1		
39	7	11/10/2010	1	0.0	0.00	N	0	1.0	0	1	N	N	K	4	1		
40	7	11/10/2010	2	10.0	0.30	O	4311	1.0	4311	1	N	N	K	4	1		
41	7	11/10/2010	3	15.0	0.30	O	4347	1.0	4347	1	N	N	K	4	1		
42	7	11/10/2010	4	20.0	0.30	O	4490	1.0	4490	1	N	N	K	4	1		
43	7	11/10/2010	5	0.0	0.00	N	0	1.0	0	1	N	N	K	4	1		
44	8	11/10/2010	7	0.0	0.00	N	0	1.0	0	1	N	N	K	4	1		
45	8	11/10/2010	9	7.0	0.30	O	4580	1.0	4580	1	N	N	K	4	1		
46	8	11/10/2010	10	10.0	0.30	O	4732	1.0	4732	1	N	N	K	4	1		
47	8	11/10/2010	11	0.0	0.00	N	0	1.0	0	1	N	N	K	4	1		
48	9	11/14/2010	1	0.0	0.00	N	0	1.0	0	1	P	P	K	4	1		
49	9	11/14/2010	2	10.0	0.30	O	52	1.0	52	1	P	P	K	4	1		
50	9	11/14/2010	3	12.0	0.30	O	52	1.0	52	1	P	P	K	4	1		
51	9	11/14/2010	4	8.0	0.30	O	59	1.0	59	1	P	P	K	4	1		
52	9	11/14/2010	5	0.0	0.00	N	0	1.0	0	1	P	P	K	4	1		
53	10	11/14/2010	7	0.0	0.00	N	0	1.0	0	1	P	P	K	4	1		
54	10	11/14/2010	8	10.0	0.30	O	175	1.0	175	1	P	P	K	4	1		
55	10	11/14/2010	9	8.0	0.30	O	160	1.0	160	1	P	P	K	4	1		
56	10	11/14/2010	10	12.0	0.30	O	153	1.0	153	1	P	P	K	4	1		
57	10	11/14/2010	12	0.0	0.00	N	0	1.0	0	1	P	P	K	4	1		
58	11	11/15/2010	1	0.0	0.00	N	0	1.0	0	1	P	P	K	4	1		
59	11	11/15/2010	2	10.0	0.30	O	739	1.0	739	1	P	P	K	4	1		
60	11	11/15/2010	3	8.0	0.30	O	716	1.0	716	1	P	P	K	4	1		
61	11	11/15/2010	4	12.0	0.30	O	1045	1.0	1045	1	P	P	K	4	1		
62	11	11/15/2010	5	0.0	0.00	N	0	1.0	0	1	P	P	K	4	1		
63	12	11/16/2010	2	0.0	0.00	N	0	1.0	0	1	P	P	K	3	1		
64	12	11/16/2010	3	10.0	0.30	O	457	1.0	457	1	P	P	K	3	1		
65	12	11/16/2010	4	20.0	0.30	O	1741	1.0	1741	1	P	P	K	3	1		
66	12	11/16/2010	5	10.0	0.30	O	436	1.0	436	1	P	P	K	3	1		
67	12	11/16/2010	6	0.0	0.00	N	0	1.0	0	1	P	P	K	3	1		
68	13	11/16/2010	9	0.0	0.00	N	0	1.0	0	1	P	P	K	3	1		
69	13	11/16/2010	10	10.0	0.30	O	382	1.0	382	1	P	P	K	3	1		
70	13	11/16/2010	11	20.0	0.30	O	318	1.0	318	1	P	P	K	3	1		
71	14	12/15/2010	3	0.0	0.00	N	0	1.0	0	1	P	P	T	3	1		
72	14	12/15/2010	4	10.0	0.65	O	8	2.3	18	1	P	P	T	3	1		
73	14	12/15/2010	5	20.0	0.65	O	140	2.3	323	1	P	P	T	3	1		
74	14	12/15/2010	6	0.0	0.00	N	0	1.0	0	1	P	P	T	3	1		
75	14	12/15/2010	7	10.0	0.30	O	80	1.0	80	1	P	P	T	3	1		
76	14	12/15/2010	8	20.0	0.30	O	100	1.0	100	1	P	P	T	3	1		
77	14	12/15/2010	9	0.0	0.00	N	0	1.0	0	1	P	P	T	3	1		

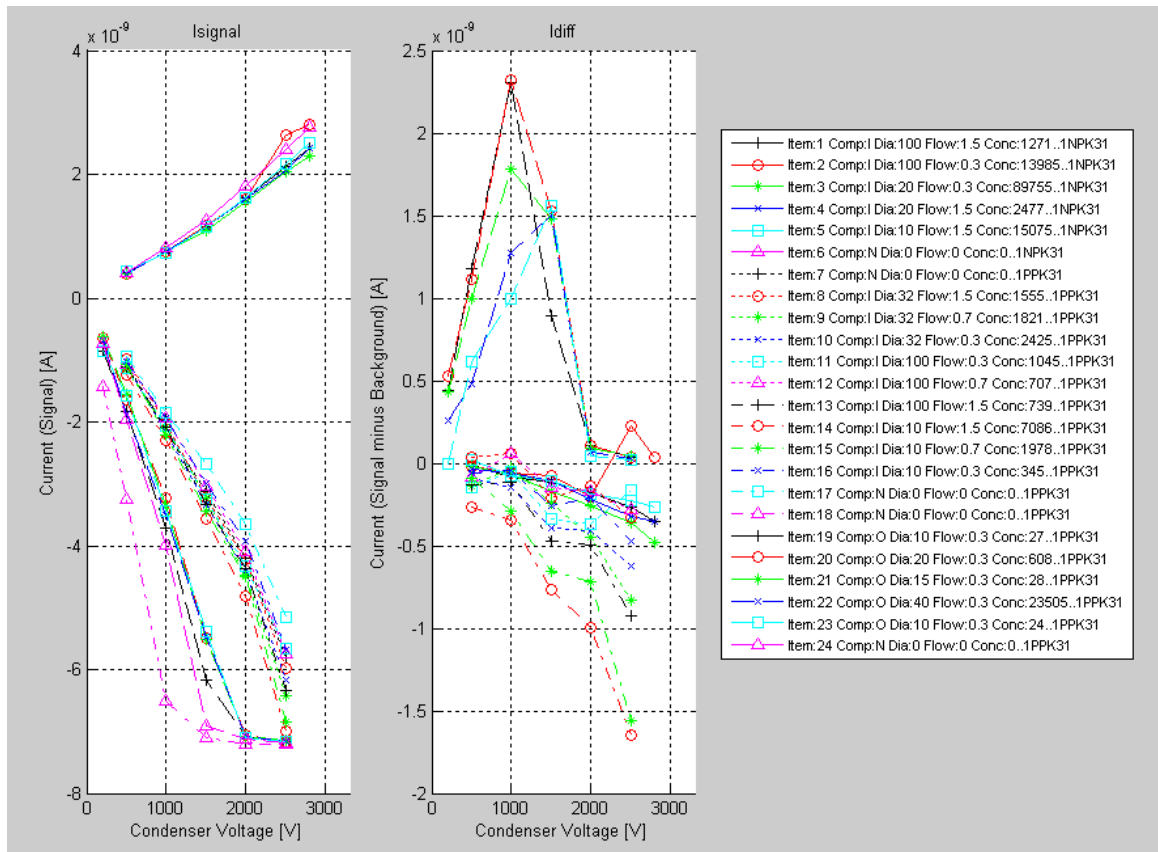


Figure 76. I_{signal} and I_{diff} for experiment sets 1 through 3.

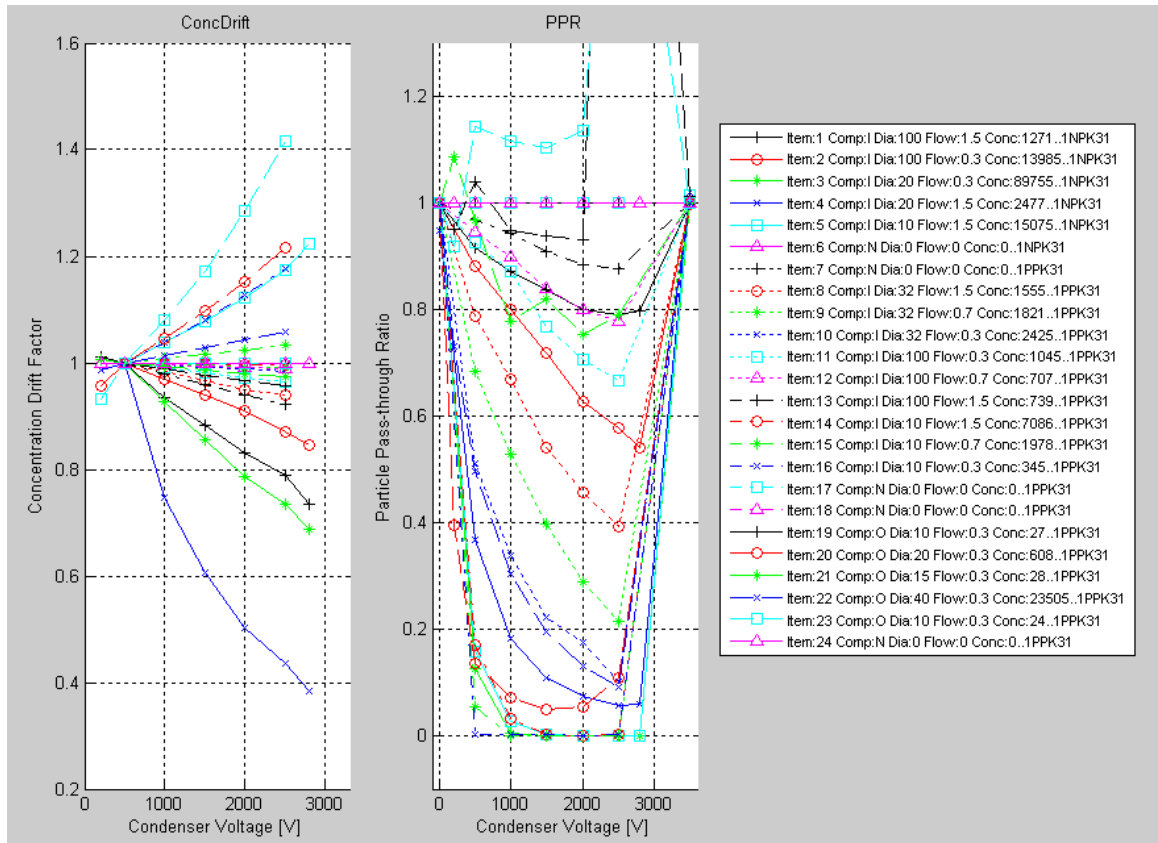


Figure 77. Concentration Drift Factor and Particle Pass-through Ratio for experiment sets 1 through 3.

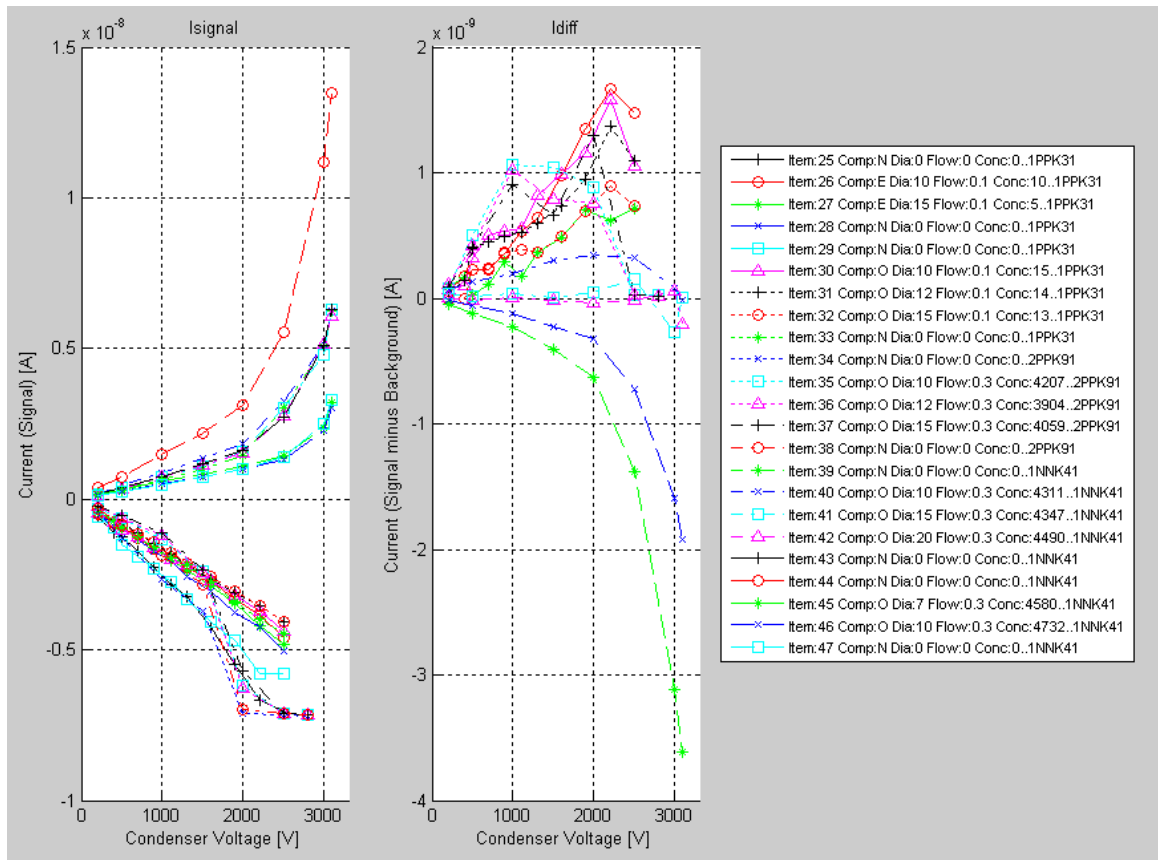


Figure 78. I_{signal} and I_{diff} for experiment sets 4 through 8.

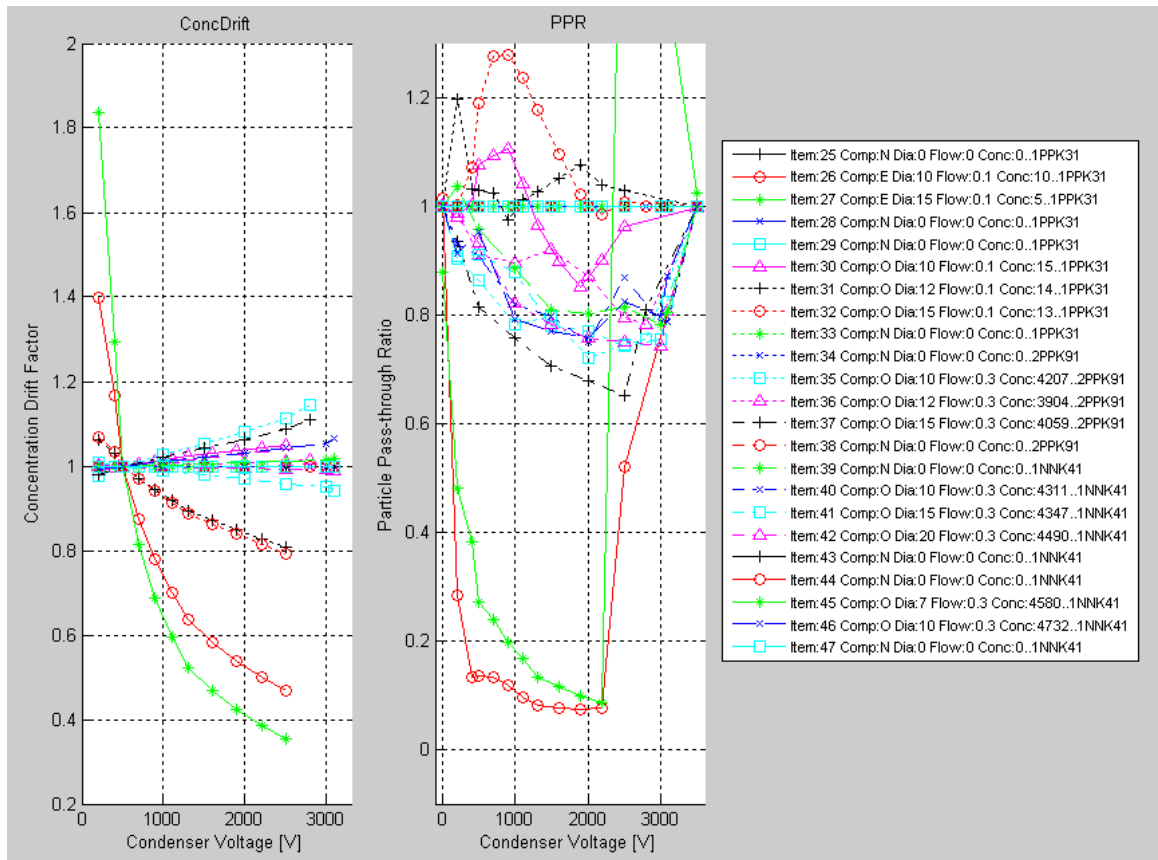


Figure 79. Concentration Drift Factor and Particle Pass-through Ratio for experiment sets 4 through 8.

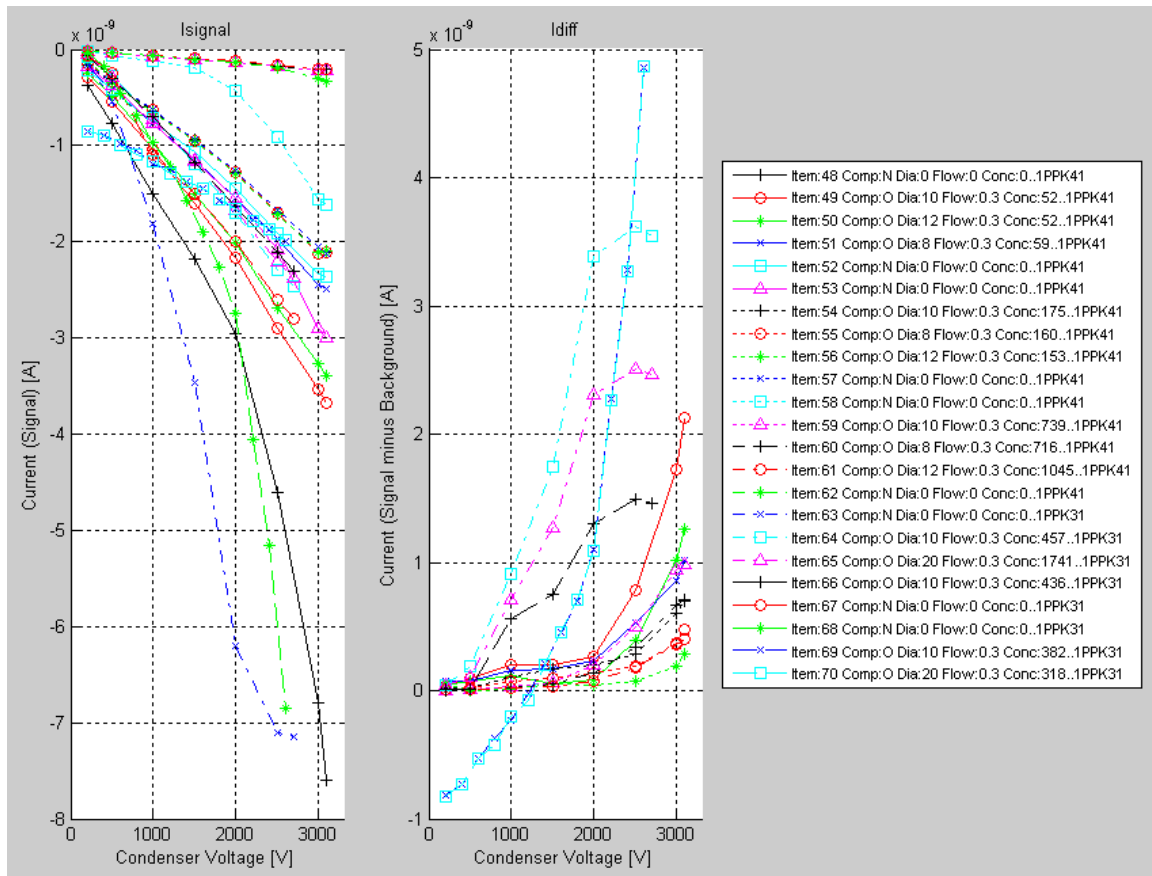


Figure 80. I_{signal} and I_{diff} for experiment sets 9 through 13.

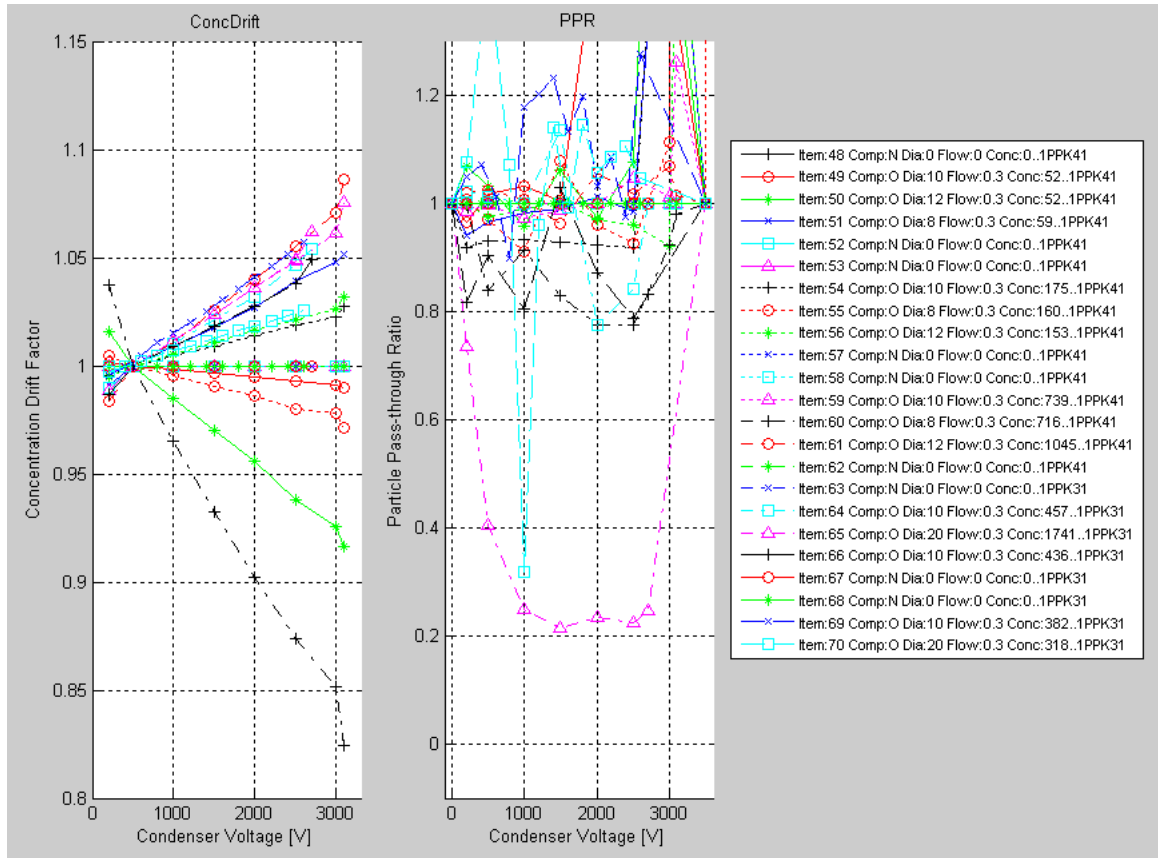


Figure 81. Concentration Drift Factor and Particle Pass-through Ratio for experiment sets 9 through 13.

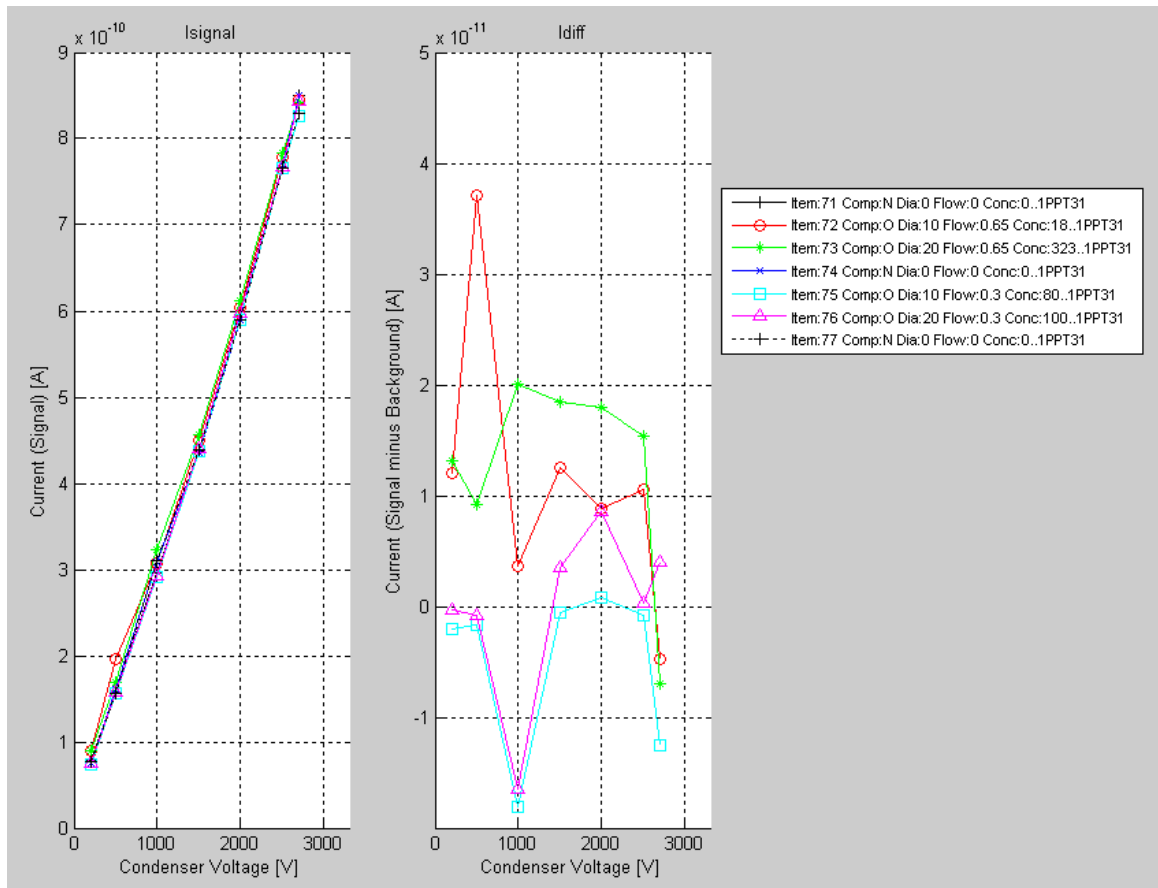


Figure 82. I_{signal} and I_{diff} for experiment set 14.

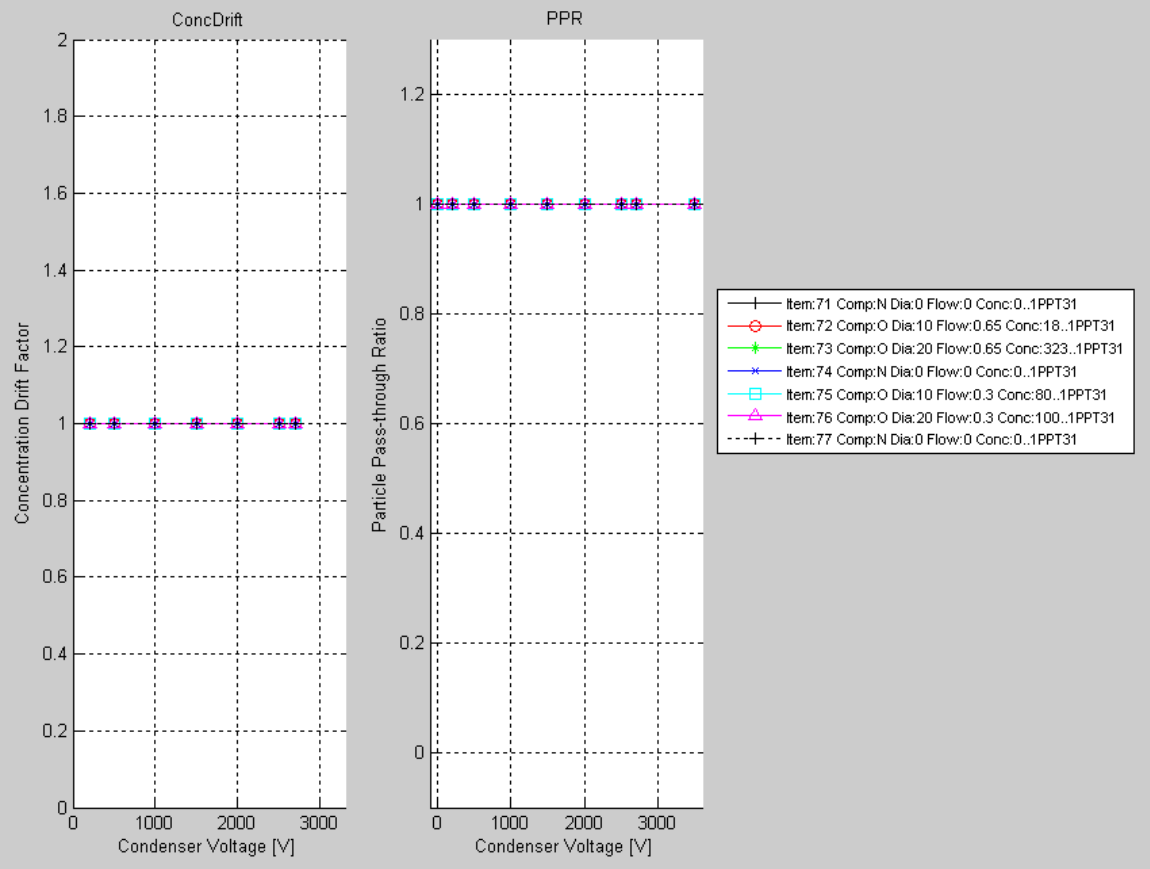


Figure 83. Concentration Drift Factor and Particle Pass-through Ratio for experiment set 14 (no data).

Appendix D. Matlab Programs

1. **Plot_cpc_lvm_14.m** is an example of the programs that processed the raw concentration (CPC .C25) and Keithley electrometer measurements (Labview .LVM)

data files:

```
% plot_cpc_lvm_14.m
% T. Barrett
% Nov 10

%%%%%%%%%%%%%%%%%%%%%%%%%%%%%%%%%%%%%%%%%%%%%%%%%%%%%%%%%%%%%%%%%%%%%%%%

cpc_file='AIM3.txt';
cpc_file_time_add= 0; %minutes
cpc_max_plot=3000; %
lvm_file='output_11.lvm'; %
exp_num_500V=3;

%%11/16 K616 data for oleic runs
before_1500V_start='17:07:15'; %file start time
lvm_background_before=[
    0
    -.03
    -.17
    -.46
    -.68
    -.97
    -1.22
    -1.58
    -1.90
    -2.27
    -2.75
    -4.05
    -5.15
    -6.85
    0
];

after_1500V_start='18:07:15'; %file start time
lvm_background_after=[
    0
    -.03
    -.17
    -.46
    -.68
```

```

-.97
-1.22
-1.58
-1.90
-2.27
-2.75
-4.05
-5.15
-6.85
0
];

%%%%%%%%%%%%%%%%%%%%%%%%%%%%%%%%%%%%%%%%%%%%%%%%%%%%%%%%%%%%%%%%%%%%%%%% 11/16/2010 oleic data %%%%%%%%%%%%%%%%%%%%%%%%%%%%%%%%%%%%%%%%%%%%%%%%%%%%%%%%%%%%%%%%%%%%%%%%%

% % output10 30s exp
% drift_windows={
%   '17:14:40' % 0V, before
%   '17:14:50'
%   '17:22:30' % 0V, after
%   '17:22:35'
% };
% experiment_windows={
%   '17:14:40' % 0V, before
%   '17:14:50'
%   '17:15:45' % 200V
%   '17:15:55'
%   '17:16:15' % 400V
%   '17:16:25'
%   '17:16:45' % 600V
%   '17:16:55'
%   '17:17:20' % 800V
%   '17:17:30'
%   '17:17:45' % 1000V
%   '17:17:55'
%   '17:18:15' % 1200V
%   '17:18:25'
%   '17:18:45' % 1400V
%   '17:18:55'
%   '17:19:15' % 1600V
%   '17:19:25'
%   '17:19:45' % 1800V
%   '17:19:55'
%   '17:20:15' % 2000V
%   '17:20:25'
%   '17:20:45' % 2200V
%   '17:20:55'
%   '17:21:15' % 2400V
%   '17:21:25'
%   '17:21:45' % 2600V
%   '17:21:55'
%   '17:22:30' % 0V, after

```

```

%      '17:22:35'
% };

% output11 30s exp
drift_windows={
    '17:24:40' % 0V, before
    '17:24:50'
    '17:32:30' % 0V, after
    '17:32:35'
};
experiment_windows={
    '17:24:40' % 0V, before
    '17:24:50'
    '17:25:40' % 200V
    '17:25:50'
    '17:26:15' % 400V
    '17:26:25'
    '17:26:45' % 600V
    '17:26:55'
    '17:27:20' % 800V
    '17:27:30'
    '17:27:45' % 1000V
    '17:27:55'
    '17:28:15' % 1200V
    '17:28:25'
    '17:28:45' % 1400V
    '17:28:55'
    '17:29:15' % 1600V
    '17:29:25'
    '17:29:45' % 1800V
    '17:29:55'
    '17:30:15' % 2000V
    '17:30:25'
    '17:30:45' % 2200V
    '17:30:55'
    '17:31:15' % 2400V
    '17:31:20'
    '17:31:45' % 2600V
    '17:31:55'
    '17:32:30' % 0V, after
    '17:32:35'
};

%%%%%%%%%%%%%%%%%%%%%%%%%%%%%%%%%%%%%%%%%%%%%%%%%%%%%%%%%%%%%%%%%%%%%%%%

fid1=fopen(cpc_file);
counter=0;

```

```

while 1
    tline = fgetl(fid1);
    if isnumeric(tline),
        break
    elseif length(tline)>10 & tline(3)==':' & tline(6)==':';
        counter=counter+1;
        cpc_timestamp(counter,:)=tline(1:8);
        cpc_conc(counter,1)=sscanf(tline(9:length(tline)),'%f');
    end
end
fclose(fid1);
cpc_timenum=datenum(cpc_timestamp)+(cpc_file_time_add/1440);

[lvm_etime,lvm_voltage,lvm_timestamp] = textread(lvm_file,'%f %f
%s');
lvm_timenum=datenum(lvm_timestamp);
lvm_min=min(lvm_voltage);
lvm_max=max(lvm_voltage);
lvm_range=0.95*lvm_max-1.05*lvm_min;

cpc_pick_index=find(cpc_timenum>min(lvm_timenum) &
cpc_timenum<max(lvm_timenum));
cpc_timenum_pick=cpc_timenum(cpc_pick_index);
cpc_conc_pick=cpc_conc(cpc_pick_index);
cpc_min=min(cpc_conc_pick);
%cpc_max=max(cpc_conc_pick(find(cpc_conc_pick<99900)));
cpc_max=max(cpc_conc_pick(find(cpc_conc_pick<cpc_max_plot)));
cpc_range=1.05*cpc_max-0.95*cpc_min;
cpc_time_min=min(cpc_timenum_pick);
cpc_time_max=max(cpc_timenum_pick);
cpc_time_range=cpc_time_max-cpc_time_min;

num_exp_timestamps=length(experiment_windows);

if length(cpc_pick_index)>0,
    experiment_windows_num=datenum(experiment_windows);
    experiment_windows_start=experiment_windows_num([1:2:num_exp_
timestamps-1]);
    experiment_windows_stop=experiment_windows_num([2:2:num_exp_t
imestamps]);
    for count_exp=1:num_exp_timestamps/2,

cpc_exp_index=find(cpc_timenum_pick>experiment_windows_start(count_e
xp) & cpc_timenum_pick<experiment_windows_stop(count_exp));
    cpc_exp{count_exp}=cpc_conc_pick(cpc_exp_index);
    cpc_exp_mean(count_exp)=mean(cpc_exp{count_exp});

lvm_exp_index=find(lvm_timenum>experiment_windows_start(count_exp) &
lvm_timenum<experiment_windows_stop(count_exp));
    lvm_exp{count_exp}=lvm_voltage(lvm_exp_index);

```



```

        lvm_exp_mean(count_exp)=mean(lvm_exp{count_exp});
    end

    display_lvm_mean=lvm_exp_mean

    drift_windows_num=datenum(drift_windows);
    drift_windows_start=drift_windows_num([1 3]);
    drift_windows_stop=drift_windows_num([2 4]);

cpc_drift_index_before=find(cpc_timenum_pick>drift_windows_start(1)
& cpc_timenum_pick<drift_windows_stop(1));

cpc_drift_index_after=find(cpc_timenum_pick>drift_windows_start(2) &
cpc_timenum_pick<drift_windows_stop(2));
    cpc_drift_indicies=[cpc_drift_index_before'
cpc_drift_index_after'];
    cpc_drift_conc=cpc_conc_pick(cpc_drift_indicies);
    cpc_drift_timenum=cpc_timenum_pick(cpc_drift_indicies);
    drift_fit=polyfit(cpc_drift_timenum,cpc_drift_conc,1);
    drift_line=polyval(drift_fit,cpc_timenum_pick);

    conc_ppr=cpc_conc_pick./drift_line;
    for count_exp=1:num_exp_timestamps/2,

cpc_exp_index=find(cpc_timenum_pick>experiment_windows_start(count_e
xp) & cpc_timenum_pick<experiment_windows_stop(count_exp));
        ppr_exp{count_exp}=conc_ppr(cpc_exp_index);
        ppr_exp_mean(count_exp)=mean(ppr_exp{count_exp});
        conc_factor_values{count_exp}=drift_line(cpc_exp_index);

conc_drift_mean(count_exp)=mean(conc_factor_values{count_exp});
    end

    lvm_background_combined=[lvm_background_before
lvm_background_after];
    before_timenum=datenum(before_1500V_start);
    after_timenum=datenum(after_1500V_start);
    time_data=[before_timenum after_timenum];
    pick_time=experiment_windows{1}; %file start
    timepick_num=datenum(pick_time);
    counter=0;
    for count_Vs=2:length(lvm_background_before)-1,
        counter=counter+1;
        Vdata=lvm_background_combined(count_Vs,:);
        Vpoly(counter,:)=polyfit(time_data,Vdata,1);
        V_pick(counter)=polyval(Vpoly(counter,:),timepick_num);
    end
    V_pick_addzeros=[0 V_pick 0];
    %lvm_diff=lvm_exp_mean'-lvm_background;
    lvm_diff=lvm_exp_mean'-V_pick_addzeros';

```

```

conc_drift_factor_vs_500V=conc_drift_mean./conc_drift_mean(exp_num_5
00V);

figure
hold on
[AX,H1,H2]=plotyy(cpc_timenum_pick,cpc_conc_pick,lvm_timenum,
lvm_voltage);
set(get(AX(1),'Ylabel'),'String','CPC Particle Concentration
[p/cm3]')
set(get(AX(2),'Ylabel'),'String','K616 Output [V]')
set(AX(1),'XTick',[])
set(AX(1),'XTickLabel',[])
set(AX(2),'XTick',[])
set(AX(2),'XTickLabel',[])
set(AX(1),'YLim',[0.95*cpc_min 1.05*cpc_max])
set(AX(1),'YTick',[ (0.95*cpc_min):cpc_range/10:(1.05*cpc_max) ])

set(AX(1),'YTickLabel',[ (0.95*cpc_min):cpc_range/10:(1.05*cpc_max) ])
set(AX(1),'YGrid','on')
set(AX(2),'YLim',[1.05*lvm_min 0.95*lvm_max])
set(AX(2),'YTick',[ (1.05*lvm_min):lvm_range/10:(0.95*lvm_max) ])

set(AX(2),'YTickLabel',[ (1.05*lvm_min):lvm_range/10:(0.95*lvm_max) ])
set(AX(1),'XLim',[cpc_time_min cpc_time_max])
set(AX(1),'XTick',[cpc_time_min:cpc_time_range/10:cpc_time_ma
x])
set(AX(1),'XTickLabel',datestr([cpc_time_min:cpc_time_range/1
0:cpc_time_max],13))
set(AX(2),'XLim',[cpc_time_min cpc_time_max])
set(AX(2),'XTick',[cpc_time_min:cpc_time_range/10:cpc_time_ma
x])
xlabel('TimeStamp')
title(['CPC (' strrep(cpc_file,'_',' ') ') and K616 ('
strrep(lvm_file,'_',' ') ')'])
set(H1,'LineStyle','-')
set(H2,'LineStyle','-')
grid on
for line_index=1:length(experiment_windows)/2,
line([experiment_windows_start(line_index)
experiment_windows_start(line_index)], [0.95*cpc_min
1.05*cpc_max], 'Color', 'g')
line([experiment_windows_stop(line_index)
experiment_windows_stop(line_index)], [0.95*cpc_min
1.05*cpc_max], 'Color', 'r')
end
plot(cpc_timenum_pick,drift_line,'b--')
line([drift_windows_start(1)
drift_windows_start(1)], [0.95*cpc_min
1.05*cpc_max], 'Color', 'b', 'LineStyle', '-.')

```

```

    line([drift_windows_stop(1) drift_windows_stop(1)], [0.95*cpc_min
1.05*cpc_max], 'Color', 'b', 'LineStyle', '-. ')
    line([drift_windows_start(2)
drift_windows_start(2)], [0.95*cpc_min
1.05*cpc_max], 'Color', 'b', 'LineStyle', '-. ')
    line([drift_windows_stop(2) drift_windows_stop(2)], [0.95*cpc_min
1.05*cpc_max], 'Color', 'b', 'LineStyle', '-. ')

%     figure
%     counter=0;
%     for count_plots=1:8,
%         counter=counter+1;
%         subplot(8,3,counter)
%         hist(cpc_exp{count_plots})
%         if counter==1, title('Particle Concentration [p/cm3]'),
end
%         counter=counter+1;
%         subplot(8,3,counter)
%         hist(ppr_exp{count_plots})
%         if counter==2, title('Particle Pass-thru Ratio'), end
%         counter=counter+1;
%         subplot(8,3,counter)
%         hist(lvm_exp{count_plots})
%         if counter==3, title('K616 Output [V]'), end
%     end

%     figure
%     plot(cpc_timenum_pick, conc_ppr)

figure

plotyy(1:num_exp_timestamps/2, ppr_exp_mean, 1:num_exp_timestamps/2, lvm_diff)

dataout=[ppr_exp_mean' lvm_diff conc_drift_factor_vs_500V']
conc_drift_500V=conc_drift_mean(exp_num_500V)

else

figure
plot(lvm_timenum, lvm_voltage)
    xlabel('TimeStamp')
title(['K616 (' strrep(lvm_file, '_', ' ') ')'])
ylabel('K616 Output [V]')
xlims=get(gca, 'Xlim');
axis([xlims 1.05*lvm_min 1.05*lvm_max])
grid on

end

```

2. NanoAPA_Distribution_Calc_DDC112.m is the program that processed the

raw TI electrometer (EVM .CSV) data files:

```
% NanoAPA_Distribution_Calc_DDC112.m
% T. Barrett
% Dec 2010

%%%%%%%%%%%%%%%%%%%%%%%%%%%%%%%%%%%%%%%%%%%%%%%%%%%%%%%%%%%%%%%%%%%%%%%%
%%%%%%%%
% Case 1 --> 15Dec, runs3-6, 10&20nm Oleic, 0.65LPM
% Case 2 --> 15Dec, runs6-9, 10&20nm Oleic, 0.3LPM

case_number = 2;

% Current Method 1 --> (Data Means - Avg(Background Means)) /
Avg(Background Means)
% Current Method 2 --> (Data Medians - Avg(Background Medians)) /
Avg(Background Medians)
% Current Method 3 --> Data Means - Avg(Background Means)
% Current Method 4 --> Data Medians - Avg(Background Medians)
% Current Method 5 --> Data Medians
% Current Method 6 --> Data Means

current_method = 6;

switch_sign = 'n';

scale_conc = 'n';

cull_outliers = 'n';

%%%%%%%%%%%%%%%%%%%%%%%%%%%%%%%%%%%%%%%%%%%%%%%%%%%%%%%%%%%%%%%%%%%%%%%%
%%%%%%%%

switch case_number

%%%%%%%%%%%%%%%%%%%%%%%%%%%%%%%%%%%%%%%%%%%%%%%%%%%%%%%%%%%%%%%%%%%%%%%%
%%%%%%%%

case 1

%% Case 1 --> 15Dec, runs3-6, 10&20nm Oleic, 0.65LPM %%

data_dir='M:\TI DDC112 EVM\15Dec2010\runs3thru6';

integration_time= 0.1; %seconds
range_max= 350; %pC
```

```

start_concentrations = [8 140];

filenames={
    'run03_V0.csv'
    'run03_V200.csv'
    'run03_V500.csv'
    'run03_V1000.csv'
    'run03_V1500.csv'
    'run03_V2000.csv'
    'run03_V2500.csv'
    'run06_V2700.csv' %replacing erroneous file
    'run04_V0.csv'
    'run04_V200.csv'
    'run04_V500.csv'
    'run04_V1000.csv'
    'run04_V1500.csv'
    'run04_V2000.csv'
    'run04_V2500.csv'
    'run04_V2700.csv'
    'run05_V0.csv'
    'run05_V200.csv'
    'run05_V500.csv'
    'run05_V1000.csv'
    'run05_V1500.csv'
    'run05_V2000.csv'
    'run05_V2500.csv'
    'run05_V2700.csv'
    'run06_V0.csv'
    'run06_V200.csv'
    'run06_V500.csv'
    'run06_V1000.csv'
    'run06_V1500.csv'
    'run06_V2000.csv'
    'run06_V2500.csv'
    'run06_V2700.csv'
};

legend_text={'10 nm, 0.65 lpm' , '20 nm, 0.65 lpm'};

%%% Whipple parameters

%Condenser properties:
A=1.18; %mm2, Condenser plate area
d=2.00; %mm, Condenser inter-plate separation

%Flow and Voltage settings:
Q=0.65; %LPM, flowarate in above experiments
V=[0 200 500 1000 1500 2000 2500 2700]; %V, voltage steps in above
experiments

%charge on one electron

```

```

e_charge=1.602e-19; %coulombs (=A*s)

%Number of devices per condenser stage
num_MEMS_cond1=1;
num_MEMS_cond2=1;

%%%%%%%%%%%%%%%%%%%%%%%%%%%%%%%%%%%%%%%%%%%%%%%%%%%%%%%%%%%%%%%%%%%%%%%%
%%%%%%%%%%%%%%%%%%%%%%%%%%%%%%%%%%%%%%%%%%%%%%%%%%%%%%%%%%%%%%%%%%%%%%%%

case 2

%% Case 2 --> 15Dec, runs6-9, 10&20nm Oleic, 0.3LPM %%

data_dir='M:\TI DDC112 EVM\15Dec2010\runs6thru9';

integration_time= 0.1; %seconds
range_max= 350; %pC

start_concentrations = [80 100];

filenames={
    'run06_V0.csv'
    'run06_V200.csv'
    'run06_V500.csv'
    'run06_V1000.csv'
    'run06_V1500.csv'
    'run06_V2000.csv'
    'run06_V2500.csv'
    'run06_V2700.csv'
    'run07_V0.csv'
    'run07_V200.csv'
    'run07_V500.csv'
    'run07_V1000.csv'
    'run07_V1500.csv'
    'run07_V2000.csv'
    'run07_V2500.csv'
    'run07_V2700.csv'
    'run08_V0.csv'
    'run08_V200.csv'
    'run08_V500.csv'
    'run08_V1000.csv'
    'run08_V1500.csv'
    'run08_V2000.csv'
    'run08_V2500.csv'
    'run08_V2700.csv'
    'run09_V0.csv'
    'run09_V200.csv'
    'run09_V500.csv'
    'run09_V1000.csv'
    'run09_V1500.csv'
    'run09_V2000.csv'

```

```

        'run09_V2500.csv'
        'run09_V2700.csv'
    };

legend_text={'10 nm, 0.3 lpm' , '20 nm, 0.3 lpm'};

%%% Whipple parameters

%Condenser properties:
A=1.18; %mm2, Condenser plate area
d=2.00; %mm, Condenser inter-plate seperation

%Flow and Voltage settings:
Q=0.3; %LPM, flowarate in above experiments
V=[0 200 500 1000 1500 2000 2500 2700]; %V, voltage steps in above
experiments

%charge on one electron
e_charge=1.602e-19; %coulombs (=A*s)

%Number of devices per condenser stage
num_MEMS_cond1=1;
num_MEMS_cond2=1;

%%%%%%%%%%%%%%%%%%%%%%%%%%%%%%%%%%%%%%%%%%%%%%%%%%%%%%%%%%%%%%%%%%%%%%%%
%%%%%%%%%%%%%%%%%%%%%%%%%%%%%%%%%%%%%%%%%%%%%%%%%%%%%%%%%%%%%%%%%%%%%%%%

end

%%%%%%%%%%%%%%%%%%%%%%%%%%%%%%%%%%%%%%%%%%%%%%%%%%%%%%%%%%%%%%%%%%%%%%%% Part I -- Acquire current signals
%%%%%%%%%%%%%%%%%%%%%%%%%%%%%%%%%%%%%%%%%%%%%%%%%%%%%%%%%%%%%%%%%%%%%%%%

current_dir=cd;
cd(data_dir)

num_files=length(filenamees);

for count_files=1:num_files,

csv_filename=filenamees{count_files};

fid=fopen(csv_filename);
fclose(fid);

raw_data=textscan(fid, '%s %f %f %*f %*f %*f', 'Delimiter', ',');
fclose(fid);

length_raw_data=length(raw_data{1});
channel=reshape(raw_data{1}, length_raw_data/4, 4);
data_count=reshape(raw_data{2}, length_raw_data/4, 4);
codes=reshape(raw_data{3}, length_raw_data/4, 4);

```

```

max_code=2^20;
max_code_current=range_max/integration_time; %pA

current=(codes/max_code)*max_code_current;

if cull_outliers == 'y',
    current_flat=current(:);
    %IQR=iqr(current_flat);
    stat_summary=summary(dataset(current_flat));
    quantiles=stat_summary.Variables.Data.Quantiles;
    IQR=quantiles(4)-quantiles(2);
    pos_outlier_min=quantiles(4)+(1.5*IQR);
    neg_outlier_max=quantiles(2)-(1.5*IQR);
    %    boxplot(current_flat)
    %    hold on
    %    plot(1,[neg_outlier_max pos_outlier_min],'x','MarkerSize',10)
    %    hold off
    %    pause
    non_outlier_index=find(current_flat>neg_outlier_max &
current_flat<pos_outlier_min);
    current_flat_culled=current_flat(non_outlier_index);
    %    subplot(121)
    %    boxplot(current_flat)
    %    xlims=get(gca,'XLim');
    %    ylims=get(gca,'YLim');
    %    subplot(122)
    %    boxplot(current_flat_culled)
    %    axis([xlims ylims]);
    %    pause
    mean_mean_current=mean(current_flat_culled);
    median_current=median(current_flat_culled);
else
    mean_current=mean(current,2);
    mean_mean_current=mean(mean_current);
    median_current=median(current(:));
    hold_all(:,count_files)=current(:);
end

end

hold_mean_mean(count_files)=mean_mean_current;
hold_median(count_files)=median_current;

end

if cull_outliers == 'n',
    groupVs_index=[ [1:8:25] 1+[1:8:25] 2+[1:8:25] 3+[1:8:25]
4+[1:8:25] 5+[1:8:25] 6+[1:8:25] 7+[1:8:25]];
    hold_all_groupVs_matrix=hold_all(:,groupVs_index);
    hold_all_groupVs_flat=hold_all_groupVs_matrix(:);

    figure

```



```

hold on
h1=boxplot(hold_all_groupVs_matrix);
ylabel('Current [pA]')
xlabel('Measurement #')
grid on
axis([0.5 num_files+0.5 -50 800])
line([4.5 4.5],[0 800],'Color','k','LineStyle',':')
line([8.5 8.5],[0 800],'Color','k','LineStyle',':')
line([12.5 12.5],[0 800],'Color','k','LineStyle',':')
line([16.5 16.5],[0 800],'Color','k','LineStyle',':')
line([20.5 20.5],[0 800],'Color','k','LineStyle',':')
line([24.5 24.5],[0 800],'Color','k','LineStyle',':')
line([28.5 28.5],[0 800],'Color','k','LineStyle',':')
end

background_before_means=hold_mean_mean(1:8);
background_before_medians=hold_median(1:8);
runA_means=hold_mean_mean(9:16);
runA_medians=hold_median(9:16);
runB_means=hold_mean_mean(17:24);
runB_medians=hold_median(17:24);
background_after_means=hold_mean_mean(25:32);
background_after_medians=hold_median(25:32);
background_avg_means=mean([background_before_means'
background_after_means'],2);
background_avg_medians=mean([background_before_medians'
background_after_medians'],2);

if current_method == 1,
    I_runA = (runA_means - background_avg_means') ./ runA_means ;
    I_runB = (runB_means - background_avg_means') ./ runB_means ;
elseif current_method == 2,
    I_runA = (runA_medians - background_avg_medians') ./
runA_medians ;
    I_runB = (runB_medians - background_avg_medians') ./
runB_medians ;
elseif current_method == 3,
    I_runA = runA_means - background_avg_means';
    I_runB = runB_means - background_avg_means';
elseif current_method == 4,
    I_runA = runA_medians - background_avg_medians';
    I_runB = runB_medians - background_avg_medians';
elseif current_method == 5,
    I_runA = runA_medians;
    I_runB = runB_medians;
elseif current_method == 6,
    I_runA = runA_means;
    I_runB = runB_means;
end

if switch_sign=='y',

```

```

        I_runA = -1* I_runA;
        I_runB = -1* I_runB;
end

if scale_conc == 'y',

start_concentrations_norm=start_concentrations/start_concentrations(
1);
    I_runA = I_runA / start_concentrations_norm(1);
    I_runB = I_runB / start_concentrations_norm(2);
end

display_before_mean=background_before_means
display_IrunA=I_runA
display_IrunB=I_runB
display_after_mean=background_after_means

%%%%%%%%%%%%%%%%%%%%%%%%%%%%%%%%%%%%%%%%%%%%%%%%%%%%%%%%%%%%%%%%%%%%%%%% Part II -- Whipple Calculation
%%%%%%%%%%%%%%%%%%%%%%%%%%%%%%%%%%%%%%%%%%%%%%%%%%%%%%%%%%%%%%%%%%%%%%%%

A_cm2=A/100;
d_cm=d/10;
C=A_cm2/(4*pi*d_cm);
Q_cm3s=Q*(1000/60);
num_Vs=length(V);
V_nozero=V(2:num_Vs);

I_runA_nozero=I_runA(2:num_Vs);
I_runB_nozero=I_runB(2:num_Vs);
IoverV_runA = I_runA_nozero./V_nozero;
IoverV_runB = I_runB_nozero./V_nozero;

kc = (Q_cm3s./(4*pi*num_MEMS_cond1*C*V_nozero));
kd = (Q_cm3s./(4*pi*(num_MEMS_cond1+num_MEMS_cond2)*C*V_nozero));

QoverV=Q_cm3s./V_nozero;

Dp_min=10.^((log10(kc)-0.197814)./(-1.985986));
Dp_max=10.^((log10(kd)-0.197814)./(-1.985986));
Dp_logmean=10.^((log10(Dp_min)+log10(Dp_max))./2);
Dp_logdiff=log10(Dp_max)-log10(Dp_min);
Dp_logdiff_1=Dp_logdiff(1,1);

for count_Vsteps= 2:num_Vs-2,
    raw_y_runA=[IoverV_runA(count_Vsteps-1)
IoverV_runA(count_Vsteps) IoverV_runA(count_Vsteps+1)];
    raw_y_runB=[IoverV_runB(count_Vsteps-1)
IoverV_runB(count_Vsteps) IoverV_runB(count_Vsteps+1)];
    raw_x=[kc(count_Vsteps-1) kc(count_Vsteps) kc(count_Vsteps+1)];
    raw_poly_runA=polyfit(raw_x,raw_y_runA,1);
    raw_poly_runB=polyfit(raw_x,raw_y_runB,1);
end

```

```

    raw_polyval_runA=polyval(raw_poly_runA,raw_x);
    raw_polyval_runB=polyval(raw_poly_runB,raw_x);
    slope_deriv_runA(count_Vsteps-1)=raw_poly_runA(1);
    slope_deriv_runB(count_Vsteps-1)=raw_poly_runB(1);
end

IoverV_set_min=min(min([IoverV_runA; IoverV_runB]));
IoverV_set_max=max(max([IoverV_runA; IoverV_runB]));
slope_deriv_set_min=min(min([slope_deriv_runA; slope_deriv_runB]));
slope_deriv_set_max=max(max([slope_deriv_runA; slope_deriv_runB]));

kc_shortened2=kc(2:length(kc)-1);
Dp_logmean_shortened2=Dp_logmean(2:length(Dp_logmean)-1);
meas_conc_based_on_slope_runA=slope_deriv_runA./(4*pi*C*e_charge);
meas_conc_slope_dlogDp_runA=meas_conc_based_on_slope_runA./Dp_logdif
f_1;
meas_conc_based_on_slope_runB=slope_deriv_runB./(4*pi*C*e_charge);
meas_conc_slope_dlogDp_runB=meas_conc_based_on_slope_runB./Dp_logdif
f_1;

max_meas_conc=max([meas_conc_slope_dlogDp_runA(:);
meas_conc_slope_dlogDp_runB(:)]);
meas_conc_slope_dlogDp_norm_runA=meas_conc_slope_dlogDp_runA./max_me
as_conc;
meas_conc_slope_dlogDp_norm_runB=meas_conc_slope_dlogDp_runB./max_me
as_conc;

figure
subplot(211)
hold on
semilogx(kc,[IoverV_runA; IoverV_runB],'-o')
legend(legend_text)
xlabel('Critical Mobility, Kc [cm2/(V s)]')
ylabel('DDC112 Current Reading / Condenser Voltage [A/V = 1/Ohm]')
%axis([min(kc) max(kc) IoverV_set_min IoverV_set_max ])
%axis([0.01 1 IoverV_set_min IoverV_set_max ])
grid on
subplot(212)
hold on
%semilogx(kc_shortened2,[slope_deriv_runA; slope_deriv_runB],'-o')
semilogx(kc,[NaN slope_deriv_runA NaN; [NaN slope_deriv_runB
NaN]],'-o')
legend(legend_text)
xlabel('Critical Mobility, Kc [cm2/(V s)]')
ylabel('slope (I/V) / kc ')
%axis([min(kc) max(kc) slope_deriv_set_min slope_deriv_set_max])
%axis([0.01 1 slope_deriv_set_min slope_deriv_set_max])
grid on

figure

```

```

semilogx(Dp_logmean_shortened2,[meas_conc_slope_dlogDp_norm_runA;
meas_conc_slope_dlogDp_norm_runB] ,'-o')
legend(legend_text)
xlabel('Theoretical Particle Diameter [nm]')
ylabel('dN/dlogDp [ (p/cm3)/(log(bin width)), normalized to maximum
value ]')
title('NanoAPA -- Particle Size Distribution')
axis([1.9 21 -.1 1.1])
set(gca,'XTick',[2:10 20])
set(gca,'XTickLabel',[2:10 20])
grid on

%%%%%%%%%%%%%%%%%%%%%%%%%%%%%%%%%%%%%%%%%%%%%%%%%%%%%%%%%%%%%%%%%%%%%%%%
%%%%%%%%%%%%%%%%%%%%%%%%%%%%%%%%%%%%%%%%%%%%%%%%%%%%%%%%%%%%%%%%%%%%%%%%

% IoverV_runA
% IoverV_runB
% start_concentrations

cd(current_dir);

```

3. Full_dataset_2.m is the program that created the project database from the

reduced data that was produced by the previous two programs:

```

% Full_dataset_2.m
% T.Barrett
% May 2011

data_spreadsheet='full_dataset.xls'; % Make sure table is sorted by
ItemNum before running this}

[item_num,txt,row] = xlsread(data_spreadsheet,'B4:B80');
[set_num,txt,row] = xlsread(data_spreadsheet,'C4:C80');
[num,test_date,row] = xlsread(data_spreadsheet,'D4:D80');
[num,run_num,row] = xlsread(data_spreadsheet,'E4:E80');
[diameter,txt,row] = xlsread(data_spreadsheet,'F4:F80');
[flowrate,txt,row] = xlsread(data_spreadsheet,'G4:G80');
[num,composition,row] = xlsread(data_spreadsheet,'H4:H80');
[CPC_conc,txt,row] = xlsread(data_spreadsheet,'I4:I80');
[bypass_factor,txt,row] = xlsread(data_spreadsheet,'J4:J80');
[APA_conc,txt,row] = xlsread(data_spreadsheet,'K4:K80');
[num_cond1,txt,row] = xlsread(data_spreadsheet,'L4:L80');
[num,cond_polarity,row] = xlsread(data_spreadsheet,'M4:M80');
[num,charge_polarity,row] = xlsread(data_spreadsheet,'N4:N80');
[num,emeter_type,row] = xlsread(data_spreadsheet,'O4:O80');
[Cond1_MEMSnum,txt,row] = xlsread(data_spreadsheet,'P4:P80');
[Cond2_MEMSnum,txt,row] = xlsread(data_spreadsheet,'Q4:Q80');

```

```

clear num txt raw

%%% Signal means *No correction made for concentration thru Vs or
run to run
Isignal{1}= 100e-11* [0.4038    0.7315    1.1442    1.6266    2.1310
2.4179];
Isignal{2}= 100e-11* [0.3950    0.7519    1.1788    1.6065    2.6246
2.8088];
Isignal{3}= 100e-11* [0.3944    0.7429    1.0888    1.5499    2.0395
2.2885];
Isignal{4}= 100e-11* [0.3814    0.7490    1.1478    1.5921    2.0740
2.4219];
Isignal{5}= 100e-11* [0.4382    0.7333    1.1524    1.6211    2.1739
2.5085];
Isignal{6}= 100e-11* [0.4150    0.8120    1.2570    1.8080    2.3970
2.7720];
Isignal{7}= 0.1e-08* [-1.0400   -2.1500   -3.1300   -4.2100   -
5.8000];
Isignal{8}= 0.1e-08* [-0.9836   -2.0197   -3.2311   -4.2169   -
5.9724];
Isignal{9}= 0.1e-08* [-1.1498   -2.0819   -3.2245   -4.4790   -
6.4186];
Isignal{10}= 0.1e-08* [-1.0938   -2.1790   -3.3412   -4.4023   -
6.1688];
Isignal{11}= 0.1e-08* [-1.1426   -2.0668   -3.2571   -4.3210   -
5.6587];
Isignal{12}= 0.1e-08* [-1.0773   -1.9373   -3.0359   -4.0878   -
5.7367];
Isignal{13}= 0.1e-08* [-1.1161   -2.0925   -3.3319   -4.3793   -
6.3338];
Isignal{14}= 0.1e-08* [-1.2394   -2.2933   -3.5737   -4.8127   -
6.9854];
Isignal{15}= 0.1e-08* [-1.0627   -2.2126   -3.4356   -4.5027   -
6.8513];
Isignal{16}= 0.1e-08* [-1.0210   -1.9337   -2.9864   -3.9251   -
5.6873];
Isignal{17}= 0.1e-08* [-0.9500   -1.8600   -2.6800   -3.6600   -
5.1500];
Isignal{18}= 0.1e-08* [-1.4300   -3.2500   -6.5000   -7.1000   -
7.2000   -7.2000];
Isignal{19}= 0.1e-08* [-0.8572   -1.8229   -3.7096   -6.1713   -
7.0780   -7.1570];
Isignal{20}= 0.1e-08* [-0.6406   -1.6418   -3.2282   -5.5025   -
7.0659   -7.1561];
Isignal{21}= 0.1e-08* [-0.6191   -1.5552   -3.3578   -5.5197   -
7.0709   -7.1440];
Isignal{22}= 0.1e-08* [-0.6911   -1.8811   -3.4943   -5.4616   -
7.0863   -7.1601];
Isignal{23}= 0.1e-08* [-0.8588   -1.5789   -3.4472   -5.3820   -
7.0965   -7.1608];

```

```

Isignal{24}= 0.1e-08* [-0.7300   -1.9600   -3.9900   -6.9100   -
7.1300   -7.1800];
Isignal{25}= 0.1e-08* [-0.5700   -1.1050   -1.2530   -1.7380   -
2.2520   -2.8300   -3.2520   -4.2650   -5.5000   -6.6640   -7.0730];
Isignal{26}= 0.1e-08* [-0.5013   -0.7911   -0.8740   -1.3098   -
1.6504   -1.9187   -2.2705   -2.7047   -3.3050   -3.8420   -4.6206];
Isignal{27}= 0.1e-08* [-0.4677   -0.7222   -0.9797   -1.3065   -
1.5826   -2.0614   -2.3511   -2.8692   -3.4582   -4.2163   -4.8204];
Isignal{28}= 0.1e-08* [-0.5500   -0.8230   -0.9300   -1.3180   -
1.7500   -2.0550   -2.5500   -3.0700   -3.7400   -4.2670   -5.0520];
Isignal{29}= 0.1e-08* [-0.6030   -0.9350   -1.5040   -1.9200   -
2.3050   -2.7540   -3.3040   -4.0800   -4.7030   -5.8000   -5.8000];
Isignal{30}= 0.1e-08* [-0.4736   -0.7772   -1.0211   -1.2297   -
1.5806   -1.9804   -2.1767   -2.7243   -3.1848   -3.7236   -4.3876];
Isignal{31}= 0.1e-08* [-0.4574   -0.6877   -0.8195   -1.1293   -
1.4723   -1.8349   -2.1524   -2.6716   -3.1074   -3.5280   -4.0557];
Isignal{32}= 0.1e-08* [-0.4409   -0.7802   -0.8451   -1.1705   -
1.4267   -1.7801   -2.1086   -2.5845   -3.0340   -3.5387   -4.0792];
Isignal{33}= 0.1e-08* [-0.3850   -0.7150   -0.9320   -1.2370   -
1.6150   -1.9650   -2.1900   -2.7300   -3.4000   -3.9750   -4.4850];
Isignal{34}= 0.1e-08* [-0.4200   -1.3000   -2.6700   -3.7200   -
7.0900   -7.1500   -7.1800];
Isignal{35}= 0.1e-08* [-0.3089   -0.6474   -1.3408   -2.3928   -
6.1706   -7.1150   -7.1408];
Isignal{36}= 0.1e-08* [-0.2516   -0.6260   -1.1851   -2.4370   -
6.2650   -7.1123   -7.1431];
Isignal{37}= 0.1e-08* [-0.2452   -0.5334   -1.1121   -2.3609   -
5.6998   -7.1104   -7.1354];
Isignal{38}= 0.1e-08* [-0.3200   -0.8500   -1.8500   -2.8500   -
6.9700   -7.1300   -7.1500];
Isignal{39}= 1e-08* [0.0100   0.0320   0.0640   0.1000   0.1450
0.3050   0.5050   0.6250];
Isignal{40}= 1e-08* [0.0181   0.0466   0.0858   0.1349   0.1838
0.3264   0.5140   0.6246];
Isignal{41}= 1e-08* [0.0164   0.0373   0.0722   0.1095   0.1579
0.3009   0.4805   0.6286];
Isignal{42}= 1e-08* [0.0140   0.0353   0.0718   0.1113   0.1529
0.2760   0.5149   0.6082];
Isignal{43}= 1e-08* [0.0150   0.0380   0.0730   0.1160   0.1600
0.2700   0.5100   0.6300];
Isignal{44}= 1e-08* [0.0370   0.0750   0.1480   0.2190   0.3100
0.5550   1.1200   1.3500];
Isignal{45}= 1e-08* [0.0150   0.0284   0.0583   0.0840   0.1083
0.1435   0.2361   0.3196];
Isignal{46}= 1e-08* [0.0130   0.0252   0.0508   0.0754   0.1011
0.1326   0.2289   0.3023];
Isignal{47}= 1e-08* [0.0100   0.0230   0.0460   0.0750   0.0990
0.1380   0.2480   0.3300];
Isignal{48}= 1e-08* [-0.0380   -0.0770   -0.1500   -0.2180   -0.2950
-0.4600   -0.6800   -0.7600];

```

```

Isignal{49}= 1e-08* [-0.0289   -0.0548   -0.1043   -0.1598   -0.2168
-0.2895   -0.3540   -0.3673];
Isignal{50}= 1e-08* [-0.0243   -0.0493   -0.0969   -0.1504   -0.2013
-0.2691   -0.3269   -0.3391];
Isignal{51}= 1e-08* [-0.0185   -0.0410   -0.0762   -0.1144   -0.1539
-0.1964   -0.2454   -0.2492];
Isignal{52}= 1e-08* [-0.0220   -0.0410   -0.0760   -0.1070   -0.1440
-0.1910   -0.2340   -0.2370];
Isignal{53}= 0.1e-08* [-0.1800   -0.3800   -0.7700   -1.1600   -
1.5400   -2.0800   -2.9000   -3.0000];
Isignal{54}= 0.1e-08* [-0.1583   -0.3443   -0.6369   -0.9448   -
1.2745   -1.7021   -2.1045   -2.1054];
Isignal{55}= 0.1e-08* [-0.1552   -0.3317   -0.6276   -0.9581   -
1.2704   -1.6988   -2.1300   -2.1101];
Isignal{56}= 0.1e-08* [-0.1173   -0.3450   -0.6593   -0.9557   -
1.2950   -1.7156   -2.1052   -2.0982];
Isignal{57}= 0.1e-08* [-0.1600   -0.3300   -0.6300   -0.9400   -
1.2600   -1.6700   -2.0500   -2.1300];
Isignal{58}= 0.1e-08* [-0.0250   -0.0650   -0.1170   -0.1960   -
0.4300   -0.9050   -1.5600   -1.6200];
Isignal{59}= 0.1e-08* [-0.0185   -0.0394   -0.0715   -0.1026   -
0.1316   -0.1770   -0.2133   -0.2187];
Isignal{60}= 0.1e-08* [-0.0183   -0.0342   -0.0654   -0.0918   -
0.1278   -0.1709   -0.2053   -0.2095];
Isignal{61}= 0.1e-08* [-0.0151   -0.0322   -0.0613   -0.0902   -
0.1202   -0.1564   -0.2003   -0.1992];
Isignal{62}= 0.1e-08* [-0.0200   -0.0340   -0.0700   -0.1030   -
0.1370   -0.1860   -0.3000   -0.3300];
Isignal{63}= 0.1e-08* [-0.1400   -0.5500   -1.8100   -3.4600   -
6.2000   -7.1000   -7.1500];
Isignal{64}= 0.1e-08* [-0.0805   -0.2731   -0.7070   -1.1964   -
1.7072   -2.2967   -2.4563];
Isignal{65}= 0.1e-08* [-0.0510   -0.2842   -0.7204   -1.1449   -
1.6676   -2.2032   -2.3782];
Isignal{66}= 0.1e-08* [-0.0679   -0.3031   -0.6986   -1.1812   -
1.6365   -2.1056   -2.3089];
Isignal{67}= 0.1e-08* [-0.0600   -0.2400   -1.1000   -1.5000   -
2.0000   -2.6000   -2.8000];
Isignal{68}= 0.1e-08* [-0.0300   -0.1700   -0.4600   -0.6800   -
0.9700   -1.2200   -1.5800   -1.9000   -2.2700   -2.7500   -4.0500
-5.1500   -6.8500];
Isignal{69}= 0.1e-08* [-0.8500   -0.8973   -0.9854   -1.0536   -
1.1979   -1.2439   -1.3693   -1.4482   -1.5728   -1.6508   -1.7748
-1.8739   -1.9920];
Isignal{70}= 0.1e-08* [-0.8557   -0.9004   -0.9928   -1.0978   -
1.1698   -1.2948   -1.3789   -1.4487   -1.5657   -1.6641   -1.7884
-1.8762   -1.9804];
Isignal{71}= 2* 1e-12* [39.3043   79.3413   148.1947   218.9903
299.6809   383.5504   424.6373];
Isignal{72}= 2* 1e-12* [44.4811   98.3291   153.1839   224.8636
301.6316   389.1492   422.2842];

```

```

Isignal{73}= 2* 1e-12* [45.0122    84.3869   161.3839   227.8435
306.1631   391.5514   421.1379];
Isignal{74}= 2* 1e-12* [37.5795    80.1882   154.5460   218.2028
294.7040   384.1384   424.6373];
Isignal{75}= 2* 1e-12* [36.9364    78.3492   145.7983   218.4073
295.0014   383.1298   413.4374];
Isignal{76}= 2* 1e-12* [37.8161    78.7238   146.6193   220.4674
298.9047   383.7017   421.7112];
Isignal{77}= 2* 1e-12* [38.3425    78.1205   155.1337   219.1532
294.4790   382.9356   414.7172];

```

```

%%% mean(Isignal)-mean(background(emeter drift corrected when
available)) *No correction made for concentration thru Vs or run to
run

```

```

Idiff{1}= 1.0e-009 * [-0.0112   -0.0805   -0.1128   -0.1814   -
0.2660   -0.3541];
Idiff{2}= 1.0e-009 * [-0.0200   -0.0601   -0.0782   -0.2015
0.2276    0.0368];
Idiff{3}= 1.0e-009 * [-0.0206   -0.0691   -0.1682   -0.2581   -
0.3575   -0.4835];
Idiff{4}= 1.0e-009 * [-0.0336   -0.0630   -0.1092   -0.2159   -
0.3230   -0.3501];
Idiff{5}= 1.0e-009 * [0.0232   -0.0787   -0.1046   -0.1869   -0.2231
-0.2635];
Idiff{6}=[];
Idiff{7}=[];
Idiff{8}= 1.0e-008 * [0.0035    0.0061   -0.0208   -0.0138   -
0.0327];
Idiff{9}= 1.0e-008 * [-0.0139   -0.0026   -0.0241   -0.0448   -
0.0830];
Idiff{10}= 1.0e-008 * [-0.0089   -0.0144   -0.0389   -0.0410   -
0.0626];
Idiff{11}= 1.0e-008 * [-0.0145   -0.0054   -0.0340   -0.0371   -
0.0166];
Idiff{12}= 1.0e-008 * [-0.0085    0.0057   -0.0147   -0.0172   -
0.0285];
Idiff{13}= 1.0e-008 * [-0.0130   -0.0116   -0.0471   -0.0498   -
0.0922];
Idiff{14}= 1.0e-008 * [-0.0263   -0.0349   -0.0763   -0.0993   -
0.1646];
Idiff{15}= 1.0e-008 * [-0.0093   -0.0288   -0.0656   -0.0721   -
0.1558];
Idiff{16}= 1.0e-008 * [-0.0062   -0.0044   -0.0261   -0.0209   -
0.0471];
Idiff{17}=[];
Idiff{18}=[];
Idiff{19}= 1.0e-008 * [0.0437    0.1176    0.2302    0.0892
0.0108    0.0039];
Idiff{20}= 1.0e-008 * [0.0524    0.1119    0.2319    0.1525
0.0107    0.0036];

```



```

Idiff{21}= 1.0e-008 * [0.0432    0.0996    0.1783    0.1477
0.0091    0.0045];
Idiff{22}= 1.0e-008 * [0.0255    0.0477    0.1270    0.1507
0.0065    0.0026];
Idiff{23}= 1.0e-008 * [-0.0002    0.0615    0.0997    0.1563
0.0046    0.0023];
Idiff{24}=[];
Idiff{25}=[];
Idiff{26}= 1.0e-008 * [0.0059    0.0178    0.0223    0.0226
0.0359    0.0537    0.0643    0.0984    0.1346    0.1666    0.1477];
Idiff{27}= 1.0e-008 * [0.0087    0.0168    0.0027    0.0112
0.0287    0.0179    0.0367    0.0486    0.0702    0.0623    0.0714];
Idiff{28}=[];
Idiff{29}=[];
Idiff{30}= 1.0e-008 * [0.0070    0.0098    0.0327    0.0504
0.0536    0.0558    0.0823    0.0987    0.1162    0.1578    0.1053];
Idiff{31}= 1.0e-008 * [0.0037    0.0138    0.0401    0.0452
0.0490    0.0528    0.0599    0.0739    0.0949    0.1367    0.1092];
Idiff{32}= 1.0e-008 * [-0.0001   -0.0010    0.0232    0.0239
0.0363    0.0384    0.0363    0.0487    0.0696    0.0898    0.0739];
Idiff{33}=[];
Idiff{34}=[];
Idiff{35}= 1.0e-008 * [0.0078    0.0506    0.1062    0.1043
0.0880    0.0029    0.0029];
Idiff{36}= 1.0e-008 * [0.0112    0.0420    0.1022    0.0791
0.0757    0.0026    0.0020];
Idiff{37}= 1.0e-008 * [0.0095    0.0407    0.0903    0.0664
0.1294    0.0024    0.0021];
Idiff{38}=[];
Idiff{39}=[];
Idiff{40}= 1.0e-009 * [0.0660    0.1280    0.1910    0.3010
0.3430    0.3190    0.0750   -0.0190];
Idiff{41}= 1.0e-009 * [0.0360    0.0200    0.0330    0.0070
0.0460    0.1510   -0.2720    0.0080];
Idiff{42}= 1.0e-009 * [0.0010   -0.0140    0.0070   -0.0120   -
0.0390   -0.0160    0.0600   -0.2070];
Idiff{43}=[];
Idiff{44}=[];
Idiff{45}= 1.0e-008 * [-0.0043   -0.0125   -0.0228   -0.0405   -
0.0632   -0.1378   -0.3116   -0.3610];
Idiff{46}= 1.0e-008 * [-0.0014   -0.0062   -0.0117   -0.0228   -
0.0319   -0.0725   -0.1595   -0.1919];
Idiff{47}=[];
Idiff{48}=[];
Idiff{49}= 1.0e-008 * [0.0036    0.0098    0.0202    0.0200
0.0262    0.0779    0.1726    0.2128];
Idiff{50}= 1.0e-008 * [0.0046    0.0074    0.0114    0.0051
0.0086    0.0393    0.1017    0.1261];
Idiff{51}= 1.0e-008 * [0.0070    0.0078    0.0159    0.0166
0.0228    0.0529    0.0853    0.1011];
Idiff{52}=[];

```

```

Idiff{53}=[];
Idiff{54}= 1.0e-009 * [0.0171    0.0242    0.1009    0.1648
0.2013    0.2839    0.6005    0.6951];
Idiff{55}= 1.0e-009 * [0.0154    0.0248    0.0766    0.0985
0.1380    0.1884    0.3704    0.4809];
Idiff{56}= 1.0e-009 * [0.0485   -0.0005    0.0112    0.0479
0.0460    0.0729    0.1906    0.2834];
Idiff{57}=[];
Idiff{58}=[];
Idiff{59}= 1.0e-009 * [0.0049    0.0157    0.0304    0.0635
0.2041    0.4967    0.9413    0.9862];
Idiff{60}= 1.0e-009 * [0.0039    0.0139    0.0259    0.0534
0.1421    0.3410    0.6658    0.7053];
Idiff{61}= 1.0e-009 * [0.0059    0.0083    0.0186    0.0323
0.0783    0.1803    0.3639    0.4013];
Idiff{62}=[];
Idiff{63}=[];
Idiff{64}= 1.0e-008 * [0.0038    0.0195    0.0915    0.1745
0.3383    0.3614    0.3544];
Idiff{65}= 1.0e-008 * [0.0046    0.0101    0.0713    0.1274
0.2302    0.2507    0.2461];
Idiff{66}= 1.0e-008 * [0.0010    0.0006    0.0560    0.0755
0.1299    0.1496    0.1460];
Idiff{67}=[];
Idiff{68}=[];
Idiff{69}= 1.0e-008 * [-0.0820   -0.0727   -0.0525   -0.0374   -
0.0228   -0.0024    0.0211    0.0452    0.0697    0.1099    0.2275
0.3276    0.4858];
Idiff{70}= 1.0e-008 * [-0.0826   -0.0730   -0.0533   -0.0418   -
0.0200   -0.0075    0.0201    0.0451    0.0704    0.1086    0.2262
0.3274    0.4870];
Idiff{71}=[];
Idiff{72}= 2* 1.0e-012 * [6.0392    18.5643    1.8136    6.2671
4.4391    5.3048   -2.3531];
Idiff{73}= 2* 1.0e-012 * [6.5703    4.6221    10.0136    9.2470
8.9706    7.7070   -3.4995];
Idiff{74}=[];
Idiff{75}= 2* 1.0e-012 * [-1.0246   -0.8052   -9.0415   -0.2707
0.4100   -0.4072   -6.2398];
Idiff{76}= 2* 1.0e-012 * [-0.1449   -0.4306   -8.2206    1.7894
4.3133    0.1647    2.0340];
Idiff{77}=[];

%%% Condenser voltage settings
Vs{1} = [500 1000 1500 2000 2500 2800];
Vs{2} = [500 1000 1500 2000 2500 2800];
Vs{3} = [500 1000 1500 2000 2500 2800];
Vs{4} = [500 1000 1500 2000 2500 2800];
Vs{5} = [500 1000 1500 2000 2500 2800];
Vs{6} = [500 1000 1500 2000 2500 2800];
Vs{7} = [500 1000 1500 2000 2500];

```



```

Vs{59} = [200 500 1000 1500 2000 2500 3000 3100];
Vs{60} = [200 500 1000 1500 2000 2500 3000 3100];
Vs{61} = [200 500 1000 1500 2000 2500 3000 3100];
Vs{62} = [200 500 1000 1500 2000 2500 3000 3100];
Vs{63} = [200 500 1000 1500 2000 2500 2700];
Vs{64} = [200 500 1000 1500 2000 2500 2700];
Vs{65} = [200 500 1000 1500 2000 2500 2700];
Vs{66} = [200 500 1000 1500 2000 2500 2700];
Vs{67} = [200 500 1000 1500 2000 2500 2700];
Vs{68} = [200 400 600 800 1000 1200 1400 1600 1800 2000 2200 2400
2600];
Vs{69} = [200 400 600 800 1000 1200 1400 1600 1800 2000 2200 2400
2600];
Vs{70} = [200 400 600 800 1000 1200 1400 1600 1800 2000 2200 2400
2600];
Vs{71} = [200 500 1000 1500 2000 2500 2700];
Vs{72} = [200 500 1000 1500 2000 2500 2700];
Vs{73} = [200 500 1000 1500 2000 2500 2700];
Vs{74} = [200 500 1000 1500 2000 2500 2700];
Vs{75} = [200 500 1000 1500 2000 2500 2700];
Vs{76} = [200 500 1000 1500 2000 2500 2700];
Vs{77} = [200 500 1000 1500 2000 2500 2700];

%%% Concentration drift through V steps
V_conc_scaling{1} = [1.0000    0.9348    0.8815    0.8305    0.7881
0.7335];
V_conc_scaling{2} = [1.0000    0.9703    0.9398    0.9088    0.8713
0.8447];
V_conc_scaling{3} = [1.0000    0.9265    0.8548    0.7863    0.7340
0.6882];
V_conc_scaling{4} = [1.0000    0.7473    0.6059    0.5029    0.4346
0.3837];
V_conc_scaling{5} = [1.0000    1.0375    1.0778    1.1215    1.1729
1.2225];
V_conc_scaling{6} = ones(1,6);
V_conc_scaling{7} = ones(1,5);
V_conc_scaling{8} = [1.0000    0.9833    0.9664    0.9500
0.9388];
V_conc_scaling{9} = [1.0000    0.9972    0.9951    0.9924
0.9903];
V_conc_scaling{10} = [1.0000    0.9962    0.9925    0.9887
0.9850];
V_conc_scaling{11} = [1.0000    0.9907    0.9816    0.9727
0.9639];
V_conc_scaling{12} = [1.0000    0.9975    0.9949    0.9916
0.9889];
V_conc_scaling{13} = [1.0000    0.9791    0.9590    0.9398
0.9228];
V_conc_scaling{14} = [1.0000    0.9990    0.9979    0.9969
0.9961];

```

```

V_conc_scaling{15} = [1.0000    1.0081    1.0163    1.0239
1.0331];
V_conc_scaling{16} = [1.0000    1.0379    1.0806    1.1269
1.1774];
V_conc_scaling{17} = ones(1,5);
V_conc_scaling{18} = ones(1,6);
V_conc_scaling{19} = [1.0120    1.0000    0.9882    0.9768    0.9656
0.9557];
V_conc_scaling{20} = [0.9577    1.0000    1.0462    1.0971    1.1530
1.2151];
V_conc_scaling{21} = [1.0070    1.0000    0.9930    0.9862    0.9795
0.9729];
V_conc_scaling{22} = [0.9866    1.0000    1.0138    1.0281    1.0426
1.0578];
V_conc_scaling{23} = [0.9315    1.0000    1.0793    1.1725    1.2840
1.4168];
V_conc_scaling{24} = ones(1,6);
V_conc_scaling{25} = ones(1,11);
V_conc_scaling{26} = [1.3992    1.1663    1.0000    0.8752    0.7780
0.7003    0.6367    0.5837    0.5388    0.5004    0.4670];
V_conc_scaling{27} = [1.8365    1.2950    1.0000    0.8145    0.6870
0.5941    0.5233    0.4675    0.4225    0.3854    0.3543];
V_conc_scaling{28} = ones(1,11);
V_conc_scaling{29} = ones(1,11);
V_conc_scaling{30} = [0.9884    0.9941    1.0000    1.0059    1.0118
1.0179    1.0241    1.0303    1.0365    1.0429    1.0493];
V_conc_scaling{31} = [1.0625    1.0303    1.0000    0.9714    0.9445
0.9189    0.8948    0.8718    0.8501    0.8277    0.8064];
V_conc_scaling{32} = [1.0686    1.0332    1.0000    0.9689    0.9397
0.9122    0.8862    0.8617    0.8384    0.8147    0.7923];
V_conc_scaling{33} = ones(1,11);
V_conc_scaling{34} = ones(1,7);
V_conc_scaling{35} = [0.9753    1.0000    1.0260    1.0534    1.0823
1.1127    1.1450];
V_conc_scaling{36} = [0.9970    1.0000    1.0030    1.0059    1.0090
1.0120    1.0150];
V_conc_scaling{37} = [0.9806    1.0000    1.0202    1.0413    1.0633
1.0862    1.1101];
V_conc_scaling{38} = ones(1,7);
V_conc_scaling{39} = ones(1,8);
V_conc_scaling{40} = [1.0004    1.0000    0.9996    0.9992    0.9988
0.9983    0.9978    0.9976];
V_conc_scaling{41} = [1.0089    1.0000    0.9896    0.9793    0.9694
0.9579    0.9516    0.9425];
V_conc_scaling{42} = [1.0016    1.0000    0.9983    0.9967    0.9950
0.9934    0.9918    0.9900];
V_conc_scaling{43} = ones(1,8);
V_conc_scaling{44} = ones(1,8);
V_conc_scaling{45} = [0.9973    1.0000    1.0027    1.0055    1.0083
1.0110    1.0138    1.0167];

```

```

V_conc_scaling{46} = [0.9909    1.0000    1.0101    1.0205    1.0310
1.0413    1.0537    1.0642];
V_conc_scaling{47} = ones(1,8);
V_conc_scaling{48} = ones(1,8);
V_conc_scaling{49} = [1.0018    1.0000    0.9982    0.9964    0.9946
0.9929    0.9911    0.9897];
V_conc_scaling{50} = [1.0156    1.0000    0.9848    0.9701    0.9559
0.9382    0.9258    0.9161];
V_conc_scaling{51} = [0.9913    1.0000    1.0089    1.0179    1.0271
1.0395    1.0481    1.0513];
V_conc_scaling{52} = ones(1,8);
V_conc_scaling{53} = ones(1,8);
V_conc_scaling{54} = [0.9954    1.0000    1.0046    1.0092    1.0139
1.0186    1.0224    1.0272];
V_conc_scaling{55} = [1.0048    1.0000    0.9952    0.9905    0.9860
0.9800    0.9779    0.9714];
V_conc_scaling{56} = [0.9947    1.0000    1.0053    1.0106    1.0161
1.0212    1.0264    1.0315];
V_conc_scaling{57} = ones(1,8);
V_conc_scaling{58} = ones(1,8);
V_conc_scaling{59} = [0.9885    1.0000    1.0117    1.0238    1.0361
1.0487    1.0616    1.0754];
V_conc_scaling{60} = [1.0375    1.0000    0.9652    0.9327    0.9024
0.8739    0.8516    0.8241];
V_conc_scaling{61} = [0.9838    1.0000    1.0111    1.0254    1.0401
1.0553    1.0709    1.0862];
V_conc_scaling{62} = ones(1,8);
V_conc_scaling{63} = ones(1,7);
V_conc_scaling{64} = [0.9898    1.0000    1.0104    1.0210    1.0319
1.0464    1.0543];
V_conc_scaling{65} = [0.9885    1.0000    1.0117    1.0239    1.0362
1.0488    1.0618];
V_conc_scaling{66} = [0.9869    1.0000    1.0092    1.0182    1.0274
1.0381    1.0490];
V_conc_scaling{67} = ones(1,7);
V_conc_scaling{68} = ones(1,13);
V_conc_scaling{69} = [0.9951    1.0000    1.0049    1.0107    1.0149
1.0200    1.0251    1.0303    1.0355    1.0408    1.0461    1.0515
1.0570];
V_conc_scaling{70} = [0.9973    1.0000    1.0023    1.0049    1.0068
1.0092    1.0115    1.0139    1.0162    1.0185    1.0209    1.0231
1.0256];
V_conc_scaling{71} = ones(1,7);
V_conc_scaling{72} = [1 1 1 1 1 1 1];
V_conc_scaling{73} = [1 1 1 1 1 1 1];
V_conc_scaling{74} = ones(1,7);
V_conc_scaling{75} = [1 1 1 1 1 1 1];
V_conc_scaling{76} = [1 1 1 1 1 1 1];
V_conc_scaling{77} = ones(1,7);

PPR{1} = [1    0.9161 0.8709 0.837    0.8002 0.7907 0.7968 0.9976];

```

```

PPR{2} = [0.9989      0.8824 0.7993 0.7181 0.6267 0.578  0.5411
0.9986];
PPR{3} = [0.9961      0.1264 0.0048 0.0003 0.0002 0.0002 0.0002
1.0023];
PPR{4} = [0.947      0.3674 0.183  0.1094 0.0736 0.0567 0.0586
1.019];
PPR{5} = [1.001      0.1568 0.0267 0.0022 0.0002 0.0003 0.0008
1.016];
PPR{6} = ones(1,8);
PPR{7} = ones(1,7);
PPR{8} = [1.0003      0.7872 0.668  0.5409 0.458  0.3928 0.9997];
PPR{9} = [1.0001      0.6847 0.5274 0.3964 0.2886 0.2139 0.9999];
PPR{10} = [0.9995      0.511  0.3385 0.2233 0.1748 0.1009 1.0005];
PPR{11} = [0.9995      0.9256 0.8704 0.7684 0.7073 0.6662 1.0005];
PPR{12} = [1.0001      0.9458 0.8997 0.8394 0.7998 0.7783 0.9999];
PPR{13} = [0.9996      0.9678 0.9443 0.9093 0.8836 0.877  1.0004];
PPR{14} = [1.0002      0.1698 0.0323 0.0027 0.0002 0.0032 0.9998];
PPR{15} = [1  0.055  0.0002 0.0001 0.0005 0.001  1];
PPR{16} = [1.0002      0.0015 0.0015 0.0016 0.0004 0.0033 0.9999];
PPR{17} = ones(1,7);
PPR{18} = ones(1,8);
PPR{19} = [1.0001      0.9506 1.0387 0.9478 0.9372 0.9303 2.8957
1.0115];
PPR{20} = [1.0001      0.3955 0.1352 0.071  0.049  0.0542 0.1079
0.9999];
PPR{21} = [1.0001      1.0871 0.9667 0.7774 0.8196 0.7522 0.7911
0.9999];
PPR{22} = [1.0004      0.7309 0.4971 0.3041 0.1948 0.1306 0.0916
0.9997];
PPR{23} = [1.0004      0.9196 1.1438 1.1164 1.1032 1.1363 1.9595
0.9989];
PPR{24} = ones(1,8);
PPR{25} = ones(1,13);
PPR{26} = [1.0136      0.2844 0.1335 0.136  0.1335 0.1187 0.0975 0.081
0.0767 0.0731 0.0775 0.5198 1.0002];
PPR{27} = [0.8781      0.4822 0.3817 0.2712 0.2397 0.1966 0.1683 0.1322
0.1151 0.0979 0.0863 1.937  1.0253];
PPR{28} = ones(1,13);
PPR{29} = ones(1,13);
PPR{30} = [1.0014      0.9989 1.0037 1.0771 1.0938 1.106  1.0415 0.9656
0.8979 0.8519 0.9019 0.962  0.9986];
PPR{31} = [1.0003      1.198  1.0309 1.0305 1.0238 0.9752 1.0131 1.0264
1.0517 1.0773 1.0388 1.0298 0.9996];
PPR{32} = [1  1.002  1.0715 1.1894 1.2774 1.2801 1.2378 1.1786 1.096
1.0232 0.9856 1.0063 1];
PPR{33} = ones(1,13);
PPR{34} = ones(1,9);
PPR{35} = [1.0005      0.9047 0.8653 0.7816 0.7966 0.72  0.7448 0.7566
0.9998];
PPR{36} = [1  0.9865 0.9107 0.8975 0.9222 0.8721 0.7957 0.782  1];

```

```

PPR{37} = [1.0001    0.9351 0.8159 0.7577 0.705   0.6783 0.6514 0.8102
1];
PPR{38} = ones(1,9);
PPR{39} = ones(1,10);
PPR{40} = [0.9999    0.9308 0.9078 0.8191 0.7965 0.7496 0.87   0.7869
0.7888 1.0001];
PPR{41} = [1  0.9087 0.9113 0.8799 0.7809 0.7694 0.743  0.7562 0.8248
1];
PPR{42} = [1.0002    0.9796 0.9323 0.8223 0.7815 0.7584 0.7495 0.7438
0.8081 0.9999];
PPR{43} = ones(1,10);
PPR{44} = ones(1,10);
PPR{45} = [0.9993    1.0381 0.9574 0.8861 0.8089 0.8026 0.8146 0.7837
0.8039 1.0007];
PPR{46} = [0.9999    0.9142 0.954  0.7932 0.7711 0.7592 0.8256 0.7967
0.8709 1.0001];
PPR{47} = ones(1,10);
PPR{48} = ones(1,10);
PPR{49} = [1.0005    0.9642 1.0181 1.0321 1.004  1.4836 1.4496 1.387
1.3461 0.9995];
PPR{50} = [1  1.07  1.0317 0.9575 1.0608 0.9717 1.0764 2.4122 1.4282
1];
PPR{51} = [0.9989    0.9414 0.9665 0.9824 0.9906 1.0115 0.984  1.8494
1.65  1.0011];
PPR{52} = ones(1,10);
PPR{53} = ones(1,10);
PPR{54} = [0.9999    0.9181 0.9316 0.9345 0.9274 0.9234 0.9194 1.9886
586.611 1.0001];
PPR{55} = [0.9996    1.0084 0.9705 0.9115 1.0799 0.9599 0.9252 1.1136
608.0677 1.0004];
PPR{56} = [1.0007    1.0012 0.975  0.9889 1.0029 0.9707 0.9603 0.9198
1.6787 0.9993];
PPR{57} = ones(1,10);
PPR{58} = ones(1,10);
PPR{59} = [0.9999    0.9858 0.9978 0.9728 0.9884 0.9998 1.0468 1.0112
1.2629 1.0001];
PPR{60} = [0.9994    0.9967 0.8406 0.913  0.8304 0.775  0.7745 0.9234
0.9807 1.0006];
PPR{61} = [0.9996    1.0193 1.0241 1.0069 0.9627 1.0579 1.0165 1.068
1.0152 1.0004];
PPR{62} = ones(1,10);
PPR{63} = ones(1,9);
PPR{64} = [1.0008    1.0215 1.013  0.9997 1.1364 0.7746 0.8408 0.9994
0.9992];
PPR{65} = [1.0005    0.7358 0.4042 0.2492 0.2153 0.2351 0.2251 0.2465
0.9995];
PPR{66} = [0.9987    0.8183 0.9032 0.806  1.0288 0.871  0.7886 0.8314
1.0013];
PPR{67} = ones(1,9);
PPR{68} = ones(1,15);

```



```

PPR{69} = [1.0003    1.0497 1.0708 1.0118 0.8992 1.1788 1.2024 1.2333
          1.1341 1.1976 1.031   1.0861 0.9743 1.2761 0.9993];
PPR{70} = [0.9999    1.0758 1.3246 1.3049 1.0728 0.3183 0.9593 1.1412
          0.992   1.1464 1.0567 1.0873 1.1069 1.0473 1.0003];
PPR{71} = ones(1,9);
PPR{72} = ones(1,9);
PPR{73} = ones(1,9);
PPR{74} = ones(1,9);
PPR{75} = ones(1,9);
PPR{76} = ones(1,9);
PPR{77} = ones(1,9);

save output.mat

```

4. Analyze_full_dataset_2.m is the program that performed the Whipple calculation, and other data analysis, on the data contained in the project database:

```

% analyze_full_dataset.m
% T.Barrett
% Jan 2011

%%%%%%%%%%%%%%%%%%%%%%%%%%%%%%%%%%%%%%%%%%%%%%%%%%%%%%%%%%%%%%%%%%%%%%%%
%%%%%%%%%%%%%%%%%%%%%%%%%%%%%%%%%%%%%%%%%%%%%%%%%%%%%%%%%%%%%%%%%%%%%%%%

plot_option = 1;
% 1: Plot the item numbers listed in <choose_items>, below.
% 2: Plot all of N composition
% 3: Plot all of O composition
% 4: Plot all of I compositions
% 5: Plot all 0.3LPM flowrates
% 6: Plot all non-zero,<>0.3LPM flowrates
% 7: Plot all 10nm diameters, no TI
% 8: Plot all non-zero,<>10nm diameters
% 9: Plot all ~N composition
%
% 10: Plot N composition for K Emeter
% 11: Plot N composition for T Emeter
%
% 12: Plot all of I compositions w/ 0.3LPM flowrate
% 13: Plot all of I compositions w/ 0.7LPM flowrate
% 14: Plot all of I compositions w/ 1.5LPM flowrate
% 15: Plot all of I compositions w/ 0.3LPM flowrate w/10nm diameter,
Kmeter
%
% 20: Plot all of O compositions w/ 0.1LPM flowrate
% 21: Plot all of O compositions w/ 0.3LPM flowrate, no TI

```

```

% 22: Plot all of 0 compositions w/ 0.65LPM flowrate --> TI , no
data
% 23: Plot all of 0 compositions w/ 0.3LPM flowrate w/10nm diameter,
Kmeter
%
% 30: Plot all PPK31, ~N
% 31: Plot all Oleic, PPK 3/4 1, ~N
%
% 32: Plot all Oleic, PPK31, ~N, <=0.3LPM, <=20nm
% 40: Plot all ~N composition, Kmeter
% 41: Plot all ~N composition, TImeter

```

```

%title_tagline=' -- all ~N datasets';
%title_tagline=' -- Oleic 0.3LPM 1PPK31';
%title_tagline=' -- IPA Flow&Diameter 1PPK31';
%title_tagline=' -- Effect of Condenser Polarity -- IPA,
1(P/N)PK31';
%title_tagline=' -- TI Electrometer, 0.3LPM';
%title_tagline=' -- TI Electrometer, 0.65LPM';
%title_tagline=' -- AAAR Oleic';
title_tagline=' ';

```

```

set_N_flowrate=0.65;

```

```

%%% Only used for option 1
%choose_items=[19 23 64 66 69 21 20 65 70 22]; %1PPK31 Oleic 0.3LPM
%choose_items=[16 15 14 10 9 8 11 12 13]; %1PPK31 IPA Flow&Diameter
%choose_items=[2 11 1 13 5 14]; %1(P/N)PK31 IPA at paired flow/dia
%choose_items=[74:77]; %TI, 0.3LPM
%choose_items=[71:74]; %TI, 0.65LPM
%choose_items=[72 73 75 76]; %TI, 0.3 and 0.65LPM, 0 composition
%choose_items=[18:24]; %AAAR Oleic
%choose_items=[1:10];
%choose_items=[1:24]; %sets 1-3
%choose_items=[25:47]; %sets 4-8
%choose_items=[48:70]; %sets 9-13
choose_items=[71:77]; %set 14
%
%choose_items=[8 9 10 11 12 13 14 15 16 20 22]; %PPK31 ~N, Isignal
pos. trend
%choose_items=[19 21 23 26 27 30 31 32]; %PPK31 ~N, Idiff pos. trend
%
%choose_items=[49 50 51 54 55 56 59 60 61 ];
%choose_items=[40 41 42 45 46];
%choose_items=[35 36 37];

```

```

plot_item_figs='n';

```

```

plot_4up_fig='y'; %plots the four vector items in the database

```

```

plot_PPR='n';

plot_6up_fig='n'; % plots the Whipple calcs on one figure

plot_Whipple='n'; % plots the whipple calcs for Idiff on three
separate figures

plot_big_Isignal='n';

plot_scatter='n';

%%%%%%%%%%%%%%%%%%%%%%%%%%%%%%%%%%%%%%%%%%%%%%%%%%%%%%%%%%%%%%%%%%%%%%%%
%%%%%%%%%%%%%%%%%%%%%%%%%%%%%%%%%%%%%%%%%%%%%%%%%%%%%%%%%%%%%%%%%%%%%%%%

A=1.18; %mm2, Condenser plate area, actual metal as designed
A_full=3.1; %mm2, Condenser plate area coverage
d=2.00; %mm, Condenser inter-plate seperation
e_charge=1.602e-19; %coulombs (=A*s)
num_MEMS_cond2=1;
sigma=2.5e-14; %S/m, Conductivity of air at 20C, CRC 74th ed.

load full_dataset_28may2011.mat
% APA_conc          Vs          data_spreadsheet  num_cond1
% CPC_conc          bypass_factor  diameter          run_num
% Idiff             charge_polarity  emeter_type      set_num
% Isignal           composition      flowrate         test_date
% V_conc_scaling    cond_polarity    item_num
% Cond1_MEMSnum     Cond2_MEMSnum     PPR

markers={
    'k-+'
    'r-o'
    'g-*'
    'b-x'
    'c-s'
%   'y-d'
    'm-^'
    'k:+'
    'r:o'
    'g:*'
    'b:x'
    'c:s'
%   'y:d'
    'm:^'
    'k-.+'
    'r-.o'
    'g-.*'
    'b-.x'
    'c-.s'
%   'y-.d'

```

'm-.^'
 'k--+'
 'r--o'
 'g--*'
 'b--x'
 'c--s'
 % 'y--d'
 'm--^'
 'k-+ '
 'r-o '
 'g-* '
 'b-x '
 'c-s '
 % 'y-d '
 'm-^ '
 'k:+ '
 'r:o '
 'g:* '
 'b:x '
 'c:s '
 % 'y:d '
 'm:^ '
 'k-.+ '
 'r-.o '
 'g-.* '
 'b-.x '
 'c-.s '
 % 'y-.d '
 'm-.^ '
 'k--+ '
 'r--o '
 'g--* '
 'b--x '
 'c--s '
 % 'y--d '
 'm--^ '
 'k-+ '
 'r-o '
 'g-* '
 'b-x '
 'c-s '
 % 'y-d '
 'm-^ '
 'k:+ '
 'r:o '
 'g:* '
 'b:x '
 'c:s '
 % 'y:d '
 'm:^ '
 'k-.+ '
 'k-.+ '

```

    'r-.o'
    'g-.*'
    'b-.x'
    'c-.s'
%   'y-.d'
    'm-.^'
    'k--+'
    'r--o'
    'g--*'
    'b--x'
    'c--s'
%   'y--d'
    'm--^'
};

A_cm2=A/100;
A_full_cm2=A_full/100;
d_cm=d/10;
C=A_cm2/(4*pi*d_cm);
sigma_cm=sigma*100;
leakage_resistance_low=d_cm/(sigma_cm*A_cm2);
leakage_resistance_high=d_cm/(sigma_cm*A_full_cm2);
num_files=length(item_num);

for pick_item=1:num_files;
% for pick_item=7;

    APA_conc_pick = round(APA_conc(pick_item));
    CPC_conc_pick = round(CPC_conc(pick_item));
    Idiff_pick = Idiff{pick_item};
    Isignal_pick = Isignal{pick_item};
    V_conc_scaling_pick = V_conc_scaling{pick_item};
    Vs_pick = Vs{pick_item};
    bypass_factor_pick = bypass_factor(pick_item);
    charge_polarity_pick = charge_polarity(pick_item);
    composition_pick = composition(pick_item);
    cond_polarity_pick = cond_polarity(pick_item);
    diameter_pick = diameter(pick_item);
    emeter_type_pick = emeter_type(pick_item);
    flowrate_pick = flowrate(pick_item);
    num_cond1_pick = num_cond1(pick_item);
    set_num_pick = set_num(pick_item);
    test_date_pick = test_date(pick_item);
    cond1_memsnum_pick = Cond1_MEMSnum(pick_item);
    cond2_memsnum_pick = Cond2_MEMSnum(pick_item);

    legend_part1=strcat('Item:',num2str(pick_item),'
Comp:',composition_pick,' Dia:',num2str(round(diameter_pick)));
    legend_part2=cellstr(strcat(' Flow:',num2str(flowrate_pick),'
Conc:',num2str(APA_conc_pick),'..',num2str(num_cond1_pick)));

```

```

legend_part3=strcat(cond_polarity_pick,charge_polarity_pick,emeter_t
ype_pick,num2str(cond1_memsnum_pick),num2str(cond2_memsnum_pick));
    hold_legend_text_part3{pick_item}=legend_part3;

legend_text{pick_item}=strcat(legend_part1,legend_part2,legend_part3
);
    %disp(legend_text{pick_item})
    %pause
    %legend_text{pick_item}=[];

    % clc
    % pick_item
    % length_Idiff_pick=length(Idiff_pick)
    % length_Isignal_pick=length(Isignal_pick)
    % length_V_conc_scaling_pick=length(V_conc_scaling_pick)
    % length_Vs_pick=length(Vs_pick)
    % pause

    if flowrate_pick==0, flowrate_pick=set_N_flowrate; end

    Q_cm3s=flowrate_pick*(1000/60);
    num_V=length(Vs_pick);
    num_MEMS_cond1=num_cond1_pick;

    kc = (Q_cm3s./(4*pi*num_MEMS_cond1*C*Vs_pick));
    kd = (Q_cm3s./(4*pi*(num_MEMS_cond1+num_MEMS_cond2)*C*Vs_pick));
    hold_kc{pick_item}=kc;
    hold_kc_log10{pick_item}=log10(kc);
    hold_kd{pick_item}=kd;
    hold_kd_log10{pick_item}=log10(kd);

    Dp_min=10.^((log10(kc)-0.197814)./(-1.985986));
    Dp_max=10.^((log10(kd)-0.197814)./(-1.985986));
    Dp_logmean=10.^((log10(Dp_min)+log10(Dp_max))./2);
    hold_Dp_min{pick_item}=Dp_min;
    hold_Dp_max{pick_item}=Dp_max;
    hold_Dp_logmean{pick_item}=Dp_logmean;
    hold_Dp_logmean_log10{pick_item}=log10(Dp_logmean);

    hold_Dp_logmean_short{pick_item}=Dp_logmean(2:length(Dp_logmean)-1);

    hold_Dp_logmean_log10_short{pick_item}=log10(Dp_logmean(2:length(Dp_
logmean)-1));
    Dp_logdiff=log10(Dp_max)-log10(Dp_min);
    Dp_logdiff_1=Dp_logdiff(1,1);

    IoverV_straight=Isignal_pick./Vs_pick;
    if length(Idiff_pick)>0,
        IoverV_background=Idiff_pick./Vs_pick;
    else

```

```

        IoverV_background=[];
    end;
    hold_IoverV_straight{pick_item}=IoverV_straight;
    hold_IoverV_background{pick_item}=IoverV_background;

    counter=0;
    slope_deriv_straight=[];
    slope_deriv_background=[];
    for count_Vsteps= 2:num_V-1,
        counter=counter+1;
        raw_x=[kc(count_Vsteps-1) kc(count_Vsteps)
kc(count_Vsteps+1)];
        raw_y_straight=[IoverV_straight(count_Vsteps-1)
IoverV_straight(count_Vsteps) IoverV_straight(count_Vsteps+1)];
        raw_poly_straight=polyfit(raw_x,raw_y_straight,1);
        raw_polyval_straight=polyval(raw_poly_straight,raw_x);
        slope_deriv_straight(counter)=raw_poly_straight(1);
        if length(Idiff_pick)>0,
            raw_y_background=[IoverV_background(count_Vsteps-1)
IoverV_background(count_Vsteps) IoverV_background(count_Vsteps+1)];
            raw_poly_background=polyfit(raw_x,raw_y_background,1);

        raw_polyval_background=polyval(raw_poly_background,raw_x);
            slope_deriv_background(counter)=raw_poly_background(1);
        end
    end

    meas_conc_straight=slope_deriv_straight./(4*pi*C*e_charge);
    meas_conc_straight_dlogDp=meas_conc_straight./Dp_logdiff_1;

    hold_meas_conc_straight_dlogDp{pick_item}=meas_conc_straight_dlogDp;
    if length(Idiff_pick)>0,

    meas_conc_background=slope_deriv_background./(4*pi*C*e_charge);

    meas_conc_background_dlogDp=meas_conc_background./Dp_logdiff_1;

    hold_meas_conc_background_dlogDp{pick_item}=meas_conc_background_dlo
gDp;
    else
        hold_meas_conc_background_dlogDp{pick_item}=[];
    end

%     max_meas_conc=max(meas_conc);
%     max_meas_conc_dlogDp=max(meas_conc_dlogDp);
%     meas_conc_dlogDp_normtomax=meas_conc_dlogDp./max_meas_conc;
%
meas_conc_dlogDp_normtoone=meas_conc_dlogDp./concs(count_files);

%     close all
    if plot_item_figs=='y',

```

```

figure(1)
set(gcf,'Position',[1          31          1280          696])
subplot(241)
%hold on
plot(hold_kc_log10{pick_item},Isignal{pick_item})
%plot(hold_kc{pick_item},Isignal{pick_item})
xlabel('Log10( Critical Mobility, Kc [cm2/(V s)] )')
%xlabel('Critical Mobility, Kc [cm2/(V s)]')
ylabel('Current Signal [A]')
grid on
%axis([0 1 -.05 1.05])
%legend(case_info_short)
title(['straight ' num2str(pick_item)])

subplot(242)
%hold on
if length(Idiff_pick)>0,
    plot(hold_kc_log10{pick_item},Idiff{pick_item})
    %plot(hold_kc{pick_item},Idiff{pick_item})
else
    plot(1,1)
end
xlabel('Log10( Critical Mobility, Kc [cm2/(V s)] )')
%xlabel('Critical Mobility, Kc [cm2/(V s)]')
ylabel('Current Signal - Background [A]')
grid on
%axis([0 1 -.05 1.05])
%legend(case_info_short)
title('background')

%
%
figure(2)
set(gcf,'Position',[645  295  560  420])
subplot(243)
%hold on
plot(hold_kc_log10{pick_item},hold_IoverV_straight{pick_item})
%plot(hold_kc{pick_item},hold_IoverV_straight{pick_item})
xlabel('Log10( Critical Mobility, Kc [cm2/(V s)] )')
%xlabel('Critical Mobility, Kc [cm2/(V s)]')
ylabel('Current Signal / Cond. Voltage [A/V = 1/Ohm]')
grid on
%axis([0 1 -.05 1.05])
%legend(case_info_short)
title('straight')

subplot(244)
%hold on
if length(Idiff_pick)>0,

plot(hold_kc_log10{pick_item},hold_IoverV_background{pick_item})
    %plot(hold_kc{pick_item},hold_IoverV_background{pick_item})

```



```

else
    plot(1,1)
end
xlabel('Log10( Critical Mobility, Kc [cm2/(V s)] )')
%xlabel('Critical Mobility, Kc [cm2/(V s)]')
ylabel('(Current Signal -Background) / Cond. Voltage [A/V =
1/Ohm]')
grid on
%axis([0 1 -.05 1.05])
%legend(case_info_short)
title('background')

subplot(247)
%hold on

plot(hold_Dp_logmean_short{pick_item},hold_meas_conc_straight_dlogDp
{pick_item})
xlabel('Theoretical Particle Diameter [nm]')
ylabel('dN/dlogDp [(p/cm3)/(log(bin width))]'')
% axis([1.9 21 -.1 1.1])
% set(gca,'XTick',[2:10 20])
% set(gca,'XTickLabel',[2:10 20])
grid on
%title('Normalization: (Data) / max(Data)')
%legend(case_info_short)
title('straight')

subplot(248)
%hold on
if length(Idiff_pick)>0,

plot(hold_Dp_logmean_short{pick_item},hold_meas_conc_background_dlog
Dp{pick_item})
else
    plot(1,1)
end
xlabel('Theoretical Particle Diameter [nm]')
ylabel('dN/dlogDp [(p/cm3)/(log(bin width))]'')
% axis([1.9 21 -.1 1.1])
% set(gca,'XTick',[2:10 20])
% set(gca,'XTickLabel',[2:10 20])
grid on
title('background')
%title('Normalization: (Data) / max(Data)')
%legend(case_info_short)

pause
end
end
end

```

```

if plot_option==1,
    plot_items=choose_items;
elseif plot_option==2,
    plot_items=[];
    counter=0;
    for i=1:num_files,
        if strcmp('N',composition{i})
            counter=counter+1;
            plot_items=[plot_items i];
            Isignal_pick=Isignal{i};
            Vs_pick=Vs{i};
            if sum(ismember(2500,Vs_pick))==1,

hold_I_2500V(counter)=Isignal_pick(find(Vs_pick==2500));
            else
                hold_I_2500V(counter)=NaN;
            end
            if cond_polarity{i}=='P' & emeter_type{i}=='K',
                hold_I_2500V(counter)=hold_I_2500V(counter)*-1;
            end
        end
    end
    figure(10)
    set(gcf,'Position',[360 441 812 481])
    plot(hold_I_2500V(1:23),'b-o','LineWidth',2)
    xlabel('Item# (in Date Order)')
    ylabel('Current (ISignal) [A] at Condenser 2500V')
    axis([0 24 0 8e-9])
    line([0 24],[2500/leakage_resistance_low
2500/leakage_resistance_low],'Color','m','LineWidth',2)
    line([0 24],[2500/leakage_resistance_high
2500/leakage_resistance_high],'Color','m','LineWidth',2)
    set(gca,'XTick',[1:1:23])
    set(gca,'XTickLabel',plot_items)
    grid on
    figure(11)
    hold on
    set(gcf,'Position',[360 441 812 481])
    plot(1:23,hold_I_2500V(1:23),'k-o','Color',[.5 .5
.5],'LineWidth',2)
    plot(25:27,hold_I_2500V(25:27),'b-o','LineWidth',2)
    xlabel('Item# (in Date Order)')
    ylabel('Current (ISignal) [A] at Condenser 2500V')
    axis([0 28 0 8e-9])
    line([0 28],[2500/leakage_resistance_low
2500/leakage_resistance_low],'Color','m','LineWidth',2)
    line([0 28],[2500/leakage_resistance_high
2500/leakage_resistance_high],'Color','m','LineWidth',2)
    set(gca,'XTick',[1:1:27])
    set(gca,'XTickLabel',plot_items)
    grid on

```

```

elseif plot_option==3,
    plot_items=[];
    for i=1:num_files,
        if strcmp('O',composition{i})
            plot_items=[plot_items i];
        end
    end
elseif plot_option==4,
    plot_items=[];
    for i=1:num_files,
        %if strcmp('E',composition{i}) | strcmp('I',composition{i})
        if strcmp('I',composition{i})
            plot_items=[plot_items i];
        end
    end
elseif plot_option==5,
    plot_items=[];
    for i=1:num_files,
        if flowrate(i)==0.3,
            plot_items=[plot_items i];
        end
    end
elseif plot_option==6,
    plot_items=[];
    for i=1:num_files,
        if flowrate(i)~=0.3 & flowrate(i)>0,
            plot_items=[plot_items i];
        end
    end
elseif plot_option==7,
    plot_items=[];
    for i=1:num_files,
        if diameter(i)==10 & strcmp('K',emeter_type{i}),
            plot_items=[plot_items i];
        end
    end
elseif plot_option==8,
    plot_items=[];
    for i=1:num_files,
        if diameter(i)~=10 & diameter(i)>0,
            plot_items=[plot_items i];
        end
    end
elseif plot_option==9,
    plot_items=[];
    for i=1:num_files,
        if ~strcmp('N',composition{i}) & strcmp('K',emeter_type{i})
            plot_items=[plot_items i];
        end
    end
elseif plot_option==10,

```

```

    plot_items=[];
    for i=1:num_files,
        if strcmp('N',composition{i}) & strcmp('K',emeter_type{i})
            plot_items=[plot_items i];
        end
    end
elseif plot_option==11,
    plot_items=[];
    for i=1:num_files,
        if strcmp('N',composition{i}) & strcmp('T',emeter_type{i})
            plot_items=[plot_items i];
        end
    end
elseif plot_option==12,
    plot_items=[];
    for i=1:num_files,
        if strcmp('I',composition{i}) & flowrate(i)==0.3
            plot_items=[plot_items i];
        end
    end
elseif plot_option==13,
    plot_items=[];
    for i=1:num_files,
        if strcmp('I',composition{i}) & flowrate(i)==0.7
            plot_items=[plot_items i];
        end
    end
elseif plot_option==14,
    plot_items=[];
    for i=1:num_files,
        if strcmp('I',composition{i}) & flowrate(i)==1.5
            plot_items=[plot_items i];
        end
    end
elseif plot_option==15,
    plot_items=[];
    for i=1:num_files,
        if strcmp('I',composition{i}) & flowrate(i)==0.3 &
diameter(i)==10 & strcmp('K',emeter_type{i})
            plot_items=[plot_items i];
        end
    end
elseif plot_option==20,
    plot_items=[];
    for i=1:num_files,
        if strcmp('O',composition{i}) & flowrate(i)==0.1
            plot_items=[plot_items i];
        end
    end
elseif plot_option==21,
    plot_items=[];

```

```

    for i=1:num_files,
        if strcmp('O',composition{i}) & flowrate(i)==0.3 &
strcmp('K',emeter_type{i})
            plot_items=[plot_items i];
        end
    end
elseif plot_option==22,
    plot_items=[];
    for i=1:num_files,
        if strcmp('O',composition{i}) & flowrate(i)==0.65
            plot_items=[plot_items i];
        end
    end
elseif plot_option==23,
    plot_items=[];
    for i=1:num_files,
        if strcmp('O',composition{i}) & flowrate(i)==0.3 &
diameter(i)==10 & strcmp('K',emeter_type{i})
            plot_items=[plot_items i];
        end
    end
elseif plot_option==30,
    plot_items=[];
    for i=1:num_files,
        if ~strcmp('N',composition{i}) &
strcmp('PPK31',hold_legend_text_part3{i})
            plot_items=[plot_items i];
        end
    end
elseif plot_option==31,
    plot_items=[];
    for i=1:num_files,
        if strcmp('O',composition{i}) &
(strcmp('PPK31',hold_legend_text_part3{i}) |
strcmp('PPK41',hold_legend_text_part3{i}))
            plot_items=[plot_items i];
        end
    end
elseif plot_option==32,
    plot_items=[];
    for i=1:num_files,
        if strcmp('O',composition{i}) &
strcmp('PPK31',hold_legend_text_part3{i}) & flowrate(i)<=0.3 &
diameter(i)<=20
            plot_items=[plot_items i];
        end
    end
elseif plot_option==40,
    plot_items=[];
    for i=1:num_files,
        if ~strcmp('N',composition{i}) & strcmp('K',emeter_type{i})

```

```

        plot_items=[plot_items i];
    end
end
elseif plot_option==41,
    plot_items=[];
    for i=1:num_files,
        if ~strcmp('N',composition{i}) & strcmp('T',emeter_type{i})
            plot_items=[plot_items i];
        end
    end
end

else
    disp('Error: incorrect plot option')
end

marker_picks=1:length(plot_items);

if plot_4up_fig=='y'

    figure(2)
    set(gcf,'Position',[1      31      1280      696])

    subplot(1,4,1)
    hold on
    counter=0;
    for i=plot_items,
        counter=counter+1;
        hold_legend_text(counter)=legend_text{i};
        plot(Vs{i},Isignal{i},markers{counter})
    end
    xlabel('Condenser Voltage [V]')
    ylabel('Current (Signal) [A]')
    grid on
    %axis([0 1 -.05 1.05])
    [legend_h,object_h,plot_h,text_strings] =
    legend(hold_legend_text);
    %set(object_h(20),'FontSize',8);
    set(object_h(1),'FontSize',8);
    %legend(hold_legend_text)
    title(['Isignal'])
    set(gca,'Xlim',[0 3300])
    %
    %     for i=plot_items,
    %         counter=counter+1;
    %         if length(Idiff{i})>0,
    %             plot(Vs{i},Vs{i}/leakage_resistance_low,'m-')
    %             plot(Vs{i},Vs{i}/leakage_resistance_high,'m-')
    %         else
    %             plot(NaN,NaN,markers{counter})
    %         end
    %     end
    %
end

```

```

subplot(1,4,2)
hold on
counter=0;
for i=plot_items,
    counter=counter+1;
    if length(Idiff{i})>0,
        plot(Vs{i},Idiff{i},markers{counter})
    else
        plot(NaN,NaN,markers{counter})
    end
    %hold_legend_text(counter)=legend_text{i};
end
xlabel('Condenser Voltage [V]')
ylabel('Current (Signal minus Background) [A]')
grid on
%legend(hold_legend_text)
title(['Idiff'])
%
%   for i=plot_items,
%   counter=counter+1;
%   if length(Idiff{i})>0,
%       plot(Vs{i},Vs{i}/leakage_resistance_low,'m-')
%       plot(Vs{i},Vs{i}/leakage_resistance_high,'m-')
%   else
%       plot(NaN,NaN,markers{counter})
%   end
%
%   end
%set(gca,'Xlim',[0 3300])
axis([0 3300 -2e-11 5e-11])

figure(3)
set(gcf,'Position',[1          31          1280          696])

subplot(1,4,1)
hold on
counter=0;
for i=plot_items,
    counter=counter+1;
    %hold_legend_text(counter)=legend_text{i};
    plot(Vs{i},V_conc_scaling{i},markers{counter})
end
xlabel('Condenser Voltage [V]')
ylabel('Concentration Drift Factor')
grid on
%axis([0 1 -.05 1.05])
%legend(hold_legend_text)
title(['ConcDrift'])
set(gca,'Xlim',[0 3300])

subplot(1,4,2)
hold on
counter=0;

```

```

    for i=plot_items,
        counter=counter+1;
        hold_legend_text(counter)=legend_text{i};
        plot([0 Vs{i} 3500],PPR{i},markers{counter})
    end
    xlabel('Condenser Voltage [V]')
    ylabel('Particle Pass-through Ratio')
    grid on
    %axis([0 1 -.05 1.05])
    [legend_h,object_h,plot_h,text_strings] =
legend(hold_legend_text);
    %set(object_h(20),'FontSize',8);
    set(object_h(1),'FontSize',8);
    %legend(hold_legend_text)
    title(['PPR'])
    set(gca,'Xlim',[-100 3600])
    set(gca,'Ylim',[-.1 3])
    %set(gca,'XTickLabel',[0:500:3000 0])
end

if plot_PPR=='y',
    figure(30)
    set(gcf,'Position',[1          31          1280          696])
    subplot(1,4,[1 2])
    hold on
    counter=0;
    for i=plot_items,
        counter=counter+1;
        hold_legend_text(counter)=legend_text{i};
        plot([0 Vs{i} 3500],PPR{i},markers{counter})
    end
    xlabel('Condenser Voltage [V]')
    ylabel('Particle Pass-through Ratio')
    grid on
    %axis([0 1 -.05 1.05])
    [legend_h,object_h,plot_h,text_strings] =
legend(hold_legend_text);
    %set(object_h(20),'FontSize',8);
    set(object_h(1),'FontSize',8);
    %legend(hold_legend_text)
    title(['PPR'])
    set(gca,'Xlim',[-100 3600])
    %set(gca,'Ylim',[-.1 1.2])
    set(gca,'Ylim',[-.1 3])
    set(gca,'XTickLabel',[0:500:3000 0])
end

if plot_6up_fig=='y',
    figure(4)
    set(gcf,'Position',[1          31          1280          696])

```



```

subplot(241)
hold on
counter=0;
for i=plot_items,
    counter=counter+1;
    hold_legend_text(counter)=legend_text{i};

plot(hold_kc_log10{i},Isignal{i},markers{counter},'LineWidth',2)
end
%plot(hold_kc{pick_item},Isignal{pick_item})
xlabel('Log10( Critical Mobility, Kc [cm2/(V s)] )')
%xlabel('Critical Mobility, Kc [cm2/(V s)]')
ylabel('Current (Signal) [A]')
grid on
%axis([0 1 -.05 1.05])
legend(hold_legend_text)
title(['Isignal'])

subplot(242)
hold on
counter=0;
for i=plot_items,
    counter=counter+1;
    if length(Idiff{i})>0,

plot(hold_kc_log10{i},Idiff{i},markers{counter},'LineWidth',2)
    else
        plot(NaN,NaN,markers{counter})
    end
end
xlabel('Log10( Critical Mobility, Kc [cm2/(V s)] )')
%xlabel('Critical Mobility, Kc [cm2/(V s)]')
ylabel('Current (Signal - Background) [A]')
grid on
%axis([0 1 -.05 1.05])
%legend(case_info_short)
title('Idiff')

subplot(243)
hold on
counter=0;
for i=plot_items,
    counter=counter+1;

plot(hold_kc_log10{i},hold_IoverV_straight{i},markers{counter},'Line
Width',2)
end
%plot(hold_kc{pick_item},hold_IoverV_straight{pick_item})
xlabel('Log10( Critical Mobility, Kc [cm2/(V s)] )')
%xlabel('Critical Mobility, Kc [cm2/(V s)]')

```

```

ylabel('Current(Signal) / Cond.Voltage [A / V = 1/Ohm]')
grid on
%axis([0 1 -.05 1.05])
%legend(case_info_short)
title('Char.Curve w/ Isignal')

subplot(244)
hold on
counter=0;
for i=plot_items,
    counter=counter+1;
    if length(Idiff{i})>0,

plot(hold_kc_log10{i},hold_IoverV_background{i},markers{counter},'Li
neWidth',2)
    else
        plot(NaN,NaN,markers{counter})
    end
end
xlabel('Log10( Critical Mobility, Kc [cm2/(V s)] )')
%xlabel('Critical Mobility, Kc [cm2/(V s)]')
ylabel('(Current(Signal-Background) / Cond.Voltage [1/Ohm]')
grid on
%axis([0 1 -.05 1.05])
%legend(case_info_short)
title('Char.Curve w/ Idiff')

subplot(247)
hold on
counter=0;
for i=plot_items,
    counter=counter+1;

%plot(hold_Dp_logmean_short{i},hold_meas_conc_straight_dlogDp{i},mar
kers{counter})

plot(hold_Dp_logmean_log10_short{i},hold_meas_conc_straight_dlogDp{i
},markers{counter},'LineWidth',2)
end
%xlabel('Theoretical Particle Diameter [nm]')
xlabel('Log10( Theoretical Dp [nm])')
ylabel('dN/dlogDp [(p/cm3)/(log(bin width))]'')
% axis([1.9 21 -.1 1.1])
% set(gca,'XTick',[2:10 20])
% set(gca,'XTickLabel',[2:10 20])
grid on
%title('Normalization: (Data) / max(Data)')
%legend(case_info_short)
title('Size Dist. w/ Isignal')

subplot(248)

```

```

hold on
counter=0;
for i=plot_items,
    counter=counter+1;
    if length(Idiff{i})>0,

%plot(hold_Dp_logmean_short{i},hold_meas_conc_background_dlogDp{i},m
arkers{counter})

plot(hold_Dp_logmean_log10_short{i},hold_meas_conc_background_dlogDp
{i},markers{counter},'LineWidth',2)
    else
        plot(NaN,NaN,markers{counter})
    end
end
xlabel('Theoretical Particle Diameter [nm]')
xlabel('Log10( Theoretical Dp [nm])')
ylabel('dN/dlogDp [(p/cm3)/(log(bin width))]' )
% axis([1.9 21 -.1 1.1])
% set(gca,'XTick',[2:10 20])
% set(gca,'XTickLabel',[2:10 20])
grid on
title('Size Dist. w/ Idiff')
%title('Normalization: (Data) / max(Data)')
%legend(case_info_short)

end

if plot_Whipple=='y',
    figure(40)
    set(gcf,'Position',[88 283 832 639])
    hold on
    counter=0;
    for i=plot_items,
        counter=counter+1;
        if length(Idiff{i})>0,

plot(hold_kc_log10{i},Idiff{i},markers{counter},'LineWidth',2)

%plot(hold_kc_log10{i},Vs{i}/leakage_resistance,markers{counter})
    else
        plot(NaN,NaN,markers{counter})
    end
end
xlabel('Log10( Critical Mobility, Kc [cm2/(V s)] )')
ylabel('Current (Signal - Background) [A]')
grid on
%axis([0 1 -.05 1.05])
legend(hold_legend_text)
% for i=plot_items,
% counter=counter+1;

```

```

%         if length(Idiff{i})>0,
%             plot(hold_kc_log10{i},Vs{i}/leakage_resistance_low,'k-
%         ')
%
plot(hold_kc_log10{i},Vs{i}/leakage_resistance_high,'k-')
%         else
%             plot(NaN,NaN,markers{counter})
%         end
%     end

title('Idiff')

figure(41)
set(gcf,'Position',[88 283 832 639])
hold on
counter=0;
for i=plot_items,
    counter=counter+1;
    if length(Idiff{i})>0,

plot(hold_kc_log10{i},hold_IoverV_background{i},markers{counter},'Li
neWidth',2)
        else
            plot(NaN,NaN,markers{counter})
        end
    end
xlabel('Log10( Critical Mobility, Kc [cm2/(V s)] )')
ylabel('(Current(Signal-Background) / Cond.Voltage [1/Ohm]')
grid on
%axis([0 1 -.05 1.05])
legend(hold_legend_text)
title('Characteristic Curve')

figure(42)
set(gcf,'Position',[88 283 832 639])
hold on
counter=0;
for i=plot_items,
    counter=counter+1;
    if length(Idiff{i})>0,

plot(hold_Dp_logmean_log10_short{i},hold_meas_conc_background_dlogDp
{i},markers{counter},'LineWidth',2)
        else
            plot(NaN,NaN,markers{counter})
        end
    end
xlabel('Log10( Theoretical Dp [nm] )')
ylabel('dN/dlogDp [(p/cm3)/(log(bin width)) ]')
% axis([1.9 21 -.1 1.1])
% set(gca,'XTick',[2:10 20])

```

```

% set(gca,'XTickLabel',[2:10 20])
grid on
title('Size Distribution')
legend(hold_legend_text)

figure(43)
set(gcf,'Position',[88 283 832 639])
hold on
counter=0;
for i=plot_items,
    counter=counter+1;
    if length(Idiff{i})>0,

plot(hold_Dp_logmean_log10_short{i},hold_meas_conc_background_dlogDp
{i},markers{counter},'LineWidth',2)
        else
            plot(NaN,NaN,markers{counter})
        end
    end
    xlabel('Log10( Theoretical Dp [nm])')
    xlabel('Theoretical Dp [nm]')
    ylabel('dN/dlogDp [(p/cm3)/(log(bin width)) ]')
%     axis([0.5 1.3 -11e10 5e10])
%     set(gca,'XTickLabel',round((10.^[0.5:.1:1.3])*10)/10)
axis([0.3 1 -4e8 3e8])
set(gca,'XTickLabel',round((10.^[.3:.1:1])*10)/10)
grid on
title('Size Distribution')
legend(hold_legend_text)
end

if plot_big_Isignal=='y',
    figure(5)
    set(gcf,'Position',[1          31          1280          696])
    subplot(1,4,[1 2 3])
    hold on
    counter=0;
    for i=plot_items,
        counter=counter+1;
        hold_legend_text(counter)=legend_text{i};
        plot(Vs{i},Isignal{i},markers{counter})
    end
    xlabel('Condenser Voltage [V]')
    ylabel('Current (Signal) [A]')
    grid on
    %axis([0 1 -.05 1.05])
    [legend_h,object_h,plot_h,text_strings] =
legend(hold_legend_text);
    %set(object_h(20),'FontSize',8);
    set(object_h(1),'FontSize',8);
    %legend(hold_legend_text)

```

```

        title(['Isignal' title_tagline])
        set(gca,'Xlim',[0 3300])
    end

    if plot_scatter=='y',
        figure(6)
        set(gcf,'Position',[ 360 111 630 587])
        counter=0;
        for i=plot_items,
            counter=counter+1;
            hold_Idiff_mean(counter)=abs(mean(Idiff{i}));
            hold_Idiff_maxabs(counter)=max(abs((Idiff{i})));
            hold_Isignal_mean(counter)=abs(mean(Isignal{i}));
            hold_Isignal_maxabs(counter)=max(abs((Isignal{i})));
            %hold_conc(counter)=APA_conc(i)*1.5/flowrate(i);
            hold_conc(counter)=APA_conc(i);
            hold_itemnum(counter)=item_num(i);
        end
        subplot(221)

        semilogx(hold_conc,hold_Isignal_mean,'o','MarkerSize',7,'MarkerFaceC
olor','w','MarkerEdgeColor','w')
        ylabel('Abs(Mean(Isignal)) [A]')
        %xlabel('APA Concentration [p/cm3]')
        grid off
        %title(['Effect of Concentration(scaled to 1.5LPM) on Idiff'
title_tagline])
        %title(['Effect of Concentration on Isignal' title_tagline])
        title(['Isignal' title_tagline])
        for j=1:length(plot_items)

            text(hold_conc(j),hold_Isignal_mean(j),num2str(hold_itemnum(j)))
            end
            subplot(223)

            semilogx(hold_conc,hold_Isignal_maxabs,'o','MarkerSize',7,'MarkerFac
eColor','w','MarkerEdgeColor','w')
            xlabel('APA Concentration [p/cm3]')
            ylabel('Max(Abs((Isignal)) [A]')
            grid off
            title(['Isignal' title_tagline])
            for j=1:length(plot_items)

                text(hold_conc(j),hold_Isignal_maxabs(j),num2str(hold_itemnum(j)))
                end
                subplot(222)

                semilogx(hold_conc,hold_Idiff_mean,'o','MarkerSize',7,'MarkerFaceCol
or','w','MarkerEdgeColor','w')
                ylabel('Abs(Mean(Idiff)) [A]')
                %xlabel('APA Concentration [p/cm3]')

```

```

    grid off
    %title(['Effect of Concentration(scaled to 1.5LPM) on Idiff'
title_tagline])
    %title(['Effect of Concentration on Idiff' title_tagline])
    title(['Idiff' title_tagline])
    for j=1:length(plot_items)

text(hold_conc(j),hold_Idiff_mean(j),num2str(hold_itemnum(j)))
    end
    subplot(224)

semilogx(hold_conc,hold_Idiff_maxabs,'o','MarkerSize',7,'MarkerFaceC
olor','w','MarkerEdgeColor','w')
    xlabel('APA Concentration [p/cm3]')
    ylabel('Max(Abs((Idiff)) [A]')
    grid off
    title(['Idiff' title_tagline])
    for j=1:length(plot_items)

text(hold_conc(j),hold_Idiff_maxabs(j),num2str(hold_itemnum(j)))

%text(hold_conc(j),hold_Idiff_maxabs(j),hold_legend_text_part3{j})
    end

    figure(7)
    subplot(211)

semilogx(hold_conc,hold_Idiff_maxabs,'o','MarkerSize',7,'MarkerFaceC
olor','w','MarkerEdgeColor','w')
    xlabel('APA Concentration [p/cm3]')
    ylabel('Max(Abs((Idiff)) [A]')
    grid off
    title(['Idiff' title_tagline])
    for j=1:length(plot_items)

text(hold_conc(j),hold_Idiff_maxabs(j),num2str(hold_itemnum(j)))

%text(hold_conc(j),hold_Idiff_maxabs(j),hold_legend_text_part3{j})
    end
    subplot(212)
    x_data=log10(hold_conc);
    poly_1_x=[min(x_data):(max(x_data)-
min(x_data))/100:max(x_data)];
    y_data=(hold_Idiff_maxabs*1E9);
    poly_1=polyfit(x_data,y_data,1);
    poly_1_y=polyval(poly_1,poly_1_x);
    corr_ItoConc=corrcoef(x_data,y_data);
    r2_ItoConc=(corr_ItoConc(1,2))^2;
    data_out=[x_data' y_data'];

    hold on

```

```

plot(x_data,y_data,'bo')
plot(poly_1_x,poly_1_y,'r-')

figure(8)
hold on
xlabel('Log10( APA Concentration [p/cm3] )')
ylabel('Max(Abs((Idiff)) [pA]')
plot(x_data,y_data,'bo')
plot(poly_1_x,poly_1_y,'r-')
grid on
title(['Slope: ' num2str(round(poly_1(1)*100)/100) ' '
[pA/Log10(p/cm3)] R-squared: ' num2str(round(r2_ItoConc*100)/100)])

end

```


Appendix E. Reynolds number calculations

	Channel Reynold's number (Rc=DV/v) for flowrate [rpm]->velocity [m/s]:	Screen Reynold's number (Rs=Lv/v) for flowrate [rpm]-> velocity [m/s]:	
@ std sea-level atm pressure (from Fluid Mechanics, Finnemore&Frantini p.733)	0.1 0.5 1.5 15	0.1 0.5 1.5 15	
temp [C]	kin_visc v [m2/s]	kin_visc v [m2/s]	
-40	9.80E-06	106 531 1594	1.55 7.73 23.19 231.91
-20	1.15E-05	91 453 1359	1.32 6.59 19.76 197.63
0	1.32E-05	79 395 1184	1.15 5.74 17.22 172.18
10	1.41E-05	74 369 1108	1.07 5.37 16.12 161.19
20	1.50E-05	69 347 1042	1.01 5.05 15.15 151.52
30	1.60E-05	65 326 977	0.95 4.73 14.20 142.05
40	1.68E-05	62 310 930	0.90 4.51 13.53 135.28
60	1.87E-05	56 279 836	0.81 4.05 12.15 121.54
80	2.09E-05	50 249 748	0.72 3.62 10.87 108.74
100	2.31E-05	45 225 676	0.66 3.28 9.84 98.39
200	3.45E-05	30 151 453	0.44 2.20 6.59 65.88
channel width [m]	channel height [m]	flow rate [l/min]	channel length [m]
2.20E-03	1.00E-03	0.5	0.03
cross-section A [m2]	cross-perimeter P [m]	avg. velocity V [m/s]	traverse time [s]
2.20E-06	hyd dia (D=4A/P) [m]	3.79	0.00792
	1.38E-03		-3+(0.7+2.75+2.3+1.0+3.3*5+0.2*4)--3 = -36mm

Figure 84. Spreadsheet for the calculation of Reynolds number. (MEMS Re.xlsx)

Appendix F. Electrical Schematics

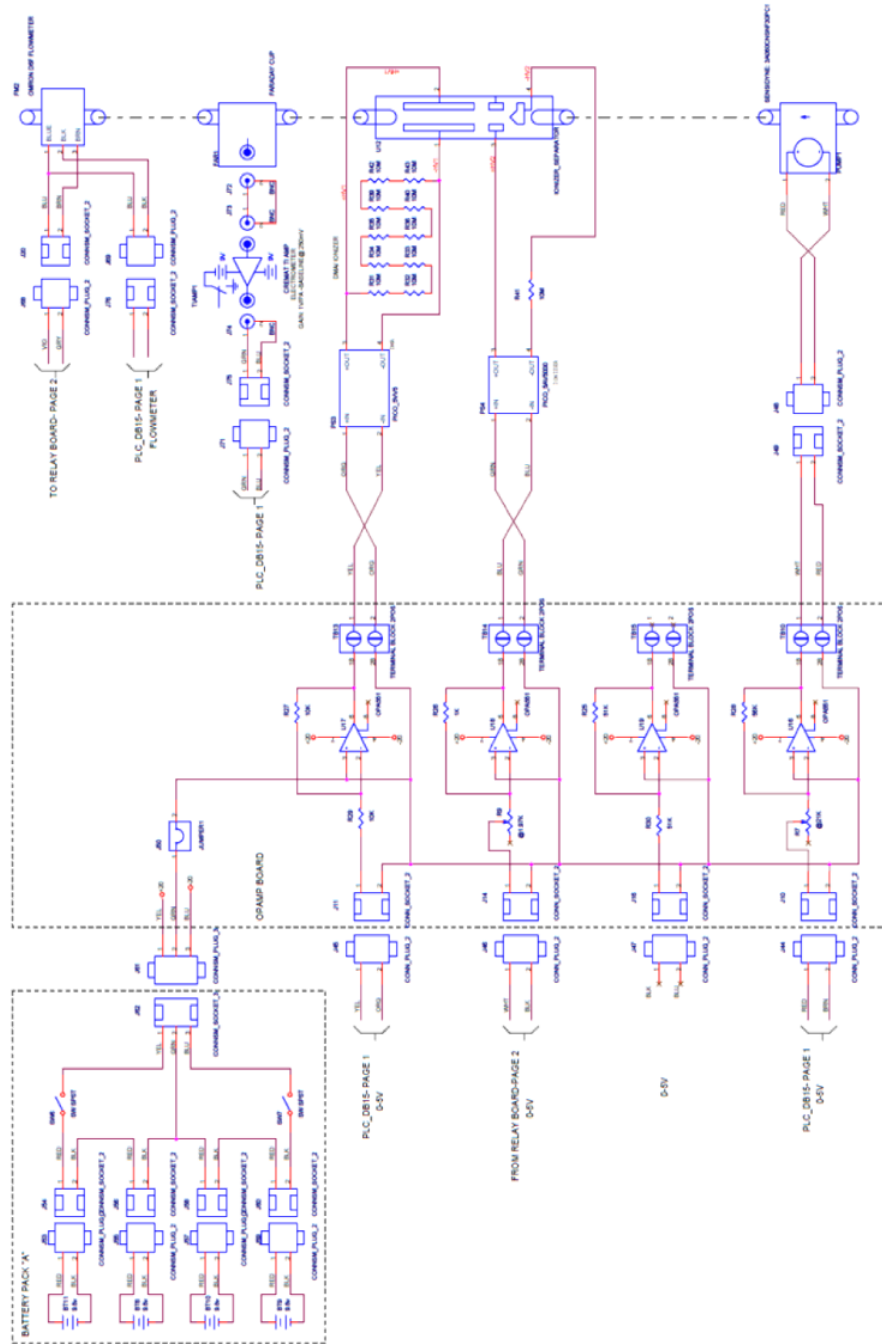


Figure 85. Electrical schematic of MicroAPA prototype (drawing by Kurt Anthony).

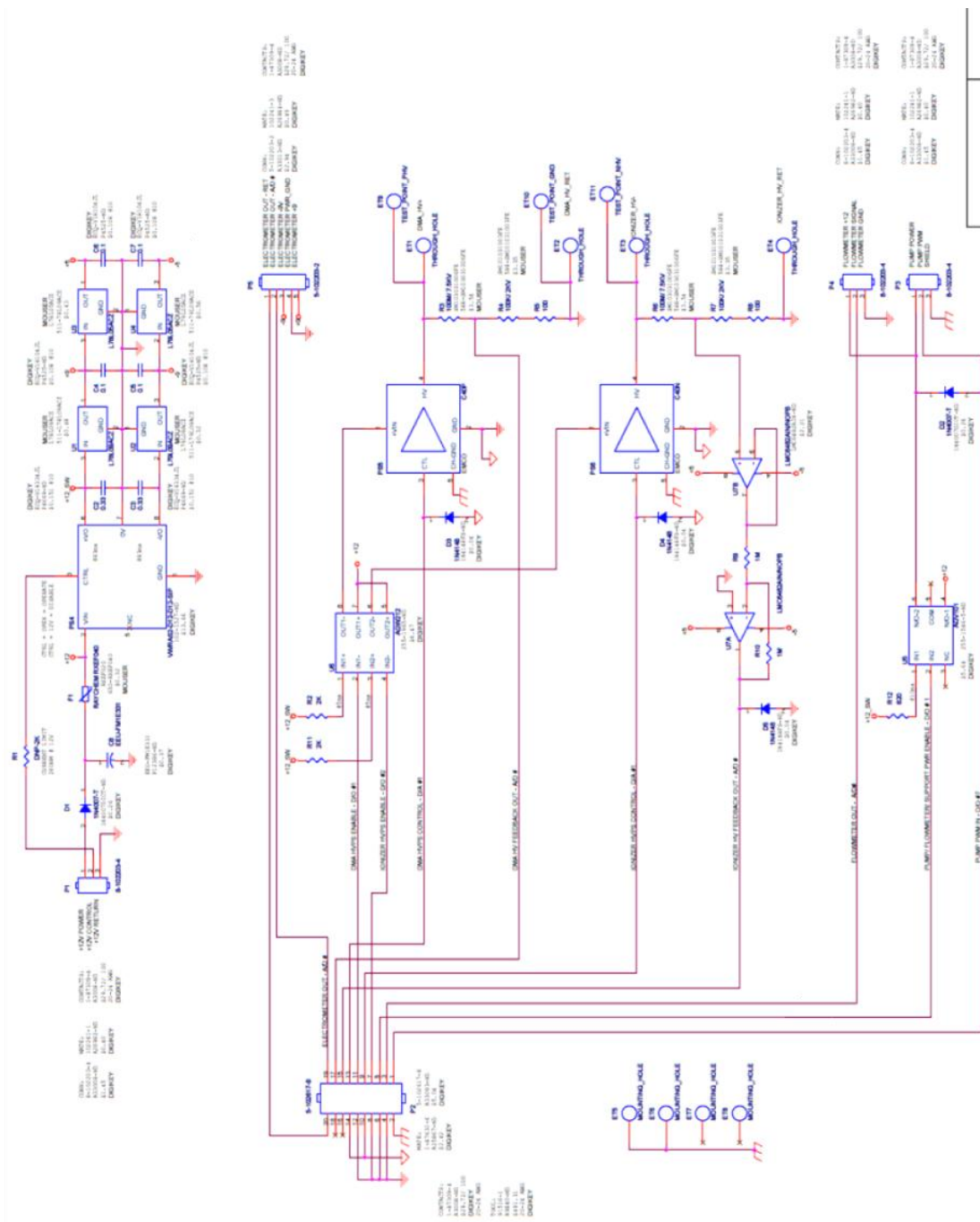


Figure 86. Electrical schematic of NanoAPAv1 instrument (drawing by Kurt Anthony).

Appendix G. Labview virtual instrument programs

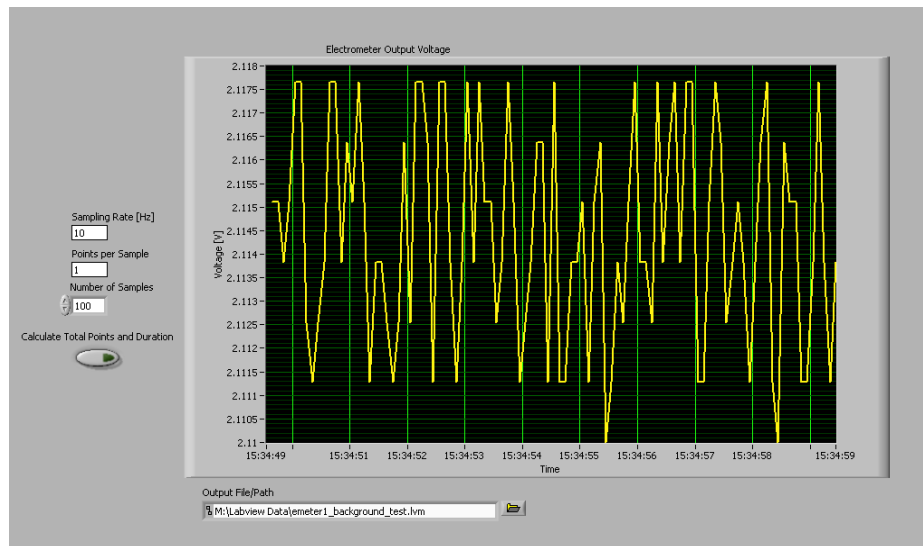


Figure 87. NanoAPA_2.vi Front Panel.

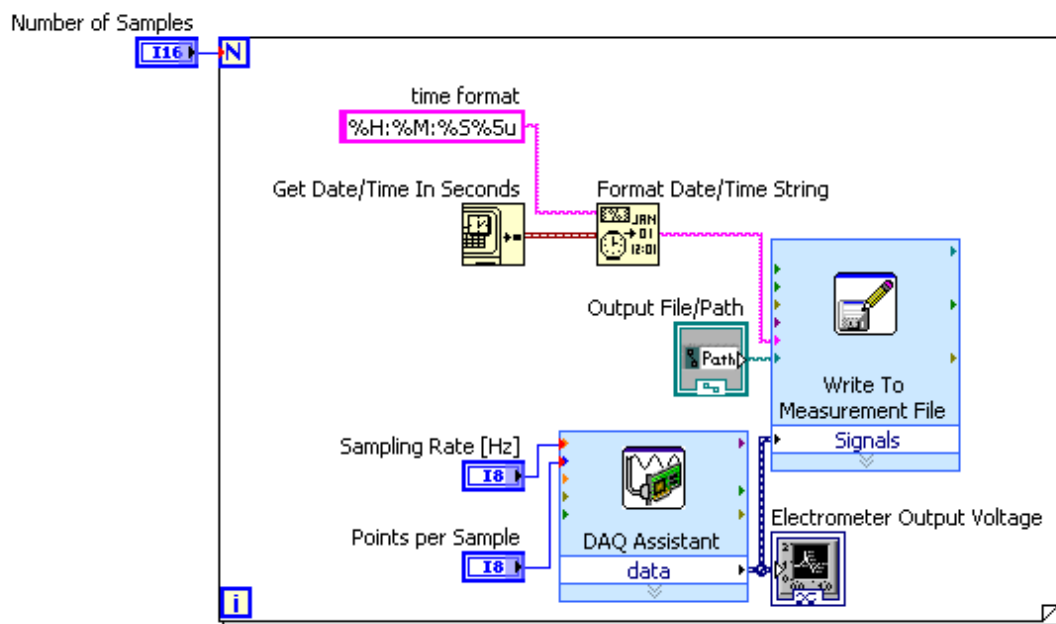


Figure 88. NanoAPA_2.vi Block Diagram.

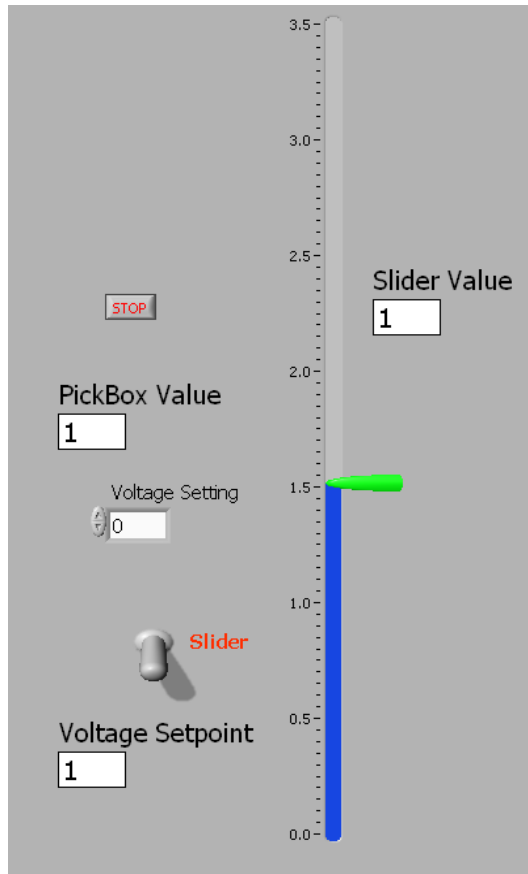


Figure 89. NanoAPA_3.vi Front Panel.

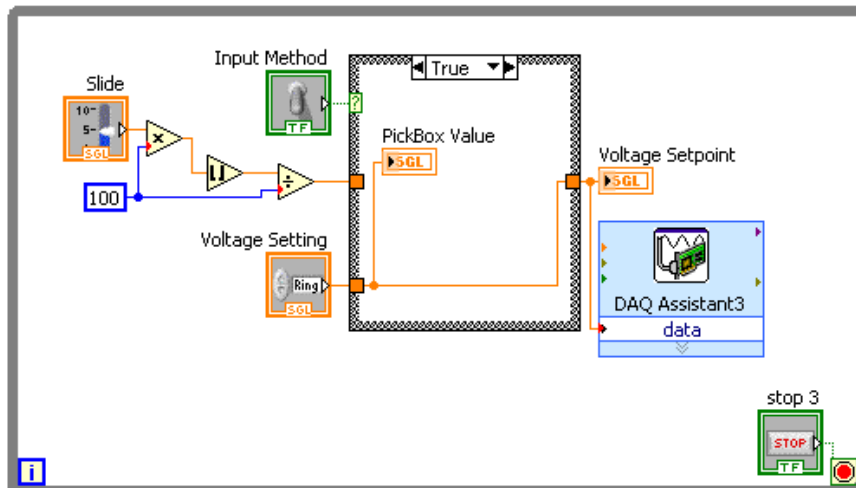


Figure 90. NanoAPA_3.vi Block Diagram.

Appendix H. TI DDC-EVM hardware and software operation

To use the TI DDC-112 EVM electrometer, install the software and setup the hardware as advised in the “DDC11xEVM-PDK User's Guide”. The software provides a user interface to set the operating parameters of the electrometer, make a current measurement, display the data, and export the data as a comma-separated text file. The front panel of the user interface is shown in Figure 91.

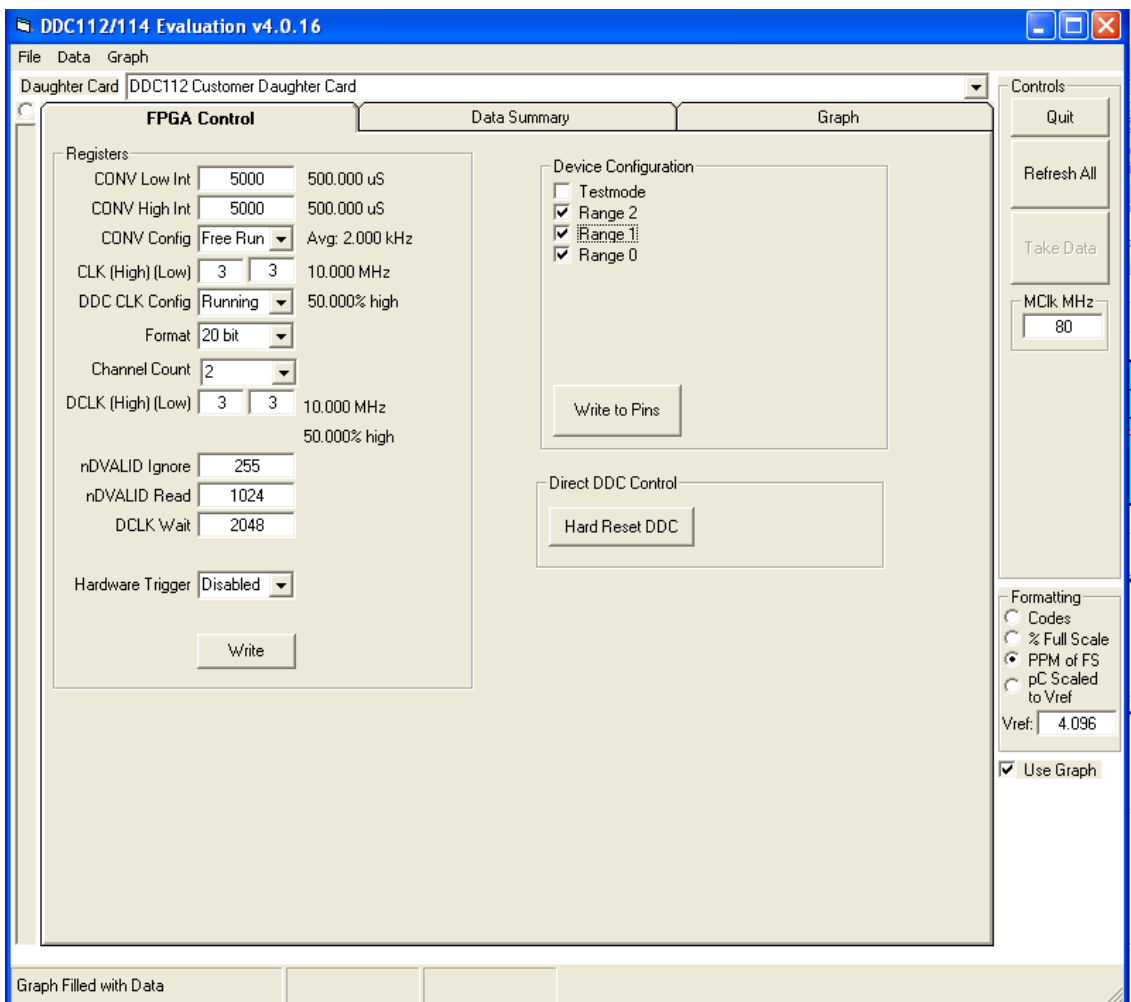


Figure 91. TI EVM Front Panel.

The DDC112 electrometer provides two channels of measurement. Each channel works by alternating cycles of collecting the charges (“integrating”) and counting the charges (“converting”); see Figure 92. Since the timing of these cycles is carefully controlled with an independent clock cycle, the measurement of very small currents can be directly determined by multiplying the number of charges collected per clock cycle by the duration of that clock cycle. If only one channel of measurement is required, the two channels can be connected together (consult User’s Guide), providing one measurement at the “common” input connection of four “channels” of data that can be averaged to increase the signal-to-noise ratio; this was the method used for all data collection in this project.

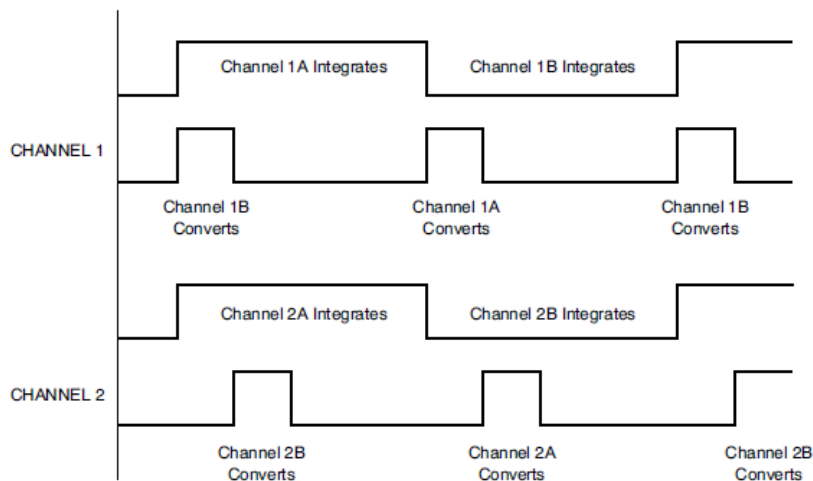


Figure 92. Integration/conversion timing of a dual DDC112 A/D converter. (DDC11xEVM-PDK User's Guide)

Most of the operating parameters were kept at their default values for the measurements made in this project. The parameters that were customized:

1. Measurement Range: To select the range of charge that the electrometer can measure per clock cycle, the check boxes labeled “Range 0/1/2” are selected according to the table shown in Table 15. A box is checked for a “1” and unchecked for a “0”. Start with the largest range -1.4 to 350pC (1-1-1) to ensure capturing all the input signal and adjust downward if needed. After the desired range is selected, push the button labeled “Write to Pins” to program the chip to this setting.

Table 15. Range selection of the DDC112 electrometer. (DDC11xEVM-PDK User's Guide)

RANGE2	RANGE1	RANGE0	C _F (pF, typ)	INPUT RANGE (pC, typ)
0	0	0	External 12.5 to 250	Up to 1000
0	0	1	12.5	-0.2 to 50
0	1	0	25	-0.4 to 100
0	1	1	37.5	-0.6 to 150
1	0	0	50	-0.8 to 200
1	0	1	62.5	-0.1 to 250
1	1	0	75	-1.2 to 300
1	1	1	87.5	-1.4 to 350

2. Set the integration time by entering identical values into the boxes marked “CONV Low/High Int”; the integration time will be shown next to the boxes.

3. Set “nDVALID Ignore” to the number of integration-time cycles to wait before recording data, which allows for signal settling. Start with a value one tenth of that used for “NDVALID Read”. If the first measurements in the data collection exhibit settling behavior, increase this parameter.

4. Set “nDVALID Read” to the number of integration-time cycles to record data for each sub-channel; the total number of data points will be double this number since the sub-channel measurements alternate.

5. Leave “DCLK Wait” at the default value of 2048, these cycles are digital clock cycles (usually 10Mz), not integration-time cycles, and are needed to allow the instrument time to read all the data collected in the run.

6. When all Register parameters are set as desired, push the button marked “Write” to program the chip with these settings.

7. To run the data collection, press the button marked “Take Data”.

8. After the run completes, the data can be viewed on the “Data Summary” and “Graph” tabs, and exported in .csv format by selecting “Save Data from Memory” from the “Data” menu.

The settings used for the TI data in the project database:

Integration time: 0.1s

nDVALID Ignore: 100

nDVALID Read: 300

Range: 7 (1-1-1)

As calibrated by the Parameter Analyzer in this project, the values of current reported by the electrometer using this method were half the actual value of current.